PROCEEDINGS

OF INTERNATIONAL SCHOOL-SEMINAR

«ACTUAL PROBLEMS OF PARTICLE PHYSICS»

Accelerator Physics,
LHC Program,
Physics (in) and (out) the Framework of Standard Model
Soft and Hard QCD Processes,
Quantum Field Theory,
Relativistic Nuclear Physics

Vol. II

PROCEEDINGS of
INTERNATIONAL SCHOOL-SEMINAR
«ACTUAL PROBLEMS OF PARTICLE PHYSICS»

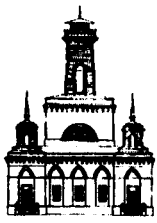

Joint Institute for Nuclear Research (Dubna, Russia),
National Center of Particle and
High Energy Physics (Minsk, Belarus),
Institute of Physics (Minsk, Belarus) &
Institute of Metal Polymer Systems (Gomel, Belarus)
of National Academy of Sciences of Belarus,
Gomel State Univiversity,
Gomel Polytechnic Institut

August 8-17, 1997 Gomel, Belarus

Accelerators physics,
LHC program,
Physics «in» and «out» the framework of Standard Model,
Soft and Hard QCD Processes,
Quantum Field Theory,
Relativistic Nuclear Physics

edited by P. Kuzhir

Vol. II

Dubna, 1998

ISBN 5-85165-517-8 (т. II)
ISBN 5-85165-519-4

CONTENTS

Volume I

* — poster

** — copies of transparences

Volume II

* — poster

** — copies of transparences

4. PHYSICS IN AND BEYOND THE FRAMEWORK OF STANDARD MODEL

4.1. Nucleon spin and radiative corrections.

Review on the Status of Spin Structure Function Measurements

H.Böttcher

DESY-IfH Zeuthen, Platanenallee 6, D-15735 Zeuthen, Germany

Results are presented on inclusive measurements of the spin structure function $g_1(x)$. The world's data on spin-dependent deep inelastic scattering are summarized. Results from recent Next-to-Leading Order (NLO) QCD analyses are given. They provide another successful test of QCD. The uncertainties arising from the low-x extrapolation of the inclusive data in absence of any measurement prevent firm conclusions about the spin structure of the nucleon. The NLO QCD analyses suggest a sizable gluon contribution to the nucleon spin. Proposals to directly probe the gluon polarisation are described.

1 Introduction

The main goal in spin physics is to reveal the spin structure of the nucleon by studying spin-dependent deep inelastic lepton-hadron scattering. The total spin of the nucleon can be written as the sum of contributions from its constituents [1]

$$\frac{1}{2} = \frac{1}{2}\Delta\Sigma + \Delta L_Q + \Delta g + \Delta L_g, \qquad (1)$$

where $\Delta\Sigma$ is the intrinsic spin carried by the quarks, ΔL_Q is the angular momentum of the quarks, Δg is the spin carried by the gluons, and ΔL_g is the angular momentum of the gluons.

While in the framework of the Quark Parton Model (QPM) $\Delta\Sigma$ is predicted to be about 0.6 the European Muon Collaboration (EMC) extracted a value of $0.06\pm0.047\pm0.069$ from measurements of the spin structure function $g_1^p(x)$ performed in 1988 [2]. This discrepancy established the so called 'spin puzzle' and stimulated a variety of experimental and theoretical activities worldwide. Recently it has been shown theoretically by investigating the Q^2 dependence of

the angular momentum [3] that $\frac{1}{2}\Delta\Sigma + \Delta L_Q \rightarrow\sim \frac{1}{4}$ and $\Delta g + \Delta L_g \rightarrow\sim \frac{1}{4}$ in the limit $Q^2 \rightarrow \infty$.

However, the definition of these quantities is a matter of discussion as the distinction between quark and gluon fields depends on the gauge chosen. All experiments to date have extracted a value for $\Delta\Sigma$ in the order of 0.3 [4] when analysing the data in the framework of the QPM and assuming SU(3) flavour symmetry. Recent NLO QCD analyses have shed more light onto the gluon contribution to the nucleon spin. However, all conclusions drawn so far concerning the spin composition of the nucleon suffer from the uncertainties arising from the low–x region where no data are available up to now. There is no final answer yet and after many years of intense studies both experimentally and theoretical, the question of how the spin of the nucleon is composed of its elementary constituents remains open.

After giving an overview of the theoretical framework the status of the measurements of the spin stucture function $g_1(x)$ will be presented and recent results from NLO QCD analyses will be discussed with a short outlook onto initiatives to directly probe the gluon polarisation in the nucleon.

2 Theoretical Framework

2.1 Inclusive Cross Section for Spin–Dependent Deep Inelastic Lepton–Nucleon Scattering

Deep inelastic scattering (DIS) is the study of lepton-nucleon scattering at a sufficient high momentum transfer. In lowest order Quantum Electro Dynamics (QED) the scattering process is described by the exchange of a virtual photon (one–photon approximation). The basic Feynman diagram is shown in Fig. 1.

The cross section for inclusive DIS of a lepton from a nucleon has the general form

$$\frac{d\sigma}{dxdQ^2} = \frac{e^4}{16\pi^2 Q^4} \times \frac{E'}{E} \times L^{\mu\nu} W_{\mu\nu}, \tag{2}$$

where $L^{\mu\nu}$ is the leptonic and $W_{\mu\nu}$ the hadronic tensor. The variables E and E' are the energies of the in-

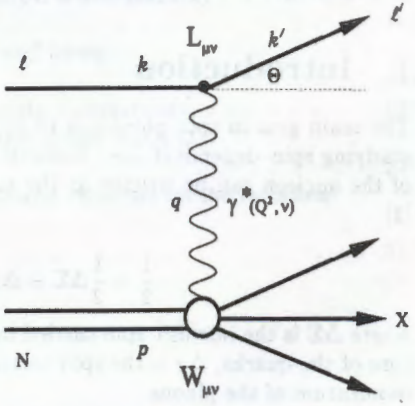

Figure 1: Deep inelastic lepton-nucleon scattering in lowest order QED.

coming and the scattered lepton, respectively, and $Q^2 = -q^2 = -(k - k') \overset{lab}{\simeq} 2EE'(1 - cos\theta))$ is the four-momentum transfer squared, with k and k' being the four-momenta of the incoming and the scattered lepton, respectively, and θ the scattering angle (see Fig. 1). The leptonic tensor is exactly determined in QED while the hadronic tensor cannot be calculated yet and, therefore, is usually expressed in terms of structure functions. Both tensors have a symmetric and an antisymmetric part where the latter contains the spin information Discussing the theoretical framework further I closely follow Ref. [5].

In the one–photon approximation (see Fig. 1) the inclusive cross section for spin–dependent DIS can be written as the sum of a spin–independent term $\overline{\sigma}$ and a spin–dependent term $\Delta\sigma$ involving the lepton helicity $h_l = \pm 1$:

$$\sigma = \overline{\sigma} - \frac{1}{2} h_l \Delta\sigma. \qquad (3)$$

The spin–independent cross section is expressed in terms of two unpolarised structure functions F_1 and F_2 which depend on Q^2 and the Bjorken scaling variable $x = Q^2/2M\nu$, where $\nu = pq/M \overset{lab}{=} E - E'$ is the energy transfer and M the nucleon mass. The variables p and q are the four–momenta of the target nucleon and the virtual photon, respectively. Its double differential form as function of x and Q^2 [6] is

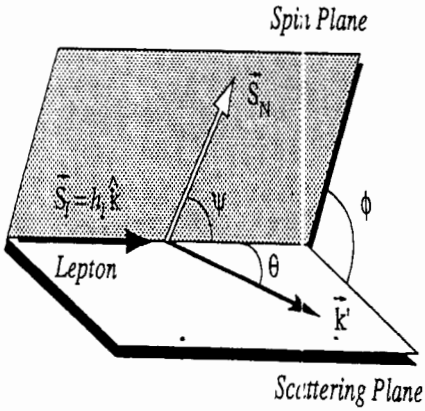

Figure 2: Definition of spin and scattering plane in polarised lepton scattering on a fixed polarised nucleon target. The figure has been taken from [5].

$$\frac{d^2\overline{\sigma}}{dxdQ^2} = \frac{4\pi\alpha^2}{Q^4 x}\left[xy^2\left(1 - \frac{2m_l^2}{Q^2}\right)F_1(x,Q^2) + \left(1 - y - \frac{\gamma^2 y^2}{4}\right)F_2(x,Q^2)\right], \qquad (4)$$

where m_l is the lepton mass, $y \overset{lab}{=} \nu/E$, and

$$\gamma^2 = \frac{4M^2x^2}{Q^2} = \frac{Q^2}{\nu}, \qquad (5)$$

a variable which approaches zero in the Bjorken limit, i.e. when Q^2 and ν approach infinity at fixed x.

The spin–dependent cross section can be expressed in terms of two polarised structure functions g_1 and g_2 which also are a function of x and Q^2. When the

directions of the lepton spin and that of the nucleon spin form an angle ψ (see Fig. 2) it can be written as [7]

$$\Delta\sigma = \cos\psi\Delta\sigma_{\parallel} + \sin\psi\cos\phi\Delta\sigma_{\perp}, \tag{6}$$

where ϕ is the azimuthal angle between the scattering plane and the spin plane. The scattering plane is defined by the three momentum vectors $\vec{k}$ and $\vec{k'}$ and the spin plane by $\vec{k}$ and the spin vector $\vec{S_N}$ of the nucleon (see Fig. 2). For longitudinally polarised leptons the spin $\vec{S_l}$ is oriented along the incoming momentum vector $\vec{k}$. The cross sections $\Delta\sigma_{\parallel}$ and $\Delta\sigma_{\perp}$ refer to the two configurations where the nucleon spin is oriented (anti)parallel and orthogonal, respectively, to the lepton spin. The variable $\Delta\sigma_{\parallel}$ is the difference between the cross sections for antiparallel and parallel spin orientations and $\Delta\sigma_{\perp}$ is the difference between the cross sections for opposite orthogonal spin orientations, i.e. at angles ϕ and $\phi+\pi$. The respective double differential cross sections as functions of x and Q^2 are given by

$$\frac{d^2\Delta\sigma_{\parallel}}{dxdQ^2} = \frac{16\pi\alpha^2 y}{Q^4}\left[\left(1-\frac{y}{2}-\frac{\gamma^2y^2}{4}\right)g_1(x,Q^2) - \frac{\gamma^2 y}{2}g_2(x,Q^2)\right] \tag{7}$$

and

$$\frac{d^3\Delta\sigma_{\perp}}{dxdQ^2d\phi} = -\cos\phi\frac{8\alpha^2 y}{Q^4}\gamma\sqrt{1-y-\frac{\gamma^2y^2}{4}}\left(\frac{y}{2}g_1(x,Q^2)+g_2(x,Q^2)\right). \tag{8}$$

At beam energies E already as high as at SLAC and at the HERA lepton ring, γ becomes small since either x is small or Q^2 is large and, hence, terms proportional to γ^2 can be neglected in first approximation. The structure function g_1 is therefore best measured in the (anti)parallel spin configuration while g_2 can be obtained from a measurement in the orthogonal configuration combined with a measurement of g_1.

2.2 Cross Section Asymmetries

Since the spin–dependent part of the cross section contributes only little to the total deep inelastic cross section it can best be determined from measurements of cross section asymmetries in which the spin–independent contribution cancels. The relevant asymmetries are

$$A_{\parallel} = \frac{\Delta\sigma_{\parallel}}{2\bar{\sigma}} \quad \text{and} \quad A_{\perp} = \frac{\Delta\sigma_{\perp}}{2\bar{\sigma}}, \tag{9}$$

which are related to the virtual photon-nucleon asymmetries A_1 and A_2 by

$$A_{\parallel} = D(A_1 + \eta A_2) \quad \text{and} \quad A_{\perp} = d(A_2 - \xi A_1). \tag{10}$$

The aymmetries A_1 and A_2 are defined by

$$A_1 = \frac{\sigma_{1/2} - \sigma_{3/2}}{\sigma_{1/2} + \sigma_{3/2}} = \frac{g_1 - \gamma^2 g_2}{F_1} \quad \text{and} \quad A_2 = \frac{2\sigma^{TL}}{\sigma_{1/2} + \sigma_{3/2}} = \gamma \frac{g_1 + g_2}{F_1}. \tag{11}$$

The variables d, η, and ξ are kinematical factors given by

$$\begin{aligned} d &= \frac{\sqrt{1 - y - \gamma^2 y^2/4}}{1 - y/2} D, \\ \eta &= \frac{\gamma(1 - y - \gamma^2 y^2/4)}{(1 - y/2)(1 + \gamma^2 y/2)}, \\ \xi &= \frac{\gamma(1 - y/2)}{1 + \gamma^2 y/2}, \end{aligned} \tag{12}$$

and D is the virtual photon depolarisation factor determining the degree of polarisation transfered from the incoming lepton to the virtual photon. The cross sections $\sigma_{1/2}$ and $\sigma_{3/2}$ refer to the absorption of a transversely polarised virtual photon by a polarised nucleon for a total photon-nucleon angular momentum component along the virtual photon axis of $1/2$ and $3/2$, respectively, and σ^{TL} is an interference cross section. The depolarisation factor D is a function of y and $R = \sigma_L/\sigma_T$, the ratio of the longitudinal and transverse photoabsorption cross sections:

$$D = \frac{y(2 - y)(1 + \gamma^2 y/2)}{y^2(1 + \gamma^2)(1 - 2m_l^2/Q^2) + 2(1 - y - \gamma^2 y^2/4)(1 + R)}. \tag{13}$$

The virtual photon-nucleon asymmetries A_1 and A_2 are bound by positivity relations [8]:

$$| A_1 | \leq 1 \quad \text{and} \quad | A_2 | \leq \sqrt{R}. \tag{14}$$

Using Eqs. (10) and (11) the longitudinal asymmetry $A_{\|}$ can be expressed as function of g_1 and A_2, and when neglecting the term proportional to A_2 the following relations are found

$$A_1 \simeq \frac{A_{\|}}{D} \quad \text{and} \quad \frac{g_1}{F_1} \simeq \frac{1}{1 + \gamma^2} \frac{A_{\|}}{D}, \tag{15}$$

where F_1 is usually expressed in terms of F_2 and R:

$$F_1 = \frac{1 + \gamma^2}{2x(1 + R)} F_2. \tag{16}$$

These relations are used to evaluate A_1 and g_1 starting from the measured longitudinal asymmetry and using parametrisations for $F_2(x, Q^2)$ and $R(x, Q^2)$.

Correspondingly one derives a relation which is used to evaluate the virtual photon-nucleon asymmetry A_2 from the measured transverse and longitudinal asymmetries $A_{\parallel}$ and $A_{\perp}$:

$$A_2 = \frac{1}{1+\eta\xi}\left(\frac{A_{\perp}}{d} + \xi\frac{A_{\parallel}}{D}\right). \tag{17}$$

As seen from Eqn. (11), A_2 has an explicit γ dependence and is therefore expected to be small at beam energies high enough. The Eqs. (11) and (17) are used to calculate g_2 from the measured asymmetries.

2.3 The Spin–Dependent Structure Function g_1

The spin structure function g_1 contains information on the quark spin orientation with respect to the nucleon spin direction. In the framework of the QPM it is given by

$$g_1(x) = \frac{1}{2}\sum_{i=1}^{n_f} e_i^2 \Delta q_i(x), \tag{18}$$

where

$$\Delta q_i(x) = \left(q_i^+(x) - q_i^-(x)\right) + \left(\overline{q_i}^+(x) - \overline{q_i}^-(x)\right), \tag{19}$$

and $q_i^+(\overline{q_i}^+)$ and $q_i^-(\overline{q_i}^-)$ are the distribution functions of quarks (antiquarks) with spin parallel and antiparallel to the nucleon spin, respectively, e_i is the electric charge of the quarks of flavour i, and n_f is the number of quark flavours involved.

In Quantum Chromo Dynamics (QCD) quarks interact by gluon exchange which gives rise to a weak Q^2 dependence of the structure functions. According to the treatment in pertubative QCD the polarised structure function $g_1(x,Q^2)$ is given by [9]

$$\begin{aligned} g_1(x,Q^2) \;=\; & \frac{1}{2}\sum_{i=1}^{n_f}\frac{e_i^2}{n_f}\int_x^1 \frac{dy}{y}\left[C_q^S(\frac{x}{y},\alpha_s(Q^2))\Delta\Sigma(y,Q^2)\right. \\ & + 2n_f C_g(\frac{x}{y},\alpha_s(Q^2))\Delta g(y,Q^2) \\ & \left. + C_q^{NS}(\frac{x}{y},\alpha_s(Q^2))\Delta q^{NS}(y,Q^2)\right], \end{aligned} \tag{20}$$

where C_q and C_g are coefficient functions, Δg is the polarised gluon distribution, and $\Delta\Sigma$ and Δq^{NS} are the singlet (S) and non-singlet (NS) combinations of the polarised quark and antiquark distributions

$$\Delta\Sigma(x,Q^2) = \sum_{i=1}^{n_f}\Delta q_i(x,Q^2), \tag{21}$$

$$\Delta q^{NS}(x,Q^2) = \frac{\sum_{i=1}^{n_f}\left(e_i^2 - \frac{1}{n_f}\sum_{k=1}^{n_f} e_k^2\right)}{\frac{1}{n_f}\sum_{k=1}^{n_f} e_k^2}\Delta q_i(x,Q^2). \tag{22}$$

The Q^2 evolution of the structure functions in QCD follows the Dokshitzer-Gribov-Lipatov-Altarelli-Parisi (DGLAP) equations [10, 11, 12]. The polarised singlet and the gluon distributions are coupled by

$$\begin{aligned}\frac{d}{dlnQ^2}\Delta\Sigma(x,Q^2) &= \frac{\alpha_s(Q^2)}{2\pi}\int_x^1 \frac{dy}{y}\left[P_{qq}^S(\frac{x}{y},\alpha_s(Q^2))\Delta\Sigma(y,Q^2)\right. \\ &\left. + 2n_f P_{qg}(\frac{x}{y},\alpha_s(Q^2))\Delta g(y,Q^2)\right], \end{aligned}\tag{23}$$

$$\begin{aligned}\frac{d}{dlnQ^2}\Delta g(x,Q^2) &= \frac{\alpha_s(Q^2)}{2\pi}\int_x^1 \frac{dy}{y}\left[P_{gq}^S(\frac{x}{y},\alpha_s(Q^2))\Delta\Sigma(y\ Q^2)\right. \\ &\left. + P_{gg}(\frac{x}{y},\alpha_s(Q^2))\Delta g(y,Q^2)\right], \end{aligned}\tag{24}$$

whereas the non-singlet distribution evolves independently of the singlet and gluon distributions:

$$\frac{d}{dlnQ^2}\Delta q^{NS}(x,Q^2) = \frac{\alpha_s(Q^2)}{2\pi}\int_x^1 \frac{dy}{y}P_{qq}^{NS}(\frac{x}{y},\alpha_s(Q^2))\Delta q^{NS}(y,Q^2). \tag{25}$$

The P_{ij} are the QCD splitting functions for polarised parton distributions.

The quark and gluon distributions, the coefficient functions, and the splitting functions depend on the mass factorization and on the renormalization scale. Setting both scales to Q^2 at leading order the coefficient functions are

$$\begin{aligned} C_q^{0,S}(\frac{x}{y},\alpha_s) &= C_q^{0,NS}(\frac{x}{y},\alpha_s) = \delta(1-\frac{x}{y}), \\ C_g^0(\frac{x}{y},\alpha_s) &= 0. \end{aligned}\tag{26}$$

In this case g_1 decouples from Δg. Beyond leading order the C_i and P_{ij} depend on the renormalization scheme. In the $\overline{MS}$ scheme the complete set of coefficient functions and the polarised splitting functions P_{qq} and P_{qg} up to order α_s^2 are given in [13] while the $\mathcal{O}(\alpha_s^2)$ corrections to the splitting functions P_{gq} and P_{gg} can be found in [14] and [15].This formalism allows a complete NLO QCD analysis of the scaling violations of the spin–dependent structure functions. In [16] the splitting and coefficient functions are transformed from the $\overline{MS}$ scheme to different factorization schemes. One of these other schemes is the Adler–Bardeen scheme which will be used later.

2.4 The First Moment of g_1, the Axial Quark Charges, and Sum Rules

A powerful tool to study the moments of structure functions is provided by the Operator Product Expansion (OPE), where the product of the leptonic and the hadronic tensors reduces to the expansion of the product of two electromagnetic currents. At leading twist the only gauge-invariant contributions are due to the non-singlet and singlet axial currents [17, 18]. Leading twist means a twist-two process where the number of partons involved in the hard process on the parton level is two [19]. Considering only the three lightest quark flavours u, d, and s the axial current operator A_k can be expressed in terms of the $SU(3)_f$ flavour matrices $\lambda_k (k = 1, ..., 8)$ and $\lambda_0 = 2I$ as [18] $A^k_\mu = \overline{\psi}\frac{\lambda_k}{2}\gamma_3\gamma_\mu\psi$. The proton matrix elements for momentum p and spin s, $\langle ps|A^i_\mu|ps\rangle$ are related to those of the neutron by assuming isospin symmetry and can be expressed in terms of the axial charge matrix elements for flavour q_i. The first moment of g_1 can be written as

$$\begin{aligned}\Gamma_1^{p(n)}(Q^2) &= \int_0^1 g_1^{p(n)}(x, Q^2)dx \\ &= \frac{C_1^S(Q^2)}{9}a_0 + \frac{C_1^{NS}(Q^2)}{12}\left[+(-)a_3 + \frac{1}{3}a_8\right], \end{aligned} \tag{27}$$

where the a_0, a_3, and a_8 are related to the axial charge matrix elements a_i for the flavour q_i by

$$\begin{aligned} a_0 &= (a_u + a_d + a_s) \\ a_3 &= (a_u - a_d) \\ a_8 &= (a_u + a_d - 2a_s). \end{aligned} \tag{28}$$

The C_1^S and C_1^{NS} are the singlet and non-singlet coefficient functions, respectively. already discussed.

It should be noted that a_u, a_d, and a_s have an implicit Q^2 dependence. The matrix element a_3 is under isospin symmetry equal to the neutron β-decay constant $|g_A/g_V|$. If exact $SU(3)_f$ symmetry is assumed for the axial flavour octet current, a_3 and a_8 can be expressed in terms of the $SU(3)_f$ coupling constants F and D obtained from neutron and hyperon β-decays [23]:

$$a_3 = F + D \quad \text{and} \quad a_8 = 3F - D. \tag{29}$$

The first moment of the polarised quark distribution for flavour q_i, defined as $\Delta q_i = \int \Delta_i(x)dx$, is the contribution of that flavour to the spin of the nucleon. In the QPM a_i is interpreted as Δq_i and a_0 as $\Delta\Sigma = \Delta u + \Delta d + \Delta s$ being the sum of the contribution of all quark flavours considered.

The **Bjorken Sum Rule** was derived by Bjorken in 1966 within the framework of current algebra [20]. It follows directly from Equ. (27) and reads

$$\Gamma_1^p(Q^2) - \Gamma_1^n(Q^2) = \frac{1}{6}\left|\frac{g_A}{g_V}\right| C_1^{NS}(Q^2). \tag{30}$$

This sum rule is considered by now to be a cornerstone of QCD. Its validation is therefore a crucial test of QCD. As a rigorous prediction it is subject to QCD corrections decribed by the non-singlet coefficient function $C_1^{NS}(Q^2)$. This function depends on the number of flavours and on the renormalization scheme. In the $\overline{MS}$ scheme it is given by

$$\begin{aligned} C_1^{NS}(Q^2) &= 1 - c_1^{NS}\left(\frac{\alpha_s(Q^2)}{\pi}\right) - c_2^{NS}\left(\frac{\alpha_s(Q^2)}{\pi}\right)^2 \\ &\quad - c_3^{NS}\left(\frac{\alpha_s(Q^2)}{\pi}\right)^3 - \mathcal{O}(c_4^{NS})\left(\frac{\alpha_s(Q^2)}{\pi}\right)^4, \end{aligned} \tag{31}$$

where the coefficients c_i^{NS} have been calculated up to the third order in α_s [21] and an estimate exists for the $\mathcal{O}(\alpha_s^4)$ [22].

In the QPM the coefficient functions are equal to unity. Using Eqn. (29) which follows from assuming exact $SU(3)_f$ symmetry Eqn. (27) can be written as

$$\Gamma_1^{p(n)} = +(-)\frac{1}{12}(F+D) + \frac{5}{36}(3F-D) + \frac{1}{3}a_s \tag{32}$$

This relation was derived by Ellis and Jaffe in 1974 and is therefore known as the **Ellis-Jaffe Sum Rule** [23]. With the additional assumption that $a_s = 0$, which in the QPM means $\Delta s = 0$, they obtained a numerical prediction for Γ_1^p and Γ_1^n using the values for the coupling constants F and D calculated from neutron and hyperon β-decays [24, 25]. In 1988 EMC [2] measured a significant smaller value for Γ_1^p than the predicted one. The interpretation of this result within the QPM implied that the contribution of the quark spins $\Delta\Sigma$ to the proton spin is small. This fact was the origin of the well-known 'spin- puzzle'.

In QCD the coefficient functions are no longer equal to unity and the Ellis-Jaffe sum rule takes the form

$$\begin{aligned} \Gamma_1^{p(n)}(Q^2) &= C_1^{NS}\left[+(-)\frac{1}{12}\left|\frac{g_A}{g_V}\right| + \frac{1}{36}(3F-D)\right] \\ &\quad + \frac{1}{9}C_1^S(3F-D), \end{aligned} \tag{33}$$

with the singlet coefficient function

$$C_1^S(Q^2) = 1 - c_1^S \left(\frac{\alpha_s(Q^2)}{\pi}\right) - c_2^S \left(\frac{\alpha_s(Q^2)}{\pi}\right)^2 - \mathcal{O}(c_3^S) \left(\frac{\alpha_s(Q^2)}{\pi}\right)^3 \qquad (34)$$

in addition to the non-singlet function C_1^{NS}. The QCD corrections have been computed up to order $\mathcal{O}(\alpha_s^2)$ [18] and there is an estimate for the third order [26].

The Interpretation of a_0 and the $U(1)$ Anomaly:

As already mentioned, in the QPM $a_0(Q^2)$ is interpreted as $\Delta\Sigma$, the contribution of the quarks to the nucleon spin. In QCD the $U(1)$ anomaly causes a gluon contribution to $a_0(Q^2)$ [27, 28, 29]. This makes $\Delta\Sigma$ dependent on the factorization scheme while a_0 is not. The decomposition of $a_0(Q^2)$ into $\Delta\Sigma$ and a gluon contribution is scheme-dependent [30]. In the Adler–Bardeen (AB) factorization scheme [31] it is

$$a_0(Q^2) = \Delta\Sigma - n_f \frac{\alpha_s(Q^2)}{2\pi} \Delta g(Q^2), \qquad (35)$$

where the last term was originally identified as the anomalous gluon contribution or the $U(1)$ anomaly. In this scheme $\Delta\Sigma$ is independent of Q^2, however, it cannot be obtained from the measured singlet axial moment $a_0(Q^2)$ without an input for $\Delta g(Q^2)$.

Recently, it was pointed out [32] that the total fraction of the nucleon spin carried by quarks, namely the sum of $\Delta\Sigma$ and the quark orbital angular momentum L_q, is scheme-independent because of an exact compensation between the anomalous contribution to $\Delta\Sigma$ and to L_q.

2.5 The Spin–Dependent Structure Function g_2

The spin structure function g_2 can be understood from the spin–flip amplitude that gives rise to the interference asymmetry $A_2 \propto g_1 + g_2$ (see Equ. 11). Wandzura and Wilczek have shown [34] that g_2 can be decomposed as

$$g_2(x, Q^2) = g_2^{WW}(x, Q^2) + \bar{g}_2(x, Q^2). \qquad (36)$$

The term g_2^{WW} is a linear function of g_1:

$$g_2^{WW}(x, Q^2) = -g_1(x, Q^2) + \int_x^1 g_1(t, Q^2) \frac{dt}{t}. \qquad (37)$$

The term $\bar{g}_2$ originates from a twist-3 contribution in the OPE [7] and is a measure of quark-gluon correlations in the nucleon [33]. In the QPM g_2 vanishes in the simplest case where the masses and transverse momenta of the quarks are neglected.

3 Results from Inclusive Data on Spin–Dependent Deep Inelastic Scattering

3.1 Summary of Experiments

The first in a series of experiment devoted to spin physics was performed at SLAC in 1975 [35]. About ten years ago the EMC experiment published the surprising result that the Ellis-Jaffe sum rule for the proton is violated [2]. In the QPM the EMC result implied that $\Delta\Sigma$, the contribution of the quark spins to the proton spin, is small and compatible with zero in contradiction to the expectations. This result initiated a number of new experiments at SLAC, CERN and DESY during the last years. All these experiments focused on high precision measurements of the spin structure function $g_1(x, Q^2)$ over the accessible kinematical range on proton, neutron, and deuteron targets. To date significant measurements of $g_1(x, Q^2)$ exist for an x-range of $0.004 \leq x \leq 0.7$. Table 1 summarizes all experiments and their kinematics.

Table 1. Summary of Experiments at SLAC, CERN, and DESY to measure spin–dependent deep inelastic scattering.

experiment	beam	target type	x-range	Q^2-range	ref.
E80 (1975)	16 GeV e^-	H–Butanol	0.10–0.50	1–3	[35]
E130 (1980)	16–23 GeV e^-	H–Butanol	0.18–0.70	3.5–10	[36]
E142 (1992)	19–26 GeV e^-	^3He	0.03–0.60	1–10	[37]
E143 (1993)	10–29 GeV e^-	NH_3/ND_3	0.029–0.80	1–10	[38]
E154 (1995)	49 GeV e^-	^3He	0.014–0.70	1–17	[39]
E155 (1997)	49 GeV e^-	NH_3/ND_3	0.014–0.70	1–17	[40]
EMC (1985)	100–200 GeV μ^-	NH_3	0.005–0.75	..–200	[2]
SMC (1992)	100 GeV μ^+	D-Butanol	0.003–0.70	1–60	[41]
SMC (1993)	190 GeV μ^+	H-Butanol	0.003–0.70	1–60	[42]
SMC (1994)	190 GeV μ^+	D-Butanol	0.003–0.70	1–60	[43]
SMC (1995)	190 GeV μ^+	D-Butanol	0.003–0.70	1–60	[44]
SMC (1996)	190 GeV μ^+	NH_3	0.003–0.70	1–60	[5, 45]
HERMES (1995)	27.5 GeV e^+	^3He	0.02–0.70	1–10	[46]
HERMES (1996)	27.5 GeV e^+	^1H	0.02–0.70	1–10	[40]
HERMES (1997)	27.5 GeV e^+	^1H	0.02–0.70	1–10	

Recent reviews can be found in [47] and [40]. In the following only results for the spin structure function g_1 and its first moment will be discussed.

3.2 Experimental Procedure for Extracting g_1

The polarised structure function g_1 is extracted from inclusive data on polarised DIS, where inclusive means that only information about the scattered lepton is used [1]. The inclusive data are analysed according to the following general strategy:

After having collected the experimental raw data certain quality and kinematic cuts are to be applied. A data sample of high quality is selected by cuts with respect to beam polarisation, target polarisation, and spectrometer performance. Kinematical cuts are applied to exclude events from the resonance region (e.g. $W^2 < 4\ GeV^2$), from the region with high radiative corrections (e.g. at HERMES $y > 0.85$), and from the region where the parametrisations used for $F_2(x, Q^2)$ and $R(x, Q^2)$ are considered not to be valid (e.g. $Q^2 < 1\ GeV^2$). From the selected data sample the experimental asymmetry

$$A_{\parallel} = \frac{N^{\uparrow\Downarrow} - N^{\uparrow\Uparrow}}{N^{\uparrow\Downarrow} + N^{\uparrow\Uparrow}} \tag{38}$$

is calculated in certain intervals of x and Q^2, where $N^{\uparrow\Downarrow}$ and $N^{\uparrow\Uparrow}$ are the number of events with antiparallel and parallel spin orientation of the incoming lepton and the target nucleon, respectively. The measured asymmetry $A_{\parallel}$ is related to the photon-nucleon asymmetry A_1 according to Eqn. (11) through

$$A_{\parallel} = f p_B p_T D A_1, \tag{39}$$

where f is the dilution factor accounting for possibly unpolarised target material, p_B and p_T are the beam and target polarisation, respectively, and D is the depolarisation factor (Eqn. (13)). At this point QED radiative corrections using the standard procedure [48] and nuclear corrections in case of a complex polarised target as ^3He [49, 50] are to be applied. The spin structure function $g_1(x, Q^2)$ can then be calculated following Eqn. (15) and (16) by

$$g_1(x, Q^2) = \frac{F_2(x, Q^2)}{2x(1 + R(x, Q^2))} A_1 \tag{40}$$

with the standard parametrisations for $F_2(x, Q^2)$ [51] and $R(x, Q^2)$ [52] as further input. A new parametrisation for F_2 has been derived in [45]. A parametrisation of R for the region $x < 0.12$ is given in [53].

After all these steps g_1 is determined as function of x at an averaged measured Q^2_m characteristic for each experiment. In order to be able to compare the measurements of different experiments one has to evolve $g_1(x, Q^2_m)$ to a common value of Q^2_0. This is done either by assuming that $A_1 \simeq g_1/F_1$ is independent of Q^2 which is experimentally justified [54] or by an NLO QCD evolution. It should

[1] Semi-inclusive data contain information about additional particles (e.g. the leading hadron) produced in the interaction.

be mentioned that in QCD the ratio g_1/F_1 is slightly Q^2-dependent because the splitting functions, with the exception of P_{qq}, are different for polarised and unpolarised parton distributions. However, in regions dominated by valence quarks the Q^2-dependence is expected to be small [55].

3.3 The Data on the Spin Structure Function g_1

At first the most recent and partly still preliminary data on g_1 measured on proton and neutron targets will be presented.

Proton data:

The SMC experiment at CERN completed data taking on a polarised proton target in September 1996. The new data [45] are plotted in Fig. 3 together with data taken in 1993. There is no indication anymore for a rise of g_1^p at low x as seen earlier [42].

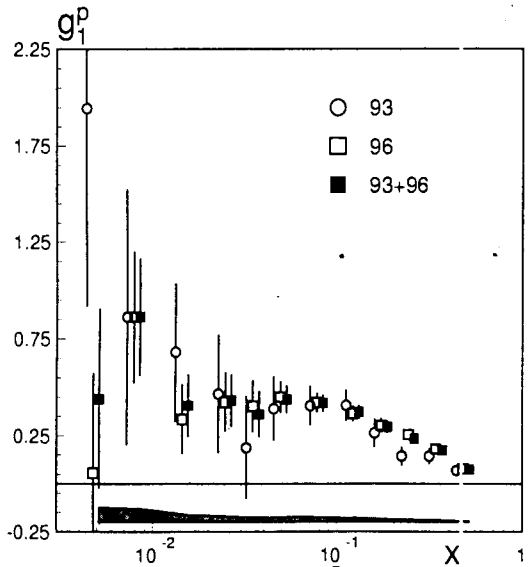

Figure 3: SMC measurements of g_1^p including the new 1996 data [45]. The shaded band indicates the systematic uncertainties.

The HERMES experiment at DESY used a polarised proton target in 1996/97. Preliminary results on the asymmetry A_1^p from the 1996 measurements are shown in Fig. 4 together with measurements from E143. At present only the statistical uncertainties of the HERMES 1996 data are shown since the systematic errors are still a matter of detailed investigations using systematic measurements performed in 1997.

At SLAC the E155 experiment started data taking on polarised proton and deuteron targets beginning of 1997 and preliminary results on g_1^p/F_1^p are shown in Fig. 5 together with the measurements from E143 and SMC.

Neutron Data:

The E154 experiment at SLAC has taken data on a polarised ^3He target which acts effectively as an polarised neutron target. The final results for g_1^n are shown

in Fig.6 together with a measurement from E142. These high quality data are comparable in precision with those on the proton.

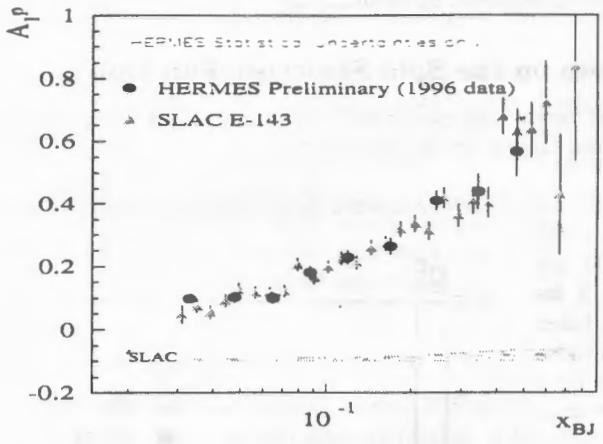

Figure 4: Preliminary results on A_1^p from HERMES compared with measurements of the ratio g_1^p/F_1^p instead of A_1^p from E143.

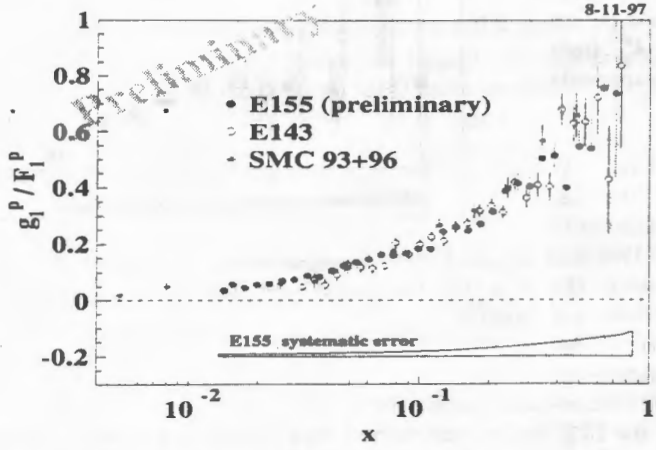

Figure 5: Preliminary results on g_1^p/F_1^p from E155. Measurements from E143 and SMC are shown for comparison [40].

The HERMES experiment at DESY has also published final results on g_1^n ob-

tained in its commissioning year (1995) which are shown in Fig.7 compared with measurements from E154.

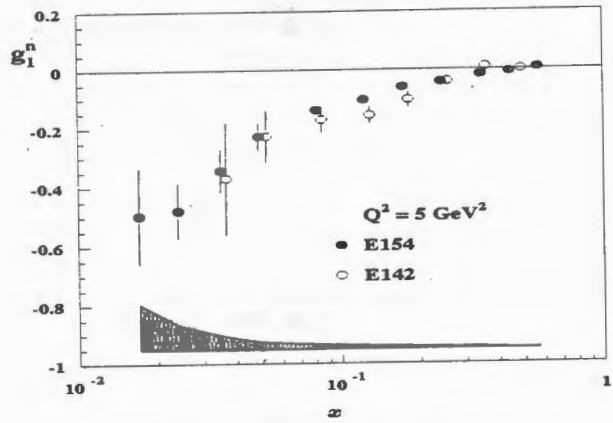

Figure 6: Final result on g_1^n from E154 together with a measurement from E142 [39].

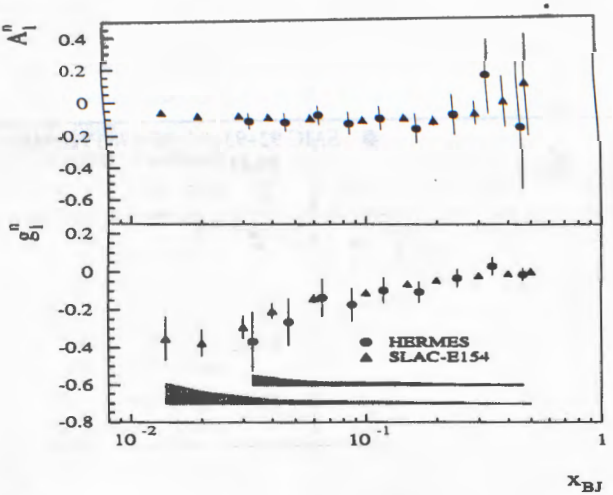

Figure 7: Final results on A_1^n and g_1^n from HERMES compared with measurements from E154.

Finally, in Fig.8 is shown a compilation done by SMC of the world data including preliminary results from HERMES, E154, and SMC 1996 running.

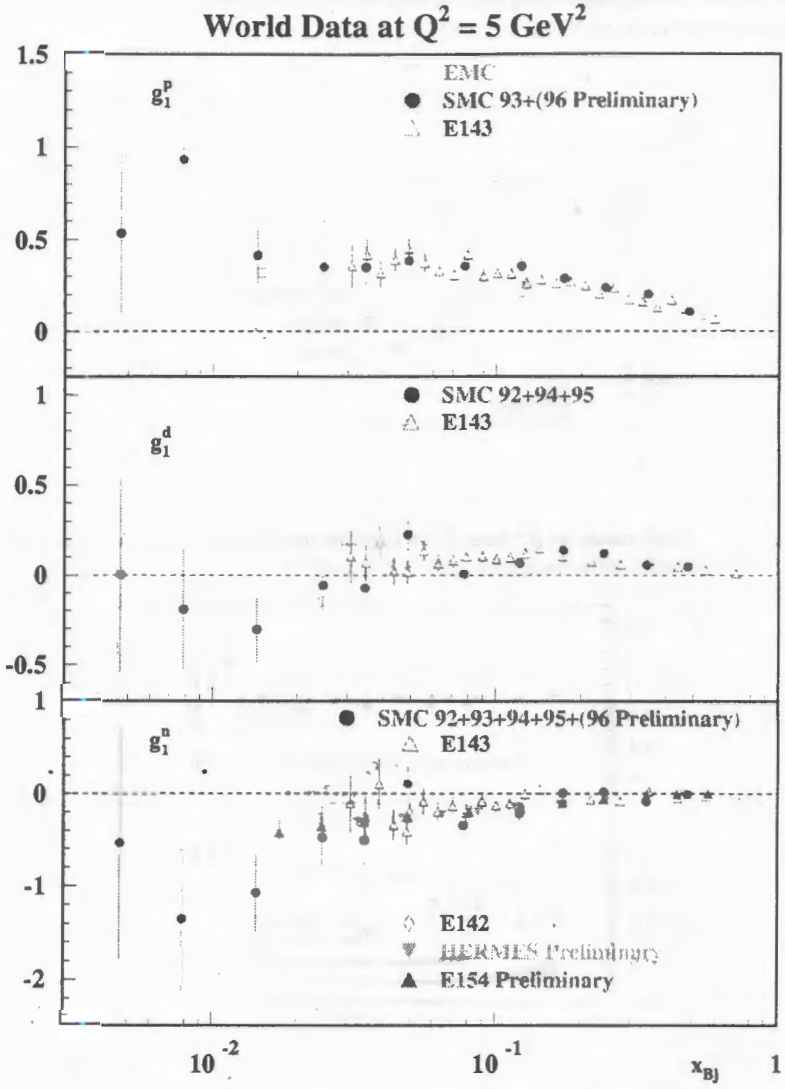

Figure 8: A compilation done by the SMC collaboration of data on $g_1(x)$ for proton, deuteron, and neutron including preliminary data from SMC(96), HERMES(95), and E154.

3.4 NLO QCD Analysis of the Data

New and more precise data for the spin structure function $g_1(x)$ and the calculation of the necessary coefficient and splitting functions opened up the possibility to carry out NLO QCD analyses of the scaling violation of g_1. Such analyses have been performed over the last years both by a number of theory groups [56, 16, 57, 58, 59] and by the experiments with each new update of their data analysis [5, 45, 60]. In quoting results only two most recent analyses will be discussed, the one performed by Altarelli et al. [59] and the one presented by SMC [5, 45].

The general procedure is to start with a parametrisation of the initial polarised parton distributions at a certain reference scale Q_0^2. The conventional form of such a parametrisation is [59]

$$\Delta f(x, Q_0^2) = N_f \eta_f x^{\alpha_f} (1-x)^{\beta_f} (1 + \gamma_f x^{\delta_f}), \tag{41}$$

where Δf stands for Δq^{NS}, $\Delta\Sigma$, and Δg, the non-singlet and singlet polarised quark distributions and the polarised gluon distribution, respectively, and α_f, β_f, γ_f, and δ_f are free parameters. The normalisation factor N_f is chosen such that $\int \Delta f(x) dx$, the first moment of Δf, is equal to η_f. It should be noted that the parameter α_f controls the low-x behaviour of the parton distributions. These distributions are then evolved using the DGLAP equations up to the values of Q^2 where the data are taken. The free parameters are determined by a best fit to all data on $g_1(x)$ used.

In the analysis presented in [59] particular care was taken in view of the small x extrapolation. Four different parametrisations A–D were chosen to probe the sensitivity to different possibilities for the parton distributions (for details see [59]). The data used were from CERN [2, 5] and SLAC [38, 39]. The strong coupling constant was assumed to be $\alpha_s(m_z) = 0.118 \pm 0.005$ [61] and the $SU(3)$ octet axial charge $a_8 = 0.579 \pm 0.025$ [25]. In Fig. 9 is shown $g_1^p(x, Q_0^2 = 10\ GeV^2)$ for the best fits using the four different parametrisations. It can be seen that $g_1^p(x)$ is predicted to turn *negative*

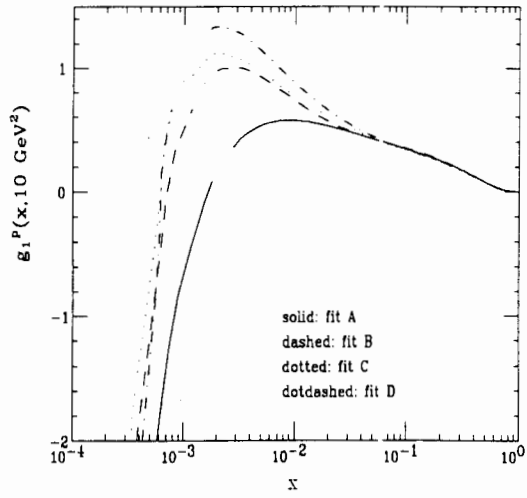

Figure 9: The function $g_1^p(x)$ from [59] showing the range of parametrisations allowed by the data.

at $x \leq 10^{-3}$ which also holds for deuteron and neutron data. The polarised gluon distribution corresponding to the parametrisations A–D used in [59] is shown in Fig. 10. As in earlier analyses also this analysis suggests a significant gluon contribution to the nucleon spin. In [59] the large *positively* polarised gluon is considered to be the reason for driving the g_1^p distribution *negative* at small x. Experimentally the gluon polarisation is completely unknown.
For the singlet first moments the following values have been obtained:

$$\Delta\Sigma = 0.45 \pm 0.04(exp) \pm 0.08(theor) \tag{42}$$

and

$$\Delta g(Q^2 = 1\ GeV^2) = 1.6 \pm 0.4(exp) \pm 0.8(theor), \tag{43}$$

leading to a value of

$$a_0(Q^2 = 10\ GeV^2) = 0.10 \pm 0.05(exp)\ {}^{+0.17}_{-0.10}\ (theor) \tag{44}$$

for the non-conserved singlet axial charge a_0. The parameter a_0 defined by $\Delta\Sigma$ and Δg according to Eqn. (35) illustrates the range of interpretation of the 'spin puzzle'. The value above is compatible with zero which was the result of the EMC experiment [2] about ten years ago. Note, however, that when using a naive Regge extrapolation at small x the value of a_0 becomes significantly different from zero as will be discussed later. There is evidence for a *positive* gluon polarisation, the amount of which is large enough to allow the conserved singlet quark density $\Delta\Sigma$ to be within one standard deviation of $a_8 \sim 0.58$ [25] which in absence of all $SU(3)$ and chiral breaking effects could be identified with the constituent spin fraction [23]. Although this could be considered as a physical explanation of the 'spin puzzle' due to the axial

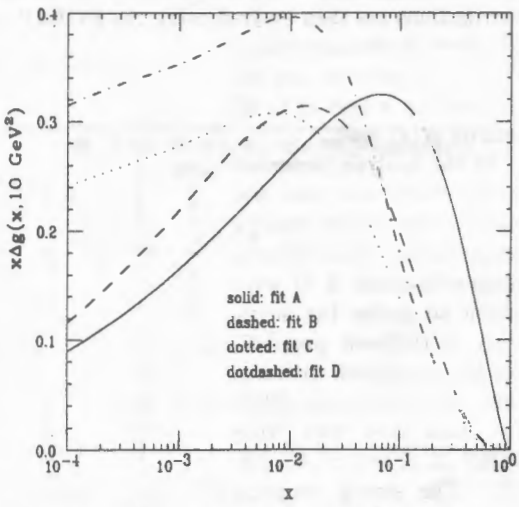

Figure 10: The $x\Delta g(x)$ distributions from [59] corresponding to the parametrisations A–D. All curves are consistent with the inclusive data used in the analysis.

anomaly, it has to be stressed that a real measurement of the gluon polarisation Δg is badly needed.

The SMC experiment has updated [45] its previously presented NLO QCD analysis [5]. Here the method developed in [16] is used. The calculation is also performed in the AB factorization scheme. In a simplification of Eqn. (41) the quark singlet, non-singlet, and gluon polarised parton distributions are parametrised at $Q_0^2 = 1\ GeV^2$ as

$$\Delta f(x, Q_0^2) = N_f \eta_f x^{a_f}(1-x)^{\beta_f}(1 + a_f x), \tag{45}$$

with the normalisation

$$N_f^{-1}(\alpha_f, \beta_f, a_f) = \int x^{a_f}(1-x)^{\beta_f}(1 + a_f x)dx. \tag{46}$$

The parameter a was set to zero in the non-singlet and gluon distributions and the exponent β was additionally fixed to 4 for the gluon (for further details see [5, 45]). The data used came from SMC [44, 5], EMC [2] and E143 [38]. The result of the NLO QCD fit for g_1^p is shown in Fig. 11.

The integral of the gluon distribution at $Q^2 = 1\ GeV^2$ was found to be $\Delta g = 0.9 \pm 0.3(exp) \pm 1.0(theor)$, corresponding to $\Delta g \sim 1.7$ at $Q^2 = 10\ GeV^2$. In this analysis the gluon contribution to the nucleon spin turned out to be also *positive* as in [59].

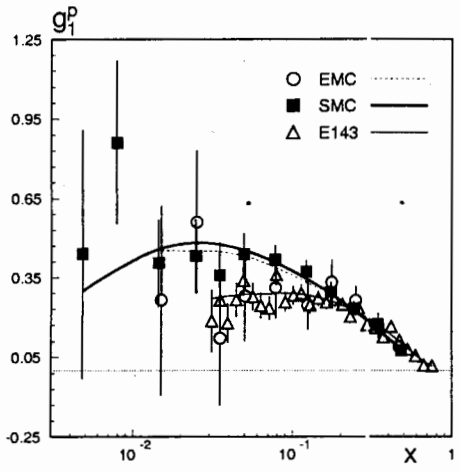

Figure 11: Published data sets on g_1^p with curves from NLO QCD fits at the measured Q^2 for each data set. The fits were done by the SMC experiment [45] using the method developed in [16].

3.5 The First Moment of g_1^p and Sum Rules

For the SMC data the contribution to **the first moment** of the proton structure function g_1^p at $Q_0^2 = 10\ GeV^2$, Γ_1^p (see Eqn. (27)), from the measured range, $0.003 < x < 0.7$, is determined to be [45]

$$\int_{0.003}^{0.7} g_1^p(x, Q_0^2)dx = 0.139 \pm 0.006(stat) \pm 0.008(syst) \pm 0.006(theor). \tag{47}$$

To estimate the contribution to Γ_1^p from the unmeasured high x region $0.7 < x < 1.0$ a constant value of $A_1^p = 0.7 \pm 0.3$ is assumed which is consistent with the data and satisfies the upper bound $A_1 \leq 1$. This conservative assumption leads to a value of

$$\int_{0.7}^{1.0} g_1^p(x, Q_0^2)dx = 0.0015 \pm 0.0006. \tag{48}$$

The main problem arises from the extrapolation into the unmeasured low–x region. The conventional method is to assume a constant g_1 in agreement with a Regge–type behaviour. Alternatively, the low–x integral from the NLO QCD fit could be used. In the case of the SMC proton data the difference is illustrated in Fig. 12.

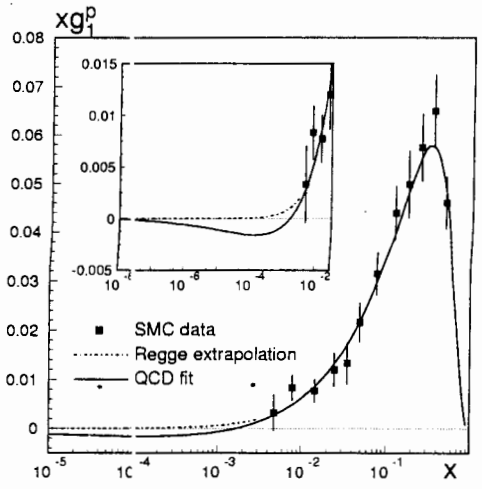

Figure 12: SMC data (squares) for xg_1^p as function of x. Shown is also the result of the NLO QCD fit (continuous line). Both at $Q_0^2 = 10\ GeV^2$. For $x < 0.003$ the extrapolation assuming Regge–type behaviour is indicated by the dashed line. The insert is a close–up extending to lower x. The figure is taken from [45].

Calculating the integrals leads to

$$\int_{0.0}^{0.003} g_1^p(x, Q_0^2)dx = \begin{array}{ll} +0.002 \pm 0.002 & (Regge) \\ -0.011 \pm 0.011 & (QCD) \end{array}. \tag{49}$$

The corresponding values for the first moment of g_1^p over the entire x range at $Q_0^2 = 10\ GeV^2$ are

$$\Gamma_1^p(Q_0^2 = 10\ GeV^2) = \begin{array}{ll} 0.142 \pm 0.006 \pm 0.008 \pm 0.006 & (Regge) \\ 0.130 \pm 0.006 \pm 0.008 \pm 0.014 & (QCD) \end{array}, \tag{50}$$

where the first error is statistical, the second is systematic, and the third arises from extrapolation and theoretical uncertainties.

Sum rules have been derived for the first moment of the polarised structure function $g_1(x)$ which are calculated according to Eqn. (27). Assuming exact $SU(3)_f$ symmetry and an unpolarised strange sea which corresponds to assuming $a_s = \Delta s = 0$ **Ellis and Jaffe** have predicted [23] for the first moment a value of

$$\Gamma_1^p(Q_0^2 = 10\ GeV^2) = 0.170 \pm 0.004. \tag{51}$$

The value extracted from the measurement is smaller and violates the Ellis-Jaffe prediction by more than 2σ. This is also demonstrated in Fig. 13 taken from a previous SMC publication [5] where results from other experiments are shown in addition. It should be noted that this conclusion holds also for the neutron and deuteron data.

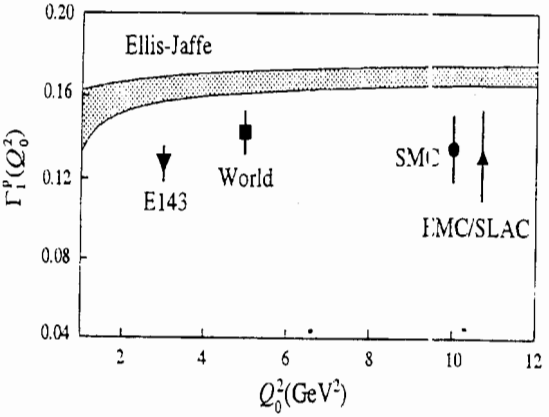

Figure 13: Comparison of the experimental results for Γ_1^p with the prediction of the Ellis-Jaffe sum rule (shaded band). The figure has been taken from [5].

Combining their proton with the deuteron data [44] SMC derived the first moment for the neutron and obtained a value for the **Bjorken** sum over the full x range using the Regge–type extrapolation of

$$\Gamma_1^p - \Gamma_1^n = 0.195 \pm 0.029, \tag{52}$$

which agrees with the theoretical prediction at $Q_0^2 = 10\ GeV^2$ of

$$\Gamma_1^p - \Gamma_1^n = \frac{1}{6}\left|\frac{g_A}{g_V}\right| C_1^{NS} = 0.186 \pm 0.003 \tag{53}$$

within 1σ. It should be noted, however, that the experimental uncertainty of about 15 % in the case of the SMC analysis is still relatively large. An alternative test of the Bjorken sum rule has been performed in [59] using the NLO QCD fit already discussed above by fixing the value for α_s and leaving g_A/g_V free. The data used there came from SMC *and* SLAC. Hence, the Bjorken sum rule was confirmed again within 1σ, but now with a better accuracy of about 8 %.

The relation between Γ_1^p, Γ_1^n, Γ_1^d, and the Bjorken sum at $Q_0^2 = 5\ GeV^2$ is illustrated in Fig. 14. As can be seen, proton, neutron, and deuteron results confirm the Bjorken sum but disagree with the Ellis-Jaffe sum rule.

The violation of the Ellis-Jaffe sum rule is not really surprising since it is connected with the assumption $\Delta s = 0$ which is not justified neither theoretical nor experimentally. As will be discussed below measurements rather indicate a slight *negative* polarisation for the strange sea. In contrast the Bjorken sum rule is fundamental, derived in 1966 from current algebra [20] before QCD became the standard model of strong interactions.

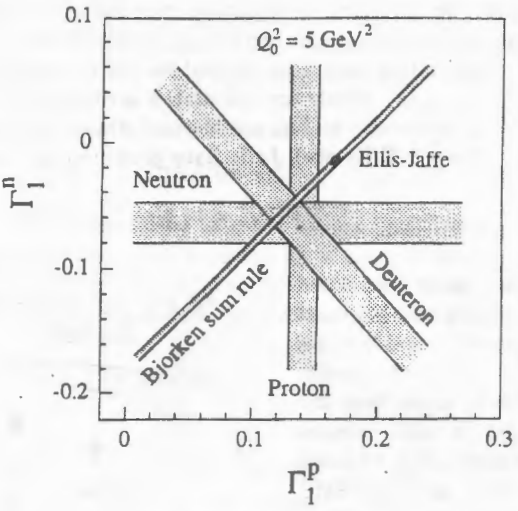

Figure 14: Comparison of the combined experimental results for Γ_1^p, Γ_1^n, and Γ_1^d with the prediction of the Bjorken and the Ellis-Jaffe sum rules at $Q_0^2 = 5\ GeV^2$. The Ellis-Jaffe prediction is indicated by the black ellipse inside the Bjorken sum rule band. The figure has been taken from [5].

As a rigorous prediction of QCD it is nowadays even used to determine the strong coupling constant α_s. Its violation would throw serious doubts on the validity of QCD. It is an experimental challenge to further reduce the experimental uncertainties in determining the Bjorken sum.

3.6 The Axial Quark Charges

Considering only the three lightest quarks u, d, and s contributing to the proton spin the first moment of g_1^p can be expressed in terms of the axial charge matrix elements according to (see Eqn. (27)).

$$\Gamma_1^p(Q^2) = \frac{C_1^S(Q^2)}{9} a_0(Q^2) + \frac{C_1^{NS}(Q^2)}{12}\left[a_3 + \frac{1}{3}a_8\right]. \qquad (54)$$

Assuming exact $SU(3)_f$ symmetry the flavour singlet axial charge $a_0(Q^2) = a_u + a_d + a_s$ can be calculated from the experimentally determined first moment Γ_1^p and from the relations $a_3 = g_A/g_V = F + D$ and $a_8 = 3F - D$, where F and D are the $SU(3)_f$ coupling constants calculated from neutron and hyperon β-decays to be $g_A/g_V = F + D = 1.2601 \pm 0.0025$ [24] and $F/D = 0.575 \pm 0.016$ [25]. The coefficient functions C_1^S and C_1^{NS} are available to 3rd order in α_s [18].

Using the relations given in Eqn. (29) the individual axial quark charges $a_u = \Delta u$, $a_d = \Delta d$, and $a_s = \Delta s$ can be calculated. This has been done by SMC for the two low-x extrapolation approaches of determining Γ_1^p adopting the larger value of the third uncertainty from the QCD analysis (see Eqn. (50)) for both approaches. The results together with the first moment Γ_1^p are given in Table 2.

Table 2. Results for the first moment Γ_1^p and the axial quark charges at $Q_0^2 = 10\ GeV^2$ from the SMC proton data [45].

Quantity	Regge approach	QCD approach
Γ_1^p	0.142 ± 0.017	0.130 ± 0.017
a_0	0.34 ± 0.17	0.22 ± 0.17
a_u	0.84 ± 0.06	0.80 ± 0.06
a_d	-0.42 ± 0.06	-0.46 ± 0.06
a_s	-0.08 ± 0.06	-0.12 ± 0.06

As can be seen, both approaches are fully compatible within the given experimental errors which are the statistical and systematic errors combined. The singlet axial charge $a_0(Q^2)$ amounts to about 0.3 in both approaches with a relatively large experimental error. There are indications for a slightly *negative* polarisation of the strange sea although compatible with zero within 2σ.

In the QPM the axial coupling $a_0(Q^2)$ is identified with $\Delta\Sigma$, the quark spin contribution to the nucleon spin. In QCD the $U(1)$ anomaly leads to a gluon contribution to $a_0(Q^2)$ which makes $\Delta\Sigma$ scheme dependent. In the Adler–Bardeen scheme the decomposition of $a_0(Q^2)$ into $\Delta\Sigma$ and Δg is given in Eqn. (35) with $\Delta\Sigma$ being independent of Q^2. The determination of $\Delta\Sigma$ and the various Δq_i from the measured a_0 and a_i requires an input value for Δg. The allowed values for $\Delta\Sigma$ and the Δq_i at $Q_0^2 = 5\ GeV^2$ are shown in Fig. 15 as function of Δg. It can be

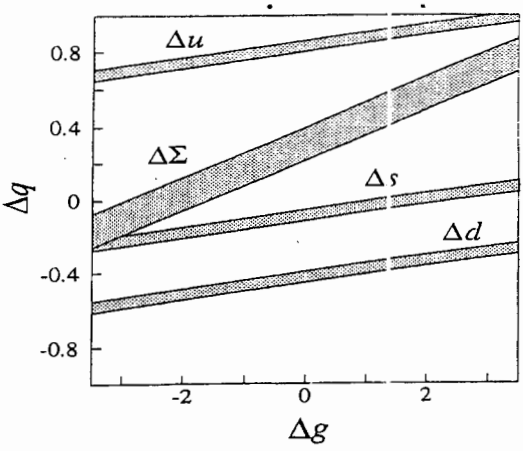

Figure 15: Quark spin contributions to the proton spin as a function of the gluon contribution at $Q_0^2 = 5\ GeV^2$ in the Adler–Bardeen scheme. The figure has been taken from [5].

seen that a value of $\Delta g(Q_0^2)$ as high as 2 would allow $\Delta\Sigma$ to be ~ 0.57, a value consistent with the constituent quark spin fraction in the nucleon suggested by the QPM, and $\Delta s \sim 0$, the value assumed by Ellis and Jaffe in deriving their sum rule [23]. In other words, a restoration of the expectations from QPM appears possible but would require a rather high value of Δg. So only a direct measurement of Δg would clarify the situation while a measurement of Δs would already help to pin down the range for Δg.

4 Conclusions

From the analysis of inclusive data on polarised DIS the following conclusions can be drawn:

- The present data are accurate enough to allow NLO QCD analyses of the scaling violation of the spin–dependent structure functions. These NLO analyses provide another successful test of QCD.
- The Bjorken sum rule is found to be confirmed within 1σ, although this presently only represents an accuracy of about 10%.
- The Ellis-Jaffe sum rule is violated by more than 2σ. This is not really surprising since its theoretical prediction is connected with the assumption of $\Delta s = 0$. The data rather indicate a slightly *negative* total polarisation of the strange sea. A value of $\Delta s = 0$ would require a value of Δg as high as 2 to be consistent with the data.
- From the NLO analyses there is evidence for a *positive* total gluon polarisation in the nucleon. The presently possible range of the gluon polarisation turned out to be large enough to allow $\Delta\Sigma$ to be consistent with the constituent quark spin fraction suggested by the QPM and Δs to be consistent with zero. Hence, direct measurements of the gluon polarisation are badly needed to resolve the situation.
- The conclusions from the NLO analyses are sensitive to the low–x extrapolation used. The values for the singlet axial charge of the nucleon a_0 extracted from the different analyses range between about 0.3 and compatible with zero. The situation can only be clarified by dedicated measurements in the low–x region which at the same time would increase our knowlegde about the gluon polarisation significantly.

5 Outlook

There are several implications of the NLO QCD analyses which are to be probed experimentally:

- Measure g_1^p in the region $x \leq 10^{-3}$, predicted to be *negative*, to verify its behaviour driven by the *positive* gluon contribution. The only possibility to do this is with a polarised proton beam in HERA which may happen, if feasible, beyond the year 2005.

- Measure the polarisation of the sea, in particular $\Delta s(x)$. This would allow to draw conclusions on Δg according to the dependency shown in Fig. 15. The measurement of semi-inclusive spin–dependent deep inelastic scattering allows a decomposition of the different components of the quark spin. There are proposals to extract information on the strange sea polarisation [62, 63] which will be pursued by the HERMES experiment beginning 1998.

- Measure the polarisation of the gluon directly. Several experimental efforts are launched to measure spin–dependent charm production which should probe the gluons via the photon-gluon fusion process. A summary of approved projects and proposals presently in discussion is given in Table 3.

Table 3. Summary of possible future initiatives to directly probe the gluon spin.

experiment	status	x_g range	$\delta(\Delta g/g)$	ref.
HERMES	1998	~ 0.3	$\sim 0.4/year$	[64]
STAR/PHENIX	~ 2000	~ 0.05–0.3	~ 0.01–0.3	[65]
COMPASS	~ 2000	~ 0.15	~ 0.1	[66]
E156	deferred	~ 0.1–0.5	~ 0.02	[67]
HERA–$\vec{e}\vec{p}$	pre-proposal stage	~ 0.02–0.2	~ 0.1	[68]
HERA–$\vec{N}$	pre-proposal stage	~ 0.01–0.4	~ 0.1	[69]
APOLLON	deferred	~ 0.4	~ 0.1	[70]

An upgrade of the HERMES spectrometer is under way to enhance charm detection which could provide first direct information on the sign of the gluon polarisation by about the year 2000. The planned experiments at CERN (COMPASS at the SPS muon beam) and BNL (STAR and PHENIX at RHIC) will provide significantly more precise information in the early years of the next decade.

Acknowledgements: I am grateful to R. Milner and A. Brüll for their support during the preparation of this review. I derived much benefit from the comprehensive presentation of the field by the SCM collaboration. I would like to thank W.-D. Nowak for stimulating discussions and the careful reading of the manuscript.

References

[1] R.L. Jaffe and A. Manohar, Nucl. Phys. **B337** (1990) 509.

[2] J. Ashman et al. (EMC), Phys. Lett. **B206** (1988) 364; J. Ashman et al. (EMC), Nucl. Phys. **B328** (1989) 1.

[3] X. Ji, Phys. Rev. Lett. **78** (1997) 610.

[4] G.K. Mallot, Proceedings of the 12th International Symposium on High-Energy Spin Physics, September 10-14, 1996, page 44.

[5] D. Adams et al. (SMC), Phys. Rev. **D56** (1997) 5330.

[6] T. Pussieux and R. Windmolders, Proc. of the Symposium on the Internal Spin Structure of the Nucleon, Yale Univ., January 5-6, 1994, World Scientific, Singapore, 1995, page 212.

[7] R.L. Jaffe, Comments Nucl. Phys. **19** (1990) 239.

[8] M.G. Doncel and E. de Rafael, Nuovo Ciment **4A** (1971) 363; P. Gnädig and F. Niedermayer, Nucl. Phys. **B55** (1973) 612.

[9] G. Altarelli, Phys. Rep. **81** (1982) 1.

[10] V.N. Gribov and L.N. Lipatov, Sov. J. Nucl. Phys. **15** (1972) 438 and 675.

[11] Y.L. Dokshitzer, Sov. Phys. JETP **46** (1977) 461.

[12] G. Altarelli and G. Parisi, Nucl. Phys. **B126** (1977) 298.

[13] E.B. Zijlstra and W.L. van Neerven, Nucl. Phys. **B417** (1994) 61.

[14] R. Mertig and W.L. van Neerven, Z. Phys. **C70** (1996) 637.

[15] W. Vogelsang, Phys. Rev. **D54** (1996) 2023.

[16] R.D. Ball, S. Forte, G. Ridolfi, Phys. Lett. **B378** (1996) 255.

[17] J. Kodaira et al., Phys. Rev. **D20** (1979) 627; J. Kodaira et al., Nucl. Phys. **B159** (1979) 99.

[18] S.A. Larin, Phys. Lett. **B334** (1994) 192.

[19] R.L. Jaffe and X. Ji, Nucl. Phys. **B 375** (1992) 527.

[20] J.D. Bjorken, Phys. Rev. **148** (1966) 1467; ibid. **D1** (1970) 1376.

[21] S.A. Larin, F.V. Tkachev, and J.A.M. Vermaseren, Phys. Rev. Lett. **66** (1991) 862; S.A. Larin and J.A.M. Vermaseren, Phys. Lett. **B259** (1991) 345.

[22] A.L. Kataev and V. Starshenko, Mod. Phys. Lett. **A10** (1995) 235; Preprint CERN/TH 94-7190 (Geneva, May 1994), hep-ph/9405294.

[23] J. Ellis and R.L. Jaffe, Phys. Rev. **D9** (1974) 1444; ibid. **D10** (1974) 1669.

[24] Particle Data Group, R.M. Barnett et al., Phys. Rev. **D54** (1996) 1.

[25] F.E. Close and R.G. Roberts, Phys. Lett. **B316** (1993) 165.

[26] A.L. Kataev, Phys. Rev. **D50** (1994) R5469.

[27] G. Altarelli and G.G. Ross, Phys. Lett. **B212** (1988) 391.

[28] A.V. Efremov and O.V. Teryaev, JINR Reprint E2-88-287, Dubna (1988).

[29] R.D. Carlitz, J.C. Collins, and A.H. Mueller, Phys. Lett. **B214** (1988) 229.

[30] H.Y. Cheng, Int. J. Mod. Phys. **A11** (1996) 5109.

[31] S. Adler and W. Bardeen, Phys. Rev. **182** (1969) 1517.

[32] X. Ji et al., Phys. Rev. Lett. **76** (1996) 740.

[33] M. Anselmino, A.V. Efremov, and E. Leader, Phys. Rep. **261** (1995).

[34] S. Wandzura and F. Wilczek, Phys. Lett. **B72** (1977) 195.

[35] M.J. Alguard et el. (E80), Phys. Rev. Lett. **37** (1976) 1261; ibid. **41** (1978) 70.

[36] G. Baum et al. (E130), Phys. Rev. Lett. **51** (1983) 1135.

[37] P.L. Anthony et al. (E142), Phys. Rev. Lett. **71** (1993) 959; Phys. Rev. **D54** (1996) 6620.

[38] K. Abe et al. (E143), Phys. Rev. Lett. **74** (1995) 346; ibid. **75** (1995) 25.

[39] K. Abe et al. (E154), Phys. Rev. Lett. **79** (1997) 26.

[40] A. Bruell, Proceedings of the XVIII International Symposium on Lepton-Photon Interactions, July 28 - August 1, 1997, Hamburg, Germany, to appear.

[41] B. Adeva et al. (SMC), Phys. Lett. **B302** (1993) 533.

[42] D. Adams et al. (SMC), Phys. Lett. **B329** (1994) 399, *erratum* Phys. Lett. **B339** (1994) 332; D. Adams et al. (SMC), Phys. Lett. **B336** (1994) 125.

[43] D. Adams et al. (SMC), Phys. Lett. **B357** (1995) 248.

[44] D. Adams et al. (SMC), Phys. Lett. **B396** (1997) 338.

[45] B. Adeva et al. (SMC), submitted to Phys. Lett. **B**, CERN-PPE/97-118.

[46] K. Ackerstaff et al. (HERMES), Phys. Lett. **B404** (1997) 383.

[47] R.G. Milner, Proceedings of the 5th International Workshop on Deep Inelastic Scattering and QCD, April 14-18, 1997, Chicago, USA, page 91.

[48] I.V. Akushevich and N.M. Shumeiko, J. Phys. **G**: Nucl. Part. Phys. **20** (1994) 513.

[49] J.L. Friar et al., Phys. Rev. **C42** (1990) 2310.

[50] C. Ciofi degli Atti et al., Phys. Rev **C48** (1993) R968.

[51] M. Arneodo et al. (NMC), Phys. Lett. **B364** (1995) 107.

[52] L. Whitlow et al. (SLAC), Phys. Lett. **B250** (1990) 193.

[53] M. Arneodo et al. (NMC), Nucl. Phys. **B483** (1997) 3.

[54] K. Abe et al. (E143), Phys. Lett. **B364** (1995) 61.

[55] T. Gehrmann and W.J. Stirling, Z. Phys. **C65** (1995) 461.

[56] J. Ellis and M. Karliner, Phys. Lett. **B341** (1995) 397.

[57] M. Glück, E. Reya, M. Stratmann, W. Vogelsang, Phys. Rev. **D53** (1996) 4775.

[58] T. Gehrmann and W.J. Stirling, Phys. Rev. **D53** (1996) 6100.

[59] G. Altarelli, R.D. Ball, S. Forte, G. Ridolfi, Nucl. Phys. **B496** (1997) 337.

[60] K. Abe et al. (E154), Phys. Lett **B405** (1997) 180.

[61] P.N. Burrows, talk at the "Cracow International Symposium on Radiative Corrections (CRAD 96)", hep-ph/9612007 (1996).

[62] St. Güllenstern et al., Phys. Lett. **B312** (1993) 166.

[63] J. Ellis, D. Kharzeev, A. Kotzinian, Z. Phys. **C69** (1996) 467.

[64] M. Amarian et al., HERMES Report 97-004, "The HERMES Charm Upgrade Program", January 24, 1997.

[65] G. Bunce et al., Particle World **3** (1992) 1.

[66] COMPASS proposal, CERN/SPSLC-96-14, March 1996.

[67] SLAC-PROPOSAL-E156, March 15, 1997.

[68] A. DeRoeck et al., Proceedings of the Workshop on Future Physics at HERA, 1995/96, volume 2, page 803, September 1996.

[69] V.A. Korotkov and W.-D. Nowak, Nucl. Phys. **A622** (1997) 78c.

[70] M. Amarian et al., The Apollon Collaboration: Proposal for an Experiment to Measure the Spin-Dependent J/ψ–Production using a Real Photon Beam at HERA, DESY.

Radiative Corrections to Moller Scattering of Polarized Particles

N. M. Shumeiko, J.G. Suarez
National Scientific and Education Center of Particle and High Energy Physics attached to Byelorussian State University

Abstract

Principal contributions to QED radiative effects for Moller scattering of polarized particles are investigated both on the Born level and taking into account radiative corrections (RC). Scattering on the case of longitudinal and transversal polarized targets is also considered. In a general way the expressions for differential cross section and polarization asymmetry (PA) have been defined, and respective graphics for longitudinal and transversal polarization asymmetries and also for radiative corrections to asymmetry are presented. All quantities are presented in terms of covariant variables. The ultrarelativistic approximation was applied for calculations. The results of a computer run are presented.

1 Introduction

For a wide serie of experiments in SLAC (E-142,E-143,E-154,E-155), it is neccesary to know the polarization of electron beam. For this aim a single arm Moller polarimeter is utilized. In order to extract (with desirable accuracy) beam polarization p_b we need to calculate theoretically, taking into account the experimental conditions, the quantities σ^{th} and A^{th} - theoretical meaning of cross section (CS) and polarization asymmetry. If the experimental data for polarization asymmetry (A^{meas}) and target polarization (p_t) are known, the ratio

$$A^{meas} = p_b p_t A^{th}, \tag{1}$$

allows to find the polarization of electron beam.

2 Method of Calculation

The Moller ($e^- + e^- \to e^- + e^-$) scattering CS of order $O(\alpha^3)$ can be written in the form (within the QED treatment)

$$\sigma = \sigma_o + \sigma_V + \sigma_R, \tag{2}$$

where each $\sigma_{o,V,R} \stackrel{\text{def}}{=} d\sigma_{o,V,R}/dy$, and $y \stackrel{\text{def}}{=} 1 - E'/E$, where E(E') is the energy of the initial (scattered) electron. σ_o is the Born (non radiative) contribution of order $O(\alpha^2)$. σ_V is the contribution of the diagrams with an additional virtual photon (V-contribution). It is constitued by contributions of vacuum polarization (sum over all generations of leptons and quarks), vertex renormalization and two-photon exchange diagrams. σ_R is the contribution of nonobservable (internal bremsstrahlung) photon radiation (R-contribution). σ_R can be divided into three parts: σ_R^F is finite when $k \to 0$ (k is the photon momentum), σ_H is the contribution of "hard photons", and it is also finite, and σ_S is the contribution of "soft photons". The latter contains infrared divergences. All σ_R^F, σ_H and σ_S may be calculated in a standard way (see, for example, [1]-[2]). According to the method of *ref.*[1], the infrared divergence vanishes when the infrared divergent part of σ_V (denoted as δ_V^λ , see, for example, [1]) is summed with the infrared divergent part of σ_R (denoted as δ_λ^R, see, for example, [1]).

As it is wellknown, the linear, exchangable and interfering diagrams give contribution to Moller scattering. For this reason the expression for differential cross section and polarization asymmetry are presented as a sum of three parts:

$$\frac{d\sigma}{dy} = \sum_l \frac{d\sigma_l}{dy}, \tag{3}$$

and

$$A = \sum_l A_l, \tag{4}$$

where l=l,e,i. In our calculations the differential cross section is presented as

$$\sigma = \sigma_o + \frac{\alpha}{\pi}(\delta_{vert} + \delta_{vac})\sigma_o + \sigma_{amm}^u + \sigma_{amm}^p + \frac{\alpha}{\pi}(\delta_k + \delta_{2\gamma}^u)\sigma_o^u +$$

$$\frac{\alpha}{\pi}(\delta_k + \delta_{2\gamma}^p)\sigma_o^p + \sigma_R^{F,u} + \sigma_R^{F,p} + \frac{\alpha}{\pi}(\delta_l + \delta^\lambda + \delta_s + \delta_1^H)\sigma_o + \sigma_2^{H,u} + \sigma_2^{H,p}, \tag{5}$$

where $\sigma_o = \sigma_o^u + \sigma_o^p$, and $\sigma_o^{u,p}$ are the spin-independent and spin-dependent Born contributions. δ_{vert} and δ_{vac} are the spin-independent finite factorized contributions of vertex and vacuum polarization corrections. $\sigma_{amm}^{u,p}$

are the spin-independent and spin-dependent contributions attributed to anomalous magnetic momentum. $\delta_{2\gamma}^{u,p}$ are the spin-independent and spin-dependent corrections due to two-photon exchange. δ_k can be written in a standard way. For references see [3]. $\sigma_R^{F,u,p}$ are the spin-independent and spin-dependent cotributions of infrared free part of R-contribution. δ_l, δ_s δ_1^H and δ^λ are spin-independent factorized corrections derived from the infrared divergent vertex contribution, finite "soft-photon" contribution, finite "hard-photon" contribution and the sum of infrared divergent parts in R and $\tilde{V}$ contributions (δ^λ). $\sigma_{2,u}^H$ and $\sigma_{2,p}^H$ are the spin-independent and spin-dependent corrections of infrared free part of hard-photon contribution. All contributions are defined in a standard way, (see, for example, references [1, 3]).

The longitudinal and transversal polarization asymmetries are, usually, defined as

$$A_l = \frac{\sigma^{\uparrow\uparrow} - \sigma^{\uparrow\downarrow}}{\sigma^{\uparrow\uparrow} + \sigma^{\uparrow\downarrow}}, \tag{6}$$

and

$$A_t = \frac{\sigma^{\uparrow\rightarrow} - \sigma^{\uparrow\leftarrow}}{\sigma^{\uparrow\rightarrow} + \sigma^{\uparrow\leftarrow}}, \tag{7}$$

The arrows show the polarization of the beam and the target, respectively. The corrected polarization asymmetry is presented as

$$A^{QED} = A_o(1 + \frac{\alpha}{\pi}(\delta_{2\gamma}^p - \delta_{2\gamma}^u)) + \sigma_{amm}^p - \sigma_{amm}^u + \frac{\sigma_o^u \sigma_R^p - \sigma_o^p \sigma_R^u}{(\sigma_o^u)^2} + O(\alpha^2), \tag{8}$$

where A_o is the Born asymmetry, and $A_o \stackrel{\text{def}}{=} A_{lo}$ or $A_o \stackrel{\text{def}}{=} A_{to}$. σ_{amm}^p and σ_{amm}^u are the spin-dependent and spin-independent contributions due to anomalous magnetic momentum. $(\sigma_o^u \sigma_R^p - \sigma_o^p \sigma_R^u)/(\sigma_o^u)^2$ is due to R-contribution. Where $\sigma_R^u = \sigma_R^{F,u} + \sigma_{2,u}^H$ and $\sigma_R^p = \sigma_R^{F,p} + \sigma_{2,p}^H$.

The radiative correction to asymmetry is defined as

$$\delta^{QED} = \frac{A^{QED}}{A_o} - 1. \tag{9}$$

3 Results

In this section the results of calculations of polarization asymmetry both for longitudinally and transversally polarized target and radiative corrections to asymmetry are presented. Numerical calculations have been carried out with the help of FORTRAN code created by the authors. For analytical calculations REDUCE code has been utilized. Graphics for asymmetries and radiative corrections can be seen in figures 1-4. Obtained results are presented in table 1.

y	A_{ol}	A_{ot}	A_l	A_t	$\delta_l(\%)$	$\delta_t(\%)$
.10	-.41282	.13334E-02	-.48454	.11093E-02	17.374	-16.807
.20	-.66387	.29711E-02	-.72840	.27305E-02	09.720	-08.943
.30	-.81058	.43023E-02	-.86688	.40466E-02	06.946	-05.147
.40	-.88520	.51717E-02	-.93473	.49056E-02	05.595	-05.194
.50	-.90438	.55191E-02	-.95268	.52324E-02	05.340	-05.823
.60	-.87293	.53009E-02	-.92673	.49923E-02	06.224	-05.233
.70	-.78220	.44700E-02	-.84584	.41523E-02	08.136	-07.233
.80	-.61358	.30365E-02	-.68504	.26956E-02	11.647	-11.224
.90	-.32977	.11483E-02	-.38357	.79126E-02	16.315	-31.092
.99	-.04891	.63291E-02	-.05877	.15068E-02	20.148	-338.07

Table 1: Results of calculations of Born asymmetries $A_{ol,ot}$, corrected asymmetries $A_{l,t}$ and radiative corrections to asymmetry $\delta_{l,t}$ for both longitudinally and transvesally polarized tagets correspondingly, for SLAC kinematics. E=50 Gev.

4 Conclusions

The calculation of the differential cross section and polarization asymmetry to Moller scattering will in the future allow to find beam polarization. For this aim it is neccesary to measure polarization asymmetry with high accuracy. Iteration procedure for theoretical calculation of polarization asymmetry can be improved, and that will lead to the increase of the accuracy when beam polarization is measured. As we can see, the corrections without cuts are very large (in any ocasion about 20%), although they will be considerably reduced when the experimental cuts will be taken into account. Analysis of the corrected polarization asymmetries in the case of longitudinally and transversally polarized targets show that in a wide kinematical range corrections are considerable. In this paper the results of calculations of differencial cross section and polarization asymmetry have been presented taking into account only the contribution of linear diagrams. Results, in which the contribution of exchangable and interfering diagrams are considered will be presented in the future. For a more accurate calculation of polarization asymmetry it is neccesary to utilize a Monte Carlo generator for Moller scattering, and the contribution of correction due to external radiation of beam particles within the target must be taken into account. This is an object for future investigations.

References

[1] Bardin D.Yu., Shumeiko N.M. Nucl. Phys. 1977. v.B127. p.242.
Bardin D.Yu., Shumeiko N.M. 1976. Dubna Preprint p_2-10113

[2] Bardin D.Yu., Shumeiko N.M. 1976. Dubna Preprint p_2-10114

[3] Kahane J. Phys. Rev. 1964. 135. B.975.

[4] Kukhto T.V., Shumeiko N.M., Timoshin S.I. Nucl. Phys. 1987. G.13. p.725

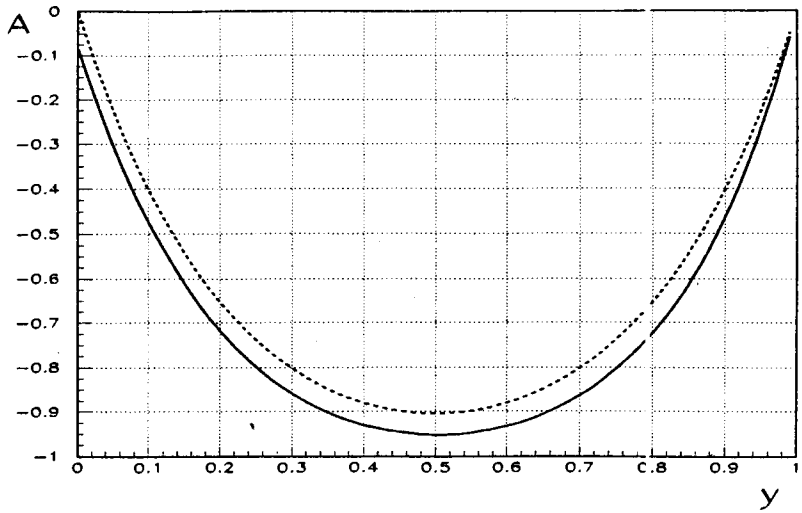

Figure 1: *y-dependence of the born asymmetry (dashed line) and corrected asymmetry (solid line) in the polarization Moller scattering for SLAC kinematics. E=50Gev.Longitudinally polarized target.*

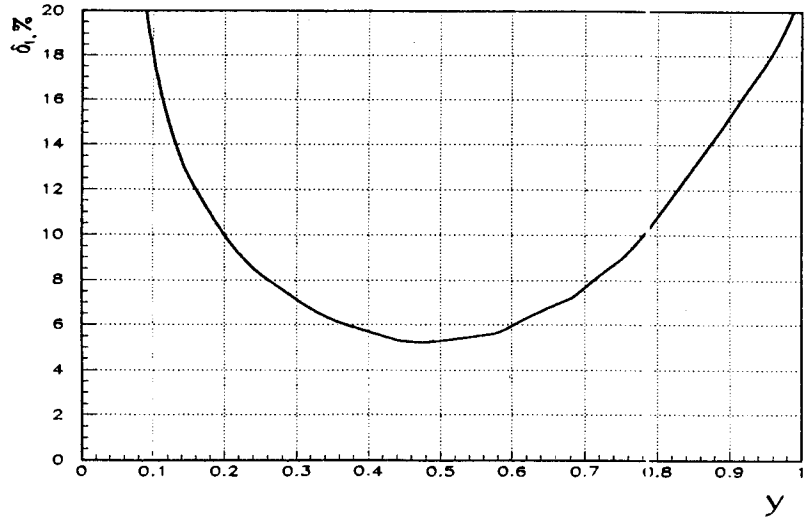

Figure 2: *The QED radiative corrections to asymmetry without experimental cuts for longitudinally polarized target.*

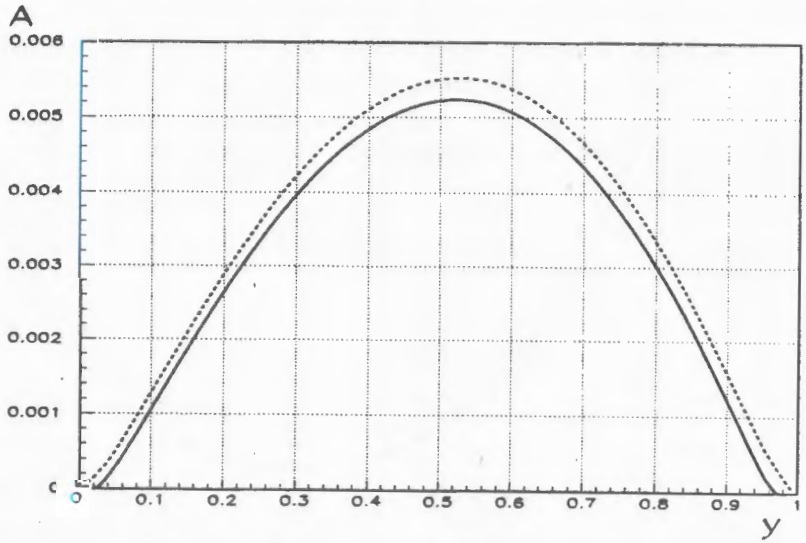

Figure 3: *y-dependence of the born asymmetry (dashed line) and corrected asymmetry (solod line) in the polarization Moller scattering for SLAC kinematics. E=50 Gev. transversally polarized target.*

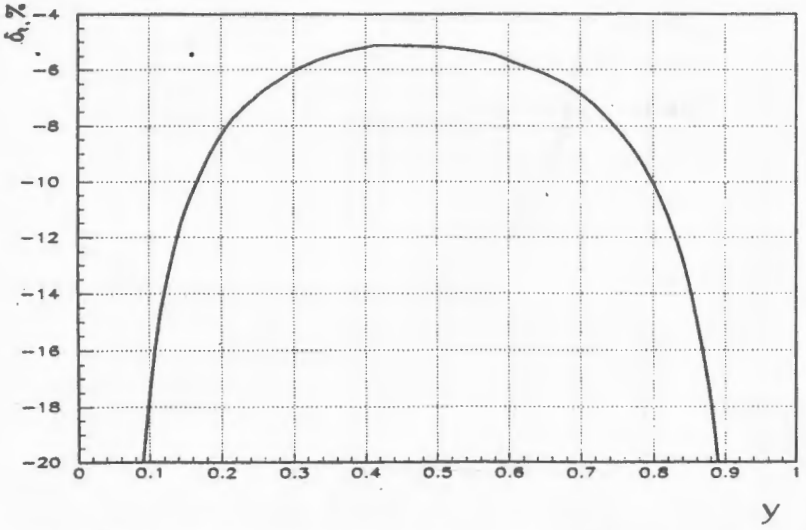

Figure 4: *The QED radiative corrections to asymmetry without experimental cuts for transversally polarized target.*

An investigation of the proton spin in deep inelastic scattering induced by charged current

S.I.Timoshin
Gomel Polytechnic Institute, Belarus

The cross sections of virtual W-boson absorbtion by polarized nucleon are calculated. The virtual W-boson-nucleon asymmetries $A_1(x)$ and $A_6(x)$ are obtained. The possibilities to extract the information about the nucleon spin structure are discussed for the polarized deep inelastic scattering (DIS) of neutrino and electrons on nucleons.

In order to study nucleon spin stucture it has been recently proposed [1] to use the processes of neutrino DIS on polarized nucleons. The analysis of the possible polarization effects was performed using a set of observable quantities. In particular several schemes for determination of quark flavors contributions to the nucleon spin were proposed.

In this paper the other approach is considered to investigate nucleon spin in reactions of DIS induced by charged current

$$\overset{(-)}{\nu} + N \to l^{(\pm)} + X, \tag{1}$$

$$l^{(\pm)} + N \to \overset{(-)}{\nu} + X. \tag{2}$$

The total cross section of virtual W-boson absorption by polarized nucleon has been calculated. The cross sections $\sigma_{1/2(3/2)}$ and $\sigma_{-1/2(-3/2)}$ (the total angular momentum of W-boson-nucleon system is $\pm 1/2$ and $\pm 3/2$ respectively) are in the scaling limit only. They are

$$\sigma_{1/2(3/2)} \sim F_1(x) - F_3(x)/2 \pm g_1(x) \mp g_6(x),$$

$$\sigma_{-1/2(-3/2)} \sim F_1(x) + F_3(x)/2 \pm g_1(x) \pm g_6(x). \tag{3}$$

With formulae (3) we can obtain two virtual W-boson-nucleon polarization asymmetries

$$A_1(x) = \frac{(\sigma_{1/2} + \sigma_{-1/2}) - (\sigma_{3/2} + \sigma_{-3/2})}{(\sigma_{1/2} + \sigma_{-1/2}) + (\sigma_{3/2} + \sigma_{-3/2})} = \frac{2xg_1(x)}{F_2(x)}, \tag{4}$$

$$A_6(x) = \frac{(\sigma_{1/2} - \sigma_{-1/2}) - (\sigma_{3/2} - \sigma_{-3/2})}{(\sigma_{1/2} - \sigma_{-1/2}) + (\sigma_{3/2} - \sigma_{-3/2})} = \frac{2xg_6(x)}{xF_3(x)} \tag{5}$$

For the process (1) the observable asymmetries $A_{\nu,\bar{\nu}}(x,y)$ [1] can be expressed through the asymmetries (4),(5)

$$A_{\nu,\bar{\nu}}(x,y) = \frac{y_1^+ A_6^{\nu,\bar{\nu}}(x) F_3^{\nu,\bar{\nu}}(x) \pm y_1^- A_1^{\nu,\bar{\nu}}(x) F_2^{\nu,\bar{\nu}}(x)}{y_1^+ F_2^{\nu,\bar{\nu}}(x) \pm y_1^- F_3^{\nu,\bar{\nu}}(x)}, \tag{6}$$

where x and y are the usual scaling variables, $y_1 = 1 - y$, $y_1^{\pm} = 1 \pm y_1^2$.

Within quark parton model (QPM) $g_{1,6}^{\nu,\bar{\nu}}(x)$ are obtained in the form

$$g_{1,6}^{\nu,\bar{\nu}}(x) = \sum_{q_i} \Delta q_i(x) \pm \sum_{\bar{q}_i} \Delta \bar{q}_i(x). \tag{7}$$

Here $q_i = (u, c, t)d, s, b$ and $\bar{q}_i = (\bar{d}, \bar{s}, \bar{b})\bar{u}, \bar{c}, \bar{t}$ in the case of (anti)neutrino scattering.

Consider the deutron polarized targed. Then

$$g_1^{\nu d}(x) = g_1^{\bar{\nu} d}(x) = 1/2[\Delta q(x) + \Delta \bar{q}(x)](1 - 3/2\omega_D) \tag{8}$$

and for the processes of leptoproduction we have

$$18/5 g_1^d(x) = [1/2(\Delta q(x) + \Delta \bar{q}(x)) - 3/5 \Delta s(x)](1 - 3/2\omega_D), \tag{9}$$

where $\Delta q(x) = \Delta u(x) + \Delta d(x) + \Delta s(x)$, $\omega_D = 0.05$ is the D-wave state probability of the deuteron. Comparing (8) and (9), we obtain approximate equality

$$g_1^d(x) \approx 5/18 g_1^{\bar{\nu} d}(x), \tag{10}$$

and in a similar way to unpolarized case [2]

$$F_2^d(x) \approx 5/18 F_2^{\nu d}(x). \tag{11}$$

Therefore using (4), (10) and (11), we come to the conclusion that

$$A_1^{(-)^{\nu d}}(x) \approx A_1^d(x), \tag{12}$$

where $A_1^d(x)$ is virtual asymmetry of leptoproduction.

Now consider the other spin-dependent structure functions (SSF) $g_6(x)$. From (7) we obtain

$$g_6^{\nu d, \bar{\nu} d} = 1/2[\Delta q(x) - \Delta \bar{q}(x) \pm (\Delta s(x) + \Delta \bar{s}(x))](1 - 3/2\omega_D) \tag{13}$$

$$g_6^{\nu d} + g_6^{\bar{\nu} d} = [\Delta q(x) - \Delta \bar{q}(x)](1 - 3/2\omega_D) \equiv [\Delta q_{val}(x)(1 - 3/2\omega_D)$$

$$g_6^{\nu d} - g_6^{\bar{\nu} d} = [\Delta s(x) - \Delta \bar{s}(x)](1 - 3/2\omega_D). \tag{14}$$

When expressions (14) are integrated over x, the contributions of valence (Δq_{val}) and strange quarks to the nucleon spin are given by

$$\Delta q_{val} = (\Gamma_6^{\nu d} + \Gamma_6^{\bar{\nu} d}) \frac{1}{1 - 3/2\omega_D}, \tag{15}$$

$$\Delta s + \Delta \bar{s} = 1/2(\Gamma_6^{\nu d} - \Gamma_6^{\bar{\nu} d}) \frac{1}{1 - 3/2\omega_D}, \tag{16}$$

where $\Gamma_j = \int_0^1 g_j(x)dx$.

The individual contributions of u and d quarks can be obtained if some additional measurable quantity is used, e.g. $a_3 = g_A/g_V = F + D = 1.2573$ [3]. Within QPM

$$a_3 = (\Delta u + \Delta \bar{u})(\Delta d + \Delta \bar{d}). \tag{17}$$

Since $\Delta q + \Delta \bar{q} = 36/5 \frac{2\Gamma_1^d}{1 - 3/2\omega_D}$, then from (16),(17) we have

$$\Delta u + \Delta \bar{u} = 1/2[(36/5\Gamma_1^d - \Gamma_6^{\nu d} + \Gamma_6^{\bar{\nu} d})(1 - 3/2\omega_D) + a_3],$$

$$\Delta d + \Delta \bar{d} = 1/2[(36/5\Gamma_1^d - \Gamma_6^{\nu d} + \Gamma_6^{\bar{\nu} d})(1 - 3/2\omega_D) - a_3]. \tag{18}$$

The SSF $g_6^{\nu d, \bar{\nu} d}(x)$ can be found using (5),(6) and taking into account (12).

Now let us discuss briefly the process (2). All results obtained above for the reactions (1) are the same as for the process (2) with the substitution

$$F_i^p, g_i^p \to F_i^{e^-} g_i^{e^-}; \quad F_i^\nu, g_i^\nu \to F_i^{e^+} g_i^{e^+}.$$

Then the asymmetries of processes (1) and (2) are correlated

$$A_{\nu,p}(x,y) = A_{e^+,e^-}(x,y); \quad A_{1,6}^{\nu,p}(x) = A_{1,6}^{e^+,e^-}(x).$$

Thus, in this paper the spin effects are considered in polarization DIS (1) and (2) induced by charged current. The cross section of virtual W-boson absorption by polarized nucleon is calculated. The asymmetries $A_1(x)$ and $A_6(x)$ are obtained. The way to estimate the contributions of valence and individual quarks to the proton spin is suggested.

References

1. Kuzhir P.P.,Timoshin S.I., Shumeiko N.M. Proc. XV Workshop on High Energy Phys. and Field Theory. Protvino, 1992.P.231; Sov.J.Nucl.Phys.1995.V.58.p.507.

2. Bilenky S.M. Introduction to diagrams of Feynman and physics of electroweak interactions.1990.

3. Particle Data Group: Montanet L. et al. Phys.Rev. 1994. V. D50. P.1173.

One-loop electroweak correction to polarization deep inelastic $\overset{(-)}{\nu}$ N–scattering

V.A. Zykunov
Gomel Polytechnic Institute, Belarus

The total electroweak radiative correction (EWC) of $O(\alpha^3)$ to the cross sections of the inclusive processes of deep inelastic scattering (DIS) of (anti)neutrino on the longitudinally and transversely polarized nucleons with the weak charge current was calculated. The on-shell renormalization scheme and Feynman gauge are used. The numerical calculations of the longitudinal polarization asymmetries taking into consideration electroweak corrections have been made.

1. The intensive experimental and theoretical investigations of spin effects in high-energy physics have been carried out in last decade. First of all it concerns to the problem of proton spin, which has appeared after EMC experiment [1]. Notwithstanding the impressive successes in the solution of this problem in experiments at CERN and SLAC [2] by the investigation of the traditional processes of lN-DIS ($l = e, \mu$) the possibilities of another deep inelastic reactions, e.g. $\overset{(-)}{\nu_\mu}$ N-DIS [3], are studied actively.

Although there are the technical difficulties in the neutrino experiments with the polarized targets, these experiments can be realized in the near future. Therefore the serious basis for the expedience of the experimental investigation of the neutrino reactions in spin physics is necessary.

For this aim in [3] the neutrino DIS on the polarized targets in the Born approximation were considered. The several schemes for the extraction of the contributions of the quarks' flavors in the nucleon spin were suggested with the help of the measurable observables (the cross sections and the asymmetries).

Naturally, the next step is the calculation and the investigation of the influence of the radiative effects on the measurable observables in polarized $\overset{(-)}{\nu}$ N-DIS. However in [4] only the one-loop electroweak correction to these processes (induced by W-boson exchange) was calculated in the unitary gauge within the renormalization scheme on mass shell.

In the present paper the total EWC (the one-loop virtual correction and the contribution of the bremsstrahlung) to the cross sections of the inclusive processes of (anti)neutrino on the polarized nucleons DIS with the weak charge current was calculated. The calculations were done within the renormalization scheme on mass shell but in Feynman gauge, since, in the first place, the unitary gauge has some defects [5] and, secondly, it's of

great interest to compare the results of the calculations of EWC in the various approaches.

2. The cross sections of the processes

$$\overset{(-)}{\nu_l}(k_1,0)+N(p,m_N)\to l^{(+)}(k_2,m_l)+X \qquad (l=\mu,e) \tag{1}$$

are given in order $O(\alpha^3)$ within the quark parton model by the cross sections of the subprocesses of (anti)neutrino scattering on the polarized (anti)quark

$$\overset{(-)}{\nu_l}(k_1,0)+\overset{(-)}{q_j}(p_1,m_j)\to l^{(+)}(k_2,m_l)+\overset{(-)}{q_{j'}}(p_2,m_{j'}) \tag{2}$$

multiplied by a parton densities. In the brackets 4-momenta and masses of the particles are given.

The cross sections (1) are written traditionally in the form

$$\left.\frac{d^2\sigma}{dxdy}\right|_{\overset{(-)}{\nu}}=\left.\frac{d^2\sigma}{dxdy}\right|^{a}_{\overset{(-)}{\nu}}+\left.\frac{d^2\sigma}{dxdy}\right|^{p}_{\overset{(-)}{\nu}}, \tag{3}$$

where x,y are the scaling variables and $Y=-q^2=-(k_1-k_2)^2$. Here the indexes 'a' and 'p' refer to the scattering of (anti)neutrino on the unpolarized nucleons and to the polarization part of the cross section (3) for the case of longitudinally ($p=\|$) or transversely ($p=\perp$) polarized nucleons.

They were obtained in order $O(\alpha^3)$ in the following way

$$\left.\frac{d^2\sigma}{dxdy}\right|^{m}_{\overset{(-)}{\nu}}=\left.\frac{d^2\sigma^B}{dxdy}\right|^{m}_{\overset{(-)}{\nu}}+\left.\frac{d^2\sigma^H_R}{dxdy}\right|^{m}_{\overset{(-)}{\nu}}+\left.\frac{d^2\sigma^F_R}{dxdy}\right|^{m}_{\overset{(-)}{\nu}}, \tag{4}$$

where $m=a,p$.

The first term of (4) factorizes into virtual one-loop correction δ_{1-loop} and the corrections relating to the bremsstrahlung of the soft photons δ^{λ}_R and δ_{soft} multiplying the Born cross section. The term δ^{λ}_R has infrared divergence, which was extracted with using of the covariant method [6] and was canceled in the sum of the corrections δ_{1-loop} and δ^{λ}_R:

$$\delta_{1-loop}+\delta^{\lambda}_R=\delta^{F}_{1-loop}=\delta_{1-loop}(\lambda^2\to z^2),$$

where $z=\frac{S_N x_1 y}{m_{j'}}$, $S_N=2pk_1$, $x_1=1-x$.

The first term in (4) has the form

$$\left.\frac{d^2\sigma^B}{dxdy}\right|^{m}_{\overset{(-)}{\nu}}=\frac{\pi\alpha^2}{2s^4_w S_0 M^4_W}\left\{\sum_{d(u)}(B^m_{\overset{(-)}{\nu}q})_0 F^m(x)(1+\delta^F_{1-loop}+\delta_{soft})+\right.$$

$$\left.+\sum_{\overline{u}(\overline{d})}(B^m_{\overset{(-)}{\nu}\overline{q}})_0 F^m(x)(1+\delta^F_{1-loop}+\delta_{soft})\right\}, \tag{5}$$

where $s_w=\sqrt{1-c^2_w}$ is the sine of the weak mixing angle, $c_w=M_W/M_Z$, $F^{a/p}(z)=f^+(z)+/-f^-(z)$ are the parton densities,

$$B^a_{\nu q} = B^a_{\bar\nu\bar q} = S^2, B^a_{\nu\bar q} = B^a_{\bar\nu q} = X^2,$$

$$B^{\parallel}_{\nu q} = -B^{\parallel}_{\bar\nu\bar q} = p^{\parallel}_N S^2, B^{\parallel}_{\bar\nu q} = -B^{\parallel}_{\nu\bar q} = p^{\parallel}_N X^2,$$

$$B^{\perp}_{\nu q} = -B^{\perp}_{\bar\nu\bar q} = p^{\perp}_N \frac{m_N}{S_N\sqrt{y_1 Y}}(-m_l^2 S^2),$$

$$B^{\perp}_{\bar\nu q} = -B^{\perp}_{\nu\bar q} = p^{\perp}_N \frac{m_N}{S_N\sqrt{y_1 Y}} 2X^2 Y,$$

p^p_N is the degree of the nucleon polarization, $y_1 = 1 - y$, $S = \xi S_N$, $X = \xi S_N y_1$; M_W, M_Z are the masses of the heavy gauge bosons, ξ is the parameter of the quark parton model. The index "0" means the replacement $\xi \to x$.

The corrections δ_{1-loop} and δ_{soft} from (5) are given in [8]. They were produced by the results of the papers [5,7] and the natural approximations $S, X, Y, M_W^2, M'^2_W \gg m_f^2, m_{f'}^2, m_l^2$ $(f, f' = \overset{(-)}{u}, \overset{(-)}{d}, \overset{(-)}{s}, \overset{(-)}{c}), Y \ll M_W^2$.

The second and the third terms in (4) are the contributions of the hard bremsstrahlung and are obtained in the form

$$\left.\frac{d^2\sigma^m_R}{dxdy}\right|^m_{\overset{(-)}{\nu}} = -\frac{\alpha^3}{2s_w^4 M_W^4}\int_x^1 \frac{d\xi}{\xi - x}\Big\{\sum_{d(u)} J(Y,v)[\frac{B^m_{\overset{(-)}{\nu}q}}{S}F^m(\xi) - \frac{(B^m_{\overset{(-)}{\nu}q})_0}{S_0}F^m(x)]$$

$$+\sum_{\bar u(\bar d)} J(Y,v)[\frac{B^m_{\overset{(-)}{\nu}\bar q}}{S}F^m(\xi) - \frac{(B^m_{\overset{(-)}{\nu}\bar q})_0}{S_0}F^m(x)]\Big\}, \qquad (6)$$

where

$$J(Y,v) = Q_l^2 - c_q Q_l Q_f L_X + c_q Q_l Q_{f'}\frac{S}{X+Y}L_A$$

$$+Q_f^2 - Q_f Q_{f'}\frac{Y}{S_X}L_u + Q^2_{f'}\frac{m^2_{f'}}{\tau},$$

$$L_X = ln\frac{X^2}{m_l^2 m_f^2}, L_A = ln\frac{(X+Y)^2}{m_l^2\tau}, L_u = ln\frac{S_X^2}{m_f^2\tau},$$

$$\tau = v + m^2_{f'}, v = S - X - Y + m_f^2 - m^2_{f'},$$

Q_j is the charge of the fermion j in the proton's charge units, $c_q = +1(-1)$ for the $\nu q, \overline{\nu q}$ $(\nu\bar q, \overline{\nu} q)$-scattering,

$$\left.\frac{d^2\sigma^F_R}{dxdy}\right|^m_{\overset{(-)}{\nu}} = -\frac{\alpha^3 y}{8s_w^4 M_W^4}\int_x^1 \frac{d\xi}{\xi}\Big\{\sum_{d(u)}[V^{\overset{(-)}{\nu}q}_{lep} - Q_f V^{\overset{(-)}{\nu}q}_{int} + Q_f^2 V^{\overset{(-)}{\nu}q}_{qua}]^m F^m(\xi)$$

$$+\sum_{\bar u(\bar d)}[V^{\overset{(-)}{\nu}\bar q}_{lep} - Q_f V^{\overset{(-)}{\nu}\bar q}_{int} + Q_f^2 V^{\overset{(-)}{\nu}\bar q}_{qua}]^m F^m(\xi)\Big\}. \qquad (7)$$

The contribution of the hard bremsstrahlung was obtained by the integration over the whole phase space of an unobserved real photon that was made analytically. The expressions for the quantities V are given in [8].

3. The numerical calculations of the asymmetries $A_{\pm}(x,y)$ and $A_{\nu,p}(x,y)$ from [3] have been made for the estimation of the EWC influence to the measurable observables in the processes (1) for $\overset{(-)}{\nu}_{\mu}$ N-DIS on the deuteron target at the energy of (anti)neutrino $E = 100\ GeV$. The parton densities [9] are used.

The influence of the total correction to the asymmetries A_+ and A_ν does not practically depend on x and y and the difference $\Delta A = A - A^{born}$ does not exceed -1%. The dependence of value $|\Delta A_+|$ on y is considerable. So, it reaches 10% at $x \leq 0.6$ and $y = 0.01$, and with the increase of y it vanishes. At large x this correction does not differ from zero over the full range of y. The value $|\Delta A_p|$ is small at $y \to 0$ over the full range of x, and with the increase of y reaches 2.5% at $x = 0.1$ and 26% at $x = 0.9$.

Thus, we have obtained formulae for the total one-loop EWC to the inclusive processes (1) in quark parton model. The analysis of the results of the numerical calculations of EWC to the polarized asymmetries shows that in the certain part of the kinematical range these corrections for some asymmetries may reach a few tens of per cents.

References

1. The EMC Collaboration. Ashman J. et.al.// Nucl.Phys. 1989. V.B328. P.1

2. Adams D et al. // Phys.Lett. 1994. V.B329. P.399.
Abe K et al. // Phys.Rev.Lett. 1995. V.74. P.346.

3. Kuzhir P., Timoshin S., Shumeiko N.// Sov.J.Nucl.Phys. 1995. V.58. P.507.

4. Kuzhir P., Shumeiko N. // The talk presented at the Xth Workshop on High Energy Physics and Quant. Field Theory. Zvenigorod, 1995.

5. Bohm M., Spiesberger H.// Nucl.Phys. 1987. V.B294. P.1081.

6. Bardin D., Shumeiko N.// Nucl.Phys. 1977. V.B127. P.242.

7. Bohm M., Spiesberger H.// Nucl.Phys. 1988. V.B304. P.749.
Bohm M., Spiesberger H., Hollik W.// Forschr.Phys. 1986. V.34. P.687.

8. Shumeiko N., Timoshin S., Zykunov V. // Sov.J.Nucl.Phys. 1997. V.60. P.1415.

9. Bourrely C., Soffer J.// CPT-95 /P.3160. 1995. 52pp.

Phenomenological Aspects of Weak-Scale Supersymmetry

Alfred Bartl

Vienna University

- Introduction
- Motivation for supersymmetry
- Minimal SUSY Model
- Breaking of SUSY
- Search for SUSY particles

e^+e^- collisions
$p\bar{p}$ collisions
ep collisions

We concentrate on phenomenological aspects of SUSY
H. Eberl, S. Kraml, T. Gajdosik, W. Majerotto, W. Porod, A. Bartl

"Minimal" **SUSY extension of Standard Model (MSSM)**

Spin 0	Spin $\frac{1}{2}$	Spin 1
Sneutrino $\tilde{\nu}_l$	Neutrino ν_l	
Slepton $\tilde{l}_{L,R}$	Lepton l	
Squark $\tilde{q}_{L,R}$	Quark q	
	Photino $\tilde{\gamma}$	Photon γ
	Wino $\tilde{W}^{\pm}$	IVB: $W^{\pm}$
	Zino $\tilde{Z}^0$	Z^0
	Gluino $\tilde{g}$	Gluon g
Higgs H_1	Higgsino $\tilde{H}_1$	
Higgs H_2	Higgsino $\tilde{H}_2$	
$H^{\pm}, H_1^0, H_2^0, H_3^0$	$\tilde{H}^{\pm}, \tilde{H}^0_{1,2}$	
H, h, A	$\tilde{W}^{\pm}\&\tilde{H}^{\pm} \rightarrow \chi_i^{\pm}, i = 1,2$ charginos	
	$\tilde{\gamma}, \tilde{Z}^0\&\tilde{H}^0_{1,2} \rightarrow \chi_i^0, i = 1...4$ neutralinos	

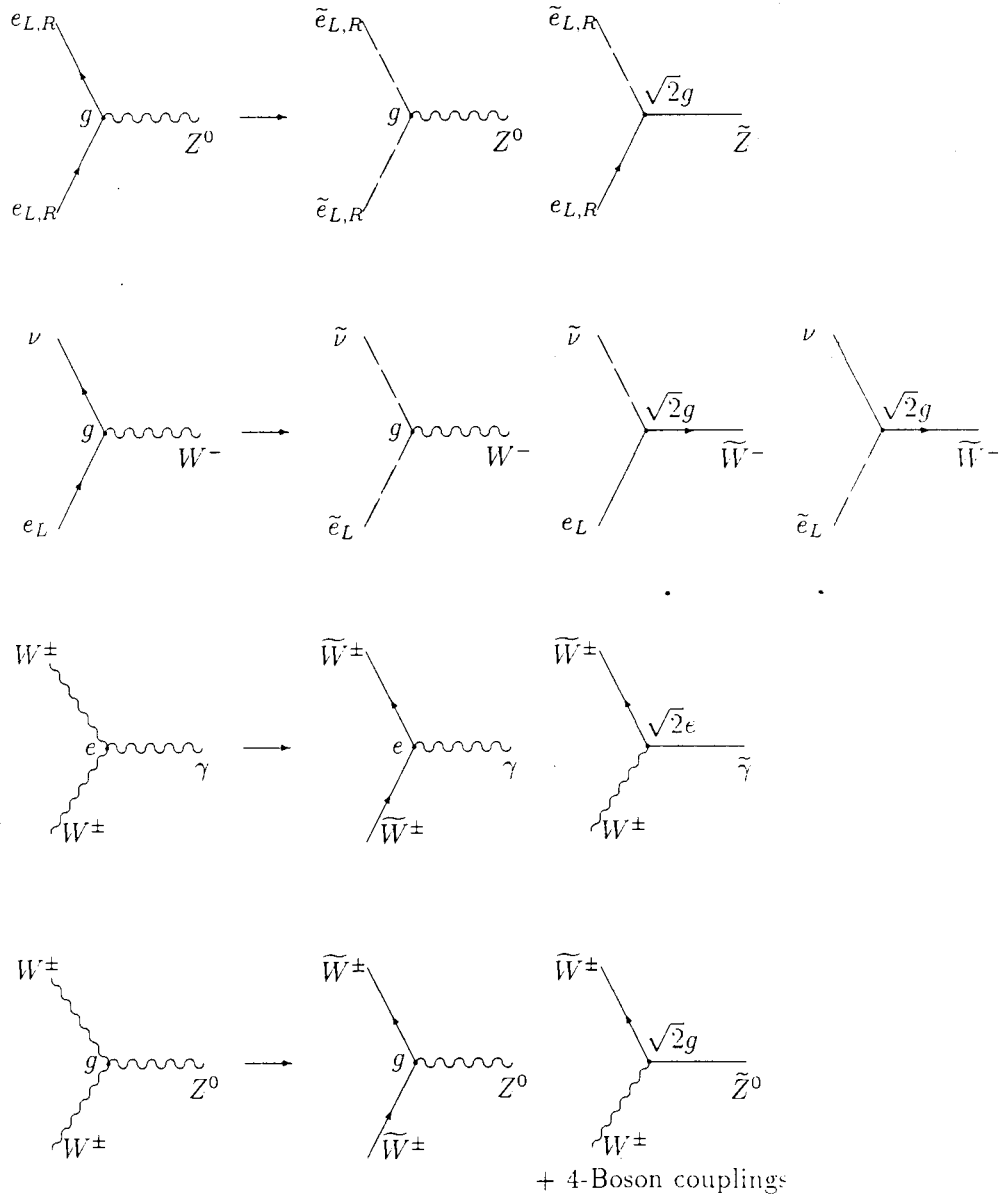

Figure 1: **Gauge interactions**

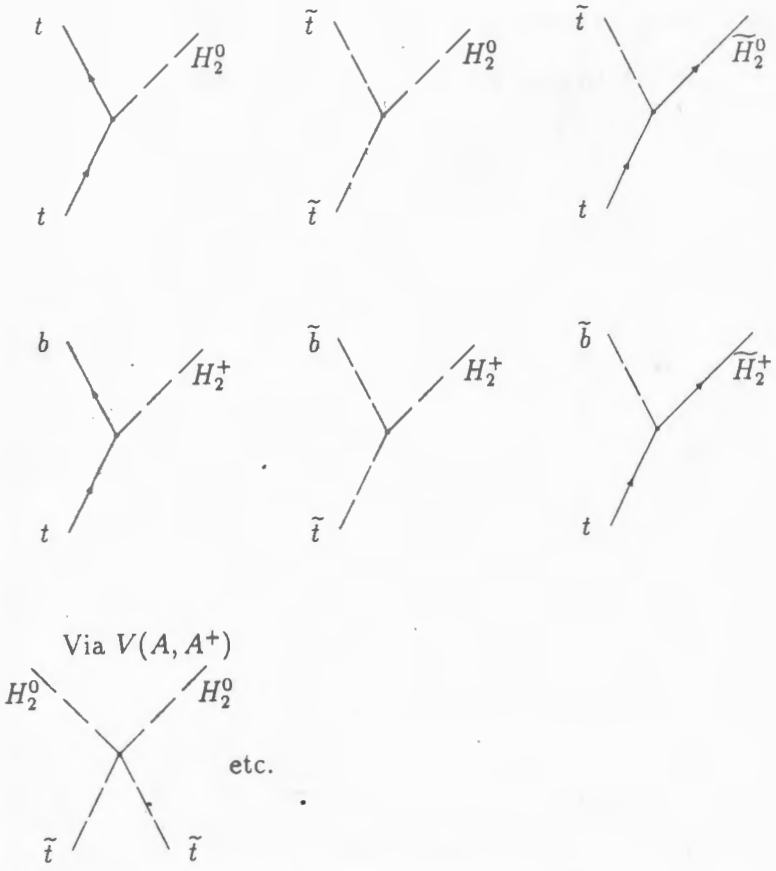

Figure 2: **Yukawa Interactions from Superpotential**

Matter field $\rightarrow$ chiral superfield
$\psi \rightarrow \Phi \sim (A, \psi_\alpha, F)$, where A – scalar, ψ_α – Weyl, F – auxiliary.

Higgs scalar $\rightarrow$ chiral superfield

Vector field $\rightarrow$ Vector superfield $V^\mu \rightarrow V \sim (V^\mu, \lambda, D)$, where V^μ – vector, λ – Weyl, D – auxiliary.

Gauge interaction of one chiral superfield with gauge vector superfield:

$$L_g = -\frac{1}{4} F^a_{\mu\nu} F_{a\mu\nu} + i\bar{\lambda}^a \bar{\sigma}^\mu D_\mu \lambda^a + (D_\mu A)^+ (D^\mu A) + i\bar{\chi}\bar{\sigma}^\mu D_\mu \chi$$

$$+ig\sqrt{2}\left(A^{+}\lambda^{a}T^{a}\chi - \bar{\chi}\bar{\lambda}^{a}T^{a}A\right) - V(A, A^{+}).$$

$$F^{a}_{\mu\nu} = \partial_{\mu}V^{a}_{\nu} - \partial_{\nu}V^{a}_{\mu} + gf^{abc}V^{b}_{\mu}V^{c}_{\nu}$$

$$D_{\mu}\lambda^{a} = \partial_{\mu}\lambda^{a} + gf^{abc}V^{b}_{\mu}\lambda^{c}$$

$$D_{\mu}\chi = \partial_{\mu}\chi - igV^{a}_{\mu}T^{a}\chi$$

Open questions in Standatd Model

Origin of electroweak symmetry breaking

Scalar Higgs field

Origin of masses ($M_W = 80GeV$)

Unification of gauge couplings ($M_{GUT} \approx 10^{16}GeV$)

GUT $\rightarrow$ how to stabilize mass of Higgs? fine-tuning problem

how to relate highly different scales?

$$M_{GUT} \sim M_W$$

hierarchy problem

SUSY solves fine-turning problem and hierarchy problem in GUT

If scalar Higgs field is elementary, then SUSY may be only consistent framework in a GUT

Radiative symmetry breaking:

Electroweak $U(2) * U(1)$ spontaneously broken simultaneously with SUGRA

Theoretical "merits" of SUSY

- SUSY algebra is only non-trivial extension of space-time symmetry in relativistic quantum field theory
- Local SUSY $\rightarrow$ supergravity (hope for a finite theory of quantum gravity)
- Superstrings + fermions $\rightarrow$ SUSY below M_{Planck}
- Non-renormalization theorems

From these follows the specific motivations for weak-scale SUSY

Supersymmetric extension of Standard model.

Eliminates quadratic divergencies of scalar Higgs field.

Mass of an elementary scalar field would "naturally" be $\Theta(M_{GUT}) \div \Theta(M_{Planck})$

SUSY is the only way we know that renders $M_{Higgs} \lesssim 1TeV$, maybe even $M_{Higgs} \approx M_{weak}$.

In SUSY GUT:

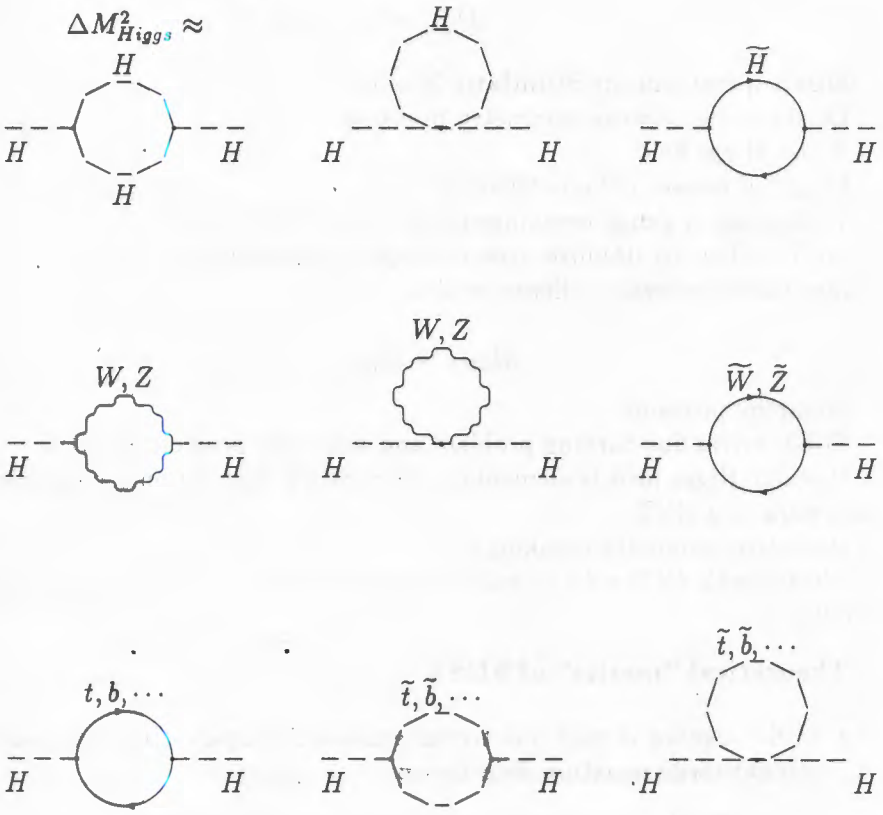

Figure 3: $\propto \ln M^2_{GUT}\,[\Theta(10^2 GeV)^2) \div \Theta(10^3 GeV)^2)]$

SUSY $\rightarrow$ Cancellation of quadratic divergence

Large $m_{top}(\gtrsim 60GeV) \rightarrow M^2_{Higgs} < 0$ for one of the Higgs states.

Radiative breaking of $SU(2) * U(1)$ is a derived consequence of SUSY breaking.

Experimental hint: gauge coupling unification.

Extra bonus: good candidate for cold dark matter (lightest SUSY

particle LSP is stable if R_p is conserved)

Unification of gauge couplings *Amadi et al. 1991*

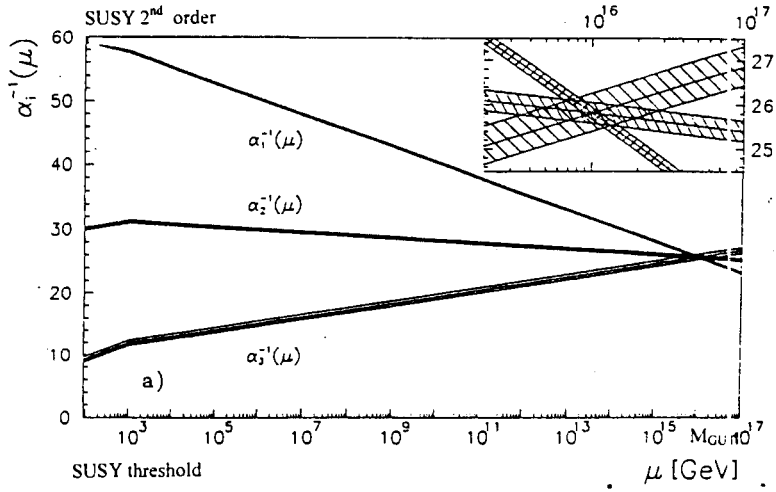

Unification of gauge couplings in minimal SUSY *Bagger et al. 1996*

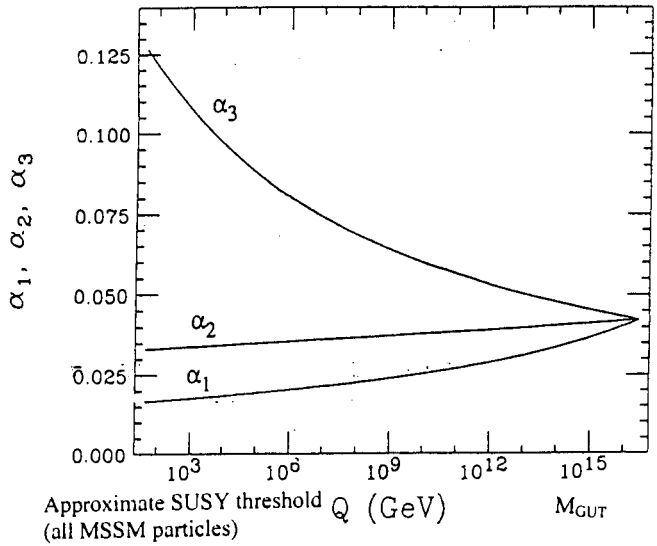

SUSY must be broken between M_W and M_{Plank}

Minimal Supersymmetric Standard Model MSSM:

SM particles + "super partners"

-2 Higgs doublets to cancel anomalies.

Break SUSY by adding "soft-breaking" terms

M_1, M_2, M_3 gaugino masses

$m_{\tilde{f}_L}, m_{\tilde{f}_R}, m_{H_1}, m_{H_2}, ..$ squark, slepton, Higgs masses

A_{ijk} trilinear couplings of scalar fields

B – bilinear Higgs coupling

altogether $\approx$ 105 new parameters.

If true, tremendous task for for experimentalists to measure all relevant parameters.

We need a theory of soft-breaking terms. What is the mechanism of SUSY breaking?

Hints for SUSY particle masses:

- Gauge couplings unification at $M_{GUT} \approx 10^{16} GeV$ works if $100 GeV \lesssim M(SUSY) \lesssim 10 TeV$
- Naturalness: $M(SUSY) \lesssim 1 TeV$

If $M(SUSY)$ increases, MSSM $\rightarrow$ SM, but MSSM becomes more and more "unnatural", fine-tuning reintroduced.

Assumption: All "soft" parameters are unified at M_{GUT}

Paradigm model: Constrained MSSM (CMSSM) minimal SUGRA (MSGM), MLES ...

Parameters $m_0, m_{1/2}, A_0, B_0, \mu_0$ at M_{GUT}

GUT scale $\rightarrow$ (renormalization group eqs.) $\rightarrow$ weak scale

Radiative EW symmetry breaking: $B \rightarrow \tan B$, $\mu^2 \rightarrow M_Z^2$

Standard set of CMSSM parameters:

$$m_0, m_{1/2}, A_0, \tan B, \text{sign } (\mu)$$

Theoretical background:

Break SUGRA in "hidden sector". Hidden sector field develops, typically at $M \sim 10^{11} GeV$

Gravity is "messenger" of SUSY breaking to visible sector:

$$M_{SUSY} \sim \frac{M^2}{M_{Planck}^2} \sim \frac{(10^{11})^2}{10^{19}} \sim 10^3 GeV$$

CMSSM can be tested experimentally. If wrong: possible to disprove
Implemented in ISASUSY, SUSYGEN...

Barger et al, de Boer et al, Kane et al, Drees-Nojiri, Pokorski et al, Ross-Roberts ...

Minimal Supersymmetric Standard Model (MSSM)

q, l, ν	$\tilde{q}, \tilde{l}, \tilde{\nu}$	
g	$\tilde{g}$	
$W^{\pm}, Z^0, \gamma$	$\tilde{W}^{\pm}, \tilde{Z}^0, \tilde{\gamma}$	charginos
$H^{\pm}, h^0, A^0, H^0$	$\tilde{H}^{\pm}, \tilde{H}_1^0, \tilde{H}_2^0$	$\tilde{\chi}_i^{\pm}, i = 1, 2$
		$\tilde{\chi}_i^0, i = 1...4$
		neutralinos

Parameters

$$M, M', \mu, \tan\beta = \frac{v_2}{v_1}, \qquad m_W^2 = \frac{1}{2}g^2(v_1^2 + v_2^2),$$

$$m_{\tilde{q}_{L,R}}, m_{\tilde{l}_{L,R}}, m_{\tilde{\nu}}, m_0$$

$$m_A, A..., m_t, m_b$$

Unification relations:

$$m_{\tilde{g}} = \frac{\alpha_s}{\alpha_1} M \approx 3M$$

$$M' = \frac{5}{3}\tan^2\Theta_W M \approx \frac{M}{2}$$

$$m^2_{\tilde{f}_{L,R}} = m_f^2 + m^2_{soft}(\tilde{f}) \pm m_D^2(f)$$

$$m^2_{soft}(\tilde{f}) = m_0^2 + C(\tilde{f})M^2$$

$$m_D^2(\tilde{f}) = m_Z^2 \cos 2\beta (T_{3L}^f - \Theta_f \sin^2\Theta_W)$$

R-parity conserved, χ_1^0 **assumed LSP**
Further constrains: RGE & boundary conditions (GUT).

$$L = L_{SUSY} + L_{soft}$$

$$L_{SUSY} = L_g + L_{Yuk} - V(A, A^+)$$

Superpotential

$$W = h_E L E^c H_1 + h_D Q D^c H_1 + h_U Q U^c H_2 + \mu H_1 H_2$$

$$L_{Yuk} = -\frac{1}{2}\frac{\partial^2 W}{\partial A_i \partial A_j}\psi_i\psi_j + h.c.$$

$$V(A, A^+) = F_i^+ F_i + \frac{1}{2}D_a^+ D_a$$

$$F_i = -\frac{\partial W}{\partial A_i}$$

$$D_a = -gA^+ T^a A$$

L_{soft} introduced by SUSY breaking
At $M_X \approx 10^{16} GeV$:

$$L_{soft} = L_M + L_S$$

$$L_M = -\frac{1}{2}\bar{M}(\lambda^a\lambda^a + \bar{\lambda}^a\bar{\lambda}^a)$$

$$L_S = -m_0^2 \mid A_i \mid^2 - B\mu h_1 h_2 - A\left(h_E \tilde{l}\tilde{e}^C h_1 - h_D \tilde{q}\tilde{d}^C h_1 - h_U \tilde{q}\tilde{u}^C h_2\right)$$

$$m_0 \approx m_{3/2}$$

Higgs Sector:

$$V_H = \mu_1^2 \mid H_1 \mid^2 + \mu_2^2 \mid H_2 \mid^2 + B\mu m_0(H_1 H_2 + h.c.) + \frac{g^2}{8\cos^2\Theta_W}(\mid H_2 \mid^2 - \mid H_1 \mid^2)^2$$

At scale M_X: $\mu_1^2 = \mu_2^2 = \mu^2 + m_0^2$

$SU(2) * U(1)$ **breaking:** $\mu_1^2\mu_2^2 < B^2\mu^2 m_0^2$
Stability: $\mu_1^2 + \mu_2^2 \geq 2 \mid B\mu m_0 \mid$

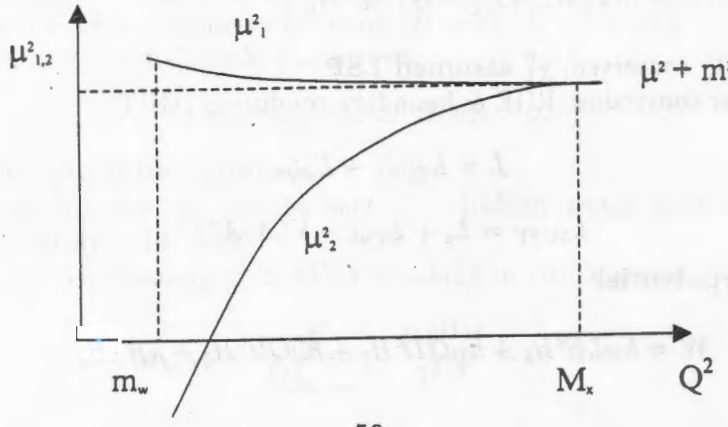

$$\frac{v_2}{v_1} = \tan\beta$$

Top quark loop:

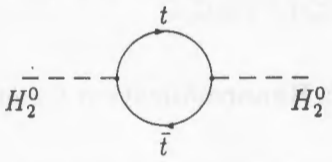

works if $m_t \gtrsim 60GeV$.

Minimum of V_H at $< H_{1,2}^0 >= \frac{1}{\sqrt{2}} v_{1,2}$

$$m_W^2 = \frac{1}{2} g^2 (v_1^2 + v_2^2), m_{H^\pm}^2 = m_W^2 + m_{H_3}^2,$$

$$m_{H_1,H_2}^2 = \frac{1}{2}\left[m_{H_3}^2 + m_Z^2 \pm \sqrt{(m_{H_3}^2 + m_Z^2)^2 - 4 m_Z^2 m_{H_3}^2 \cos^2 2\beta}\right]$$

$$\tan\beta = v_2/v_1, \mid m_{H_\pm} \mid \geq m_W, \mid m_{H_1} \mid \geq m_Z, \mid m_{H_2} \mid \leq m_Z \mid \cos 2\beta \mid$$

$$H_2^0 \to h^0, H_1^0 \to H^0, H_3^0 \to A^0$$

RGE's

Masses of squarrks and sleptons:

1st and 2nd generation:

$$\begin{aligned}
m_{\tilde{\nu}}^2 &= m_0^2 + 0.79M^2 + 0.50 m_Z^2 \cos 2\beta \qquad m_{\tilde{L}}^2 \\
m_{\tilde{e}_L}^2 &= m_0^2 + 0.79M^2 - 0.28 m_Z^2 \cos 2\beta \qquad m_{\tilde{L}}^2 \\
m_{\tilde{e}_R}^2 &= m_0^2 + 0.23M^2 - 0.23 m_Z^2 \cos 2\beta \qquad m_{\tilde{E}}^2 \\
m_{\tilde{u}_L}^2 &= m_0^2 + 10.8M^2 + 0.36 m_Z^2 \cos 2\beta \qquad m_{\tilde{Q}}^2 \\
m_{\tilde{u}_R}^2 &= m_0^2 + 10.1M^2 + 0.15 m_Z^2 \cos 2\beta \qquad m_{\tilde{U}}^2 \\
m_{\tilde{d}_L}^2 &= m_0^2 + 10.8M^2 - 0.43 m_Z^2 \cos 2\beta \qquad m_{\tilde{Q}}^2 \\
m_{\tilde{d}_R}^2 &= m_0^2 + 10.1M^2 - 0.07 m_Z^2 \cos 2\beta \qquad m_{\tilde{D}}^2
\end{aligned}$$

3rd generation:

$$M_{\tilde{t}}^2 = \begin{pmatrix} m_{\tilde{t}_L}^2 + m_t^2 & -m_t(A_t + \mu cot\beta) \\ -m_t(A_t + \mu cot\beta) & m_{\tilde{t}_R}^2 + m_t^2 \end{pmatrix}$$

$$M_{\tilde{b}}^2 = \begin{pmatrix} m_{\tilde{b}_L}^2 + m_b^2 & -m_b(A_b + \mu \tan\beta) \\ -m_b(A_b + \mu \tan\beta) & m_{\tilde{b}_R}^2 + m_b^2 \end{pmatrix}$$

$\tilde{b}_L - \tilde{b}_R$ **mixing** non negligible for $\tan \gtrsim 10$.

Constrained MSSM (CMSSM)

Minimal $N = 1$ Supergravity together with **Renormalization Group Equations**

Different assumptions about boundary conditions lead to restrictions on soft-breaking parameters

Radiative electroweak breaking

Gauge couplings unification at M_{GUT}

Yukava couplings unification ($\lambda_b = \lambda_t$) at M_{GUT}

Proton decay

Dark matter density

$b \to s + \gamma$

Naturalness

⋮

de Boer et al: "Low $\tan\beta$" "High $\tan\beta$" solution

Kane et al: $m_h^0 \lesssim 146 GeV$ in general

expect $76 GeV \lesssim m_h^0 \lesssim 107 GeV$ for $m_t = 135 GeV$

also $100 GeV \lesssim M, m_0 \lesssim 400 GeV$ most probable

Pokorski et al: $M, m_0 \gtrsim 200 GeV$ for $\tan\beta = 30, m_t = 120 GeV$

$M \gtrsim 50 GeV, m_0 \gtrsim 200 GeV$ for $\tan\beta = 40, m_t = 160 GeV$

Kelley et al: MSSM and "flipped" $SU(5)$

Arnowitt et al: $m_h^0 < 105 GeV, m_{\tilde{\chi}_1^\pm} < 100 GeV$ possible

Barbieri et al, Barger et al, Borzumati, Dress et al, Ellis et al,..: $h^0, \tilde{\chi}_1^\pm, \tilde{t}, \tilde{l}$ may be in LEP II reach.

Evolution of SUSY particle masses *Bagger et al.*

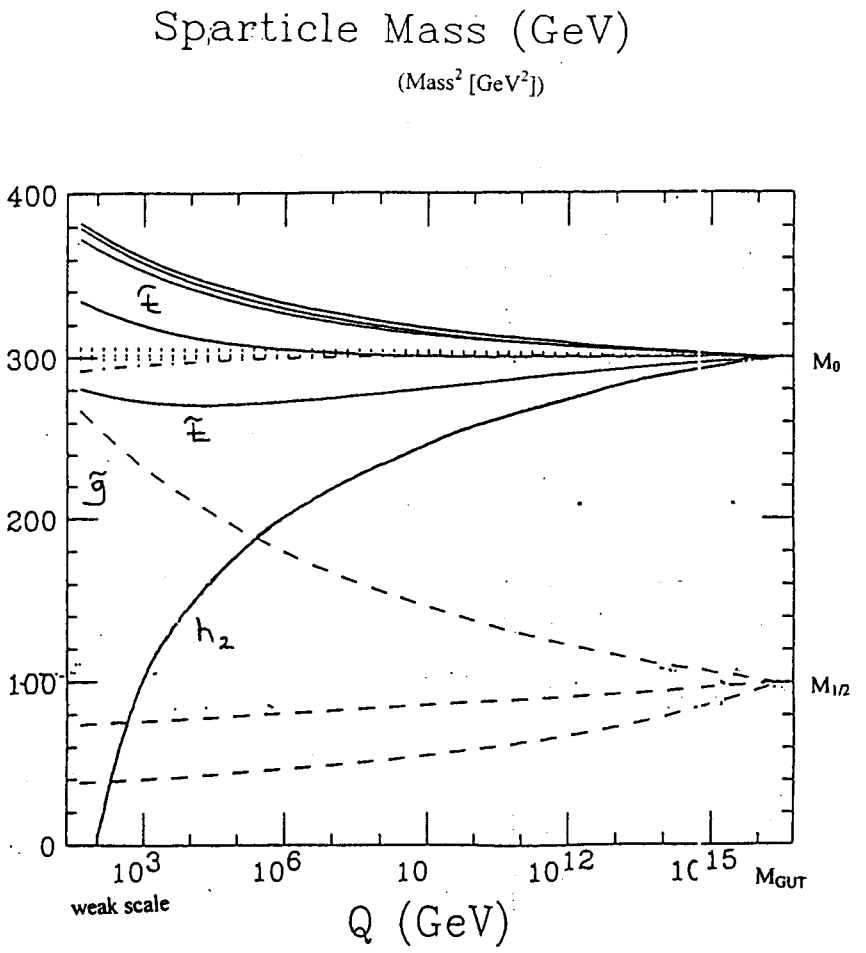

Argument for constraining SUSY masses:
Naturalness

Barbieri-Giudice:

M_Z depends om EWSB, therefore on "soft" SUSY parameters

Define: $C(M_Z^2, p) := \mid \frac{p}{M_Z^2} \frac{\partial M_Z^2}{\partial p} \mid$ p any SUSY parameter

$C(M_Z^2, p)$ is a measure of sensitivity of M_Z on p

Demand: $C(M_Z^2, p) < 10$ for example

Anderson-Castano take

$$\gamma(M_Z^2, p) := \frac{C(M_Z^2, p)}{\bar{C}}$$

as a measure of naturalness, with

$$\bar{C}^{-1} = \frac{\int_{p_-}^{p_+} dp p f(p) C^{-1}(M_Z^2, p)}{\int_{p_-}^{p_+} dp p f(p)}$$

$f(p)$: probability density of p, e.g. $f(p) = 1$ or $f(p) = 1/p$

$p_\pm$: expected range of parameter p

This gives $m_{\tilde{g}} \lesssim 800GeV, m_{\tilde{q}} \lesssim 700GeV, m_{\tilde{\chi}_1^\pm} \lesssim 250GeV$, "most natural" values are $m_{\tilde{g}} \approx m_{\tilde{q}} \approx 250GeV$

LEP2 range is "most natural". This is true, however, only in CMSSM.

Present mass limits

LEP:

Charged SUSY particles:

$$m \gtrsim 60 - 80GeV, m_{\tilde{\chi}_1^0} \gtrsim 13GeV, m_{\tilde{\chi}_2^0} \gtrsim 60 - 80GeV$$

Higgs: $m_{h^0} \gtrsim 62GeV, (m_{A^0} \gtrsim 62GeV)$

Tevatron:

$m_{\tilde{g}} \gtrsim 173GeV$ if $\tan\beta = 4, \mu = -400GeV$
$m_{\tilde{g}} \gtrsim 216GeV$ if $m_{\tilde{g}} = m_{\tilde{q}}$
$m_{\tilde{q}} \gtrsim 150GeV$ if $m_{\tilde{g}} < 500GeV$

$40GeV \lesssim m_{\tilde{t}_1} \lesssim 100GeV$ excluded if $m_{\tilde{t}_1} - m_{\tilde{\chi}_1^0} \gtrsim 30GeV, \tilde{t}_1 \to C\tilde{\chi}_1^0$

Which parameters of MSSM are excluded by experiment?

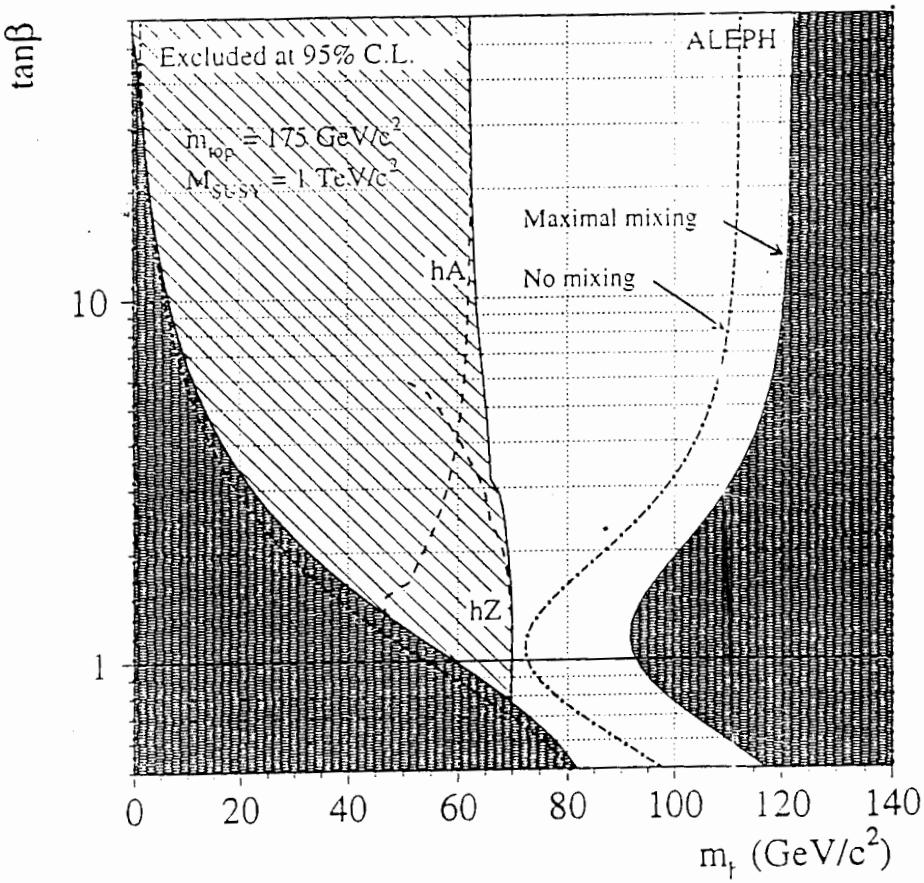

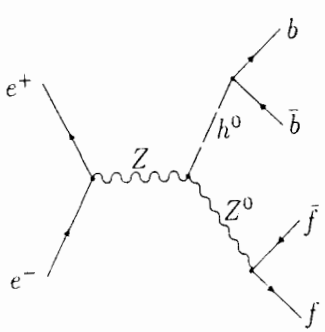

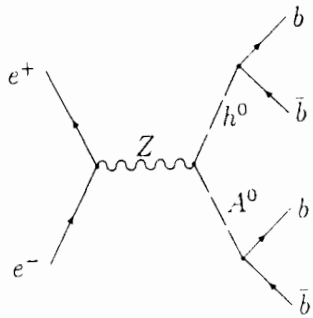

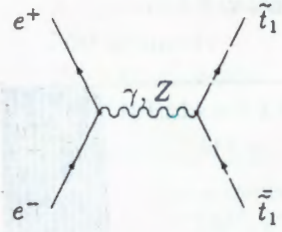

The 95 % C.L. excluded regions assuming that the $\tilde{t}_1$ decays into $c\tilde{\chi}_1^0$.

(a) The excluded regions in the $(\Theta_{\tilde{t}}, m_{\tilde{t}_1})$ plane. The solid line shows the limit for a mass difference $\Delta m (= m_{\tilde{t}_1} - m_{\tilde{\chi}_1^0}) \geq 10 GeV$, and the dotted line for $\Delta m \geq 5 GeV$. The cross hatched region has already been excluded by the search at LEP1.

(b) The excluded regions in the $(m_{\tilde{t}_1}, m_{\tilde{\chi}_1^0})$ plane, for a mixing angle of $\tilde{t}_1$ of 0.0 (solid line) and 0.98 rad (dotted line). The cross hatched region has already been excluded by the search at LEP1. The singly hatched region has been excluded by D0 Collaboration. The dash-dotted straight line shows the kinematic limit for the $\tilde{t}_1 \rightarrow c\tilde{\chi}_1^0$ decay.

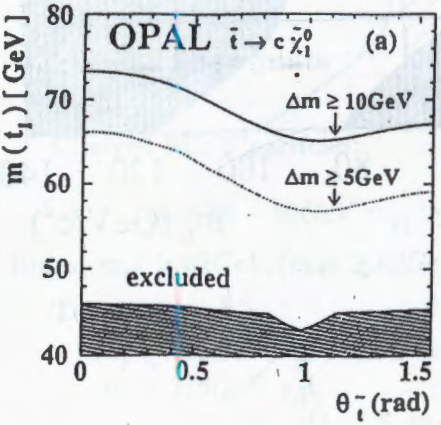

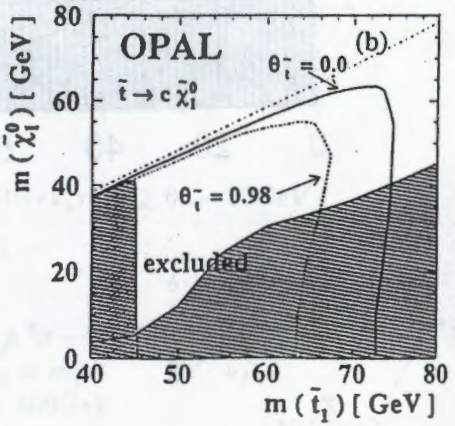

Basic principle of MSSM particle searches:

$R_p = (-)^{3B+L+2S}$ conserved

SUSY particles produced in pairs

Lightest SUSY particle is stable and only weakly interacting (like neutrino)

A SUSY particle decays into LSP and known particles (maybe in cascades)

Signal for SUSY: Events with **missing energy-momentum** carried by the invisible LSP.

Machines:

e^+e^- : LEP, SLC, e^+e^- LC (NLC, JLC, CLIC)

pp : Tevatron $p - \bar{p}$, LHC, Eloisatron

$e - p$: HERA, LEP/LHC

Strategy:

Look for **excess of events** for characteristic final states (compared to SM prediction)

Search for SUSY

$p - p$ Collisions:

Strongly interacting SUSY particles: Gluino, Squarks

Neutral Higgses (Wilczek mechanism, $g - g$ fusion quark loops)

Sleptons, Charginos, Neutralinos (via Drell-Yan, smaller cross sections).

$e^+ - e^-$ Annihilation:

Neutral and Charged Higgses

Electro-weakly interacting SUSY particles:

Sleptons, Sneutrinos, Squarks, Charginos ($\tilde{W}^\pm - \tilde{H}^\pm$ mixings)

Neutralinos ($\tilde{\gamma} - \tilde{Z}^0 - \tilde{H}_i^0$ mixings)

Also in $\gamma - \gamma$, $e^\pm - \gamma$, $e^- - e^-$ reactions

$e - p$ Collisions:

Associated production of Slepton-Squark, Slepton-Chargino or Neutralino Squark pairs (gluon fusion)

Neutral Higgs ($\gamma - g$ fusion)?

(If R_p: single squark production via $eq\bar{q}$ coupling)

SUSY at Hadron colliders

$p - \bar{p}$: Tevatron, $\sqrt{s} \approx 2TeV$ (CERN $Sp\bar{p}S$)

$p-p$ LHC, $\sqrt{s} \approx 14TeV$ (Eloisatron ?)

$$pp \to \tilde{g}\tilde{g} + X, pp \to \tilde{q}\bar{\tilde{q}} + X, pp \to \tilde{g}\tilde{q} + X,$$

have largest cross sections of all SUSY particles (*Barnett et al, Baer et al*)

Gluino $\tilde{g}$, squarks $\tilde{q}$, decay into charginos $\tilde{\chi}_i^{\pm}$ and neutralinos $\tilde{\chi}_i^0$, until $\tilde{\chi}_1^0$ (LSP) is reached (*Bartl et al*)

Also associated production with $\tilde{\chi}_i^{\pm}, \tilde{\chi}_i^0$ is possible:

$$pp \to \tilde{g}\tilde{\chi}_i^{\pm} + X, \tilde{g}\tilde{\chi}_i^0 + X, \tilde{q}\tilde{\chi}_i^{\pm} + X, \tilde{q}\tilde{\chi}_i^0 + X (Baer\ et\ al)$$

Drell-Yan production:

$$pp \to \tilde{\chi}^{\pm}\tilde{\chi}_i^0 + X, \tilde{\chi}_i^+\tilde{\chi}_j^- + X, \tilde{\chi}_i^0\tilde{\chi}_j^0 + X,$$

$$pp \to \tilde{l}^+\tilde{l}^- + X ... (Barbieri\ et\ al,\ Baer\ et\ al)$$

May be detectable at LHC if $m \lesssim 200GeV$, large $t\bar{t}$ background.

SUSY Higgses MSSM

Tree level: $m_{H^{\pm}}^2 \mid_0 = m_W^2 + m_A^2$

$$m_{h,H}^2 \mid_0 = \frac{1}{2}\left[m_A^2 + m_Z^2 \mp \sqrt{(m_A^2 + m_Z^2)^2 - 4m_A^2 m_Z^2 \cos^2 2\beta}\right]$$

$$m_W, m_A < m_{H^{\pm}}, m_h < m_Z < m_H, m_h < m_A < m_H$$

Rad. correction:

$m_h^2 = m_h^2 \mid_0 + \Delta^0, m_{H^{\pm}}^2 = m_{H^{\pm}}^2 \mid_0 + \Delta^{\pm}$, (*J. Ellis et al, R. Barbieri et al, Y. Dkada et al, S. Pokorski et al, H. Haber et al, A. Yamada ...*)

$\Delta^0 \propto \frac{m_t^4}{m_W^2}, \Delta^{\pm} \propto m_t^2$

m_h could go up to $120GeV$, h^0 could be beyond LEP200 reach, and in mass region not easily accessable at LHC

$m_A < m_h$ possible, $m_{H^{\pm}} < m_W$ possible.

At EE500: If no Higgs particle is found, then MSSM is disproved, but SUSY is not disproved.

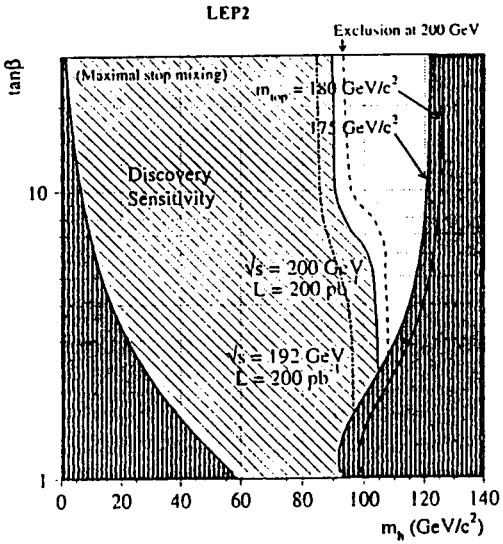

SUSY in e^+e^- collisions (SLC, LEPI & II, KEK)

$$e^+e^- \to \tilde{\chi}_1^0\tilde{\chi}_1^0, \tilde{\chi}_1^0\tilde{\chi}_2^0, \tilde{\chi}_1^0\tilde{\chi}_3^0, \tilde{\chi}_2^0\tilde{\chi}_2^0, ..$$

$$e^+e^- \to \tilde{\chi}_1^+\tilde{\chi}_1^-,$$

$$e^+e^- \to \tilde{e}_{L,R}^+\tilde{e}_{L,R}^-, \tilde{\mu}_{L,R}^+\tilde{\mu}_{L,R}^-, \tilde{\tau}_{L,R}^+\tilde{\tau}_{L,R}^-, \tilde{\nu}\bar{\tilde{\nu}}, \tilde{q}_{L,R}\bar{\tilde{q}}_{L,R}, ..$$

$\tilde{\chi}_1^0$ not seen (lightest SUSY particle)

Characteristic signatures from SUSY particle decays:

$$\tilde{\chi}^\pm \to l^\pm + \nu(\bar{\nu}) + \tilde{\chi}_1^0, \quad \tilde{\chi}^\pm \to q + \bar{q}^{'} + \tilde{\chi}_1^0,$$

$$\tilde{l}_R \to l + \tilde{\chi}_1^0, \quad \tilde{l}_L \to l + \tilde{\chi}_1^0, \quad \nu_L + \tilde{\chi}_1^\pm$$

$$\tilde{\chi}_i^0 \to l^+ + l^- + \tilde{\chi}_1^0, \quad i = 2,3$$

$$\tilde{\chi}_i^0 \to q + \bar{q} + \tilde{\chi}_1^0, \tilde{\chi}_i^0 \to \nu + \bar{\nu} + \tilde{\chi}_1^0,$$

$$\tilde{\chi}_i^0 \to \gamma + \tilde{\chi}_1^0, \tilde{\chi}_i^0 \to h(A) + \tilde{\chi}_1^0,$$

(*Barbieri et al, Ellis et al, Hidaka et al, Bartl et al, Chen et al*)

Candidates for lightest visible SUSY particle (LVSP): $\tilde{\chi}_1^\pm, \tilde{e}_R, \tilde{\mu}_R, \tilde{\tau}_1, \tilde{t}_1, \tilde{b}_1, \tilde{\chi}_2^0$.

$$e^+e^- \to \tilde{\chi}_1^+\tilde{\chi}_1^- \to l^+ + l^- + \tilde{\chi}_1^0 + \tilde{\chi}_1^0 \qquad \text{two-sided events}$$

$$e^+e^- \to \tilde{\chi}_2^+\tilde{\chi}_1^- \to l^+l^- + \tilde{\chi}_1^0 + \tilde{\chi}_1^0 \qquad \text{one-sided events}$$

Cononical signature for SUSY: **Missing** $E, \vec{p}$

SUSY at LEP200

$\sqrt{s} = 190 GeV \qquad \int L \approx 500 pb^{-1}$

$e^+ + e^- \to \tilde{\chi}_i^+ + \tilde{\chi}_j^-$

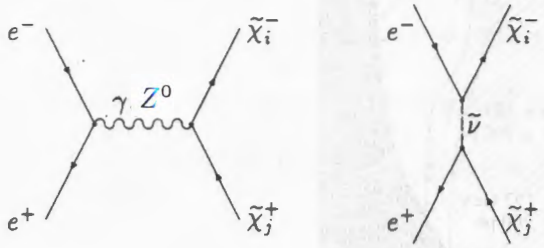

$e^+ + e^- \to \tilde{\chi}_i^0 + \tilde{\chi}_j^0$

$e^+ + e^- \to \tilde{e}_{L,R}^+ + \tilde{e}_{L,R}^-$

$e^+ + e^- \to \tilde{\nu}_e + \bar{\tilde{\nu}}_e$

$e^+ + e^- \to \tilde{\mu}_{L,R}^+ + \tilde{\mu}_{L,R}^-, \quad \tilde{q}_{L,R} + \bar{\tilde{q}}_{L,R}, \quad \left[\tilde{t}_1 + \bar{\tilde{t}}_1, \quad \tilde{b}_1 + \bar{\tilde{b}}_1, \quad \text{mixing}\right]$

Main Standard Model background

$e^+ + e^- \to W^+ + W^-$ *Chen et al. Phys. Rep.*

LEP200

$e^+ + e^- \to \tilde{\chi}_1^+ + \tilde{\chi}_1^-$

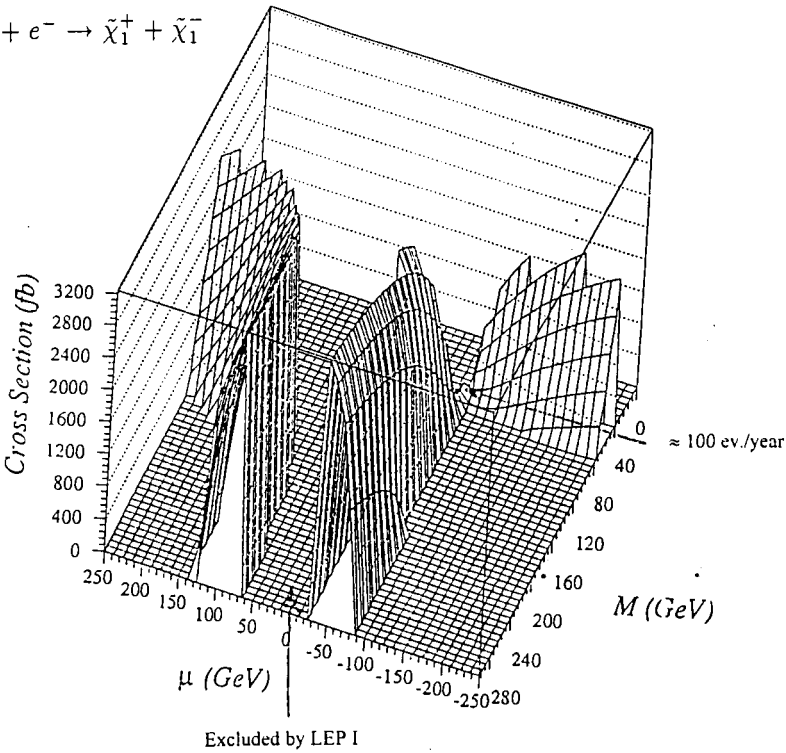

$\sqrt{s} = 190GeV, \quad \tan\beta = 1.4, \quad m_{\tilde{\nu}} = 100GeV$

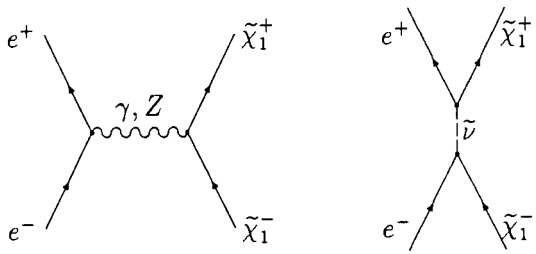

LEP2 Report
$\sigma\left(e^+e^- \to \tilde{\chi}_1^+\tilde{\chi}_1^-\right)$.

Chargino production cross section at LEP2, $\sqrt{s} = 190GeV$, as a function of $m_{\tilde{\chi}_1^\pm}$. We show the ranges obtained by varying $M_2, \mu, \tan\beta$ and $m_{\tilde{\nu}_e}$ throughout the parameter space, requiring $m_{\tilde{\nu}_e} > 45GeV$. The solid and dotted lines correspond to the maximum production rates. The dashed (dash-dotted) line corresponds to the minimum cross section if $m_{\tilde{\nu}_e} = 2TeV$ ($m_{\tilde{\nu}_e} = 200GeV$).

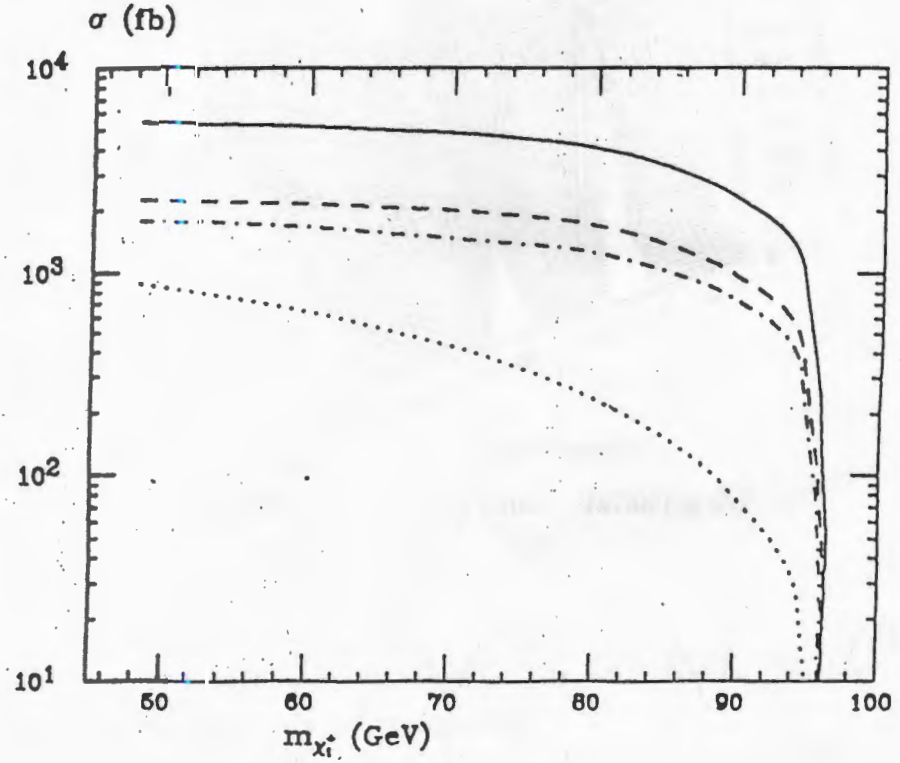

LEP2: $e^-e^+ \to \tilde{t}_1\bar{\tilde{t}}_1$

5σ discovery reach (left) and 95 % CL limits (right) for the $\tilde{t}$ search at $190GeV$. The solid (dashed) lines correspond to maximal (minimal) coupling to the Z. The shaded area corresponds to the current 95 % CL Tevatron limits.

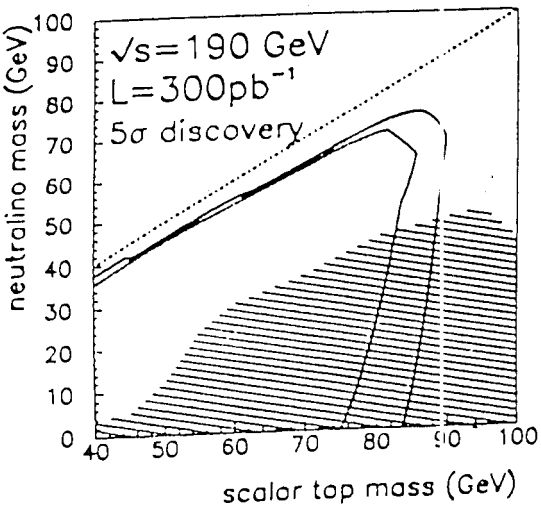

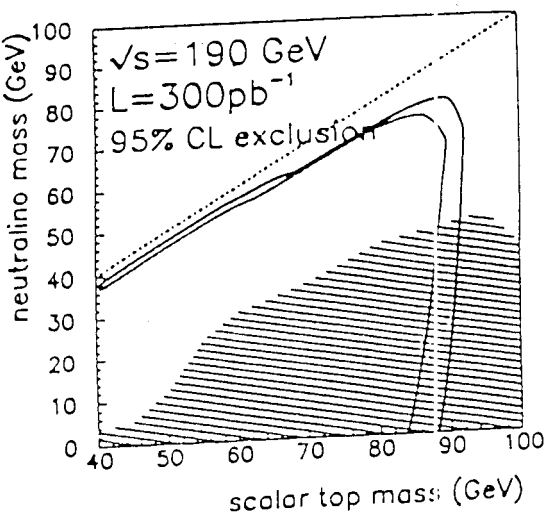

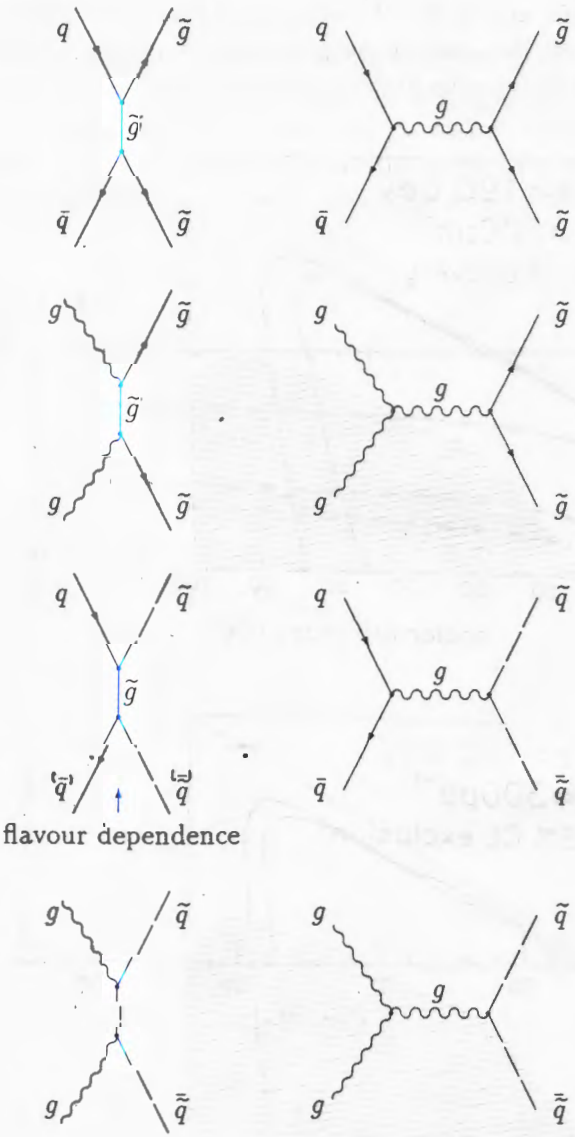

Figure 4: $p + p \rightarrow \tilde{g} + \tilde{g} + X$, $p + p \rightarrow \tilde{q} + \tilde{\bar{q}} + X$

Possible TEVATRON Upgrades

Run "1B": Peak luminosity $\approx 2 * 10^{31} cm^{-2} s^{-1}$, 18 months $\rightarrow 100 pb^{-1}$

Main injector: L $\approx 10^{32} cm^{-2} s^{-1}$, Run "II" $2 fb^{-1}$
CDF, D0: proposed upgrades
Ideas how to bridge time between LEP and LHC:
$TeV*$: $L \approx 2 * 10^{32} cm^{-2} s^{-1}$ Run "II - stretch" $\rightarrow 10 fb^{-1}$
Incremental CDF and D0 upgrades
$TeV33$: $L \approx 10^{33} cm^{-2} s^{-1} \rightarrow 25 fb^{-1} -:- 100 fb^{-1}$? CDF, D0 ?

SUSY mass reach expected:
$\int L = 2 fb^{-1}$: $m_{\tilde{g}/\tilde{q}} \lesssim 390 GeV$, $m_{\tilde{l}} \lesssim 150 GeV, m_{\tilde{\chi}^{\pm}} \lesssim 210 GeV$
$\int L = 25 fb^{-1}$: $m_{\tilde{g}/\tilde{q}} \approx 400 GeV$, $m_{\tilde{l}} \lesssim 180 GeV, m_{\tilde{\chi}^{\pm}} \lesssim 250 GeV$

$TeV*, TeV33$ $\sqrt{s} = 2 TeV$

$p\bar{p} \rightarrow \tilde{\chi}_1^{\pm} \tilde{\chi}_2^0 X \rightarrow l^{\pm} l^{+} l^{-} + \not{p}_T$

□ A: $BR(\tilde{\chi}_2^0 \rightarrow \text{invisible}) > 90\%$
* B: large destructive interference in leptonic decays
× C: $BR(\tilde{\chi}_2^0 \rightarrow h^0 \tilde{\chi}_1^0) > 50\%$
o D: all other cases.

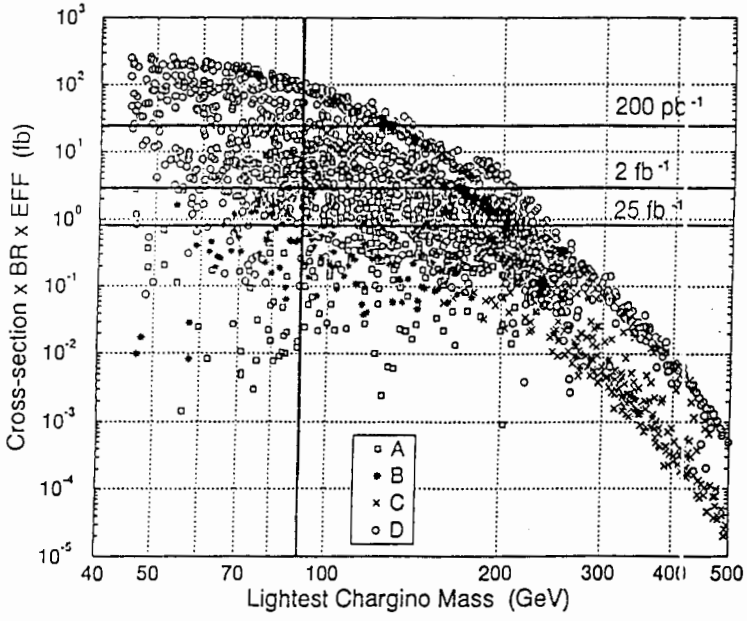

Squark production LHC

$pp \to \tilde{u}\bar{\tilde{u}} + X, \quad t\bar{\tilde{t}} + X, \quad b\bar{\tilde{b}} + X, \quad m_{\tilde{g}} = m_{\tilde{q}}$

Rad. corr. (*Beenakker et al.*) not included.

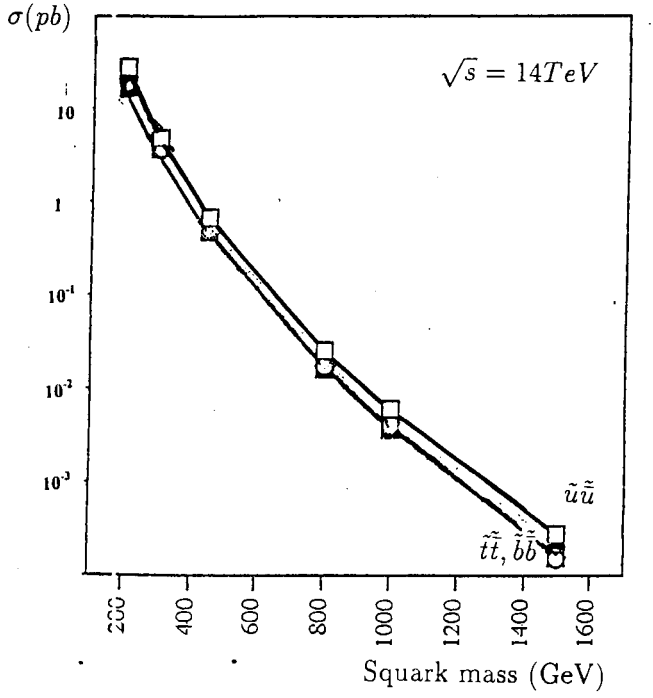

Cascade Decay of heavy SUSY Particles:

$$\tilde{e}_L \to e + \tilde{\chi}^0_K, \quad \nu + \tilde{\chi}^-_K,$$

$$\tilde{g} \to q\bar{q} + \tilde{\chi}^0_K(\tilde{\chi}^0_1), \quad \to q\bar{q}' + \tilde{\chi}^\pm_i, \quad \to g + \tilde{\chi}^0_i(\tilde{\chi}^0_1),$$

$$\tilde{e}_R \to e + \tilde{\chi}^0_K, \quad \tilde{\nu} \to \nu + \tilde{\chi}^0_K, \quad \to e + \tilde{\chi}^+_K$$

$$\tilde{q}_{L,R} \to q + \tilde{\chi}^0_K(\tilde{\chi}^0_1), \quad \tilde{q}_L \to q' + \tilde{\chi}^\pm_i$$

$$\tilde{\chi}^0_K \to Z^0 + \tilde{\chi}^0_l, \quad \to W^\pm + \tilde{\chi}^\mp_l, \quad \to H^0_i + \tilde{\chi}^0_l, \quad H^\pm + \tilde{\chi}^\mp_l,$$

$$\tilde{\chi}^\pm_K \to Z^0 + \tilde{\chi}^\pm_l, \quad \to W^\pm + \tilde{\chi}^0_l, \quad \to H^0_i + \tilde{\chi}^\pm_l, \quad H^\pm + \tilde{\chi}^0_l$$

until $\tilde{\chi}^0_1$ is reached (LSP)

Missing-energy signature may be strongly reduced.

Decay into $H^0_i, H^\pm$ may reduce leptonic signal.

Decays:

$$\tilde{g} \to q + \bar{q} + \tilde{\chi}_i^0, \quad t + \bar{t} + \tilde{\chi}_i^0, \quad \text{if} \quad M_{\tilde{q}} > m_{\tilde{g}}$$

$$q + \bar{q}' + \tilde{\chi}_i^{\pm}, \quad t + \bar{b} + \tilde{\chi}_i^-, \quad \bar{t} + b + \tilde{\chi}_i^+$$

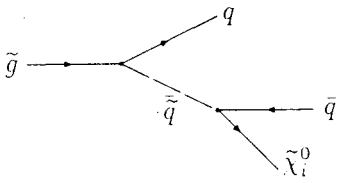

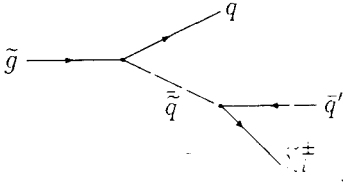

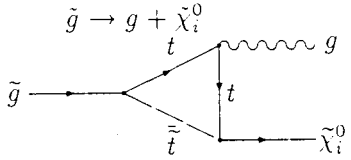

if $m_{\tilde{q}} < m_{\tilde{g}}$

$$\tilde{q}_{L,R} \to q + \tilde{\chi}_i^0, \quad \tilde{t}_{L,R} \to t + \tilde{\chi}_i^0 \quad \tilde{t}_L - \tilde{t}_R \quad \text{mixing}$$

$$\tilde{u}_L \to d + \tilde{\chi}_i^+, \quad \tilde{t}_L \to b + \tilde{\chi}_i^+ \quad \tilde{b}_L - \tilde{b}_R \quad \text{mixing}$$

$$\tilde{d}_L \to u + \tilde{\chi}_i^-, \quad \tilde{b}_L \to t + \tilde{\chi}_i^- \quad \tilde{t}_1, \tilde{b}_1 \quad \text{may be much lighter}$$

Cascades

A. Bartl, W. Majerotto, B. Moblacher, N. Oshimo, S. Stippel
Also: H. Baer et al, R. Barbieri et al., R. Barnett et al.

Signatures of $\tilde{q}\bar{\tilde{q}}$ pairs:

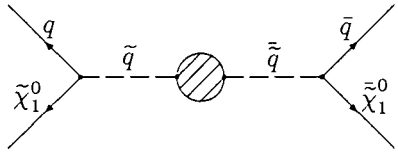

Figure 5: 2 jets, large $p_{T\text{miss}}$

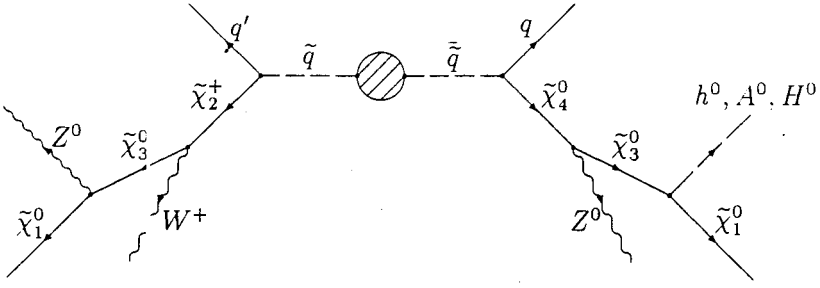

Figure 6: jets, $W^{\pm}$'s, Z^0's, Higgses, reduced $p_{T\text{miss}}$

Signatures of $\tilde{g}\tilde{g}$ pairs:

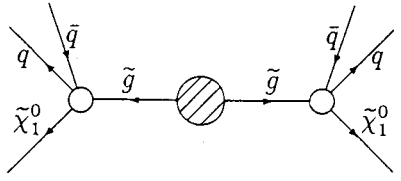

Figure 7: 4 jets, large $p_{T\text{miss}}$

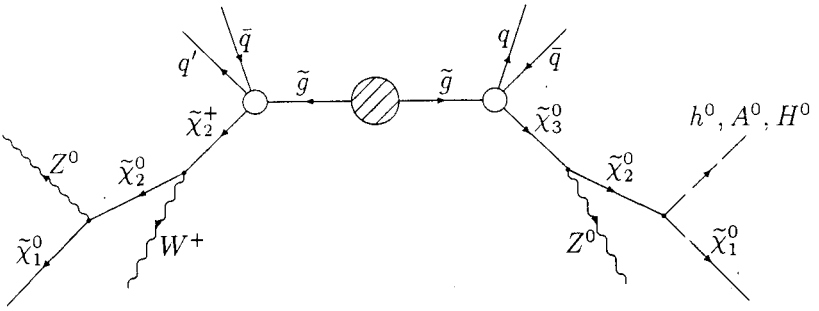

Figure 8: jets, $W^{\pm}$' s, Z^{0}' s, Higgses, reduced $\not{p}_{Tmiss}$

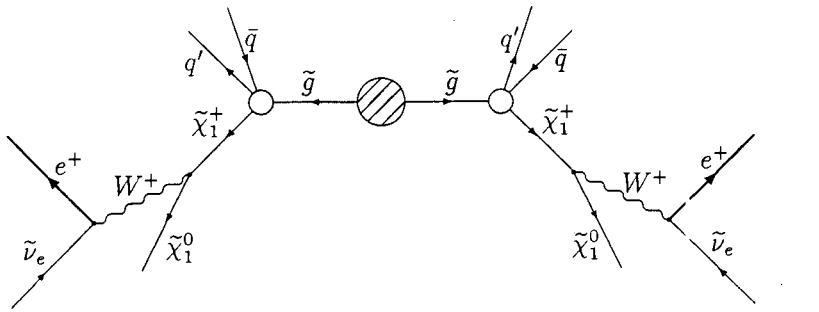

Figure 9: same-sign dileptons ($\tilde{g}$ Majorana)

gluino → neutralinos / charginos $m_{\tilde{g}} = 750GeV$

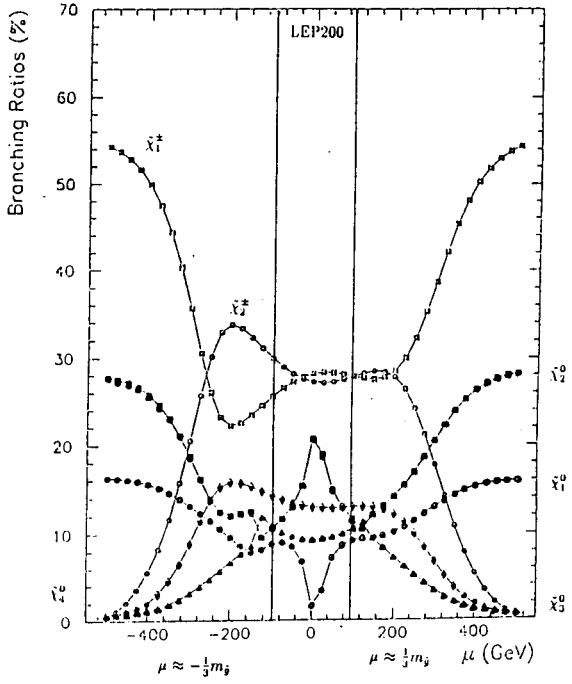

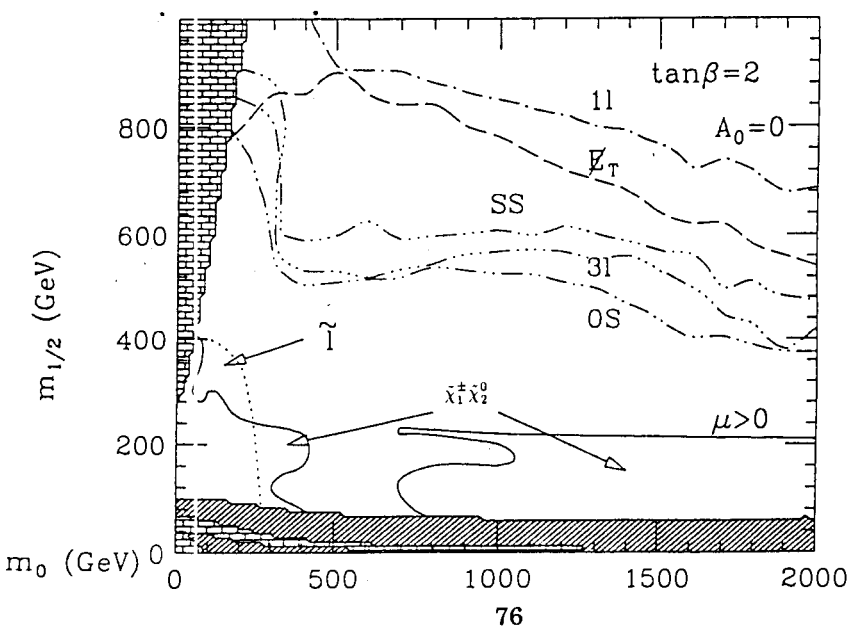

m SUGRA at LHC

R_p conserved, $\tilde{\chi}_1^0$ is LSP $\rightarrow \not{E}_T$

Reach in $m_0 - m_{1/2}$ plane by 1-lepton, same-sign 2-lepton, opposite-sign 2-lepton, 3-lepton signals, $\tilde{\chi}_1^\pm, \tilde{\chi}_2^0$ and $\tilde{l}\tilde{l}$ production.

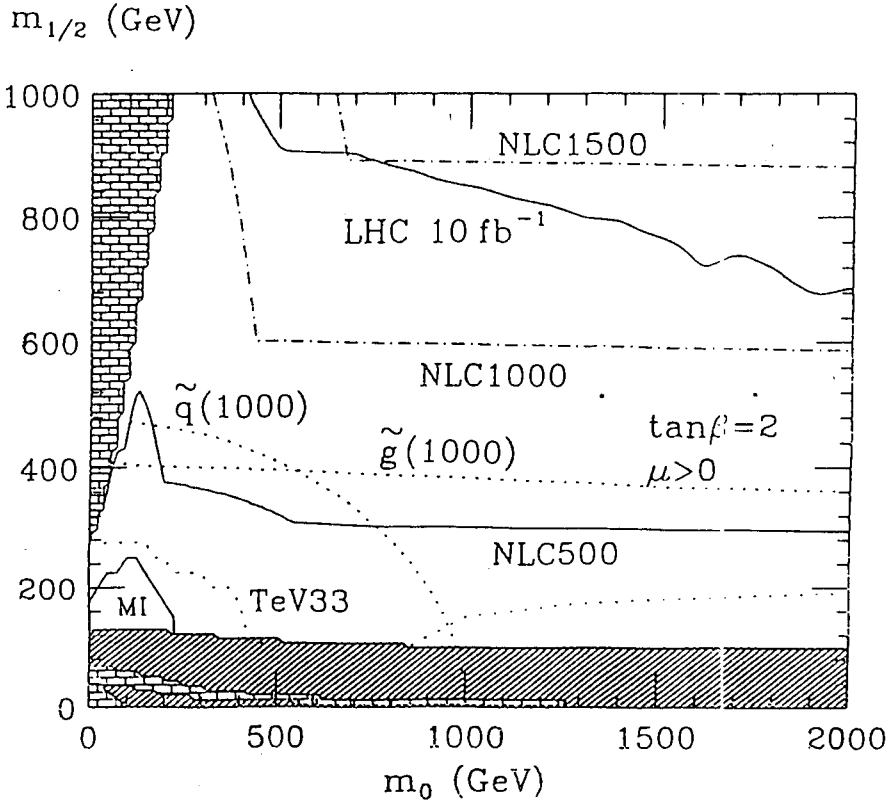

Hadronic Final States in Deep Inelastic Scattering at HERA

N. H. Brook
Dept. of Physics & Astronomy,
University of Glasgow,
Glasgow, United Kingdom.

Abstract

This lecture contains a brief introduction to HERA and deep inelastic scattering (DIS), before going on to highlight some of the measurements of the hadronic final state in DIS performed by the H1 and ZEUS collaborations.

1 The HERA Accelerator and Detectors

The HERA accelerator, located at DESY in Hamburg, is an electron-proton collider. It is 6.3 km in circumference and collides positrons (or electrons) at $\simeq$ 27 GeV with protons at 820 GeV. There are four interaction regions two containing general purpose, hermetic detectors (H1 and ZEUS); another experiment (HERMES) investigating the spin distributions of the quarks in protons and neutrons; and another (HERA-B) planning to measure CP violation in the B-system. The H1 and ZEUS detectors took first data in 1992.

The ZEUS detector is shown in figure 1. The asymmetric design of the detector reflects the proton energy being significantly higher than that of the electron beam.

The tracking system consists of a vertex detector (VXD) [1] and a central tracking chamber (CTD) [2] enclosed in a 1.43 T solenoidal magnetic field. Immediately surrounding the beampipe is the VXD which consists of 120 radial cells, each with 12 sense wires. The CTD, which encloses the VXD, is a drift chamber consisting of 72 cylindrical layers, arranged in 9 superlayers. Superlayers with wires parallel to the beam axis alternate with those inclined at a small angle to give a stereo view. A forward tracking detector is employed in the forward region to detect tracks in the proton direction and consists of three 12-layer planar drift chambers sandwiched

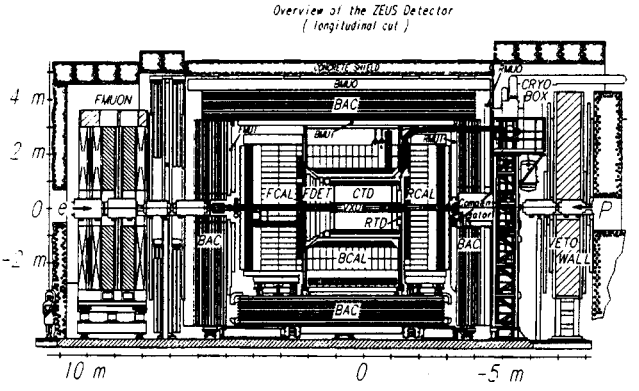

Figure 1: *Cross sectional view of the ZEUS detector*

with pairs of transition radiation detectors. In the rear direction there is an additional 12-layer planar drift chamber known as the rear tracking detector (RTD).

Outside the solenoid is the uranium-scintillator calorimeter (CAL) [3], which is divided into three parts: forward, barrel and rear covering the polar regions 2.6° to 36.7°, 36.7° to 129.1° and 129.1° to 176.2°, respectively. The CAL covers 99.7% of the solid angle, with holes of 20×20 cm^2 in the centres of the forward and rear calorimeters to accommodate the HERA beam pipe. Each of the calorimeter parts is subdivided into towers which are segmented longitudinally into electromagnetic (EMC) and hadronic (HAC) sections. The small angle rear tracking detector (SRTD) [4], which is attached to the front face of the rear calorimeter, measures the impact point of charged particles at small angles with respect to the positron beam direction.

The iron return yoke for the magnet is instrumented with proportional counters. This backing calorimeter (BAC) measures any hadronic energy which 'leaks out' out of the main calorimeter. Beyond that and in the forward direction there are further detectors for muon detection.

Downstream of the main detector in the proton direction, six measuring stations are installed in the proton ring for detecting forward scattered protons. Beyond the final station, further downstream, is a forward neutron calorimeter. In the electron direction, two lead scintillator calorimeters placed -35 m and -107 m from the interaction point measure the lumi-

nosity and tag events with a small momentum transfer [5].

A fuller description of the ZEUS detector can be found in reference [6]. The H1 detector is of a very similar layout as ZEUS and a description can be found in reference [7].

2 DIS Kinematics

The event kinematics of deep inelastic scattering, DIS, are determined by the negative square of the four-momentum transfer at the positron vertex, $Q^2 \equiv -q^2$, and the Bjorken scaling variable, $x = Q^2/2P \cdot q$, where P is the four-momentum of the proton. In the Quark Parton Model (QPM), the interacting quark from the proton carries the four-momentum xP. The variable y, the fractional energy transfer to the proton in its rest frame, is related to x and Q^2 by $y \simeq Q^2/xs$, where $\sqrt{s}$ is the positron-proton centre of mass energy. Because the H1 and ZEUS detectors are almost hermetic the kinematic variables x and Q^2 can be reconstructed in a variety of ways using combinations of electron and hadronic system energies and angles [8].

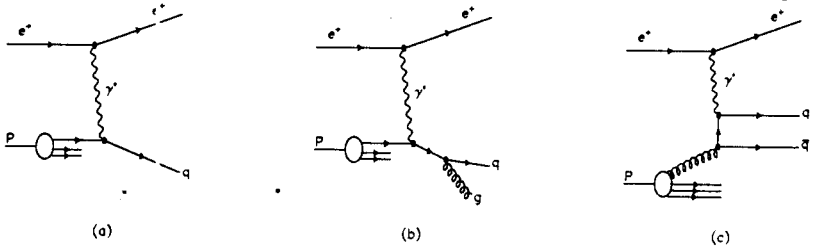

Figure 2: (a) QPM (b) QCDC and (c) BGF diagrams

In QPM there is a 1+1 parton configuration, fig. 2a, which consists of a single struck quark and the proton remnant, denoted by "+1". At HERA energies there are significant higher-order Quantum Chromodynamic (QCD) corrections: to leading order in the strong coupling constant, α_s, these are QCD-Compton scattering (QCDC), where a gluon is radiated by the scattered quark and Boson-Gluon-Fusion (BGF), where the virtual boson and a gluon fuse to form a quark-antiquark pair. Both processes have 2+1 partons in the final state, as shown in fig. 2. There also exists calculations for the higher, next-to-leading (NLO) processes.

Perturbative QCD does not predict the absolute value of the parton densities within the proton but determines how they vary from a given

input. For a given initial distribution at a particular scale Altarelli-Parisi (DGLAP) evolution [9] enables the distributions at higher Q^2 to be determined. DGLAP evolution resums the leading $\log(Q^2)$ contributions associated with a chain of gluon emissions. At large enough electron-proton centre-of-mass energies there is a second large variable $1/x$ and, therefore, it is also necessary to resum the $\log(1/x)$ contributions. This is acheived by using the BFKL equation [10].

3 Jet Physics

To relate the hadronic final state to the underlying hard partonic behaviour it is generally necessary to apply a jet algorithm. The JADE algorithm [11] has been used in the following analyses as it was, at the time, the only algorithm which allowed comparison to the NLO calculations (PROJET [12] and DISJET [13]). The JADE algorithm is a cluster algorithm based on the scaled invariant mass-squared

$$y_{ij}^{\mathrm{JADE}} = \frac{2E_iE_j(1-\cos\theta_{ij})}{W^2} \ .$$

for any two objects i and j assuming that these objects are massless. W^2 is the squared invariant mass of the hadronic final state and θ_{ij} is the angle between the two objects of energies E_i and E_j. The minimum y_{ij} of all possible combinations is found. If the value of this minimum y_{ij} is less than the variable cut-off parameter y_{cut}, the two objects i and j are merged into a new object by adding their four-momenta and the process is repeated until all $y_{ij} > y_{cut}$. The surviving objects are called jets which represent the underlying partonic structure that is dependent on α_s.

Figures 3a–d show the ZEUS jet rates using data taken in 1994, R_{1+1}, R_{2+1} and R_{3+1} as a function of y_{cut} for data compared with the DISJET and PROJET NLO QCD calculations for three Q^2 intervals $120 < Q^2 < 240$ GeV^2, $240 < Q^2 < 720$ GeV^2, $720 < Q^2 < 3600$ GeV^2, and the combined region $120 < Q^2 < 3600$ GeV^2. There is good agreement between the corrected $1+1$ and $2+1$ jet rates and the NLO QCD calculation over most of the range in y_{cut} shown. Both programs agree well in their prediction of the jet-rate dependence as a function of y_{cut}.

The values of $\alpha_s(Q)$ extracted by the H1 [14] and ZEUS [15] collaboration as a function of Q are shown in Fig. 4. The value of α_s was determined by varying the Λ scale parameter in the QCD calculation until the best fit

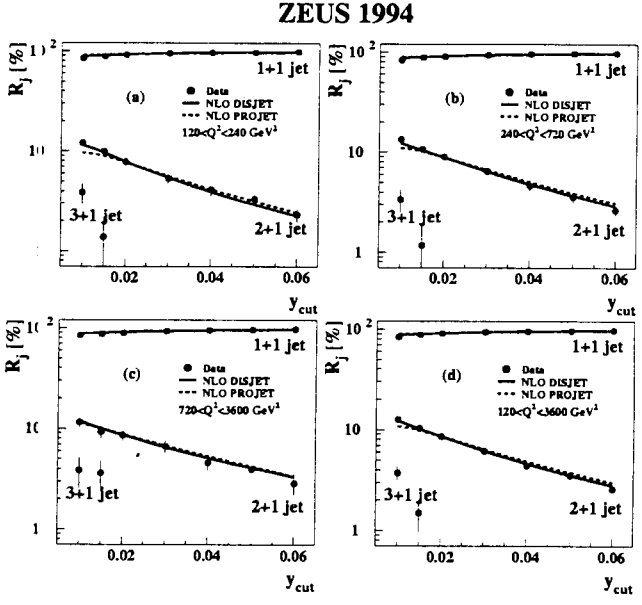

Figure 3: *Jet production rates R_j as a function of the jet resolution parameter y_{cut} for Q^2 in the range (a) $120 < Q^2 < 240\ GeV^2$, (b) $240 < Q^2 < 720\ GeV^2$, (c) $720 < Q^2 < 3600\ GeV^2$, and (d) $120 < Q^2 < 3600\ GeV^2$. Only statistical errors are shown. Two NLO QCD calculations, DISJET and PROJET, each with the value of $\Lambda_{\overline{MS}}$ obtained from the fit at y_{cut}=0.02, are also shown.*

to the ratio R_{2+1} was obtained at a particular value of y_{cut}. The measured α_s decreases with increasing Q, consistent with the running of the strong coupling constant, with Q^2 taken as the scale. In addition the figure shows the curves for $\Lambda^{(5)}_{\overline{MS}} = 100$, 200, and 300 MeV. An extrapolation to $\alpha_s(M_z)$ yields:

$$\text{H1 93}: \quad \alpha_s(M_z) = 0.123 \pm 0.012(\text{stat}) \pm 0.013(\text{syst.})$$
$$\text{ZEUS 94}: \quad \alpha_s(M_z) = 0.117 \pm 0.005(\text{stat})^{+0.005}_{-0.004}(\text{exp.}) \pm 0.007(\text{th.})$$

which are consistent with other values obtained from a large variety of different processes as shown Fig. 4 (see [16] for references). Even with the current statistics the HERA measurements are already competitive with those made elsewhere.

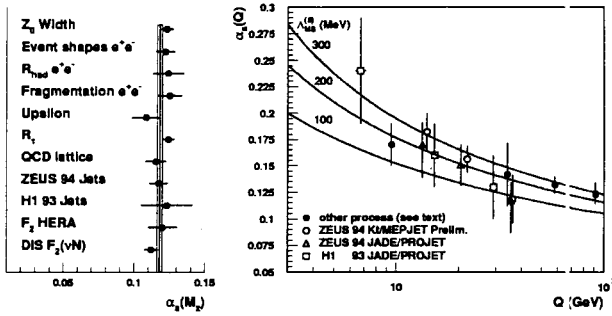

Figure 4: *Left: Values and total error of $\alpha_s(M_Z)$ from various processes. The solid line indicates the world average and the band its total error. Right: $\alpha_s(Q)$ from HERA (open symbols) and other processes with increasing Q (closed circles): Γ_Υ and $\sigma_{\rm had}/\sigma_{\rm tot}$, event shapes and $\Gamma_{\rm hadron}/\Gamma_{\rm lepton}$ in e^+e^-.*

Recently two new, more flexible NLO calculations (MEPJET [17] and DISENT [18]) have become available allowing the experiments to analyze the data using any particular jet algorithm. The k_T algorithm [19] is particularly suited for DIS as it allows factorization between the beam fragmentation and the hard process [20]. The ZEUS collaboration has reanalyzed [21] their 1994 data using this algorithm. The preliminary values of $\alpha_s(Q)$ obtained in the three bins of Q are shown (with statistical errors only) in Fig. 4 and are consistent with the results obtained with the JADE algorithm.

4 Event Shapes

A natural frame in which to study the dynamics of the hadronic final state in DIS is the Breit frame [22]. In this frame the exchanged virtual boson is purely space-like with 3-momentum $\mathbf{q} = (0, 0, -Q)$, the incident quark carries momentum $Q/2$ in the positive Z direction, and the outgoing struck quark carries Q/2 in the negative Z direction. A final state particle has a 4-momentum p^B in this frame, and is assigned to the current region if p_Z^B is negative, and to the target frame if p_Z^B is positive. The advantage of this frame lies in the maximal separation of the outgoing parton from

radiation associated with the incoming parton and the proton remnant, thus providing the optimal environment for the study of the fragmentation of the outgoing parton.

Event shape variables have been investigated in e^+e^- experiments and used to extract the strong coupling constant $\alpha_s(M_Z)$ independent of any jet algorithm, see *eg* ref. [23]. H1 have recently performed a similar analysis [24] in deep inelastic scattering in the current fragmentation region of the Breit frame.

The event shape dependence on Q (or energy dependence) can be due to the logarithmic change of the strong coupling constant $\alpha_s(Q) \propto 1/\ln Q$, and/or power corrections (hadronisation effects) which are expected to behave like $1/Q$. Recent theoretical developments suggest that $1/Q$ corrections are not necessarily related to hadronisation, but may instead be a universal soft gluon phenomenon associated with the behaviour of the running coupling at small momentum scales [25, 26].

H1 have analysed a number of infrared safe (ie independent of the number of partons produced) event shape variables. Their definitions are given below, where the sums extend over all hadrons h (being a calorimetric cluster in the detector or a parton in the QCD calculations) with four-momentum $p_h^B = \{E_h^B, \mathbf{p}_h^B\}$ The current hemisphere axis $\mathbf{n} = \{0, 0, -1\}$ coincides with the virtual boson direction.

- **Thrust T_c**

$$T_c = \max \frac{\sum_h |\mathbf{p}_h^B \cdot \mathbf{n}_T|}{\sum_h |\mathbf{p}_h^B|} \qquad \mathbf{n}_T \equiv \text{thrust axis},$$

- **Thrust T_z**

$$T_z = \frac{\sum_h |\mathbf{p}_h^B \cdot \mathbf{n}|}{\sum_h |\mathbf{p}_h^B|} = \frac{\sum_h |\mathbf{p}_{z\,h}^B|}{\sum_h |\mathbf{p}_h^B|} \qquad \mathbf{n} \equiv \text{hemisphere axis},$$

- **Jet Broadening B_c**

$$B_c = \frac{\sum_h |\mathbf{p}_h^B \times \mathbf{n}|}{2 \sum_h |\mathbf{p}_h^B|} = \frac{\sum_h |\mathbf{p}_{\perp\,h}^B|}{2 \sum_h |\mathbf{p}_h^B|} \qquad \mathbf{n} \equiv \text{hemisphere axis},$$

- **Scaled Jet Mass ρ_c**

$$\rho_c = \frac{M^2}{Q^2} = \frac{(\sum_h p_h^B)^2}{Q^2}.$$

A common characteristic of the mean event shape values $\langle 1 - T_c \rangle$, $\langle 1 - T_z \rangle$, $\langle B_c \rangle$ and $\langle \rho_c \rangle$ is the fact that they exhibit a clear decrease with rising Q, fig. 5. This is due to fact that the energy flow becomes more collimated along the event shape axis as Q increases, a phenomenon also observed in e^+e^- annihilation experiments.

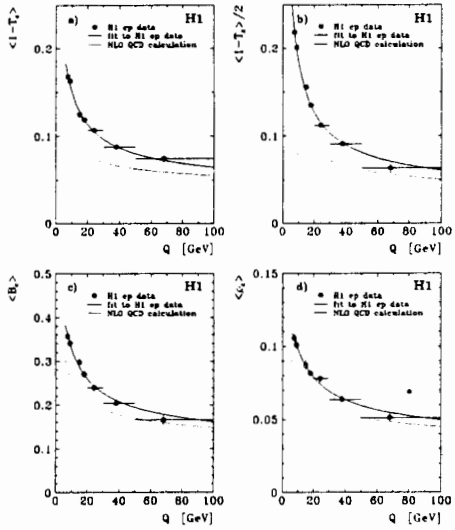

Figure 5: *Mean event shape variables as a function of Q for* **a)** $\langle 1 - T_c \rangle$, **b)** $\langle 1 - T_z \rangle / 2$, **c)** $\langle B_c \rangle$, *and* **d)** $\langle \rho_c \rangle$. *H1 DIS ep data (•, errors include statistics and systematics) are compared with QCD fits (—) and second order QCD calculations (· · ·)*

H1 showed by fitting to the data in fig. 5 all the event shape variables can be well described by just the first order power corrections $\propto 1/Q$, without the need for any higher order corrections. The second order perturbative QCD parton predictions are also shown and their discrepancies with the data show that the power corrections are substantial at low values of Q, but become less important with increasing energy.

The analysis of the event shapes give results consistent with each other for $\bar{\alpha}_0$, the power correction parameter thus supporting the prediction of universality [25], and also gives consistent values of $\alpha_s(M_Z)$. The results of the fit are $\bar{\alpha}_0 = 0.491 \pm 0.003$ (exp) $^{+0.079}_{-0.042}$ (theory) for the power correction

parameter and $\alpha_s(M_Z) = 0.118 \pm 0.001$ (exp) $^{+0.007}_{-0.006}$ (theory) for the strong coupling constant in the $\overline{\rm MS}$ scheme. These values are compatible with those extracted by e^+e^- experiments [27]

5 Fragmentation Functions

Fragmentation functions represent the probability for a parton to fragment into a particular hadron carrying a certain fraction of the parton's energy. Fragmentation functions incorporate the long distance, non-perturbative physics of the hadronization process in which the observed hadrons are formed from final state partons of the hard scattering process and, like structure functions, cannot be calculated in perturbative QCD, but can be evolved from a starting distribution at a defined energy scale. If the fragmentation functions are combined with the cross sections for the inclusive production of each parton type in the given physical process, predictions can be made for the scaled momentum, x_p, spectra of final state hadrons. Small x_p fragmentation is significantly affected by the coherence (destructive interference) of soft gluons [28], whilst scaling violation of the fragmentation function at large x_p allows a measurement of α_s [29].

In e^+e^- annihilation the two quarks are produced with equal and opposite momenta, $\pm\sqrt{s}/2$. This can be compared with a quark struck from within the proton with outgoing momentum $-Q/2$ in the Breit frame. In the direction of the struck quark (the current fragmentation region) the particle momentum spectra, $x_p = 2p^B/Q$, are expected to have a dependence on Q similar to those observed in e^+e^- annihilation [30, 31, 32] at energy $\sqrt{s} = Q$.

The inclusive charged particle distributions [33, 34], $(1/\sigma_{tot})d\sigma/dx_p$, are shown in figure 6 plotted in bins of fixed x_p as a function of Q^2. For $Q^2 > 80$ GeV^2 the distributions rise with Q^2 at low x_p and fall-off at high x_p and high Q^2. By measuring the amount of scaling violation one can ultimately measure the amount of parton radiation and thus determine α_s. Below $Q^2 = 80$ GeV^2 the fall off is due to depopulation of the current region.

The results can be compared to the next-to-leading order (NLO) QCD calculations, as implemented in CYCLOPS [35], of the charged particle inclusive distributions in the restricted region $Q^2 > 80$ GeV^2 and $x_p > 0.1$, where the theoretical uncertainties are small, unaffected by the hadron mass effects which are not included in the fragmentation function. This

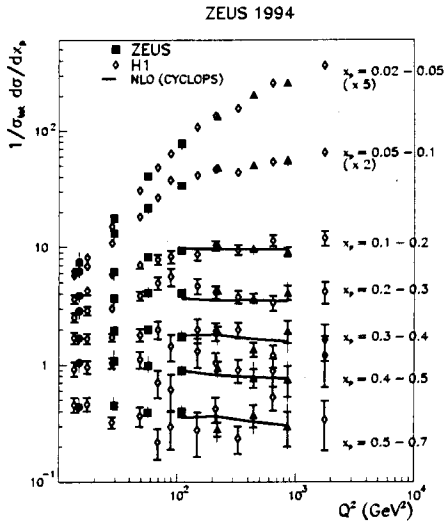

Figure 6: *The inclusive charged particle distribution, $1/\sigma_{tot}\ d\sigma/dx_p$, in the current fragmentation region of the Breit frame compared to the NLO calculation, CYCLOPS [35].*

comparison is shown in figure 6. The NLO calculation combines a full next-to-leading order matrix element with the MRSA′ parton densities (with a $\Lambda_{\overline{\rm MS}} = 230$ MeV) and NLO fragmentation functions derived by Binnewies et al. from fits to e^+e^- data [36]. The data and the NLO calculations are in good agreement, supporting the idea of universality of quark fragmentation.

The peak position of the $\xi = \ln(1/x_p)$ distributions, ξ_{peak}, was evaluated. Figure 7 shows the distribution of $\xi_{\rm peak}$ as a function of Q for the HERA data [33, 37, 38] and of $\sqrt{s}$ for the e^+e^- data. Over the range shown the peak moves from $\simeq 1.5$ to 3.0, equivalent to the position of the maximum of the corresponding momentum spectrum increasing from $\simeq 400$ to 900 MeV. The HERA data points are consistent with those from TASSO [39] data and a clear agreement in the rate of growth of the HERA points with the e^+e^- data [39, 40] is observed.

The increase of $\xi_{\rm peak}$ can be approximated phenomenologically by the straight line fit $\xi_{\rm peak} = b\ \ln(Q) + c$ also shown in figure 7. Also shown is the statistical fit to the data when $b = 1$ which would be the case if the QCD cascade was of an incoherent nature, dominated by cylindrical phase space. (A discussion of phase space effects is given in [41].) In such

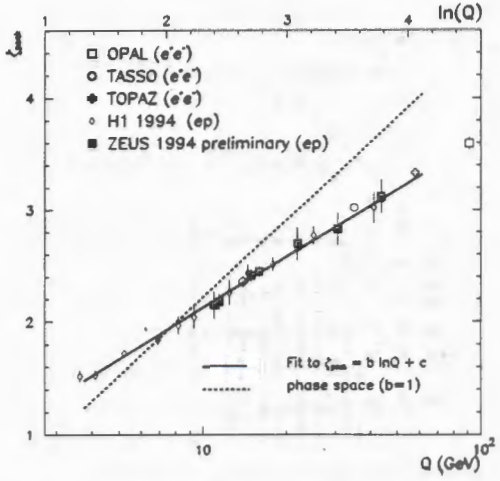

Figure 7: ξ_{peak} *as a function of* Q. *The HERA data are compared to results from OPAL, TASSO and TOPAZ. A straight line fit of the form* $\xi_{peak} = b\ ln(Q) + c$ *to the ZEUS* ξ_{peak} *values is indicated as well as the line corresponding to* $b = 1$, *discussed in the text.*

a case, the logarithmic particle momentum spectrum would be peaked at a constant value of momentum, independent of Q. The observed gradient is clearly inconsistent with $b = 1$ and therefore inconsistent with cylindrical phase space thus supporting the coherent nature of gluon radiation.

6 BFKL versus DGLAP Evolution

In the DGLAP parton evolution scheme [9] the parton cascade follows a strong ordering in transverse momentum $k^2_{Tn} \gg k^2_{Tn-1} \gg ... \gg k^2_{T1}$, while there is only a soft (kinematical) ordering for the fractional momentum $x_n < x_{n-1} < ... < x_1$. However for low-$x$ at HERA the BFKL scheme [10] could well be the dominant scheme. In this scheme the cascade follows a strong ordering in fractional momentum $x_n \ll x_{n-1} \ll ... \ll x_1$, while there is no ordering in transverse momentum.

BFKL evolution can be enhanced by studying DIS events which contain an identified jet of longitudinal momentum fraction $x_{jet} = p_z(j)/E_{proton}$ (in the proton direction) which is large compared to Bjorken x [42]. By tagging a forward jet with $p_T(j) \simeq Q$ this allows minimal phase space for DGLAP

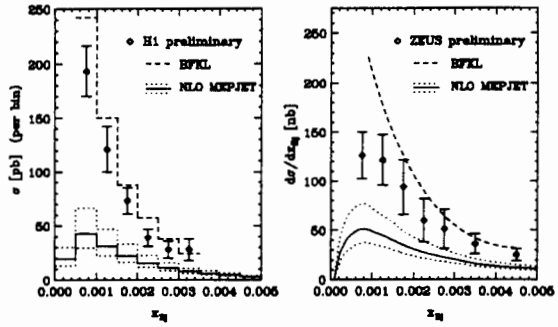

Figure 8: *Forward jet cross section at HERA as a function of Bjorken x within (a) the H1 [44] and (b) the ZEUS [45] acceptance cuts. The BFKL result of Bartels et al. [46] is shown as the dashed line. The solid and dotted line give the NLO MEPJET result and a measure for the uncertainity of NLO prediction through changes in the choice of scale.*

evolution while the condition $x_{jet} \gg x$ leaves BFKL evolution active. This leads to the forward jet production cross section in BFKL dynamics being larger than that of the $\mathcal{O}(\alpha_S^2)$ QCD calculation with DGLAP evolution [43].

In Fig. 8, recent data from H1 [44] and ZEUS [45] are compared with BFKL predictions [46] and fixed order QCD predictions as calculated with the MEPJET [17] program at NLO. The conditions $p_T(j) \simeq Q$ and $x_{jet} \gg x$ are satisfied in the two experiments by slightly different selection cuts. H1 selects events with a forward jet of $p_T(j) > 3.5$ GeV (in the angular region $7^\circ < \theta(j) < 20^\circ$) with

$$0.5 < p_T(j)^2/Q^2 < 2\,, \qquad x_{jet} \simeq E_{jet}/E_{proton} > 0.035\,; \qquad (1)$$

while ZEUS triggers on somewhat harder jets of $p_T(j) > 5$ GeV and $\eta(j) < 2.4$ with

$$0.5 < p_T(j)^2/Q^2 < 4\,, \qquad x_{jet} = p_z(j)/E_{proton} > 0.035\,. \qquad (2)$$

Fig. 8 shows that both experiments observe substantially more forward jet events than expected from NLO QCD. A very rough estimate of the uncertainty of the NLO calculation is provided by the two dotted lines, which correspond to variations by a factor 10 of the renormalisation and

factorisation scales μ_R^2 and μ_F^2. A recent BFKL calculation (dashed lines) gives a better agreement with the data. The overall normalisation in this calculation is uncertain and the agreement may be fortuitous, indeed it should also be noted that both experiments observe more centrally produced dijet events than predicted by the NLO QCD calculations. Further careful investigation is necessary before claiming that BFKL is the mechanism for this enhanced forward jet production.

7 Conclusions

To understand the underlying QCD processes in DIS it is necessary to study the hadronic final state. At the current level of understanding, QCD works well and describes the HERA data. As the precision of the HERA data improves and the NLO QCD calculations become available the framework of QCD is being tested more thoroughly. As yet it is not possible to say conclusively whether the effects of BFKL dynamics are being observed in the HERA data, much theoretical and experimental work is in progress to define and measure variables that will allow a definitive statement.

Acknowledgements

I would like to thank the organising committee for inviting me to the school and providing such a pleasant and enjoyable environment.

References

[1] C. Alvisi et al., Nucl. Inst. Meth. A305 (1991) 30.

[2] N. Harnew et al., Nucl. Inst. Meth. A279 (1989) 290; B. Foster et al., Nucl. Phys. B (Proc. Suppl.) 32 (1993) 181; B. Foster et al., Nucl. Inst. Meth. A338 (1994) 254.

[3] M. Derrick et al., Nucl. Inst. Meth. A309 (1991) 77; A. Andresen et al., Nucl. Inst. Meth. A309 (1991) 101; A. Bernstein et al., Nucl. Inst. Meth. A336 (1993) 23.

[4] ZEUS Collab., M. Derrick et al., Z. Phys. C72 (1996) 399.

[5] J. Andruszków et al., DESY 92-066 (1992).

[6] ZEUS Collab., The ZEUS Detector, Status Report 1993, DESY 1993.

[7] H1 Collaboration, I. Abt et al., DESY preprint 93-103 (1993), Nucl. Instr. Meth. A386 (1997) 310 (Vol 1) and *ibid.* p.348 (Vol 2).

[8] S. Bentvelsen, J. Engelen and P. Kooijman, Proceedings of the 1991 Workshop on Physics at HERA, DESY Vol. 1 (1992) 23.

[9] G. Altarelli and G. Parisi, Nucl. Phys. 126 (1977) 297; V.N. Gribov and L.N. Lipatov, Sov. J. Nucl. Phys. 15 (1972) 438 and 675; Yu. L. Dokshitzer, Sov. Phys. JETP 46 (1977) 641.

[10] E.A. Kuraev, L.N. Lipatov and V.S. Fadin, Sov. Phys. JETP 45 (1977) 199; Y.Y. Balitsky and L.N. Lipatov, Sov. J. Nucl. Phys. 28 (1978) 282.

[11] JADE Collab., W. Bartel et al., Z. Phys. C33 (1986) 23;
JADE Collab., S. Bethke et al., Phys. Lett. B213 (1988) 235.

[12] D. Graudenz, CERN-TH.7420/94 (1994), to appear in Comp. Phys. Comm.

[13] T. Brodkorb and E. Mirkes, Univ. of Wisconsin, MAD/PH/821 (1994).

[14] H1 Collab., T. Ahmed et al., Phys. Lett. B346 (1995) 415.

[15] ZEUS Collab., M. Derrick et al., Phys. Lett. B363 (1995) 201.

[16] Particle Data Group, R.M. Barnett et al., Phys. Rev. D54 (1996).

[17] E. Mirkes and D. Zeppenfeld, Phys. Lett. B380 (1996) 205.

[18] S. Catani and M. Seymour, Nucl. Phys. B 485 (1997) 291 and hep-ph/9605323;

[19] S. Catani, Y. Dokshitzer and B. Webber, Phys. Lett. B285 (1992) 291.

[20] B. R. Webber, J. Phys. G19 (1993) 1567.

[21] T. Trefzger, Proc. of the Int. Workshop on DIS and Related Phenomena, ed. G. D'Agostini and A. Nigro, Rome, 1996.

[22] R.P. Feynman, "Photon-Hadron Interactions", Benjamin, N.Y. (1972).

[23] S. Bethke, Proceedings *QCD 94*, Montpellier, ed. S Narison, Nuc . Phys. B (Proc. Suppl.) 39 B, C (1995), p. 198.

[24] H1 collab., C. Aloff et al., DESY-97-098. [hep-ex/9706002]

[25] B.R. Webber, Proceedings *Workshop on Deep Inelastic Scattering and QCD*, Paris (1995), eds. J.F. Laporte and Y. Sirois, p. 115; M. Dasgupta and B.R. Webber, preprint Cavendish-HEP-96/5 and hep-ph/9704297.

[26] Yu.L. Dokshitzer and B.R. Webber, Phys. Lett. B 352 (1995) 451; Z. Kunszt, P. Nason, G. Marchesini and B.R. Webber, *Z Physics at LEP 1*, eds. G. Altarelli, R. Kleiss and C. Verzegnassi, CERN 89-08, vol. 1, p. 373.

[27] PLUTO Collaboration, Ch. Berger et al., Z. Phys. C 12 (1982) 297; Mark II Collaboration, A. Peterson et al., Phys. Rev. D 37 (1988) 1; TASSO Collaboration, W. Braunschweig et al., Z. Phys. C 45 (1989) 11 and Z. Phys. C 47 (1990) 187; AMY Collaboration, Y.K. Li et al., Phys. Rev. D 41 (1990) 2675; DELPHI Collaboration, P. Abreu et al., Z. Phys. C 73 (1997) 229.

[28] Yu. Dokshitzer, V. Khoze, A. Mueller and S. Troyan, "Basics of Perturbative QCD", Editions Frontières, Gif-sur-Yvette, France (1991).

[29] G. Altarelli et al., Nucl. Phys. B160 (1979) 301; P. Nason and B. R. Webber, Nucl. Phys. B421 (1994) 473.

[30] Yu. Dokshitzer et al., Rev. Mod. Phys. 60 (1988) 373.

[31] A. V. Anisovich et al., Il Nuovo Cimento, A106 (1993) 547.

[32] K. Charchuła, J. Phys. G19 (1993) 1587.

[33] H1 collab., C. Adloff et al., DESY-97-158 [hep-ex/9707005 fig. 2 amended 15th August 1997]

[34] ZEUS collab., J. Breitweg et al., DESY-97-183.

[35] D. Graudenz, CERN-TH/96-52; D. Graudenz, CYCLOPS program and private communication.

[36] J. Binnewies et al., Z Phys C65 (1995) 471.

[37] ZEUS Collaboration, M. Derrick et al., Z. Phys. C67 (1995) 93.

[38] H1 Collaboration, S. Aid et al., Nucl. Phys. 445B (1995) 3.

[39] TASSO Collab., W. Braunschweig et al., Z. Phys. C47 (1990) 187; TASSO Collab., W. Braunschweig et al., Z. Phys. C22 (1984) 307.

[40] OPAL Collab., M. Akrway et al., Phys. Lett. B247 (1990) 617. TOPAZ Collab., R. Itoh et al., Phys. Lett. B345 (1995) 335.

[41] E.R. Boudinov, P.V. Chliapnikov and V.A. Uvarov, Phys. Lett. B309 (1993) 210.

[42] A.H. Mueller, Nucl. Phys. B (Proc. Suppl.) 18C (1990) 125; J. Phys. G17 (1991) 1443; J. Kwiecinski, A.D. Martin and P.J. Sutton, Phys. Rev. D46 (1992) 921; W.K. Tang, Phys. Lett. B278 (1992) 363.

[43] E. Mirkes and D. Zeppenfeld, Phys. Rev. Lett. 78 (1997) 428 [hep-ph/9609231].

[44] M. Wobisch, to appear in proceedings of DIS97 (and references therein).

[45] S. Wölfle, to appear in proceedings of DIS97

[46] J. Bartels et al., Phys. Lett. B384 (1996) 300 [hep-ph/9604272].

CP Violation and Future 'B-Factories'

N. H. Brook
Dept. of Physics & Astronomy,
University of Glasgow.
Glasgow, United Kingdom.

Abstract

This lecture contains a brief introduction to CP violation in the B system before discussing future experimental programmes and their CP reach in the B system.

1 CP Violation in the B-system

Quark mixing in the standard model is described by the Cabibbo-Kobayashi-Maskawa (CKM) matrix [1], eqn(1). Conventionally the u, c and t quarks are unmixed and the mixing is described by the 3×3 V_{CKM} matrix operating on the d, s and b quarks. The matrix elements of V_{CKM} can, in principle, be determined by measuring the charged current coupling to the $W^{\pm}$ bosons.

$$V_{CKM} \equiv \begin{pmatrix} V_{ud} & V_{us} & V_{ub} \\ V_{cd} & V_{cs} & V_{cb} \\ V_{td} & V_{ts} & V_{tb} \end{pmatrix} \tag{1}$$

The CKM matrix is unitary ie $V_{CKM}^{\dagger} V_{CKM} = 1$, which leads to 9 unitarity conditions expressed in terms of the matrix elements. There are several (approximate) parameterisations of the CKM matrix, one of the more popular approaches is that of Wolfenstein [2], eqn(2), where the matrix elements are expressed in terms of powers of $\lambda = \sin\theta_c$, where θ_c is the Cabibbo angle. As can be seen from this parameterisation, the 9 complex elements of the matrix can be expressed in terms of 4 independent variables; three real parameters A, λ and ρ and an imaginary part of a complex number, η. The 18 parameters of the CKM matrix can be reduced to 4 because of the unitarity constraints and the arbitrary nature of the relative quark phases [3]. It is the complex phase in the V_{CKM} that leads to CP violation in the standard model.

$$V_{\text{Wolfenstein}} = \begin{pmatrix} 1 - \frac{1}{2}\lambda^2 & \lambda & A\lambda^3(\rho - i\eta) \\ -\lambda & 1 - \frac{1}{2}\lambda^2 & A\lambda^2 \\ A\lambda^3(1 - \rho - i\eta) & -A\lambda^2 & 1 \end{pmatrix} \tag{2}$$

The unitarity condition

$$V_{ud}V_{ub}^* + V_{cd}V_{cb}^* + V_{td}V_{tb}^* = 0$$

is of particular interest since $V_{ud} \simeq V_{tb} \simeq 1$ and $V_{ts}^* \simeq -V_{cb}$. This allows us to depict this condition as a triangle in the complex plane, as shown in fig 1. The angles of the triangle α, β and γ are related to the phase and can be measured in CP violating B-decays.

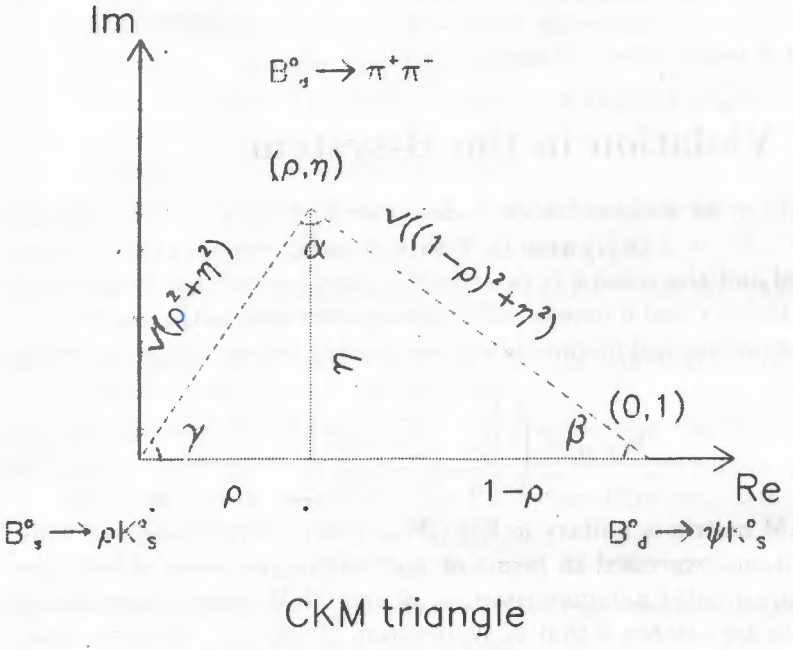

Figure 1: *The CKM unitarity triangle in the Wolfenstein parameterisation*

The non-closure of this triangle ie $\alpha + \beta + \gamma \neq \pi$ would suggest that our understanding of CP violation within the Standard Model was incomplete. Physics beyond the Standard Model can be further investigated, for example, by measuring CP asymmetries in several B decays that depend on the same unitarity angle or studying decays where zero asymmetries are expected in the Standard Model.

CP violation in the B system should be observable through the phenomenon of $B^0 - \bar{B}^0$ mixing, see for example [4]. This $B^0 - \bar{B}^0$ mixing is dominated by box-diagrams with virtual $t-$quarks, fig 2.

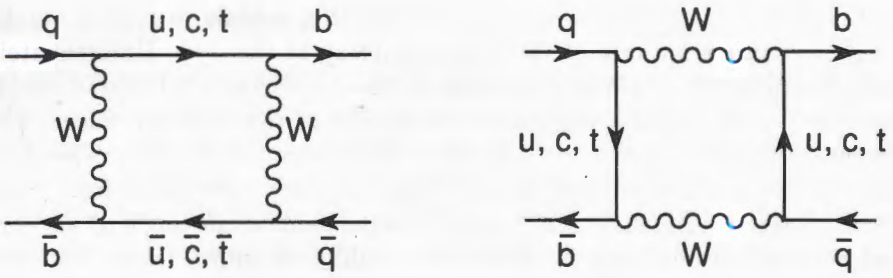

Figure 2: $B^0 - \bar{B}^0$ *mixing diagrams.*

The following decays

$$\begin{aligned} B_d^0 &\rightarrow J/\psi K_s^0 \\ B_d^0 &\rightarrow \pi^+\pi^- \\ B_s^0 &\rightarrow \rho K_s^0 \end{aligned} \tag{3}$$

are into a CP eigenstate. If this is coupled with only a single diagram contributing to the decay, CP asymmetries can be constructed which are directly related to the angles of the unitarity triangle. For example, these conditions occur for the decay mode $B_d^0 \rightarrow J/\psi K_s^0$. Here the number of B_d^0 which decay at time t (where t is expressed in units of lifetime) is proportional to

$$n(t) \propto e^{-t}(1 + \sin 2\beta \sin xt) \tag{4}$$

and the number of $\bar{B}_d^0$ is proportional to

$$\bar{n}(t) \propto e^{-t}(1 - \sin 2\beta \sin xt) \tag{5}$$

where the mixing parameter, $x = \Delta M/\Gamma \simeq 0.67$, is the ratio of the mass difference of the eigenstates to their decay rate. The CP asymmetry can then be defined as

$$a(t) = \frac{n(t) - \bar{n}(t)}{n(t) + \bar{n}(t)} = \sin 2\beta \sin xt.$$

By integrating eqns. (4) and (5) over time a similar asymmetry can be constructed which is proportional to $\sin 2\beta$. (Although for coherent B production ie the $B\bar{B}$ pair is produced in a definite CP state, this time

integrated asymmetry is zero.) In addition this channel is experimentally very promising because of the dilepton decay of the J/ψ. Unfortunately additional decay diagrams contribute to the other channels listed in eqn(3) so there is no longer a complete cancellation of the hadronic matrix elements in the CP asymmetry. The $B_d^0 \to \pi^+\pi^-$ channel, which is dependent on the angle α is predicted to have large hadronic corrections from 'penguin' diagrams, fig. 3. The $B_s^0 \to \rho K_s^0$ (dependent on the angle γ) also has additional hadronic contributions but, in addition, suffers from a very low branching fraction. Fortunately there are, of course, many other channels which can be used to measure CP violation, eg see ref. [5].

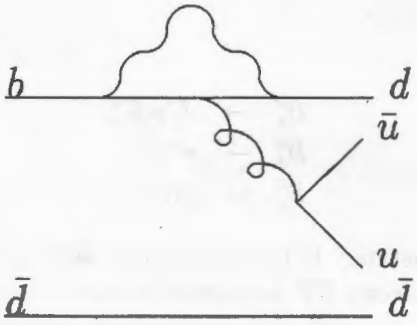

Figure 3: *'Penguin' contribution to* $B_d^0 \to \pi^+\pi^-$ *decay*

2 B-Production Facilities

Because of the small visible branching ratios of decays to CP eigenstates, $\mathcal{O}(10^{-5})$, a large number of B meson must be produced in order to study CP violation in the B system. There are two complimentary ways to achieve the necessary large number of B mesons. The first is at e^+e^- colliders at centre of mass energy of 10 GeV to produce the $\Upsilon(4S)$ which then decays to two B mesons. Alternatively high energy hadron machines, where there is a large cross section for $b\bar{b}$ production, can be used to produce the B mesons. The pros and cons of the various approaches are discussed in this sections.

2.1 e^+e^- Colliders

B meson production via e^+e^- colliders is being pursued at laboratories in the United States (Cornell and SLAC) and Japan (KEK). The luminosity at these machines is of the $\mathcal{O}(10^{33})$ cm^{-2}s^{-1} which is equivalent to approximately 4 $b\bar{b}$ pairs produced every second. Because the B mesons produced from the decay of $\Upsilon(4S)$ are coherent it is necessary to be able to measure the time separation between the two B's in order to measure the CP asymmetry through $B^0 - \bar{B}^0$ mixing. To give the $\Upsilon(4S)$ sufficient boost to allow the two B^0 decay vertices to be reconstructed and thus the distance between the two B mesons to be measured, the beam energies at SLAC and KEK are asymmetric. The Cornell B-facility has symmetric beam energies and will be unable to measure CP asymmetry through $B^0 - \bar{B}^0$ mixing though there are possibilities to measure CP violation through the decays of charged B's. The KEK and SLAC facilities are asymmetric with $e^-(e^+)$ energies of 3.5 GeV (8 GeV) and 3.1 GeV (9 GeV) respectively. The need for the large luminosity and the asymmetric beam energies poses great challenges on the machine design. The advantages of this approach is the very clean production environment of the $\hat{2}$ B mesons, with no underlying event from which to extract the signal. By running at the mass of $\Upsilon(4S)$ it is not possible, simply by kinematic contraints, to study the B_s system. In order to study the B_s system the machine can be operated with energies at the mass of $\Upsilon(5S)$ but the cross sections are much smaller.

2.2 Hadron Colliders

The high energy hadron machines, Tevatron and HERA (in fixed target mode with a wire target inserted into the proton beam halo), are already producing large numbers of B mesons. The LHC will produce even greater numbers. At the Tevatron the $b\bar{b}$ production rate is $\mathcal{O}(10^4)$ Hz and at LHC it will be $\mathcal{O}(10^5)$ Hz compared to the $\simeq$ 4 Hz at SLAC and KEK. The problem in this approach is achieving high enough reconstruction and tagging efficiencies in order to extract a sufficient number of B's to measure CP violation. The LHC has an additional benefit over the Tevatron and HERA because with the increasing centre of mass energy the ratio of the $b\bar{b}$ cross section over the total inelastic cross section also increases. All the hadron machines also have the advantage that they can study B_s mesons.

3 The Experiments

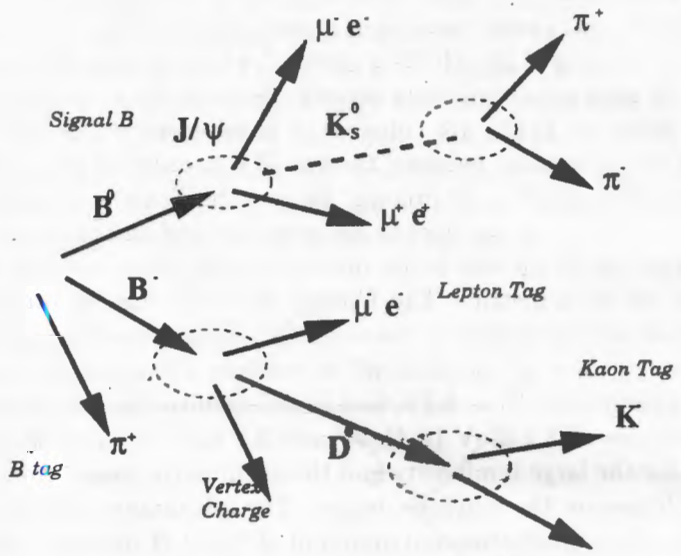

Figure 4: *Example of B tagging.*

To measure CP violation it is not only necessary to measure the decay of the B meson but also to tag its initial flavour via the decay of the accompanying B, as shown schematically in fig. 4. The generic detector requirements for an experiment to study B decays are that it has good resolution on measuring the decay time and the mass of decayed B mesons and has particle identification to allow a good initial flavour tag of the B meson. The characteristics of the detectors designed to study CP violation are discussed below.

3.1 BELLE

The BELLE detector [6] is the experimental apparatus being designed for the KEK B factory. A schematic of the detector is shown in figure 5. The detector consist of a silicon vertex detector (SVD) situated just outside the beampipe. Surrounding that there is a cylindrical wire drift chamber (CDC) that measures charged tracks which extends to a radius of 90 cm. Particle identification is provided by dE/dx measurements in the CDC, and aerogel Čerenkov counter and time of flight (TOF) arrays situated radially

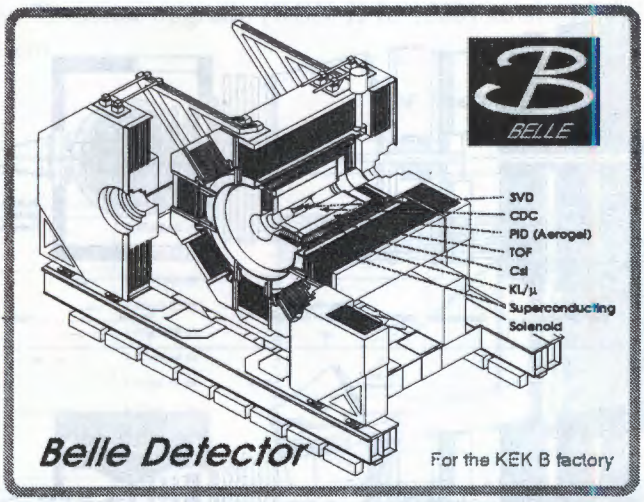

Figure 5: *Schematic of the BELLE detector at the KEK B factory.*

around the CDC. Inside the superconducting solenoid is a electromagnetic calorimeter manufactured from CsI(Tl) crystals. The iron return yoke of the 1.5 Tesla solenoid is interspersed with arrays of detectors for measuring muons and K_L^0 mesons. The design of the equivalent detector, BaBar, at the SLAC B factory is discussed in ref. [7].

3.2 HERA-B

To guarantee the observation of standard model CP violation in B decays (after folding in the detector efficiencies), interactions at the HERA-B detector have to occur approximately 4 times for every one of the 10 MHz bunch crossings of the HERA machine. The HERA-B experiment is essentially a fixed target experiment with a wire target in the beam halo [8]. A schematic of the HERA-B spectrometer is shown in fig. 6. It has a single dipole momentum spectrometer situated 4.5 m downstream of the target. Directly downstream of the target wires, but before the magnet, there is a silicon vertex detector of length of $\sim$ 2 m. The main tracking system uses a variety of technologies dependent on the distance away from the beam (Si-strips, microstrip gas counters and honeycomb-drift chambers at ever increasing radii from the beam.) This is followed by a ring imaging Čerenkov

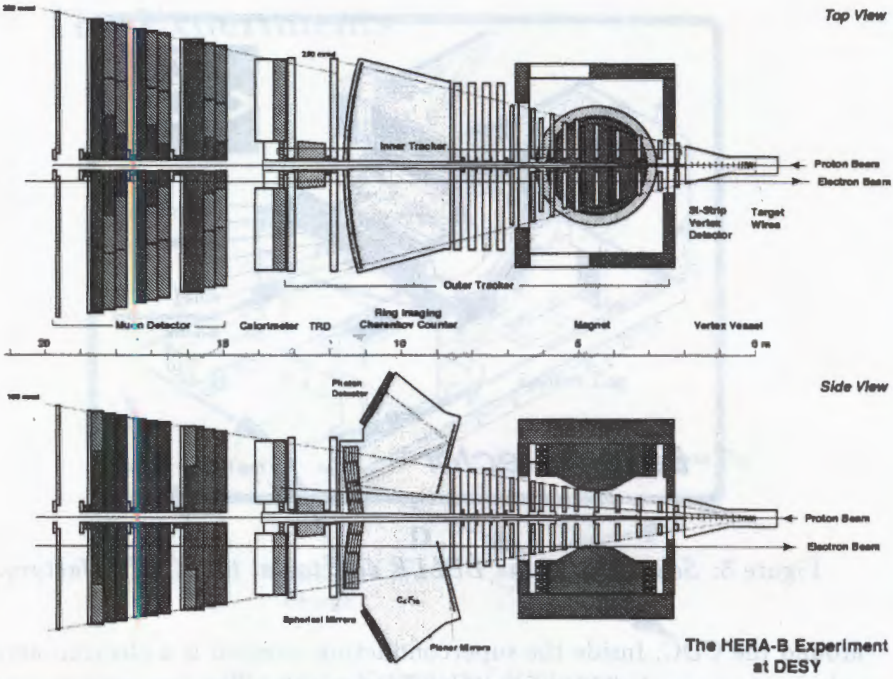

Figure 6: *Schematic of the HERA-B detector at DESY.*

(RICH) detector to tag the charged kaon and a transition radiation detector to improve electron identification. There are additional large tracking chambers immediately behind the RICH and in front of the calorimeter. The electromagnetic calorimetry is designed to use Lead/Scintillator and Tungsten/Scintillator. This is followed by a conventional muon system with four chamber layers at various depths in the absorber. The muon chambers are essential for the triggering of HERA-B when the J/ψ decays to two muons.

3.3 CDF and D0

There is already a very active B physics program at the CDF detector at the Tevatron. The B meson lifetime measurements, fig. 7, are already competetive with those of the combined LEP experiments. This proves that it is possible to extract B physics from the hostile experimental environment of the hadron colliders. Both CDF [9] and D0 [10] are hoping

to exploit the Tevatron upgrade (RUN II in 1999) to study CP violation in the B-system.

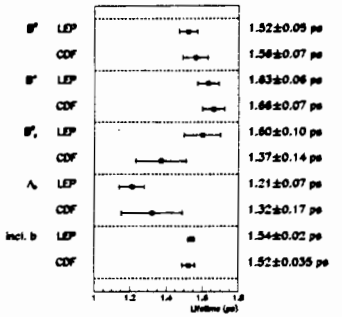

Figure 7: *A comparison of CDF and LEP B meson lifetime measurements.*

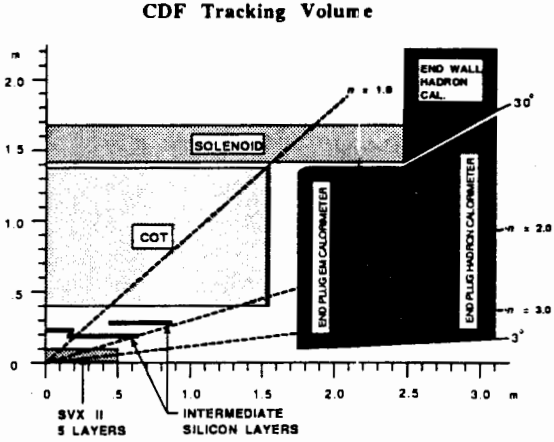

Figure 8: *Longitudinal View of the CDF II Tracking System.*

CDF are proposing a new tracking system for Run II, fig. 8. At large radii they will have a central outer tracker (COT) of an open drift chamber design. Inside this component there is a silicon inner tracker compromising of two components: a micro-vertex detector (SVX II) at very small radii and two additional layers of silicon at intermediate radii. The current forward calorimetry is going to be replaced with a new scintillating tile plug calorimeter. New chambers will be added to the current muon system to close gaps in the azimuthal acceptance and the forward acceptance will be improved. The trigger will also be upgraded to allow track finding at level-1 and the ability to trigger on large impact parameter tracks at level-2.

A major element of the D0 upgrade is their new inner tracking system which will be located insides a new 2 Tesla superconducting solenoid. It will consist of an inner silicon vertex detector, surrounded by eight superlayers of scintillating fibre tracker. In the forward region, on the face of the end calorimeter cryostats, and in the central region, located between the solenoid and the inner radius of the calorimeter cryostat, a scintillator based pre-shower detector will be installed. The trigger upgrades will include tracking triggers at level-1 and an upgraded level-2 muon triggers.

3.4 ATLAS and CMS

The ATLAS [11] and CMS [12] detectors at the LHC are optimised for high luminosity physics. But initial low luminosity running will allow these general purpose detectors to used for B physics. Both detectors are installing silicon vertex detectors close to the beampipe. More detailed discussion of these detectors and their physics performance can be found elsewhere in these proceedings [13].

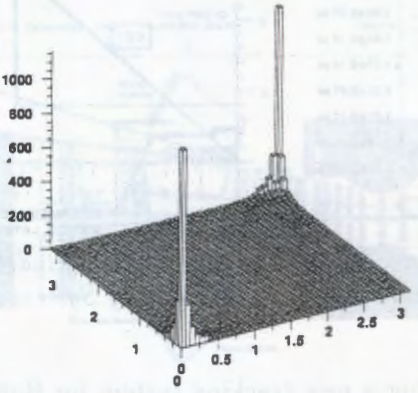

Figure 9: *Production angle of B vs. angle of* $\overline{\mathrm{B}}$ *in the laboratory (in units of rad.) at LHC calculated using the the PYTHIA Monte Carlo generator [14].*

3.5 LHC-B

At high energy hadron colliders the produced B and $\bar{B}$ mesons are correlated in the forward direction (ie close to the proton beam direction). Figure 9 shows the angular distribution of the $B\bar{B}$ mesons in the laboratory frame at LHC. This is due to the relatively low mass production of b quark pairs at collider energies. This production mechanism lends itself to dedicated experiments that are of a forward, planar design, reminiscent of those used in fixed target experiments.

Such an experiment, LHC-B, has been proposed for the LHC [15]. Its layout is shown in figure 10. LHC-B is a forward single-dipole spectrometer It consists of a silicon microvertex detector, a tracking system, aerogel

and gas RICH detectors, electromagnetic and hadronic calorimeter and a muon filter. LHC-B will be allowed to run with a defocussed beam in their interaction area which would give a nominal running luminosity $\mathcal{L} = 1.5 \times 10^{32}\ \mathrm{cm}^{-2}\mathrm{s}^{-1}$.

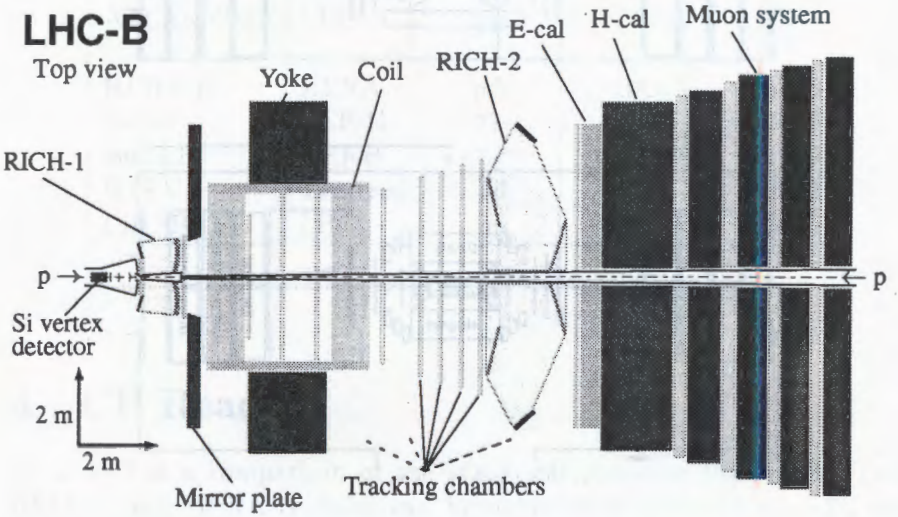

Figure 10: *Top view of the LHC-B detector*

3.6 BTeV

Recently a similarly motivated experiment (BTeV) has submitted a expression of interest at Fermilab [16]. The schematic layout of the BTeV proposal is shown in figure 11. The baseline description of the detector has a dipole magnet centred on the interaction region, thus providing the basis for a two-arm spectrometer. A vertex pixel detector (inside the magnetic field) provides high resolution tracking near the interaction. The baseline design has seven downstream tracker stations of straw tubes along both arms of the spectrometer. For identification of electromagnetic final states and kaons there is electromagnetic calorimetry and a RICH detector respectively, with a toroidal magnetic detector for muon identification and measurement. The BTeV detector relies heavily on the vertex detector for triggering of the B events.

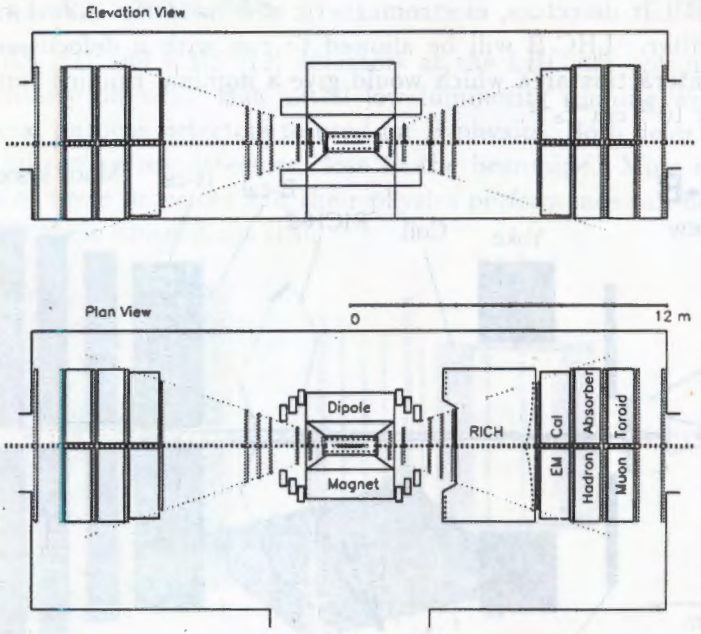

Figure 11: *Schematic Layout of the BTeV detector*

3.7 Experimental Recap

Table 1 summarises the experiments discussed previously in this section. The SLAC and KEK B factories are due to take first data before the turn of the century. Though it is important to remember that new accelerators often take 2-3 years to reach their design goals. HERA-B is already partially instrumented and is already taking data in situ in order to debug and test some of their detector components. They have already achieved the multiple interaction per bunch crossing that is necessary to meet their design considerations. CDF and D0, like the experiments at the e^+e^- machines, are due to take data again before the end of the century. With their already proven track record in B physics they should be in a good position to be the first to observe CP violation in the B system. Beyond that LHC-B and BTEV (in addition ATLAS and CMS) should be in a good position to further test and even overconstrain the unitarity triangle of CP violation in the standard model and perhaps any new physics

beyond.

Experiment	Machine	Collision Type	Centre of Mass Energy	Start
CDF/D0	Tevatron	$p\bar{p}$	2TeV	1999
ATLAS/CMS	LHC	pp	14TeV	2005
HERA-B	HERA	pN	40GeV	1998
BaBar	PEP-II	e^+e^-	$\Upsilon(4S)$	1999
BELLE	KEKB	e^+e^-	$\Upsilon(4S)$	1999
BTEV	Tevatron	$p\bar{p}$	2TeV	2002
LHC-B	LHC	pp	14TeV	2005

Table 1: *Properties of the experiments*

4 CP Reach

In table 2 is a comparison of the statistical precision that BaBar (and BELLE) and HERA-B claim can be achieved in measuring $\sin 2\alpha$ and $\sin 2\beta$ for one year's running at design luminosity. The two experiments are comparable in the $B^0 \to J/\Psi K_s^0$ channel, but there are other channels that BaBar can use, because of the clean event environment, to extract the angle α. For measuring $\sin 2\beta$ at first glance the two experiments are again comparable, but the figures quoted in the table are for zero background. HERA-B will have a background in $B^0 \to \pi^+\pi^-$ channel and the quoted figures need to be modified by a factor $\sqrt{1 + B/S}$ where B/S is the ratio of background to signal. It is thought that a value of $B/S < 1$ can be achieved [17].

Table 3 reviews the accuracy that the experiments at hadron colliders hope to achieve from 10^7 seconds running. Besides the accuracy on $\sin(2\alpha)$ and $\sin(2\beta)$, the measurement precision and upper limit of γ and x_s (comparable to x in the B_d system) are listed, which need the B_s mesons to be detected and tagged. The figures show that the dedicated experiment at the LHC, LHC-B, has by far the best reach in measuring the parameters of CP violation. It is also worth noting that the performance of the Tevatron general purpose detectors are comparable to result expected from HERA-B and thus the e^+e^- B factories. (It should be noted though the clean

Decay Channel	BaBar	HERA-B
$J/\Psi K^0_s$ evts		
$\Delta \sin 2\beta$	± 0.10	± 0.13
All channels		
$\Delta \sin 2\beta$	± 0.06	± 0.13
$\pi^+\pi^-$		
$\Delta \sin 2\alpha$	± 0.20	± 0.14
$\rho^\pm\pi^\pm$		
$\Delta \sin 2\alpha$	± 0.11	
All channels		
$\Delta \sin 2\alpha$	± 0.085	± 0.14

Table 2: *A comparison of the experimental accuracy of the BaBar and HERA-B experiments*

experimental environment in e^+e^- allows them to make a more complete study of rare B-decays.)

	CDF/D0	HERA-B	ATLAS/CMS	LHC-B	BTeV
$\Delta \sin(2\alpha)$	~ 0.10	~ 0.14	0.10/0.07	0.039	0.1
$\Delta \sin(2\beta)$	~ 0.10	~ 0.13	0.02/0.07	0.023	0.042
$\Delta\gamma$				$6 - 16°$	
x_s		≤ 17	≤ 34	≤ 55	≤ 30

Table 3: *A comparison of the experimental accuracy and reach of the experiments at hadron facilities. All but BTeV data taken from ref. [18]. BTeV limits from their EoI [16].*

5 Conclusions

There is a strong program of future experiments planning to study CP violation in the B system. The first generation experiments start taking data in the next few years. Second generation experiments are already being planned to extend the measurement of CP violation. The experiments will over constrain the unitarity triangle and perhaps indicate new physics beyond the Standard Model.

References

[1] M. Kobayashi and T. Maskawa, Prog. Theor. Phys. 49 (1973) 652.

[2] L. Wolfenstein, Phys. Rev. Lett. 51 (1983) 1945.

[3] J. L. Rosner, 'The Cabibbo-Kobayashi-Maskawa Matrix', in B Decays (World Scientific), ed. S. Stone.

[4] Y. Nir and H. R. Quinn, 'Theory of CP Violation in B Decays', in B Decays (World Scientific), ed. S. Stone.

[5] I. Dunietz, 'CP Violation with Additional B Decays', in B Decays (World Scientific), ed. S. Stone.

[6] BELLE Collab., M. T. Cheng et al., Technical Design Report, KEK-Report 95-1.

[7] BaBar Collab., D. Boutigny et al., Technical Design Report, SLAC-R-95-457.

[8] HERA-B Collab., E. Hartouni et al., Technical Design Report, DESY-PRC-95/01.

[9] CDF Collab., R. Blair et al., The CDF II Detector Technical Design Report, FERMILAB-Pub-96/390-E.

[10] D0 Collab., The D0 Upgrade: The Detector and its Physics, Fermilab Pub-96/357-E.

[11] ATLAS Collab., W. W. Armstrong et al., ATLAS Technical Proposal, CERN/LHCC/94-43.

[12] CMS Collab., G. L. Bayatian et al., CMS Technical Proposal, CERN/LHCC/94-38.

[13] I. Vichou, 'Physics with the ATLAS dtector at LHC', to appear in these proceedings;
I. Efthymiopouos, 'Overview of the ATLAS Detector at LHC', to appear in these proceedings;
G. Snow, 'CMS General Overview and Physics Performance', to appear in these proceedings;
R. Ribeiro, 'The Tracking System of CMS', to appear in these proceedings;
D. Barney, 'The CMS Crystal Calorimeter', to appear in these proceedings.

[14] T. Sjöstrand, Computer Physics Commun. 39 (1986) 347;
H.-U. Bengtsson and T. Sjöstrand, Computer Physics Commun. 46 (1987) 43.

[15] LHC-B Collab., K. Kirsebom et al., LHC-B Letter of Intent, CERN/LHCC 95-5.

[16] BTeV Collab.,A. Santoro et al., BTeV: An Expression of Interest for a Heavy Quark Program at C0, BTeV-pub-97/2

[17] I. Abt, Proceedings of Beauty'96, Nucl. Instr. Meth. A384 (1996), 113.

[18] Proceedings of Beauty'96, Nucl. Instr. Meth. A384 (1996).

Polarization as a tool to study Z' vs. anomalous gauge coupling effects at the LC

A. A. Pankov

Gomel Polytechnical Institute, Gomel, 246746 Belarus

We show that the availability of longitudinally polarized electron beams at a $500\,GeV$ Linear Collider would allow, from an analysis of the reaction $e^+e^- \to W^+W^-$, to set stringent bounds on the couplings of a Z' of the most general type. In addition, to some extent, it would be possible to disentangle observable effects of the Z' from analogous ones due to competitor models with anomalous trilinear gauge couplings.

Introduction

It has been recently suggested [1] that theoretical models with one extra $Z \equiv Z'$ whose couplings to quarks and leptons are not of the 'conventional' type would be perfectly consistent with all the available experimental information from either LEP1 [2] and SLD [3] or CDF [4] data. Starting from this observation, a detailed analysis has been performed of the detectability in the final two-fermion channels at LEP2 of a Z' whose fermion couplings are arbitrary (but still family independent) [5]. Also, in [5] the problem of distinguishing this model from competitor ones (in particular, from a model with anomalous gauge couplings) has been studied.

The final two-fermion channel is not the only one where virtual effects generated by a Z' can manifest themselves. The usefulness of the final W^+W^- channel in e^+e^- annihilation to obtain improved information on some theoretical properties of such models, has already been stressed in previous papers in the specific case of longitudinally polarized beams for models of 'conventional' type (e.g., E_6, LR, *etc.*), showing that the role of polarization in these cases would be essential [6].

The aim of this note is that of considering whether the search for *indirect* effects of a 'unconventional' Z' in the W^+W^- channel would benefit from the availability of longitudinal polarization of initial beams, as it is the case for the 'conventional' situation. We shall show that in the parameter space the expected experimental sensitivity in the polarized processes is by far better than in the unpolarized case. For what concerns the differentiation from other sources of nonstandard effects, in particular those with anomalous gauge couplings, we shall also show that the characteristic feature of such a Z' would be the existence of certain peculiar properties of different observables, all pertaining to the final W^+W^- channel. All our discussions assume that longitudinal electron polarization will be available at the future $500\,GeV$ linear Collider (LC).

Constraints for general Z' parameters

The starting point will be the expression of the invariant amplitude for the process

$$e^+ + e^- \to W^+ + W^-. \tag{1}$$

In Born approximation, this can be written as a sum of a t-channel and of an s-channel component: $\mathcal{M}^{(\lambda)} = \mathcal{M}_t^{(\lambda)} + \mathcal{M}_s^{(\lambda)}$, where $\lambda = \pm 1/2$ is the electron helicity. Since we will concentrate on the sensitivity of process (1) to general features of Z'-exchange effects and their comparison to analogous effects in models with anomalous gauge couplings, we consider only the s-channel amplitudes. Accounting for one extra Z:

$$\mathcal{M}_s^{(\lambda)} = \left(-\frac{1}{s} + \frac{g_{WWZ_1}(v_1 - 2\lambda a_1)}{s - M_{Z_1}^2} + \frac{g_{WWZ_2}(v_2 - 2\lambda a_2)}{s - M_{Z_2}^2} \right) \times \mathcal{G}^{(\lambda)}(s, \theta). \tag{2}$$

$\mathcal{G}^{(\lambda)}(s, \theta)$ is a kinematical coefficient, depending also on the final W's helicities. For simplicity we omit its explicit form, which and can be found in the literature [7]. Eq. (2) shows two possible sources of effects from, respectively, the 'light' and the 'heavy' neutral gauge bosons Z_1 and Z_2.

The first one is the modification of the Z couplings, due to the presence of the extra Z', that can be induced, e.g., through the mechanism of $Z - Z'$ mixing. To account for this fact, the 'light' Z is now denoted as Z_1, and the same convention applies to its vector and axial-vector couplings to electrons v_1, a_1 and to the trilinear gauge coupling g_{WWZ_1}. The second effect is the actual heavy Z exchange denoted as Z_2, with analogous notations for its physical couplings.[1]

Eq. (2) can be conveniently rewritten in the same form as the Standard Model (SM):

$$\mathcal{M}_s^{(\lambda)} = \left(-\frac{g_{WW\gamma}}{s} + \frac{g_{WWZ}(v - 2\lambda a)}{s - M_Z^2} \right) \times \mathcal{G}^{(\lambda)}(s, \theta), \tag{3}$$

where the 'effective' gauge boson couplings $g_{WW\gamma}$ and g_{WWZ} are defined as:

$$g_{WW\gamma} = 1 + \Delta_\gamma = 1 + \Delta_\gamma(Z_1) + \Delta_\gamma(Z_2), \tag{4}$$

$$g_{WWZ} = \cot\theta_W + \Delta_Z = 1 + \Delta_Z(Z_1) + \Delta_Z(Z_2), \tag{5}$$

with

$$\begin{aligned} \Delta_\gamma(Z_1) &= v \cot\theta_W \left(\frac{\Delta a}{a} - \frac{\Delta v}{v} \right) (1 + \Delta\chi)\, \chi; \\ \Delta_\gamma(Z_2) &= v\, g_{WWZ_2} \left(\frac{a_2}{a} - \frac{v_2}{v} \right) \chi_2, \end{aligned} \tag{6}$$

$$\Delta_Z(Z_1) = \Delta g_{WWZ} + \cot\theta_W \left(\frac{\Delta a}{a} + \Delta\chi \right); \qquad \Delta_Z(Z_2) = g_{WWZ_2} \frac{a_2}{a} \frac{\chi_2}{\chi}. \tag{7}$$

We have introduced electrons SM couplings normalized as: $v = (T_{3,e} - 2Q_e\, s_W^2)/2 s_W c_W$; $a = T_{3,e}/2 s_W c_W$ with $T_{3,e} = -1/2$; $s_W = \sin\theta_W$; $c_W = \cos\theta_W$. Moreover: $\Delta v = v_1 - v$, $\Delta a = a_1 - a$ and $\Delta g_{WWZ} = g_{WWZ_1} - \cot\theta_W$. Finally, neglecting gauge boson widths:

$$\chi(s) = \frac{s}{s - M_Z^2}; \qquad \chi_2(s) = \frac{s}{s - M_{Z_2}^2}; \qquad \Delta\chi(s) = -\frac{2 M_Z \Delta M}{s - M_Z^2}, \tag{8}$$

[1] In Eq. (2), the couplings to W^+W^- of both Z_1 and Z_2 have been tacitly assumed of the usual Yang-Mills form.

where $\Delta M = M_Z - M_{Z_1}$ is the Z-Z_1 mass-shift, of the order of $150 - 200\,MeV$ according to most recent estimates [8, 9] (notice $\Delta M > 0$ if this is due to $Z - Z'$ mixing).

It should be stressed that, not referring to specific models, the parametrization (3)-(5) is both general and useful for phenomenological purposes, in particular to compare different sources of nonstandard effects contributing finite deviations (6) and (7) to the SM predictions.

We now focus on the effects of the heavy Z on polarized observables. The general expression for the cross section of process (1) with longitudinally polarized electron and positron beams can be expressed as

$$\frac{d\sigma}{d\cos\theta} = \frac{1}{4}\left[(1+P_L)\left(1-\bar{P}_L\right)\frac{d\sigma^+}{d\cos\theta} + (1-P_L)\left(1+\bar{P}_L\right)\frac{d\sigma^-}{d\cos\theta}\right], \quad (9)$$

where P_L and $\bar{P}_L$ are the actual degrees of electron and positron longitudinal polarization, respectively, and $\sigma^{\pm}$ are the cross sections for purely right-handed and left-handed electrons. We consider the cross section for polarized electrons and unpolarized positrons ($\bar{P}_L = 0$). Explicit expressions for the polarized cross can be found in [7, 10].

We reserve the notations σ^L and σ^R for the cross sections with $P_L = -0.9$ and $P_L = 0.9$, respectively, which seem to be realistically obtainable at the LC [11]. Our numerical analysis to assess the sensitivity of σ^L and σ^R to Δ_γ and Δ_Z follows the χ^2 procedure adopted in [10]. We represent the effect of non-standard couplings introduced above by the relative deviation of the cross section from the SM prediction:

$$\Delta \equiv \frac{\Delta\sigma}{\sigma_{SM}} = \frac{\sigma - \sigma_{SM}}{\sigma_{SM}}, \quad (10)$$

which is a function of Δ_γ and Δ_Z.

If a nonvanishing value of Δ was experimentally measured at some level of accuracy, the values of such parameters could be determined and possibly used to learn about the properties of the related nonstandard

physics. Alternatively, in the case of no observation, one could derive numerical bounds on Δ_γ and Δ_Z, and therefore constrain the various extended models, at some confidence level. In this regard, assuming small deviations, Δ is expressed as a linear combination of Δ_γ and Δ_Z with coefficients which, generally, increase with s. Conversely, the SM cross section decreases as $1/s$ (at least) due to the gauge cancellation among the various amplitudes. Therefore, if we parametrize the sensitivity of process (1) to δ_γ and δ_Z by, e.g., the ratio $\mathcal{S} = \Delta/(\delta\sigma/\sigma)$ with $\delta\sigma/\sigma$ the attainable statistical uncertainty on the SM cross section, such sensitivity is expected to increase with energy, even at fixed integrated luminosity (basically, as $\mathcal{S} \propto \sqrt{L_{int} s}$).

By specifying λ, Eq. (3) directly shows that

$$\Delta\sigma^- \propto \Delta_\gamma - \Delta_Z \cdot g_e^L \chi; \qquad \Delta\sigma^+ \propto \Delta_\gamma - \Delta_Z \cdot g_e^R \chi, \tag{11}$$

where $g_e^R = v - a = \tan\theta_W \simeq 0.55$ and $g_e^L = v + a = g_e^R(1 - 1/2s_W^2) \simeq -0.64$. Thus, by themselves, σ^- (or σ^{unpol}) and σ^+ only provide correlations among Δ_γ and Δ_Z, rather than true limits. These correlations can be represented as bands in the $\Delta_\gamma - \Delta_Z$ plane with a width proportional to the corresponding sensitivities, and a relative angle of approximately 60 degrees. In contrast to the unpolarized case, finite allowed ranges for Δ_γ and Δ_Z are obtained from the intersection of the two bands.

Quantitatively, for the LC500 with an assumed $L_{int} = 50\, fb^{-1}$ and P_L as above, one can derive the following 95% CL allowed ranges [10]:

$$\begin{aligned} -0.002 < \Delta_\gamma < 0.002 \\ -0.004 < \Delta_Z < 0.004. \end{aligned} \tag{12}$$

We now consider the application of the model-independent limits (12) to the case of an extra Z of extended gauge origin, generated by an E_6 symmetry. For such extended models one can write in Eqs. (4)-(7):

$$(v_1, a_1) \simeq (v + v'\phi, a + a'\phi) \Rightarrow (\Delta v, \Delta a) \simeq (v'\phi, a'\phi), \tag{13}$$

$$(v_2, a_2) \simeq (-v\phi + v', -a\phi + a'), \tag{14}$$

and

$$\Delta g_{WWZ} \simeq 0, \qquad g_{WWZ_2} \simeq -\cot\theta_W \phi. \tag{15}$$

Here, ϕ is the $Z - Z'$ mixing angle, and v', a' are the Z' vector and axial-vector couplings with electrons. The actual values of such couplings for the specific E_6 models (η, ψ and χ) can be found in the literature [12]. The above relations become equalities in linear approximation in the, expectedly small, angle ϕ, and give for Eqs. (6) and (7):

$$\Delta_\gamma = v \cot\theta_W \phi \left(\frac{a'}{a} - \frac{v'}{v}\right)\left(1 - \frac{\chi_2}{\chi} + \Delta\chi\right)\chi, \tag{16}$$

$$\Delta_Z = \cot\theta_W \left[\phi \frac{a'}{a}\left(1 - \frac{\chi_2}{\chi}\right) + \Delta\chi\right]. \tag{17}$$

Neglecting $\Delta\chi$ as being quadratic in ϕ, these relations show that every specific model is represented in linear approximation by a straight line in the $(\Delta_\gamma, \Delta_Z)$ plane, of equation:

$$\Delta_Z = \Delta_\gamma \frac{1}{v\chi} \frac{(a'/a)}{(a'/a) - (v'/v)}. \tag{18}$$

Such relation does not depend on either ϕ or M_{Z_2}, but only on ratios of the fermionic couplings.

The combination of (12) and (18) can be easily translated into limits on ϕ and M_{Z_2}. For the considered energy and luminosity of LC500, the typical bounds on ϕ are of the order of few $\times\ 10^{-3}$ for $M_{Z_2} \geq 1 TeV$, and much more restrictive for smaller values of M_{Z_2} (up to one order of magnitude in the extreme case $M_{Z_2} \simeq \sqrt{s}$). The detailed analysis of different specific models is worked out in [10] and references there. At the LC1000, the numerical results can be obtained according to the scaling law $\sqrt{L_{int} s}$.

Comparison with a model with anomalous gauge couplings

The extra heavy neutral gauge boson Z' would produce virtual effects in the final W^+W^- channel that, in principle, could mimic those of a model with anomalous trilinear gauge boson couplings [13]. Therefore, the identification of such an effect, if observed at the LC, becomes a relevant problem. The relevant trilinear WWV interaction which conserves $U(1)_{e.m.}$, C and P, can be written as ($e = \sqrt{4\pi\alpha_{em}}$) [7]:

$$\begin{aligned}
\mathcal{L}_{eff} &= -ie(1+\delta_\gamma)\left[A_\mu\left(W^{-\mu\nu}W^+_\nu - W^{+\mu\nu}W^-_\nu\right) + F_{\mu\nu}W^{+\mu}W^{-\nu}\right] \\
&- ie\,(\cot\theta_W + \delta_Z)\left[Z_\mu\left(W^{-\mu\nu}W^+_\nu - W^{+\mu\nu}W^-_\nu\right) + Z_{\mu\nu}W^{+\mu}W^{-\nu}\right] \\
&- ie\,x_\gamma F_{\mu\nu}W^{+\mu}W^{-\nu} - ie\,x_Z Z_{\mu\nu}W^{+\mu}W^{-\nu} \\
&+ ie\frac{y_\gamma}{M_W^2}F^{\nu\lambda}W^-_{\lambda\mu}W^{+\mu}_{\nu} + ie\frac{y_Z}{M_W^2}Z^{\nu\lambda}W^-_{\lambda\mu}W^{+\mu}_{\nu}\,, \qquad (19)
\end{aligned}$$

where $W^\pm_{\mu\nu} = \partial_\mu W^\pm_\nu - \partial_\nu W^\pm_\mu$ and $Z_{\mu\nu} = \partial_\mu Z_\nu - \partial_\nu Z_\mu$. In the SM at the tree-level, the anomalous couplings in (19) vanish: $\delta_\gamma = \delta_Z = x_\gamma = x_Z = y_\gamma = y_Z = 0$.

For the explicit form of helicity amplitudes for process (1) corresponding to (19) we refer to [7]. Here, for practical purposes, the Yang-Mills parts and their deviations proportional to δ_γ and $\delta_Z = g_{WWZ} - cot\theta_W$ are reported separately from the anomalous 'magnetic' and 'quadrupole' terms.

While in the previous case of the Z' the deviations Δ_γ and Δ_Z have an explicit (although numerically not quite significant) s-dependence through Eqs. (6) and (7), the anomalous trilinear gauge boson couplings are considered as effective *constants*. As a consequence, we assume $\delta_\gamma \equiv 0$ to ensure $U(1)_{e.m.}$ gauge invariance. In the framework where anomalous gauge couplings arise from effective theories with $SU(2) \times U(1)$ gauge symmetry, representing low-energy expansions of the non-standard weak interaction [14], finite δ_γ (and in any case it must be $\delta_\gamma(0) = 0$) only occurs at next-to-leading dimension level [15]. Furthermore, it can be shown

that the assumption of 'custodial' global $SU(2)$ symmetry of the New Physics, which naturally accounts for the smallness of the $\Delta\rho$ parameter, would require $\delta_\gamma = 0$ also at the higher, dim=8, level because the relevant operator would not respect this symmetry.

In most generality, Eq. (19) introduces five independent parameters into the analysis, and therefore the determination of suitable experimental observables, depending on subsets of anomalous gauge boson couplings, is a problem by itself (see, for example, refs. [16]).

Concerning the distinction between Z' and anomalous gauge boson coupling effects, one can try to define observables which are 'orthogonal' to the Z' mode. To this purpose, they should depend only on the x_V, y_V couplings that are specific of (19), but not on δ_Z which would represent an effect in common with the Z' model. Some attempts are presented in Ref. [10].

Concerning a possible discrimination between the Z' model of Sect. 2 and the model considered in this section, a strategy could be the following. If a signal is observed in either σ^L and/or σ^R and also in at least one of the 'orthogonal' observables defined above, we can conclude that it is due to the model with anomalous gauge couplings, and we can try to derive the values of some of them by properly analyzing the observed effects [16]. If, conversely, only σ^L and/or σ^R show an effect, we are left with the possibility that both models are responsible for such deviations. In this situation, we still have a simple tool to try to distinguish among the two models, which uses the observation that, under the assumption that only δ_V and Δ_V are effective, the expressions of the consequent deviations of the integrated cross sections σ^L and σ^R are, respectively:

$$\Delta\sigma^{R,L} \simeq \Delta\sigma^{\pm} \propto \delta_\gamma - \delta_Z g_e^{R,L} \chi, \tag{20}$$

and

$$\Delta\sigma^{R,L} \simeq \Delta\sigma^{\pm} \propto \Delta_\gamma - \Delta_Z g_e^{R,L} \chi. \tag{21}$$

Here, both Δ_V and δ_V have been taken nonvanishing, and $g_e^{L,R} = v \pm a$ are the left- and right-handed electron couplings, respectively. However, recalling that $\delta_\gamma = 0$ in the case of anomalous trilinear gauge boson couplings, using the experimental value of $s_W^2 \simeq 0.23$, one has for such a model the very characteristic feature

$$\Delta\sigma^L \simeq \left(1 - \frac{1}{2s_W^2}\right) \Delta\sigma^R = -1.17\Delta\sigma^R, \tag{22}$$

where the explicit expressions of g_e^L and g_e^R have been used. If, on the contrary, the effect is due to a model with a Z', no *a priori* relationship exists between $\Delta\sigma^L$ and $\Delta\sigma^R$. Accordingly, from inspection of these two quantities, if they are found not to be related by Eq. (22) to a given confidence level, one would conclude that the observed effect should be due to the general extra Z discussed in Sect. 2. Then, depending on the actual values of the experimental deviations, a determination of the two parameters Δ_γ and Δ_Z might be carried on.

Actually, if the deviations of $\sigma^{L,R}$ satisfy the correlation Eq. (22), a small residual ambiguity would remain. Although the possibility that in a model with both Δ_γ and Δ_Z nonvanishing the correlation Eq. (22) is satisfied just by chance seems rather unlikely, one cannot exclude it *a priori*. Should this be the real situation, further analysis, e.g., in the different final fermion-antifermion channel would be required. The discussion of this essentially unlikely case can be performed, but is beyond the purpose of this note.

Concluding remarks

We have shown in this paper that the availability of longitudinal electron beam polarization at the LC would be very useful for the study of the most general model with one extra Z from an analysis of the final W^+W^- channel. In principle, it would also be possible to discriminate this model from a rather 'natural' competitor one where anomalous gauge

boson couplings are present. This could be done by analyzing suitable experimental variables, all defined in the same W^+W^- final channel. All these facts allow us to conclude that polarization at the LC would be, least to say, a highly desirable opportunity.

References

[1] P. Chiappetta, J. Layssac, F. M. Renard and C. Verzegnassi, Phys. Rev. D **54** (1996) 789; G. Altarelli, N. Di Bartolomeo, F. Feruglio, R. Gatto and M. Mangano, Phys. Lett. **B375** (1996) 292.

[2] For an updated review see, e.g., A. Blondel, talk at the *28th International Conference on High Energy Physics*, 25-31 July 1996, Warsaw, Poland.

[3] For an updated review see, e.g., M. W. Grünewald, talk at the *28th International Conference on High Energy Physics*, 25-31 July 1996, Warsaw, Poland.

[4] E. Buckley-Geer, FERMILAB-Conf-95/316-E (1995), Proceedings of the *EPS Conference on High Energy Physics*, Brussels, Belgium (1995).

[5] G. Montagna, F. Piccinini, J. Layssac, F. M. Renard and C. Verzegnassi, Z. Phys. C **75** (1997) 641. Montpellier Report PM 96-25 (1996).

[6] A. A. Pankov and N. Paver, Phys. Rev. D **48** (1993) 63.

[7] G. Gounaris, J. Layssac, G. Moultaka and F. M. Renard, Int. J. Mod. Phys. A **8** (1993) 3285.

[8] G. Altarelli, CERN report CERN-TH-96-265, presented at the *NATO Advanced Study Institute on Techniques and Concepts of High-Energy*

Physics, St. Croix, U.S. Virgin Islands (1996); CERN report CERN-TH.7464/94, Proceedings of the Workshop on *Radiative Corrections: Status and Outlook*, (Gatlinburg, Tenn., USA, 1994), ed. B. L. Ward, World Scientific 1995.

[9] K. S. Babu, C. Kolda and J. March-Russell, Phys. Rev. D **54** (1996) 4635.

[10] A.A. Pankov, N. Paver and C. Verzegnassi, hep-ph/9701359, to appear in Int. J. Mod. Phys. **A**.

[11] C. Y. Prescott, Proceedings of the Workshop *Physics and Experiments with Linear e^+e^- Colliders*, (Waikoloa, Hawaii, 1993), eds. F. A. Harris, S. L. Olsen, S. Pakvasa and X. Tata, (World Scientific, Singapore 1993), p. 379.

[12] For a review see, e.g.: J. L. Hewett, T. G. Rizzo, Physics Reports **183** (1989) 193.

[13] A. A. Pankov and N. Paver, Phys. Lett. **B393** (1997) 437.

[14] See, e.g., K. Hagiwara, S. Ishihara, R. Szalapski and D. Zeppenfeld, Phys. Lett. B **283** (1992) 353; Phys. Rev. D **48** (1993) 2182; and references there.

[15] G. Gounaris and F. M. Renard, Z. Phys. C **59** (1993) 133.

[16] V. V. Andreev, A. A. Pankov and N. Paver, Phys. Rev. D **53** (1996) 2390.

Renormalization group and searching for new physics beyond Standard Model

Vladimir Skalozub

Dnipropetrovsk University, Dnipropetrovsk 320625, Ukraine
e-mail: skalozub@ff.dsu.dp.ua

The renormalization group equation for the effective Lagrangian describing effects of new physics beyond the Standard Model at low energies is derived. It is applied for investigation of $2 \to 2$ scattering processes with ordinary particles. In one-loop order specific relations between the parameters of the Lagrangian appear which depend on the underlying model of particle physics. As an example the Standard Model with heavy Higgs boson is investigated.

1. Introduction

One of important nowadays problems is a searching for new physics beyond the Standard Model (SM) (the Glashow-Salam-Weinberg theory and QCD) which may exhibit itself at an energy scale $\sqrt{s} \sim \Lambda, \Lambda >> m_t$ - mass of t-quark. Among possible ways for its solution very popular is the construction of the effective Lagrangians (EL) which, as usually is believed, are obtained as a result of decoupling of the virtual heavy particles in the scattering amplitudes of light particles from the SM [1],[2]. EL contain the effective operators (EO), which can be generated either by the tree level virtual states of heavy particles having masses $\sim \Lambda$ or by the virtual heavy particle loops. Obviously, the EO of the latter type are suppressed by at least one degree of Λ^{-1} as compared with the former ones. It is usually assumed that EL and EO are the remnants of some unknown at present time renormalizable gauge theory [3],[4]. But, as a rule, any actual properties of EO called forth by the renormalizability are not used in the calculations of scattering processes. In the present work it will be discussed which kind of information about EO can be derived from the basic requirement that the fundamental theory is to be a renormalizable one. That, in particular, means the EO have to satisfy the renormalization group (RG) equations. Our consideration is based on the RG equation in $\overline{MS}$ scheme and a decoupling theorem [5], giving possibility to proceed from high to low energies taking into account the presence of different mass scales [6], [7]. The content is as follows. In Sect. 2 a necessary information about EL and RG equations in $\overline{MS}$ scheme is given. In Sect. 3 we specialize that for the case of $2 \to 2$ scattering processes. Then,

to make clear our approach we consider the processes including W- and Z- bosons in the SM with very heavy Higgs particles considered as the threshold of "new" physics. Sect. 5 contains brief discussion of the results and prospects.

2. Effective Lagrangians and RG equations

In what follows, we will consider the EL as the sum of the scattering amplitudes of SM particles in initial and final states with external momenta $p_{ext} << \Lambda_i$:

$$\mathcal{L}_{eff.} = \sum_j T_j, \tag{1}$$

where Λ_i are the heavy particle masses. In this case the virtual contributions of heavy particles in amplitudes T_j are separated in the form of local amplitudes (EO) containing the SM fields, their derivatives and masses, $O_{j,d}$, having increasing energy dimensions d which are suppressed by the corresponding degrees of heavy mass [5]:

$$T_j = T_j^{SM} + T_j^{\Lambda}, \qquad T_j^{\Lambda} = \sum_{d>4} \frac{1}{\Lambda^{d-4}} \alpha_{j,d} O_{j,d}. \tag{2}$$

The EO are produced at low energies $\sqrt{s} << \Lambda$ when the propagators $\sim \frac{1}{p^2-\Lambda^2}$ with a good accuracy can be approximated by $-\frac{1}{\Lambda^2}$. Amplitudes T_j^{SM} are to be calculated in the SM and T_j^{Λ} describe deviations from SM due to virtual heavy particles. The dimensionless parameters $\alpha_{j,d}$ characterize the heavy particle physics. They are model dependent and expressed through dimensionless coupling constants. At present time the distinction from zero of any $\alpha_{j,d}$ is not determined reliably, although the values of many of them are strictly limited by experiments [2], [8]. In papers [4], [3] it was studied which sets of EO entering the EL could be produced in different gauge theories containing the SM as a subgroup. To realize that the various renormalizable types of couplings between vector, fermion and scalar fields have been analyzed and the operators appeared at tree- and loop- levels were determined. However, in such a way it is not possible to find out the coefficients $\alpha_{j,d}$, since their values are model dependent. Therefore, it is assumed the coefficients are arbitrary parameters which should be fixed by experiments. On the contrary, the parameters in eq.(2) are not free ones but specialized by the initial theory. One can ask a question: which correlations between $\alpha_{j,d}$ take place in different cases? This will be the problem discussed below.

More definitely, we shall investigate the ratios of $\alpha_{j,d}$ entering the EL which have to realize as the consequence of the RG equation for $\mathcal{L}_{eff.}$. Existence of RG equation is a fundamental property of any renormalizable theory. As it is occurred, it gives possibility to connect the parameters $\alpha_{j,d}$ for a number of processes that would be useful for future experiments. As a prospect, one would hope that different correlations between the parameters, calculated for chosen set of scattering processes at different variants of underlining theories, will give information about the unique one selected on the ground of comparisons with experimental data.

In renormalizable theory RG equations can be written for any objects - running coupling constants $\bar{\lambda}(g^2)$, Green's functions, S-matrix elements, etc. These equations mean that if a subtraction point μ in the momentum plane is shifted, $\mu \to mu + \Delta\mu$, then all the parameters - couplings λ_a, masses m_i, fields ϕ_i - can be changed in such a way that the considered functions F of the parameters remain unchanged:

$$\mathcal{D}_{RG} F(\lambda_a, \phi_i, m_i, \mu) = 0, \tag{3}$$

$$\mathcal{D}_{RG} = \frac{d}{dln\mu} = \frac{\partial}{\partial ln\mu} + \sum_a \beta_a \frac{\partial}{\partial \lambda_a} - \sum_X \dot{\gamma}_X \frac{\partial}{\partial lnX},$$

where the running parameters are defined with the β-functions

$$\frac{d\lambda_a(\mu)}{dln\mu} = \beta_a(\lambda_a) \tag{4}$$

and the anomalous dimensions

$$\frac{dln\hat{X}(\mu)}{dln\mu} = -\gamma_X(\lambda_a). \tag{5}$$

In what follows, we shall use a dimension regularization and the $\overline{MS}$ scheme of renormalizations [9]. In this case β- and γ- functions are independent of particle masses and all mass dependencies are concentrated in the scattering amplitudes. Therefore, a possibility for moving along an energy scale from high to low values appears. The RG operator $\mathcal{D}_{RG}$ is the same either at high energies, $E >> \Lambda$ and at low energies $E << \Lambda$, but it is expressed in terms of different parameter sets. At high energies all particles contribute. At low energies, the virtual heavy states are decoupled and β- and γ- functions have to be expressed through light particle loops, only. In the latter case the amplitudes are expanded in a power series in $1/\Lambda$

and the RG operator, acting on any function, does not change its order in $1/\Lambda$.

These properties of RG operator in the $\overline{MS}$ scheme give reasons for application of the RG method to the EL describing new physics beyond the SM at low energies $E << \Lambda_i$.

Having in mind general reasons mentioned above, let us apply the RG formalism to the EL (1). First, let us consider a renormalizable theory generalizing the SM which contains N heavy particles with the masses $\Lambda_n, (n = 1, ..., N)$. We denote the light SM particles as ϕ for bosons (W-, Z-bosons, photons, gluons, and Higgs's boson) and f for fermions (leptons and quarks). The only SM mass parameter is v - vacuum expectation value of scalar field. As λ_a we denote all the coupling constants, $\lambda_a = g^2, g'^2, g_s, G_f, \lambda, \lambda_{heavy}$, where first three couplings correspond to $SU(2)_L, U(1)_y$ and $SU(3)_c$ subgroups of the SM; G_f is Yukawa coupling, λ is a self-interaction of SM; scalar field and λ_{heavy} is couplings of heavy particles.

The low energy EL, as any renormalized amplitude, satisfies the RG equation (3) with the entering parameters defined in eqs. (4), (5). Below, to distinguish the objects,a, of complete model we will mark them by "hat": $\hat{a}$. So, in the above formulae one has to substitute $a \to \hat{a}$. In the low energy region (which mainly is of interest for us), $p_{ext.} << \Lambda$, the amplitudes T_j are expanded in series in small values ,$p_{ext.}\hat{\Lambda}_n \ll 1$, $\frac{\hat{v}}{\hat{\Lambda}_n} \ll 1$, $\frac{\hat{\phi}}{\hat{\Lambda}_n} \ll 1$, $\frac{\hat{f}}{\hat{\Lambda}_n^{3/2}} \ll 1$:

$$T_j = \hat{\alpha}_{j,4}\left(\hat{\lambda}_a, \ln\frac{\hat{\Lambda}_n}{\mu}, \ln\frac{\hat{v}}{\mu}, \frac{\hat{\Lambda}_n}{\hat{\Lambda}_{n'}}\right)\hat{O}_{j,4} + \\ + \sum_{d>4}\sum_{n_i}\frac{\hat{\alpha}_{j,d}^{n_1...n_{d-4}}\left(\hat{\lambda}_a, \ln\frac{\hat{\Lambda}_n}{\mu}, \ln\frac{\hat{v}}{\mu}, \frac{\hat{\Lambda}_n}{\hat{\Lambda}_{n'}}\right)\hat{O}_{j,d}}{\hat{\Lambda}_{n_1}...\hat{\Lambda}_{n_{d-4}}}, \qquad (6)$$

where the amplitudes $\hat{O}_{j,d}$ are built from parameters $\hat{v}, \hat{\phi}/\hat{v}, \hat{f}/\hat{v}^{3/2}$ and have the dimensions $[mass]^d$.

At low energies, $E << \Lambda_n$, after the decoupling of heavy field contributions the running parameters have to be determined by the effective theory, only [6]. These parameters contain the SM loops and independ of heavy particle physics. This point is very important. It gives possibility to concentrate all the EL dependencies on the heavy particles in the parameters $\alpha_{j,d}$.

Thus we accentuate, running of low energy parameters is determined by the same equations (3), (4) and (5), however in this case the $\beta-$ and $\gamma-$ functions take into account the loops of SM particles, only. As the sewing conditions we choice the coincidence of parameters at $\mu = \Lambda$:

$$\lambda_a \mid_{\mu=\Lambda} = \hat{\lambda}_a \mid_{\mu=\Lambda}, \qquad X \mid_{\mu=\Lambda} = \hat{X} \mid_{\mu=\Lambda} . \tag{7}$$

This yields

$$\begin{aligned} \lambda_a &= \hat{\lambda}_a + a_{\lambda_a} \ln \frac{\hat{\Lambda}^2}{\mu^2} + b_{\lambda_a} \left[\ln \frac{\hat{\Lambda}^2}{\mu^2} \right]^2 + ...; \\ X &= \hat{X} \left(1 + a_X \ln \frac{\hat{\Lambda}^2}{\mu^2} + b_X \left[\ln \frac{\hat{\Lambda}^2}{\mu^2} \right]^2 + ... \right). \end{aligned} \tag{8}$$

These series give possibility to express the EL through the running low energy parameters. The decoupling theorem guarantees an absorption of heavy particle contributions by $\lambda_a(\mu), X(\mu)$ in such a way that the explicit dependencies of $\alpha_{j,d}$ on $log\frac{\Lambda^2}{\mu^2}$ disappear [6], and the terms $\hat{\alpha}_{j,4}\hat{O}_{j,4}$ been expressed through the SM parameters convert into the amplitude T_j^{SM}:

$$\mathcal{L}_{eff} = \sum_j T_j^{SM} + \sum_{j,d>4} \sum_{n_i} \frac{\alpha_{j,d}^{n_1 ... n_{d-4}} \left(\lambda_a, \ln \frac{v}{\mu}, \frac{\Lambda_n}{\Lambda_{n'}} \right) C_{j,d}}{\Lambda_{n_1} ... \Lambda_{n_{d-4}}}. \tag{9}$$

where the amplitudes $O_{j,d}$ have the dimensions d and are constituted from the parameters $v, p_{ext.}/v, f/v^{3/2}$.

As it follows from the analysis in ref.[6], at energies $E << \Lambda_n$ the RG operator $\mathcal{D}_{\hat{a}}$ and the operator $\mathcal{D}_a$ are the same ones but expressed through different sets of parameters: in both cases we have the same RG equation.

Now, applying the RG operator to the EL (9) we obtain in each order in $1/\Lambda_n$:

$$\mathcal{D} T_j^{SM} = 0; \qquad \mathcal{D} \left(\sum_{n_i} \frac{\alpha_{j,d}^{n_1 ... n_{d-4}} (\lambda_a, \ln \frac{v}{\mu}, \frac{\Lambda_n}{\Lambda_{n'}}) O_{j,d}}{\Lambda_{n_1} ... \Lambda_{n_{d-4}}} \right) = 0. \tag{10}$$

These relations are general and take place independently of computation schemes or approximations. In the most cases it is sufficient to take into account tree- and one-loop orders of eq. (10), that will be investigated in

detail below. Let us denote the n-loop contribution to the value a as $a^{(n)}$. Then we have

$$\mathcal{D}^{(0)} = \frac{\partial}{\partial \ln \mu}, \qquad \mathcal{D}^{(1)} = \sum_a \beta_a^{(1)} \frac{\partial}{\partial \lambda_a} - \sum_X \gamma_X^{(1)} \frac{\partial}{\partial \ln X}. \tag{11}$$

Since in the $\overline{MS}$-scheme, $\frac{\partial \lambda_a}{\partial \ln \mu} = 0$, $\frac{\partial X}{\partial \ln \mu} = 0$, from eq.(10) it follows:

$$\mathcal{D}^{(0)} \alpha_{j,d}^{n_1 \dots n_{d-4}(0)} = \frac{\partial}{\partial \ln \mu} \alpha_{j,d}^{n_1 \dots n_{d-4}(0)} = 0, \tag{12}$$

$$-\sum_{n_i} \frac{O_{j,d}^{(0)}}{\Lambda_{n_1}^{(0)} \dots \Lambda_{n_{d-4}}^{(0)}} \mathcal{D}^{(0)} \alpha_{j,d}^{n_1 \dots n_{d-4}(1)} = \sum_{n_i} \mathcal{D}^{(1)} \left[\frac{\alpha_{j,d}^{n_1 \dots n_{d-4}(0)} O_{j,d}^{(0)}}{\Lambda_{n_1}^{(0)} \dots \Lambda_{n_{d-4}}^{(0)}} \right]. \tag{13}$$

The first of these relations simply means that a tree amplitude is independent of $ln\mu$. The second one will be considered as an equation for parameters $\alpha_{j,d}$. This remark requires some comments.

Usually, RG equations are used to improve the results of perturbation theory. However, the structure of eqs.(10) and (13) show that they can be specialized for calculation of the correlations between the parameters $\alpha_{j,d}$ for a number of processes. The reasons are as follows. As it was noted before, in specified renormalizable theory the coefficients $\alpha_{j,d}$ in the EL (1) are defined numbers. In this case the relation (13) is just the identity which relates the tree operators $O_{j,d}$ with that of one- loop order due to renormalizability. But if the model is not specified (unknown), the equation (13) implements nontrivial relations between formally arbitrary parameters which take place due to supposed renormalizability of the model. This circumstance is closely connected with our consideration of the EO $O_{j,d}$ as the S-matrix amplitudes. In the next section we will consider that in more detail for scattering processes $2 \to 2$.

3. RG equation for $2 \to 2$ scattering processes

To calculate $\mathcal{D}^{(0)} \alpha_{j,d}^{n_1 \dots n_{d-4}(1)}$ let us remind that in the $\overline{MS}$-scheme the dependence on $ln\mu$ enters together with the pole term $\frac{2}{4-D}$, where D is the momentum space dimension. So, to find the left hand side of eq.(13) it is sufficient to calculate the pole part of $\alpha^{(1)}$.

Now, let us turn to determination of the dependence $\frac{\partial}{\partial \ln \mu} \alpha_{j,d}^{n_1 \dots n_{d-4}(1)}$ (r)n $\alpha_{j,d}^{n_1 \dots n_{d-4}(0)}$ for the scattering process $2 \to 2$ in the order $1/\Lambda^2$. In the most simple case the EL are generated in tree approximation when the heavy particle propagators $\frac{1}{p^2 - \Lambda^2}$ are substituted by the effective contact

interactions $\sim -\frac{1}{\Lambda^2} + O(\frac{p^2}{\Lambda^4})$. Then the problem is reduced to scattering of ordinary particles on the external field produced by the heavy virtual state. The scattering should be calculated in one-loop order.

To proceed further, let as denote the amputated one-particle irreducible vertexes of the effective low energy theory describing interaction of the two SM particles with heavy one as $\Gamma_i = \Gamma_i^{(0)} + \Gamma_i^{(1)} + ...(i = 1, 2, ..)$. Let $F_i^{(0)}$ is a product of the SM fields entering the vertex $\Gamma_i^{(0)}$. In order $1/\Lambda^2$ the tree-level EL equals to $\frac{1}{\Lambda^2}\Gamma_i^{(0)}\Gamma_j^{(0)}F_i^{(0)}F_j^{(0)}$, and the one-loop corrections to the initial, i, and final, j, scattering amplitudes on the "external field" equal $\frac{1}{\Lambda^2}\Gamma_i^{(1)}\Gamma_j^{(0)}F_i^{(0)}F_j^{(0)}$ and $\frac{1}{\Lambda^2}\Gamma_i^{(0)}\Gamma_j^{(1)}F_i^{(0)}F_j^{(0)}$, respectively. Then we have for the EO $O_{ij,6}^{(0)}$:

$$\alpha_{ij,6}^{(0)}O_{ij,6}^{(0)} = \Gamma_i^{(0)}\Gamma_j^{(0)}F_i^{(0)}F_j^{(0)},$$
$$\alpha_{ij,6}^{(1)vertex}O_{ij,6}^{(0)} = \left(\Gamma_i^{(1)}\Gamma_j^{(0)} + \Gamma_i^{(0)}\Gamma_j^{(1)}\right)F_i^{(0)}F_j^{(0)}. \qquad (14)$$

Since the vertexes enter multiplicatively the EL, the equation (13) is resulted in the following relation for Γ_i:

$$-\frac{\partial}{\partial \ln \mu}\Gamma_i^{(1)} = \left[\sum_a \beta_a^{(1)}\frac{\partial}{\partial \lambda_a} - \gamma_v^{(1)}\frac{\partial}{\partial \ln v} - \sum_\phi N_{i,\phi}\gamma_\phi^{(1)} - \right.$$
$$\left. - \sum_f N_{i,f}\gamma_f^{(1)} + \frac{1}{2}\gamma_\Lambda^{(1)\prime}\right]\Gamma_i^{(0)}, \qquad (15)$$

where $N_{i,\phi}, N_{i,f}$ are numbers of fields in the vertex $\Gamma_i^{(0)}$.

Taken for a specific renormalizable theory, it is just the identity. The one-loop vertex, describing scattering on the heavy particle external field, stands in the left-hand side. The one-loop $\beta^{(1)}$- and $\gamma^{(1)}$– functions of light particles enter into right-hand side, as well as the corresponding vertex function in tree-approximation. Due to renormalizability, an algebraic structure of the $\Gamma_i^{(1)}$ pole part coincides with the structure of $\Gamma(0)_i$, that leads to the equality of both sides in eq. (15). But if the model in not known, this equation can be used to obtain information about the parameters $\alpha_{j,d}$. Being the consequence of renormalizability it, in a sense, takes the place of the tree unitarity condition which is a necessary condition for the renormalizability at high energies.

To find correlations between $\alpha_{j,d}$ one has to represent the vertex $\Gamma_i^{(0)}$ in the form of product of an arbitrary number $A_i^{(0}$, which to be determined,

and the amplitude $V_i^{(0)}$ constructed from momenta $p_{ext.}$ and , possibly, v, and where the structure of interaction with the "external field" is also taken into account:

$$\begin{aligned} \Gamma_i^{(0)} &= A_i^{(0)} V_i^{(0)}, \\ \alpha_{ij,6}^{(0)} &= A_i^{(0)} A_i^{(0)}, \qquad O_{ij,6}^{(0)} = F_i^{(0)} V_i^{(0)} F_i^{(0)} V_i^{(0)}. \end{aligned} \tag{16}$$

Since a one-loop correction contains the SM particles only, its divergent part is to be a linear superposition of the parameters $A_i^{(0)}$:

$$\begin{aligned} \tfrac{\partial}{\partial \ln \mu} \quad & \Gamma_i^{(1)} = \sum_k f_{ik}^{(1)} A_k^{(0)} V_i^{(0)}, \\ \tfrac{\partial}{\partial \ln \mu} \quad & \alpha_{ij,6}^{(1)vertex} = \sum_k f_{ik}^{(1)} A_k^{(0)} A_j^{(0)} + \sum_k f_{jk}^{(1)} A_k^{(0)} A_i^{(0)}, \end{aligned} \tag{17}$$

where k marks the sort of particles inside loops and the coefficients $f_{ik}^{(1)}$ are explicitly calculated in terms of the SM variables. Then the equations for coefficients $A_i^{(0)}$ follow from eq. (15):

$$\begin{aligned} -\sum_k f_{ik}^{(1)} A_k^{(0)} = \quad & \left[\sum_a \beta_a^{(1)} \frac{\partial}{\partial \lambda_a} - \gamma_v^{(1)} \frac{\partial V_i^{(0)}}{\partial \ln v} - \sum_\phi N_{i,\phi} \gamma_\phi^{(1)} - \right. \\ & \left. - \sum_f N_{i,f} \gamma_f^{(1)} + \frac{1}{2} \gamma_\Lambda^{(1)\prime} \right] A_i^{(0)}. \end{aligned} \tag{18}$$

Thus, if the vertex structure is chosen, the renormalizability of initial model implemented in the relation (15) may serve as a tool to find relations between $A_i^{(0)}$ and, hence, $\alpha_{j,d}$.

In the next section, as the most simple example, we will apply eq.(18) to the SM with a heavy Higgs boson. In this case the theory contains only one heavy particle. Moreover, the SM is well studied and the possibility to compare the results followed from eq. (18) with the exact known forms of $\Gamma_i^{(0)}$ will also appear.

4. EO in SM with heavy scalar particle

Let us consider the Higgs particle mass, m_H, as the threshold of new physics. Light particles is to be photon, W- and Z-bosons and fermions, f. To the Higgs field interactions with two light particles one has to refer the Yukawa interaction $-G_f(\bar{f}f)H$ and the boson interactions

$\Gamma^{(0)}_{WWH} W^+_\alpha W^{-\alpha} H$, $\Gamma^{(0)}_{ZZH} Z_\alpha Z^\alpha H$. The coupling constants G_f are dimensionless and $\Gamma^{(0)}_{WWH}$, $\Gamma^{(0)}_{ZZH}$ have a dimensionality of mass. In the order $1/m_H^2$ the following tree level EO are produced:

$$\begin{aligned}
\mathcal{O}^{(0)}_{ff_1f_1} &= \frac{G_f G_{f_1}}{m_H^2}(\bar{f}f)(\bar{f}_1 f_1) = \frac{\alpha^{(0)}_{ff_1f_1}}{m_H^2}(\bar{f}f)(\bar{f}_1 f_1), \\
\mathcal{O}^{(0)}_{ffWW} &= -\frac{G_f \Gamma^{(0)}_{WWH}}{m_H^2}(\bar{f}f) W^+_\alpha W^{-\alpha} = \frac{\alpha^{(0)}_{ffWW}}{m_H^2}(\bar{f}f) W^+_\alpha W^{-\alpha}, \\
\mathcal{O}^{(0)}_{WWWW} &= \frac{\Gamma^{(0)2}_{WWH}}{2m_H^2} W^+_\alpha W^{-\alpha} W^+_\beta W^{-\beta} = \frac{\alpha^{(0)}_{WWWW}}{m_H^2} W^+_\alpha W^{-\alpha} W^+_\beta W^{-\beta}, \\
\mathcal{O}^{(0)}_{WWZZ} &= \frac{\Gamma^{(0)}_{WWH}\Gamma^{(0)}_{ZZH}}{m_H^2} W^+_\alpha W^{-\alpha} Z_\beta Z^\beta = \frac{\alpha^{(0)}_{WWZZ}}{m_H^2} W^+_\alpha W^{-\alpha} Z_\beta Z^\beta
\end{aligned} \tag{19}$$

and analogously the operators $\mathcal{O}^{(0)}_{ffZZ}$ and $\mathcal{O}^{(0)}_{ZZZZ}$.

Now, let us assume for the moment that the couplings $\Gamma^{(0)}$ are not known. Our goal here is to derive the correlations between the parameters $\alpha^{(0)}$, which follow from renormalizability of the SM. We apply the equation (15) to solve this problem.

The only mass parameter in the considered case is the scalar field vacuum expectation value $v = \frac{2m_W}{g} = \frac{2m_Z}{\sqrt{g^2+g'^2}} = \frac{m_f}{G_f}$.

Let us consider the vertexes WWH and ZZH. The gauge fields enter the theory via the covariant derivatives together with their coupling constants. Therefore, $\Gamma^{(0)}_{WWH} \sim g^2$. Z-bosons is the superposition of the neutral components of the $SU(2)_I$- and $U(1)_Y$- fields. So, the vertex ZZH contains both of couplings g, g' but remains a quadratic form. Taking into account the dimensions of the vertexes we parametrize them as follows:

$$\begin{aligned}
\Gamma^{(0)}_{WWH} &= v A^{(0)}_{WWH}, \qquad A^{(0)}_{WWH} = \xi_1 g^2, \\
\Gamma^{(0)}_{ZZH} &= v A^{(0)}_{ZZH}, \qquad A^{(0)}_{ZZH} = \xi_2 g^2 + \xi_3 g'^2,
\end{aligned} \tag{20}$$

where ξ_1, ξ_2, ξ_3 are arbitrary numbers. We are going to find the ratios between them. Parametrizing the values G_{WWH} and G_{ZZH}, which correspond to $8\pi^2 \sum\limits_k f^{(1)}_{ik} A^{(0)}_k$ in eq.(17),

$$\frac{\partial}{\partial \ln \mu^2}\Gamma^{(1)}_{WWH} = \frac{v}{16\pi^2} G_{WWH}, \qquad \frac{\partial}{\partial \ln \mu^2}\Gamma^{(1)}_{ZZH} = \frac{v}{16\pi^2} G_{ZZH}, \tag{21}$$

where $\Gamma^{(1)}_{WWH}, \Gamma(1)_{ZZH}$ are the amputated one-particle- irreducible vertex functions of low energy theory, one obtains from eq. (18):

$$
\begin{aligned}
-G_{WWH} &= 8\pi^2\left[\tilde{\beta}_g^{(1)}\frac{\partial}{\partial g^2} - \tilde{\gamma}_v^{(1)} - 2\tilde{\gamma}_W^{(1)} + \frac{1}{2}\tilde{\gamma}_{m_H}^{(1)\prime}\right] A^{(0)}_{WWH}, \\
-G_{ZZH} &= 8\pi^2\left[\tilde{\beta}_g^{(1)}\frac{\partial}{\partial g^2} + \tilde{\beta}_{g'}^{(1)}\frac{\partial}{\partial g'^2} - \tilde{\gamma}_v^{(1)} - 2\tilde{\gamma}_Z^{(1)} + \frac{1}{2}\tilde{\gamma}_{m_H}^{(1)\prime}\right] 2A^{(0)}_{ZZH}
\end{aligned}
\tag{22}
$$

Here, the $\tilde{\beta}-$ and $\tilde{\gamma}$-functions take into account all the SM particles except Higgs's boson , H, and the factor 2 infront $A^{(0)}_{ZZH}$ is due to the identity of Z-bosons. By eliminating of $\tilde{\gamma}'_{m_H}$ and introducing the standard definition $g'^2 = g^2 tg^2\theta_W$ and $m_W^2 = m_Z^2 cos^2\theta_W$ eq.(22) can be written in the form

$$
\begin{aligned}
\frac{A^{(0)}_{WWH}}{2A^{(0)}_{ZZH}}G_{ZZH} - G_{WWH} &= 8\pi^2 A^{(0)}_{WWH}\Bigg[2\left(\tilde{\gamma}_Z^{(1)} - \tilde{\gamma}_W^{(1)}\right) + \\
&+ \frac{\tilde{\beta}_g^{(1)}}{g^2} - \frac{A^{(0)}_{WWH}}{A^{(0)}_{ZZH}}\frac{\xi_2\tilde{\beta}_g^{(1)} + \xi_3\tilde{\beta}_{g'}^{(1)}}{\xi_1 g^2}\Bigg].
\end{aligned}
\tag{23}
$$

As is seen, after expressing $\tilde{\beta}_{g'}^{(1)}$-function through $\tilde{\beta}_g^{(1)}, \tilde{\gamma}_{m_Z}^{(1)}, \tilde{\gamma}_{m_W}^{(1)}$ the terms with $\tilde{\beta}_g^{(1)}$ are cancelled exactly.

Calculation of $\tilde{\gamma}^{(1)}_{Z,W}, \tilde{\gamma}^{(1)}_{m_Z,m_W}$ is reduced to the determination of the coefficients standing at the pole terms in the one-loop W- and Z-boson mass operators, $\delta\tilde{\Sigma}^{(1)}_{WW}, \delta\tilde{\Sigma}^{(1)}_{ZZ}$, when the light particles only to be taken into account:

$$
\begin{aligned}
\tilde{\gamma}_Z^{(1)} &= -\frac{1}{2}\lim_{D\to 4}(4-D)\frac{\partial}{\partial p^2}\delta\tilde{\Sigma}^{(1)}_{ZZ}(p^2), \\
\tilde{\gamma}_{m_Z}^{(1)} &= \lim_{D\to 4}(4-D)\frac{\delta\tilde{\Sigma}^{(1)}_{ZZ}(m_Z^2)}{m_Z^2}
\end{aligned}
\tag{24}
$$

(and analogously for W-bosons).

These calculations have been done in the Feynman-t'Hooft gauge and actually are very simple. The dependencies of the right-hand side and left-hand side in eq. (23) on the Yukawa coupling are given by the fermion loops,

$$
\delta\tilde{\Sigma}^{(1)fermi}_{ZZ}(p^2) = -\frac{1}{8\pi^2(4-D)}\frac{g^2}{2cos^2\theta_W}\sum_f\left\{\left[1 + \right.\right.
$$

$$+\left(1-4sin^2\theta_W \mid Q_f \mid\right)^2\Big]\frac{p^2}{6}-m_f^2\Big\}$$

$$\delta\tilde{\Sigma}^{(1)ferm}_{WW}(p^2)=-\frac{1}{8\pi^2(4-D)}\frac{g^2}{2}\sum_f(\frac{p^2}{3}-m_f^2)+$$

$$G^{ferm}_{WWH}=-g^2\sum_f\frac{m_f}{v}G_f,\qquad G^{ferm}_{ZZH}=-\frac{g^2}{cos^2\theta_W}\sum_f\frac{m_f}{v}G_f,\qquad(25)$$

where $\sum_f$ means the sum over all fermions, Q_f is a fermion charge expressed in the proton charge units. Equating the coefficients at $G_f(m_f)$ in eq.(23) gives

$$\frac{A^{(0)}_{WWH}}{2A^{(0)}_{ZZH}}=cos^2\theta_W=\frac{\xi_1}{2\xi_3}cos^2\theta_W,\qquad(26)$$

Hence we find $\xi_2=\xi_3=\xi_1/2$ and

$$A^{(0)}_{WWH}=\xi_1 g^2,\qquad A^{(0)}_{ZZH}=\frac{1}{2cos^2\theta_W}\xi_1 g^2.\qquad(27)$$

Thus, one can see that the dependencies of the vertexes WWH and ZZH appear even if the fermionic sector only is considered. Now, let us simplify eq. (23) using eq.(27):

$$G_{ZZH}cos^2\theta_W-G_{WWH}=$$

$$=8\pi^2A^{(0)}_{WWH}\lim_{D\to4}(4-D)\Big[\left(\frac{\delta\tilde{\Sigma}^{(1)}_{ZZ}(m_Z^2)}{m_Z^2}-\frac{\partial}{\partial p^2}\delta\tilde{\Sigma}^{(1)}_{ZZ}(p^2)\right)-$$

$$-\left(\frac{\delta\tilde{\Sigma}^{(1)}_{WW}(m_W^2)}{m_W^2}-\frac{\partial}{\partial p^2}\delta\tilde{\Sigma}^{(1)}_{WW}(p^2)\right)\Big]=$$

$$=8\pi^2A^{(0)}_{WWH}\lim_{D\to4}(4-D)\left[\frac{\delta\tilde{\Sigma}^{(1)}_{ZZ}(0)}{m_Z^2}-\frac{\delta\tilde{\Sigma}^{(1)}_{WW}(0)}{m_W^2}\right].\qquad(28)$$

Calculation of the values G_{ZZH}, G_{WWH}, $\delta\tilde{\Sigma}^{(1)}_{ZZ}(0)$, $\delta\tilde{\Sigma}^{(1)}_{WW}(0)$ c in one-loop order gives

$$G_{WWH}=\frac{3g^2}{2}\left(A^{(0)}_{WWH}+A^{(0)}_{ZZH}cos^2\theta_W\right)-$$

$$-\frac{g^4}{4}\left(1+\frac{3}{2}tg^2\theta_W\right)-g^2\sum_f\frac{m_f}{v}G_f,$$

$$G_{ZZH} = 3g^2 A^{(0)}_{WWH} cos^2\theta_W - \frac{g^4}{4} cos^2\theta_W \Big(1 - 2tg^2\theta_W +$$

$$+3tg^4\theta_W\Big) - \frac{g^2}{cos^2\theta_W} \sum_f \frac{m_f}{v} G_f,$$

$$8\pi^2 \lim_{D\to 4}(4-D)\left[\frac{\delta\tilde{\Sigma}^{(1)}_{ZZ}(0)}{m_Z^2} - \frac{\delta\tilde{\Sigma}^{(1)}_{WW}(0)}{m_W^2}\right] =$$

$$= g^2 cos^4\theta_W \left(-\frac{13}{4} tg^2\theta_W - \frac{5}{2} tg^4\theta_W + \frac{3}{4} tg^6\theta_W\right). \quad (29)$$

Substituting eqs. (29) and (27) in eq.(28) leads to the equation for ξ_1:

$$\left(\frac{11}{8\xi_1} - 6\right) tg^2\theta_W + \left(\frac{1}{4\xi_1} - 3\right) tg^4\theta_W + \frac{3}{8\xi_1} tg^6\theta_W =$$

$$= -\frac{13}{4} tg^2\theta_W - \frac{5}{2} tg^4\theta_W + \frac{3}{4} tg^6\theta_W, \quad (30)$$

and finally we obtain $\xi_1 = 1/2$.

As the result we come to conclusion, in the considered case the RG equation gave possibility not only to connect with each other the vertexes WWH and ZZH but also to calculate them explicitly

$$\Gamma^{(0)}_{WWH} = \frac{1}{2} v g^2, \qquad \Gamma^{(0)}_{ZZH} = \frac{1}{4cos^2\theta_W} v g^2, \quad (31)$$

that exactly coincides with the SM result. To complete, let us adduce the relations appearing between the parameters of the EL:

$$\frac{\alpha^{(0)}_{ffWW}}{\alpha^{(0)}_{ffZZ}} = \frac{2\alpha^{(0)}_{WWWW}}{\alpha^{(0)}_{WWZZ}} = \frac{\alpha^{(0)}_{WWZZ}}{2\alpha^{(0)}_{ZZZZ}} = 2cos^2\theta_W. \quad (32)$$

The above simple example shown that the renormalizability of the theory implemented in the equation (18) can be used to reduce the number of independent parameters in the EL. Specific correlations between the parameters corresponding to different processes, naturally, depend on models containing new heavy particles.

5. Discussion of results

Let us note a number of features of the approach proposed.As it was realized, the investigation of the effective operators is reduced to investigation of the scattering processes of different in general case particles

on the external field produced by the heavy particle. The interaction with the external field has to be taken into account in tree approximation. The renormalizability of the fundamental theory implemented in the existence of the RG equation for the low energy EL (1) serves in order to determine a number of relations between scattering processes. The latter fact is very important, since just the relations between $\alpha_{j,d}$ entering the EL would give information about fundamental theory.

Formal mathematical cause of that is originated from the basic property of the vertexes in a renormalizable theory - recurrence of the tree-level algebraic structure by the divergent part of the radiation corrections. The second point is the presence in different RG equations of the same anomalous dimension corresponding to the heavy particle "external field". It can be excluded from the system of one-loop RG equations and resulted in defined ratios between coefficients parametrizing the vertexes and hence between the parameters $\alpha_{j,d}$. Different parametrizations connected with different groups of symmetry will lead to numerically different correlations between chosen parameters $\alpha_{j,d}$.

We complete our discussion with the remark that RG equations give a possibility to obtain information about new physics beyond the SM energy scale investigating scattering processes with ordinary particles at low energies. In a sense, at low energies the one-loop RG equations substitute the condition of the tree unitarity for scattering amplitudes which has been used at high energies to determine the renormalizable theory. So, the developed method seems to be more informative than formulation of not well defined conditions (such as a naturality condition) usually discussed in literature [2], [10], when the EL approach is applied.

References

[1] H. Georgi, Annual review of nuclear and particle science 43, 209 (1994).

[2] J. Wudka, Int.J.Mod.Phys. A9, 2301 (1994).

[3] W. Buchmuller and Wyler, Nucl. Phys. B268, 621 (1986).

[4] C. Arzt, M.B. Einhorn, J. Wudka, B433, 41 (1995).

[5] T. Appelquist and J. Carazzone, Phys. Rev. D11, 2856 (1975).

[6] M. Bando, T. Kugo, N. Naekawa and H. Nakano, Phys. Lett. B301, 83 (1983).

[7] M. Bando, T. Kugo, N. Naekawa and H. Nakano, Progress Theor. Phys. 90, 405 (1993).

[8] K. Hagiwara et. al., Phys. Rev. D48, 2182 (1993).

[9] G. 'tHooft, Nucl. Phys. B62, 444 (1973).

[10] M. Bilenky and A. Santamaria, hep-ph/9503257 7 Mar 1995.

Electroweak phase transition in strong magnetic field

Michael Bordag[a] and Vladimir Skalozub[b]

[a] *Leipzig University,*
[b] *Dniepropetrovsk State University, 320625 Ukraine*

Phase transitions induced by high temperatures and strong magnetic fields are investigated in the Standard model. The one-loop effective potential and the ring diagram corrections are calculated and investigated for different values of field, temperature and the Higgs boson mass m_H. All other particles - fermions and bosons - are taken into account with their actual values of masses. It is shown that the symmetry restoration is the second type phase transition for $m_H \geq M_w$. The magnetic field essentially changes the parameters of the phase transition at high temperatures. It is shown that the fields $H > 3 \cdot 10^24G$ could not be realized in early universe. The vacuum structure is briefly discussed.

1.Introduction

The concept of symmetry restoration at high temperature has been intensively used in studying the evolution of the Universe at its early stages. Nowadays it gives a possibility to investigate various problems of cosmology and particle physics [1],[2]. In particular, the type of the electroweak phase transition and hence a further evolution of the universe depends on the mass m_H of the Higgs boson. Most investigations of the electroweak phase transition have included into consideration a high temperature environment as the main ingredient [2], [3]. But in recent a few years cogent arguments followed from different approaches in favour of the presence of strong magnetic fields at that stage have appeared [5], [6](recent review on the magnetic fields in the universe is Ref.[7]). So, the phase transition at high temperature and strong fields has to be of interest . Moreover, at present time when all masses of fundamental particles, except m_H, are known there is a possibility to investigate in details the phase transition as the function of this parameter .This, in particular, will give a possibility to determine the properties of the vacuum. its structure and to specify a so-called metastability bound on m_H [3],[4].

One of possibilities to have strong magnetic fields in the electroweak phase transition epoch was clarified by Vachaspati [5]. From his analysis it follows that under very general conditions the fields $H \sim T_i^2$ in the patches of sub-horizon scales can be generated during a large class of grand unified transitions [6],[7], where T_i is transition temperatures. The

second one is formation of the Savvidy vacuum magnetic state at high temperature ($H \sim gT^2, g$ is gauge coupling constant) [13, 14],[23]. In latter case only the abelian field configurations could arise spontaneously since they are sourceless. For many problems it is important to estimate the field strengths presented, but it is difficult to realize that without detailed investigations within specific models. Usually, only one type of fields is considered. Therefore, results obtained in such a way give an upper estimate of the field. This remark is relevant to the our present investigation. The discussed "primordial" fields are usually considered as seed fields responsible for generation of the observed magnetic fields in galaxies [7].

Various aspects of the phase transitions in magnetic fields at high temperature have been investigated by many authors [8]-[14]. In Refs. [11],[18] the phase transitions derived with the effective potential (EP) of the bosonic part of the Salam-Weinberg model and the vacuum structures of the phases have also been described. In Ref.[14] in addition to the temperature and magnetic fields a chemical potential was incorporated. But the role of the fermions has not been investigated in details. However, due to a rather heavy t-quark mass, $m_t \simeq 175$ Gev, an unbounded global minimum of the EP is produced in addition to the electroweak local one for not very heavy Higgs's scalars [3]. As will be shown, strong magnetic fields influence essentially the phase transition dynamics realized in this case.Another aspect of the electroweak phase transition, which also was not investigated but plays an important role, is the influence of the so-called ring diagrams at high temperature and strong field. At zero field it was investigated in details in Refs.[15],[16] where it has been shown the importance of these diagrams for determining the type of the phase transition.

In the present lecture we discuss the electroweak phase transition at high temperature and constant strong magnetic fields H . We calculate and investigate the one-loop effective potential and the contributions of ring diagrams. In contrast to previous considerations we include the content of all bosons and fermions with the corresponding masses. So, the only free parameter remains the mass m_H. As we shall see, the influence of fermions (mainly heavy quarks) is of great importance. It also will be shown that for values of mass $m_H \geq M_w$ the electroweak phase transition is of the second type one. Moreover, a magnetic field acts not only to stimulate generation of the electroweak minimum but also it

removes the potential barrier separating this state from the unbounded global minimum produced by the heavy fermions. At any temperature there exist a corresponding field at which the metastable vacuum could not produced at all. This property will be used to find an upper limit on the field strengths at the transition epoch. Fermions affect both the phase transition and the vacuum structure appeared. The lecture is organized as follows. In Sects.2,3 the one-loop contributions of bosons and fermions to the EP $V^{(1)}(T, H, \phi_c)$ are calculated in the form convenient for numerical study. In Sect.4 the contribution of ring diagrams is calcu ated. Further in Sect.5 we investigate symmetry behaviour for the number values of the mass m_H and fields H considering the cases when only the one-loop EP is taken into account and when in addition the ring diagrams are included. The description of vacuum structures and the discussion of the results obtained are given in Sect.6.

2. Boson contributions to $V^{(1)}(T, H, \phi_c)$

The Lagrangian of the boson sector of the Salam-Weinberg model is

$$L = -\frac{1}{4}F^a_{\mu\nu}F^{\mu\nu}_a - \frac{1}{4}G_{\mu\nu}G^{\mu\nu} + (D_\mu\Phi)^+(D^\mu\Phi) + \frac{m^2}{2}(\Phi^+\Phi) - \frac{\lambda}{4}(\Phi^+\Phi)^2, \quad (1)$$

where the standard notations are introduced

$$F^a_{\mu\nu} = \partial_\mu A^a_\nu - \partial_\nu A^a_\mu + g\varepsilon^{abc}A^b_\mu A^c_\nu,$$
$$G_{\mu\nu} = \partial_\mu B_\nu - \partial_\nu B_\mu,$$
$$D_\mu = \partial_\mu + \frac{1}{2}igA^a_\mu\tau^a + \frac{1}{2}ig'B_\mu. \quad (2)$$

The vacuum expectation value of the field Φ is

$$< \Phi >= \frac{1}{\sqrt{2}}\begin{pmatrix} 0 \\ \phi_c \end{pmatrix}. \quad (3)$$

The fields corresponding to the W-,Z-bosons and photons respectively, are

$$W^\pm_\mu = \frac{1}{\sqrt{2}}(A^1_\mu \pm iA^2_\mu),$$

$$Z_\mu = \frac{1}{\sqrt{g^2+g'^2}}(gA^3_\mu - g'B_\mu),$$
$$A_\mu = \frac{1}{\sqrt{g^2+g'^2}}(g'A^3_\mu + gB_\mu). \quad (4)$$

The external e ectromagnetic field is introduced by splitting the potential in two parts: $A_\mu = \bar{A}_\mu + A^R_\mu$, where A^R describes a radiation field and $\bar{A} = (0, 0, Hx^1, 0)$ corresponds to the constant magnetic field directed along the third axis. We make use of the gauge-fixing conditions [22]

$$\partial_\mu W^{\pm\mu} \pm ie\bar{A}_\mu W^{\pm\mu} \mp i\frac{g^2\phi^2}{4\xi}\phi^\pm = C^\pm(x), \quad (5)$$

$$\partial_\mu Z^\mu - \frac{i}{\xi'}(g^2+g'^2)^{1/2}\phi_z = C_z, \quad (6)$$

where $e = gsin\theta_w, tang\theta_w = g'/g, \phi^\pm, \phi_z$ are the Goldstone fields, ξ, ξ' are the gauge fixing parameters, $C^\pm, C_z$ are arbitrary functions and ϕ_c is a scalar condensate value. In what follows, all calculations will be done in the general relativistic renormalizable gauge (5),(6) and after that we set $\xi, \xi' = 0$ choosing the unitary gauge.

To compute the EP $V^{(1)}$ in the background magnetic field let us introduce the proper time,s, representation for the Green functions

$$G^{ab} = -i\int_0^\infty ds \exp(-isG^{-1\,ab}) \quad (7)$$

and use the method of Ref.[17], allowing in a natural way to incorporate the temperature into this formalism. A basic formula of Ref.[17] connecting the Matsubara- Green functions with the Green functions at zero temperature is needed,

$$G^{ab}_k(x, x'; T) = \sum_{-\infty}^{+\infty}(-1)^{(n+[x])\sigma_k} G^{ab}_k(x - [x]\beta u, x' - n\beta u), \quad (8)$$

where $G^{ab}_k$is the corresponding function at $T = 0, \beta = 1/T, u = (0, 0, 0, 1)$, the symbol $[x]$ means a whole part of $x_4/\beta, \sigma_k = 1$ in the case of physical fermions and $\sigma_k = 0$ for boson and ghost fields. The Green functions in the right-hand side of formula (8) are the matrix elements of the operators

G_k computed in the states $\mid x', a)$ at $T = 0$, and in the left-hand side the operators are averaged in the states with $T \neq 0$. The corresponding functional spaces U^0 and U^T are different but in the limit of $T \to 0$ U^T transforms into U^0.

The one-loop contribution into EP is given by the expression

$$V^{(1)} = \frac{1}{2} Tr \log G^{ab}, \tag{9}$$

where G^{ab} stands for the propagators of all the quantum fields $W^{\pm}, \phi^{\pm}, ...$ in the background magnetic field H. In the s-representation the calculation of the trace can be done in accordance with formula [20]

$$Tr \log G^{ab} = -\int_0^{\infty} \frac{ds}{s} tr \exp(-isG_{ab}^{-1}) \tag{10}$$

Details of calculations based on the s-representation and the formula (8) can be found, for example,in Refs.[17],[18],[23]. The terms with $n = 0$ in Eqs.(8), (9) give zero temperature expressions for Green's functions and effective potential $V^{(1)}$, respectively. They are the only terms possessing divergences. To eliminate them and uniquely fix the potential we use the following renormalization conditions at $H, T = 0$[18]:

$$\frac{\partial^2 V(\phi, H)}{\partial H^2} \mid_{H=0, \phi=\delta(0)} = \frac{1}{2}, \tag{11}$$

$$\frac{\partial V(\phi, H)}{\partial \phi} \mid_{H=0, \phi=\delta(0)} = 0, \tag{12}$$

$$\frac{\partial^2 V(\phi, H)}{\partial \phi^2} \mid_{H=0, \phi=\delta(0)} = \mid m^2 \mid, \tag{13}$$

where $V(\phi, H) = V^{(0)} + V^{(1)} + \cdots$ is the expansion in a number of loops and $\delta(0)$ is the vacuum value of a scalar field determined in a tree approximation.

It is convenient for what follows to introduce the dimensionless quantities: $h = H/H_0 (H_0 = M_w^2/e), \phi = \phi_c/\delta(0), K = m_H^2/M_w^2$, $B = \beta M_w, \tau = 1/B = T/M_w, \mathcal{V} = V/H_0^2$ and $M_w = \frac{g}{\sqrt{2}}\delta(0)$.

After reparametrization the scalar field potential is directly expressed in terms of the ratio K,

$$\mathcal{V}^{(0)} = \frac{h^2}{2} + K(-\frac{\phi^2}{4} + \frac{\phi^4}{8}). \tag{14}$$

The renormalized one-loop EP is given by the sum of the functions

$$\mathcal{V}_1 = \mathcal{V}^{(0)} + \mathcal{V}^{(1)}(\phi, H, K) + \omega^{(1)}(\phi, h, K, \tau), \tag{15}$$

where $\mathcal{V}^{(1)}$ is the one-loop EP at $T = 0$, which has been studied already in Ref.[22]. It has the form:

$$\mathcal{V}^{(1)} = \mathcal{V}^{(1)}_{w,z} + \mathcal{V}^{(1)}_{\phi}, \tag{16}$$

where

$$\begin{aligned}
\mathcal{V}^{(1)}_{w,z} = \; & \frac{3\alpha}{\pi} \; [\mu^2 Log\Gamma_1(\frac{1}{2} + \frac{\phi^2}{2h}) + h^2\zeta'(-1) + \frac{1}{16}\phi^4 \\
& - \frac{1}{8}\phi^4 log\frac{\phi^2}{2h} + \frac{1}{24}h^2 - \frac{1}{24}h^2 log(2h)] \\
& + \frac{\alpha}{2\pi}[-2h^2 + (h^2 + h\phi^2)log(h + \phi^2) + (h^2 - h\phi^2)log \mid h - \phi^2 \mid] \\
& + i\frac{1}{2}\alpha h(\phi^2 - h)\theta(h - \phi^2)
\end{aligned} \tag{17}$$

$$\begin{aligned}
\mathcal{V}^{(1)}_{\phi} = \; & K \quad sin^2\theta_w(-\phi^2 + \frac{1}{2}\phi^4) \\
& + \frac{3\alpha}{4\pi}(1 + \frac{1}{2cos^2\theta})(\frac{1}{2}\phi^4 log\phi^2 - \frac{3}{4}\phi^4 + \phi^2) \\
& + \frac{\alpha K^2}{32\pi}[(\frac{9}{2}\phi^4 - \frac{3}{4}\phi^2 + \frac{1}{2})log \mid \frac{3\phi^2 - 1}{2} \mid - \frac{27}{4}\phi^4 + \frac{21}{2}\phi^2]
\end{aligned} \tag{18}$$

and $\omega^{(1)}$ is the temperature dependent contribution to the EP determined by the terms of formulae (8),(9) with $n \neq 0$.

We outline the used calculation procedure considering the W-boson contribution as an example [23],

$$\omega^{(1)}_w = \frac{\alpha}{2\pi}\int_0^\infty \frac{ds}{s^2}\, e^{-is(\phi^2/h)}\Big[\frac{1 + 2\cos 2s}{\sin s}\Big]\sum_1^\infty \exp(ihB^2n^2/4s). \tag{19}$$

As Eq.(17), this expression contains an imaginary part for $h > \phi^2$ appeared due to the tachyonic mode $\varepsilon^2 = p_3^2 + M_w^2 - eH$ in the W-boson spectrum [22]. It can be explicitly calculated by means of an analytic continuation taking into account the shift $s\beta s - i0$ in the s- plane. Fixing $\phi^2/h > 1$ one

can rotate clockwise the integration contour in the s-plane and direct it along the negative imaginary axis. Then, using the identity

$$\frac{1}{\sinh s} = 2\sum_{p=0}^{\infty} e^{-s(2p+1)} \tag{20}$$

and integrating over s in accordance with the standard integral

$$\int_0^{\infty} ds s^{n-1} \exp(-\frac{b}{s} - as) = 2(\frac{a}{b})^{n/2} K_n(2\sqrt{ab}), \tag{21}$$

$a, b > 0$, one can represent the expression (19) in the form

$$Re\omega_w^{(1)} = -4\frac{\alpha}{\pi}\frac{h}{B}(3\omega_0 + \omega_1 - \omega_2), \tag{22}$$

where

$$\omega_0 = \sum_{p=0}^{\infty}\sum_{n=1}^{\infty} \frac{x_p}{n} K_1(nBx_p); x_p = (\phi^2 + h + 2ph)^{1/2}. \tag{23}$$

$$\omega_1 = \sum_{n=1}^{\infty} \frac{y}{n} K_1(nBy), y = (\phi^2 - h)^{1/2} \tag{24}$$

and in the region of parameters $\phi^2 < h$ after analytic continuation

$$\omega_1 = -\frac{\pi}{2}\sum_{n=1}^{\infty} \frac{\mid y \mid}{n} Y_1(nB \mid y \mid), \tag{25}$$

$$\omega_2 = \sum_{n=1}^{\infty} \frac{z}{n} K_1(nBz), z = (\phi^2 + h)^{1/2}, \tag{26}$$

and $K_n(x), Y_n(x)$ are the Macdonald and Bessel functions, respectively. The imaginary part of $\omega_w^{(1)}$ is given by the expression

$$Im\omega_2 = -2\alpha\frac{h}{B}\sum_{n=1}^{\infty} \frac{\mid y \mid}{n} J_1(nB \mid y \mid), \tag{27}$$

$J_n(x)$is Bessel function. As is well known, the imaginary part of EP is signaling the instability of a system [20]. In what follows we shall consider

mainly the symmetry behaviour described by the real part of the EP and processes connected with $\mathrm{Im}\Omega$ will be discussed in Sect.6.

Carrying out similar calculations for the Z- and Higgs bosons, we obtain [11]:

$$\omega_z = -6\frac{\alpha}{\pi}\sum_{n=1}^{\infty}\frac{\phi^2}{\cos^2\theta_w n^2 B^2}K_2(\frac{nB\phi}{\cos\theta}) \tag{28}$$

$$Re\omega_\phi = \left\{ \begin{array}{c} -2\frac{\alpha}{\pi}\sum\frac{t^2}{B^2n^2}K_2(nBt) \\ \alpha\sum\limits_{n=1}^{\infty}\frac{|t|^2}{n^2B^2}Y_2(nB\mid t\mid) \end{array} \right\}. \tag{29}$$

where the variable $t = [K_w(\frac{3\phi^2-1)}{2})]^{1/2}$ at $3\phi^2 > 1$ and series with the function $Y_2(x)$ has to be calculated at $3\phi^2 < 1$. The corresponding imaginary part will also be considered in Sect.6.

The above expressions (16),(22),(28),(29) will be used in numerical studying of the symmetry behaviour at different H, T. In fact, there is a cancellation of a number of terms from the zero-temperature contributions given Eqs.(16) and T-depended terms. This fact has a general nature and can be used as a good check of the correctness of calculations.

3. Fermion contributions to $V^{(1)}(H,T,\phi)$

To find the explicit form of the fermion contribution to the EP let us consider the standard unrenormalized expression written in the s - representation [21]:

$$V_f^{(1)} = -\frac{}{8\pi^2}\sum_{n=-\infty}^{\infty}(-1)^n\int_{-\infty}^{+\infty}\frac{ds}{s^3}e^{-(m^2s+\beta^2n^2/4s)}(eHs)cotheHs, \tag{30}$$

m is a fermion mass. Here, we have incorporated the equation (8) to include a temperature dependence. In what follows, we shall take into account the contributions of all fermions - leptons and quarks - with their masses known at present time. Usually, considering a symmetry behaviour without field one restricts himself by a t-quark contribution only. But in the case of an external field applied this is not a good idea, since the dependence of $V^{(1)}$ on H is a complicated function of the ratio m_f^2/eH. So, at some fixed values of H, T different dependencies on H will contribute for fermions with different masses. Hence, a very complicate dependence on the field takes place in general. We include this in a total, carrying out a numerical calculations and summing up over all the fermions. Now, separating a zero temperature contribution by means of the relation $\sum\limits_{-\infty}^{+\infty} =$

$1 + 2\sum_{1}^{\infty}$ and introducing the parameter $K_f = m_f^2/M_w^2 = 2G_{Yukawa}^2/g^2$, we obtain for the zero temperature fermion contribution to the dimensionless EP ,

$$\begin{aligned}
\mathcal{V}_f(h,\phi) = \; & \tfrac{\alpha}{4\pi} \sum_f K_f^2(-2\phi^2 + \frac{3}{2}\phi^4 - \phi^4 log\phi^2) \\
& - \frac{\alpha}{\pi}\sum_f (q_f^2 \frac{h^2}{6} \log \frac{2 \mid q_f \mid h}{K_f}) \\
& - \frac{\alpha}{\pi}\sum_f [2q_f^2 h^2 \log \Gamma_1(\frac{K_f\phi^2}{2 \mid q_f \mid h}) + (2\zeta'(-1) - \frac{1}{6})q_f^2 h^2 \\
& + \frac{1}{8}K_f^2\phi^4 + (\frac{1}{4}K_f^2\phi^4 - \frac{1}{2}K_f \mid q_f \mid h\phi^2) \log \frac{2 \mid q_f \mid h}{K_f\phi^2}] \quad (31)
\end{aligned}$$

where q_f is a fermion electric charge, the sum

$$\sum_f = \sum_{f=1}^{3}(leptons) + 3\sum_{f=1}^{3}(quarks) \quad .$$

counts the contributions of leptons and quarks with their electric charges. The Γ_1 function is defined as follows (see, for example, survey [22]):

$$\log \Gamma_1(x) = \int_0^x dy \log \Gamma(y) + \frac{1}{2}x(x-1) - \frac{1}{2}x \log(2\pi). \quad (32)$$

The finite temperature part can be calculated in a way, described in the previous section. In the dimensionless variables it looks as follows:

$$\begin{aligned}
\omega_f \; = \; & -4\frac{\alpha}{\pi}\sum_f \Big\{\sum_{p=0}^{\infty}\sum_{n=1}^{\infty}(-1)^n \Big[\frac{(2ph + K_f\phi^2)^{1/2}h}{Bn} K_1((2ph + K_f\phi^2)^{1/2}Bn) \\
& + \frac{(2p+2)h + K_f\phi^2)^{1/2}}{Bn} h K_1(((2p+2)h + K_f\phi^2)^{1/2}Bn)\Big]\Big\} \quad (33)
\end{aligned}$$

Again, a number of terms from Eqs.(31) and (33) are cancelled being summed up, as in the bosonic sector.

These two expressions and the boson contributions obtained in Sect.2 will be used in numerical investigations of symmetry behaviour. More

precise, we consider the difference $V'(H,T,\phi) = ReV(H,T,\phi) - ReV(H, T,\phi = 0)$ giving possibility to determine the symmetry restoration. As was mentioned in Introduction, we will consider the EP of two types - the one-loop contribution and the sum of that and the ring diagrams which are the next corrections.

4. Contribution of ring diagrams

It was shown by Carrington [16] that at $T \neq 0$ a consistent calculation of the EP based on generalized propagators, which include the polarization operator insertions, requires the ring diagrams to be added simultaneously with the one-loop contributions. These diagrams essentially affect the phase transition at high temperature and zero field [15],[16]. Their importance at T and $H \neq 0$ was also pointed out in literature [13],[14] but, as far as we know, these contributions have not been calculated, yet. So, we are going to fill in this gap.

As is known [15], the sum of ring diagrams describes a dominant contribution of great distances. It differs from zero only in the case when massless states appear in a system. So, this type of diagrams has to be calculated when a symmetry restoration is investigated. To find the correction $V_{ring}(H,T)$ at high temperature and magnetic field the polarization operators of the Higgs particle, photon and Z-boson at the considered background have to be calculated. Just these calculations have been announced in Refs.[13], [14]. Then, $V_{ring}(H,T)$ is given by series depicted in figures 1,2.

Here, a dashed line describes Higgs particles, the wavy lines represent photons and Z-bosons, the blobs represent the polarization operators in the limit of zero momenta. As also is known [16], in order to calculate the contribution of ring diagrams not the complete polarization operators $\Pi_{\mu\nu}(k,T,H)$ but only their limiting expressions at zero momenta $\Pi_{00}(k = 0,T,H)$ are sufficient. This limit is named the Debye mass and can be calculated also from the effective potential of special type. The latter considerably simplifies our task.

Now, let us turn to calculations of $V_{ring}(H,T)$.This part of EP is given by the standard expression [15],[16],[13]:

$$V_{ring} = -\frac{1}{12\pi\beta} Tr\{[M^2(\phi) + \Pi_{00}(0)]^{3/2} - M^3(\phi)\}, \qquad (34)$$

where trace means the summation over all the contributing states, $M(\phi)$ is a tree mass of corresponding state and $\Pi_{00}(0) = \Pi(k = 0,T,H)$ for the

Higgs particle and $\Pi_{00}(0) = \Pi_{00}(k = 0, T, H)$ are the zero-zero components of the polarization operators in the magnetic field taken at zero momenta. The above contribution has order $\sim g^3(\lambda^3)$ in coupling constant whereas the two-loop terms are to be of order $\sim g^4$. As $\Pi_{00}(0)$ the high temperature limits of polarization functions have to be substituted which are of orders $\sim T^2$ for leading terms and $\sim g\phi_c T, (gH)^{1/2}T, \phi_c, (gH)^{1/2}/T << 1$ for subleading ones.

For the next step of calculations, we remind that the effective potential is the generating functional of the one-particle irreducible Green functions at zero momenta transferred. So, to have $\Pi(0)$ we can just calculate the second derivative with respect to ϕ of the potential $V^{(1)}(H, T, \phi)$ in the limit of high temperature ,$T >> \phi, (eH)^{1/2}$ and set $\phi = 0$. This limit can be calculated by means of the Mellin transformation technique (see for example [23]) and the result looks as follows:

$$\begin{aligned} V^{(1)}(H, \phi, T\beta\infty) &= [\Big(\frac{C_f}{12}\phi_c^2 + \frac{\alpha\pi}{2cos^2\theta_w}\phi_c^2 + \frac{g^2}{16}\phi_c^2\Big)T^2] \\ &+ [\frac{\alpha\pi}{6}(3\lambda\phi_c^2 - \delta^2(0))T^2 - \frac{\alpha}{cos^3\theta}\phi^3 T \\ &- \frac{\alpha}{3}(\frac{3\lambda\phi_c^2 - \delta^2(0)}{2})^{3/2}T] \\ &- \frac{1}{2\pi}(\frac{1}{4}\phi_c^2 + gH)^{3/2}T + \frac{1}{4\pi}eHT(\frac{1}{4}\phi_c^2 + eH)^{1/2} \\ &+ \frac{1}{2}eHT(\frac{1}{4}\phi_c^2 - eH)^{1/2}, \end{aligned} \tag{35}$$

The parameter $C_f = \sum_{i=1}^{3} G_{il}^2 + 3\sum_{i=1}^{3} G_{iq}^2$ determines the fermion contribution of the order $\sim T^2$ having relevance to our problem. We also omitted $\sim T^4$ contributions to the EP. The terms of the type $\sim log[T/f(\phi, H)]$ cancel the logarithmic terms in the temperature independent contributions (15),(30). Considering the high temperature limit we restrict ourselves by linear and quadratic in T terms, only.

Now, differentiating this expression twice with respect to ϕ and setting then $\phi = 0$, we obtain

$$\begin{aligned} \Pi_\phi(0) &= \frac{\partial^2 V^{(1)}(\phi, H, T)}{\partial\phi^2}\,|_{\phi=0} \\ &= \frac{1}{24\beta^2}\Big(6\lambda + \frac{6e^2}{\sin^2 2\theta_w} + \frac{3e^2}{\sin^2\theta_w}\Big) + \sum_f 2G_f^2/\beta^2 \end{aligned}$$

$$+ \quad \frac{(eH)^{1/2}}{8\pi \sin^2\theta_w \beta} e^2 (3\sqrt{2}\zeta(-\frac{1}{2},\frac{1}{2}) - 1). \qquad (36)$$

The terms $\sim T^2$ in Eq.(36) give standard contributions to temperature mass squared coming from the boson and fermion sectors. The H-dependent term is negative since the difference in the brackets is

$$3\sqrt{2}\zeta(-\frac{1}{2},\frac{1}{2}) - 1 \simeq -0,39.$$

Formally, this may result in the negativeness of the $\Pi(0)_\phi$ for very strong fields $(eH)^{1/2} > T$. But this happens in the range of parameters where asymptotic expansion is not valid. Substituting expression (36) into Eq.(34) we obtain (in the dimensionless variables),

$$\mathcal{V}^{\phi}_{ring} = -\frac{1}{12B}\Big\{(\frac{3\phi^2-1}{2}K + \Pi_\phi(0)\Big\}^{3/2} + \frac{\alpha}{3B}K(\frac{3\phi^2-1}{2})^{3/2}. \qquad (37)$$

As one can see, the last term of this expression cancels the term in Eq.(35), which becomes imaginary at $3\phi^2 < 1$. This is an important property which prevents the infrared instability at high temperature.

To calculate the H-dependent Debye masses of photons and Z-bosons the following procedure will be used. We calculate the one-loop EP of the W-bosons and fermions in a magnetic field and some "chemical potential", μ, which plays the role of the auxiliary parameter. Then, by differentiating them twice with respect to μ and setting $\mu = 0$ the mass squared m_D^2 will be found. Let us demonstrate that in more detail for the case of fermion contributions where the result is known.

The temperature dependent part of the one-loop EP of constant magnetic field and a non-zero chemical potential induced by an electron-positron vacuum polarization is [21]:

$$V^{(1)}_{ferm.} = -\frac{1}{4\pi^2}\sum_{l-1}^{\infty}(-1)^{l+1}\int_0^\infty \frac{ds}{s^3} exp(\frac{-\beta^2 l^2}{4s} - m^2 s) eHs coth(eHs) cosh(\beta l \mu), \qquad (38)$$

where m is the electron mass, $e = g sin\theta_w$ is electric charge and a proper-time representation is used.Its second derivative with respect to μ taken at $\mu = 0$ can be written in the form,

$$\frac{\partial^2 V^{(1)}_{ferm.}}{\partial \mu^2} = \frac{eH}{\pi^2}\beta^2 \frac{\partial}{\beta^2}\sum_{l=1}^{\infty}(-1)^{l+1}\int_0^\infty \frac{ds}{s} exp(-m^2 s - \beta^2 l^2/4s) coth(eHs). \qquad (39)$$

Expanding $coth(eHs)$ in series and integrating over s in accordance with formula (21) we obtain in the limit of $T >> m, (eH)^{1/2}$:

$$\sum_{l=1}^{\infty}(-1)^{l+1}[\frac{8m}{\beta l}K_1(m\beta l) + \frac{2}{3}\frac{(eH)^2 l\beta}{m}K_1(m\beta l) + \cdots] \qquad (40)$$

Series in l can easily be calculated by means of the Mellin transformation (see, for example, Refs.[23],[14]). To have the Debye mass squared it is necessary to differentiate Eq.(39) with respect to β^2 and to take into account the relation of the parameter μ with the zero component of the electromagnetic potential : $\mu ßieA_0$ [13]In this way we obtain finally,

$$m_D^2 = g^2 sin^2\theta_w(\frac{T^2}{3} - \frac{1}{2\pi^2}m^2 + O((m\beta)^2, (eH\beta^2)^{\cdot}). \qquad (41)$$

This is the well known result calculated from the photon polarization operator (see for example [19]). As we see, the dependence on H appears in the order $\sim T^{-2}$. To find the total fermion contribution to m_D^2 one should sum up expression (41) over all fermions and substitute their electric charges.

To calculate m_D^2 for Z-bosons it is sufficient to take into account the fermion couplings with Z-field. It can be done by substituting $\mu ßi(g/2cos\theta_w + gsin^2\theta_w)$ and the result differs from Eq. (41) by the coefficient at the bracket in the right-hand side which have to be replaced, $g^2 sin^2\theta ßg^2(\frac{1}{4cos^2\theta_w} + tang^2\theta_w)$. One also should add the terms coming due to the neutral currents and the part of fermion-Z-boson interaction which is not reproduced by the above replacement:

$$m_D^{2'} = \frac{g^2}{8cos^2\theta_w}(1 + 4sin^4\theta_w)T^2. \qquad (42)$$

Now, let us apply this procedure for the case of the W-boson contribution. The corresponding EP (temperature dependent part) calculated at non-zero T, μ in the unitary gauge looks as follows,

$$V_w^{(1)} = -\frac{eH}{8\pi^2}\sum_{l=1}^{\infty}\int_0^{\infty}\frac{ds}{s^2}exp(-m^2 s - l^2\beta^2/4s) \qquad (43)$$

$$[\frac{3}{sinh(eHs)} + 4sinh(eHs)]cosh(\beta l\mu).$$

All the notations are obvious. The first term in the squared brackets gives the triple contribution of the charged scalar field and the second one is due to the interaction with a W-boson magnetic moment. Again, after differentiation twice with respect to μ and setting $\mu = 0$ it can be written as

$$\frac{\partial^2 V_w^{(1)}}{\partial \mu^2} = \frac{eH}{2\pi^2}\beta^2 \frac{\partial}{\partial \beta^2} \sum_{l=1}^{\infty} \int_0^{\infty} \frac{ds}{s} exp(-\frac{m^2 s}{eH} - \frac{l^2\beta^2 eH}{4s}) \qquad (44)$$

$$[\frac{3}{sinh(eHs)} + 4sinh(eHs)].$$

Expanding $sinh^{-1}s$ in series over Bernoulli's polynomials,

$$\frac{1}{sinhs} = \frac{e^{-s}}{s} \sum_{k=0}^{\infty} \frac{B_k}{k!}(-2s)^k, \qquad (45)$$

and carrying out all the calculations described above, we obtain for the W- boson contribution to m_D^2 of the electromagnetic field,

$$m_D^2 = 3g^2 sin^2\theta_w [\frac{1}{3}T^2 - \frac{1}{2\pi}T(m^2 + gsin\theta_w H)^{1/2} - \frac{1}{8\pi^2}(gsin\theta_w H) \qquad (46)$$

$$+O(m^2/T^2, (gsin\theta_w H/T^2)^2)].$$

As is seen, spin does not contribute to the Debye mass in the leading order. The second very important point is that the linear in T term has negative sign. This leads to the generation of the magnetic field at high temperature. More detailed it was discussed in Ref. [13].

The contribution of the W-boson sector to the Z-boson mass m_D^2 is given by expression (46) with the replacement $g^2 sin^2\theta_w ß g^2 cos^2\theta_w$.

Summing up the expressions (41) and (46) and substituting them in Eq.(34), we obtain the photonic part V_{ring}^{γ} where it is also necessary to express masses in terms of the vacuum value of the scalar condensate ϕ_c. In the same way the contribution of Z-bosons V_{ring}^{z} can be calculated. The only difference is an additional mass term of Z -field and the additional term in the Debye mass due to the neutral current $\sim \bar{\nu}\gamma_\mu \nu Z_{mu}$. These three fields - ϕ, γ, Z ,- which becomes massless in the restored phase, contribute into $V_{ring}(H,T)$ in the presence of the magnetic field. At zero field there is also a term due to the W-boson loops in Figs.1,2 . But when $H \neq 0$ the charged particles acquire $\sim eH$ masses. The corresponding fields remain short-range ones in the restored phase of the vacuum and

therefore do not contribute. A separate consideration should be spared to the tachyonic mode in the W-boson spectrum . We also shall discuss it in details below. Here, it only worth to mention that this mode is connected with a spin interaction and does not influence the $G_{00}(k)$ component of the W-boson propagator. So, the "Coulomb-like charged field" is short-rang one when an external magnetic field is switched on.

5. Symmetry behaviour in a magnetic field at high temperature Having obtained the one-loop EP described by formulae (16),(22), (28)-(33) and the ring diagrams contribution V_{ring} we are going to investigate the symmetry behaviour at high temperature and strong magnetic fields. We shall present that in two steps. First, we consider the sum of the three and one-loop effective potentials as the function of ϕ^2 at various fixed H, T and K . Then, we shall add the term V_{ring} and calculate the symmetry behaviour for the total EP at the same fixed H, T, K. This will clarify the role of the plasmon contributions in the magnetic field. Since our EP by construction contains as an input all the fundamental particles, we shall obtain new information about the electroweak phase transition.

As usually [22], to investigate symmetry behaviour let us consider the difference $\mathcal{V}' = Re[\mathcal{V}(h,\phi,K,\beta) - \mathcal{V}(h,\phi = 0,\beta)]$ which describes the possibility of symmetry restoration. More precise, we consider the real part of this function. The imaginary part describing the instability of the state because of the unstable mode in the W-boson spectrum will be discussed separately. Below, we consider the case when the mass m_H is equal to M_w. Typical curves for small fields h and different values of β are plotted in Fig.3.

It is seen that the well known symmetry restoration (for the heavy fermion case) takes place. There are two minima - local, produces due to the Higgs mechanism, and and global one, generated due to heavy fermion contributions. At low temperatures (big β) the local metastable minimum is disposed near the value $\phi^2 = 1$ that corresponds to the spontaneously broken symmetry. With a temperature increasing the local minimum becomes shallower and at $\beta \sim 0.1$ removes to the value $\phi^2 = 0$ that signals the symmetry restoration. At the same time the barrier separating two minima is increasing in height and width suppressing tunneling to the global unbounded from below minimum.

In Fig.4 we present the influence of the field on the symmetry behaviour at low temperature. As is seen, an increase in h leads to the getting deeper of the local minimum and to the growing up the barrier which separates

the minima. In this way the magnetic field prevents the tunneling to the global minimum.

Now, let us investigate symmetry behaviour at high temperature and strong magnetic fields. Typical picture is shown in Fig.5. From the plot it follows that the field acts as a temperature decreasing and stimulates the symmetry breaking. First the metastable vacuum is generated under the field increasing. When the field strength is growing further the potential barrier between the local and global vacua is diminishing and the depth of the former one is getting smaller. At $h \geq 3$ the electroweak minimum disappears at all. This picture is typical and realized at any high temperature. Therefore, it is possible to obtain an upper limit on the magnetic field strength requiring that the electroweak vacuum must be a long living state. From the above analysis one could conclude that the fields $H \geq 3H_0 = M^2/e \sim 3 \cdot 10^24G$ have not been generated in the early universe. In the opposite case our world would never been realized and the system from the very beginning suppose to be in the global minimum. Similar symmetry behaviour (with slightly different values of h, β) has also been determined for $K = 2$. Summarizing the above results we note that fermions affect in a very essential way the symmetry behaviour in the field H.

Now, let us include in our consideration the contribution of $V_{corr.}$. In Fig. 6 the curves a),b) show the symmetry behaviour for intermediate temperatures and small fields. The case a) corresponds to the one-loop EP and b) - to the total EP including the ring diagram effect. The curves c), d) describe correspondingly the same potentials for the middle values of fields. From the plot it follows that $V_{corr.}$ is inessential for intermediate h, β. But it is important for small h when this contribution acts to remove the separation barrier and stimulate the transition to the global vacuum state.

In Fig.7 the influence of the ring diagrams is represented for small β. We see again that with $V_{corr.}$ included (curve b))the influence of the field is resulted in the removing of the barrier and in this way the transition to the global minimum is stimulated. This effect is important for the cosmology scenario with the primordial magnetic field. In particular, it means that to have the long-leaving metastable minimum the bound value of the Higgs boson mass have to be increased as compared with the zero field case discussed in literature [3],[4]. Another important possibility arises for the fixed value of K. in this case to have a realized metastable vacuum an

upper limit on possible field strengths should be derived, as we discussed before.

6. Discussion

Let us discuss the vacuum stability in a magnetic field. This problem is connected with the presence in the W-boson spectrum the mode $p_0^2 = M_w^2 - eH$ which becomes unstable for $H > M_w^2/e$. The evolution of this state and its consequences have been investigated by many authors in various approaches [24],[22],[12]. For the considered case of high temperatures this problem was studied only for the bosonic part of electroweak theory been included [11],[18],[12]. In Refs. [12] the classical equations of W, Z and ϕ fields were solved and the results that at high temperature the symmetry is restored and the magnetic field is screened by the W- boson and Z-boson condensates have been obtained. The key point in this approach is the assumption that the symmetry restoration is the second type phase transition which can be taken into account by adding the term $\sim \phi^2 T^2$ in field equations. In Refs.[11],[18] the vacuum structures at high temperatures generated due to the evolution of the unstable mode for different values of the parameter K have been described . In these papers both the classical equations and the one-loop EP were included. The latter is obligatory because of the complicated behaviour of the EP in the intermediate range of temperatures and magnetic fields. But the conclusion about the final vacuum state was not derived.

The present investigation based on the complete EP with fermions included shown that symmetry restoration is really to be the second type phase transition (for values of K considered ,$m_H > M_w$). Therefore, the results of Ref. [12] seam to be relevant. However, at finite temperature not only the terms $\sim \phi^2 T^2$ but also a number of other terms dependent on H, T, ϕ (see Eqs.(41), (46)) are generated. These terms as well as the Debye mass of charged W- bosons should be included in the effective Lagrangian describing the evolution of the instability. Thus, a complete investigation of the instability evolution requires an additional calculations. But for the cases of intermediate states shown in figures 4 - 6, when the imaginary part $ImV^{(1)}$ is small, the results of Refs.[11],[25] are relevant. So, one can arrive at the qualitative picture that the evolution of the unstable mode in these states is resulted in the lattice vacuum structure formed from $W-, Z-$ and scalar fields.

As follows from the results of Sect.4 , the role of fermions is very essential in the symmetry dynamics. Actually, their contribution deter-

mines the properties of the phase transition due to magnetic field. We have seen that at low temperature the field acts to prevent the phase transition from the metastable to stable minimum of the EP. Since the charged fermions and gauge bosons oppositely influence the symmetry behaviour in a magnetic field, for the actual values of particle masses these two contributions compensate each other and the position of the metastable minimum remains near the initial point $\phi^2 = 1$ for any values of h. The influence of the field is expressed in the change of the potential barrier separating two minima. As is also occurred, at high temperatures the role of the ring diagrams is important (as also takes place at $h = 0$ [15],[16]).Their effect is resulted in an essential modification of the form of the EP curves (see figures 5-7) for the same fixed h. Thus, we conclude that the EW phase transition in a magnetic field acquires substantial changes. For its detailed investigation it is necessary to calculate the bubble nucleation parameters, the metastability bound on m_H, etc. which are characteristics of the first type phase transition. That will be the topic for future.

Other interesting problem which can be studied on the base of the obtained results is the generation of the chromomagnetic field in massless non-abelian theories at $T \neq 0$. This problem has also intensively been investigated [23],[23] but a final conclusion about the phenomenon was not derived because of the gluon Debye masses at non-zero field required for that have not been calculated. Now these masses can be easily obtained from Eq. (46) at the value of the scalar field $\phi = 0$. More precise, to have the result corresponding to the massless Yang-Mills theory in abelian magnetic field it is necessary also to substitute the factor 3 counting the number of polarizations of W-boson to factor 2 - the number of gluon polarizations. We obtain

$$m_L^2 = g^2[\frac{2}{3}T^2 - \frac{1}{\pi}T(gH)^{1/2} - \frac{1}{4\pi^2}gH + O(gH/T^2)], \qquad (47)$$

g is the gauge coupling constant. Hence it is seen that the second term has the negative sign and therefore the field has to be spontaneously generated at high temperatures (for details on this point see Ref.[13]). Naturally, the same has relevance to the phase with restored symmetry in the Standard model. One of possible ways to stabilize this state was proposed in Ref. [13]. It consists in spontaneous generation of the gauge field electrostatic potential. But to have a final conclusion about this mechanism it is

necessary to consider a common generation of these fields. This also is the problem for future.

As a conclusion we would like to note that the electroweak phase transition in primordial magnetic fields acquires substantial modifications which would be resulted in new interesting phenomena of young Universe described by the Standard model.

One of the authors (V.S.) expresses kind gratitude to colleagues from Institute of Theoretical physics University of Leipzig for hospitality and the DAAD programme for financial support of his stay at Leipzig in period when this work had been carried out.

References

[1] D. Kirzhnits, JETP Lett. 15, 529 (1972)

[2] A.D. Linde, Particle Physics and Inflationary Cosmology (Harwood Academic, New York, 1990)

[3] M. Sher, Phys. Rep. 179, 273 (1989)

[4] J.R. Espinosa, Preprint DESY 96-107 IEM-FT-96-133, June 1996

[5] T. Vachaspati, Phys. Lett. B265, 258 (1991)

[6] P.H. Brandenberger, A-C. Davis, A.M. Matheson and M. Troden, Phys. Lett. B 293, 287 (1992)

[7] K. Enquist, astro-ph/9707300 28 July 1997.

[8] J. Chakrabarti, Phys. Rev. D28 , 2657 (1983); ibd D29 1859 (1984)

[9] M. Reuter and W. Dittrich, Phys. Lett. 144B , 99 (1984)

[10] J. Fujimoto and T. Fukuyama, Z. Phys. C19 , 11 (1983)

[11] V.V. Skalozub, Sov. J. Nucl. Phys. 45, 1058 (1987)

[12] J. Ambjorn and P. Olesen , Nucl. Phys. B315, 606 (1989); B330 , 193 (1990)

[13] A.O.Starinets, S.A. Vshivtsev and V.Ch. Zhukovskii, Phys. Lett. B322, 287 (1994)

[14] A.S. Vshivtsev, V,Ch. Zhukovsky and A.O. Starinets Z. Phys. C, (1993)

[15] K. Takahashi, Z. Phys. C26 , 601 (1985)

[16] M. Carrington, Phys. Rev. D45 , 2933 (1992)

[17] A. Cabo, Fortschr. Phys. 29, 495 (1981)

[18] Yu.Yu. Reznikov and V.V. Skalozub, Sov. J. Nucl. Phys. 46 , 1085 (1987)

[19] A.S. Vshivtsev, V. Ch. Zhukovsky, B.V. Magnitsky and A.V. Tatarintsev, Preprint - 89 -21/ 98 , Inst. Nucl. Phys. Moscow State Univ., Moscow, 1989

[20] J. Schwinger, Phys. Rev. 82 , 664 (1951)

[21] P. Elmfors, D. Persson and B-S. Skagerstam, Phys. Rev. Lett. 71 (1993) 480

[22] V.V. Skalozub, Sov. J. Part. Nucl. 16, 445 (1985)

[23] V.V. Skalozub, Int. J. Mod. Phys. A 11, 5643 (1996)

[24] H.B. Nielsen and M. Ninomiya, Nucl.Phys. B163, 57 (1980); B169, 309 (1980); J. Ambjorn and P. Olesen, Nucl. Phys. B170, 265 (1980)

[25] S. MacDowell and O. Törnquist, Phys. Rev. D45, 3833 (1992)

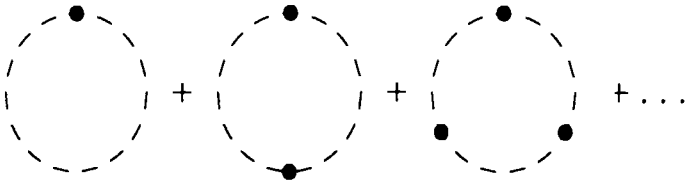

Fig.1

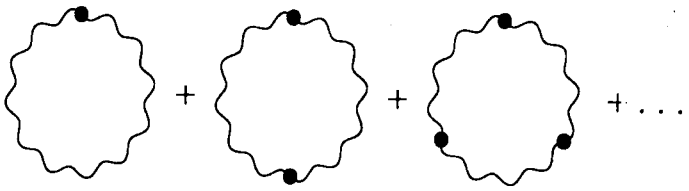

Fig.2

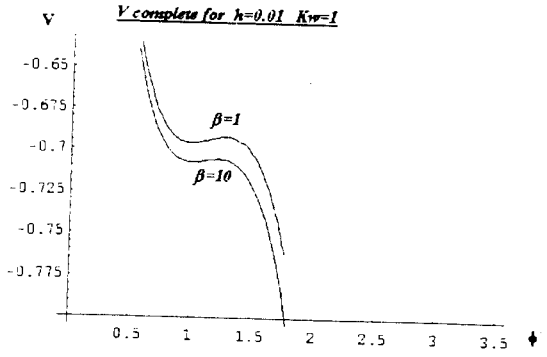

Fig.3

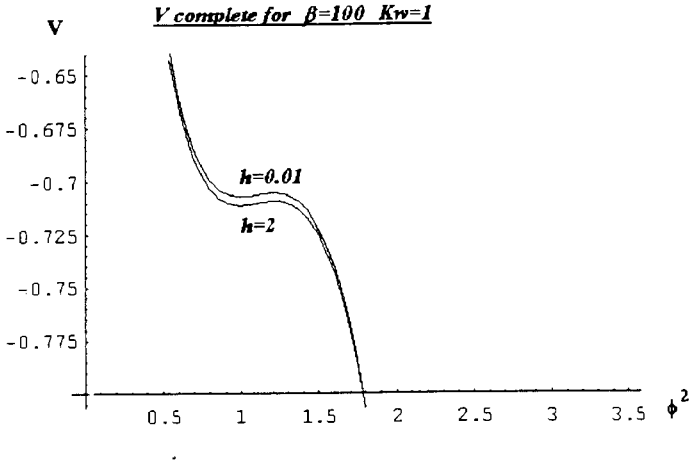
V complete for β=100 Kw=1
V
-0.65
-0.675
-0.7
-0.725
-0.75
-0.775
h=0.01
h=2
0.5
1
1.5
2
2.5
3
3.5
ϕ2

Fig.4

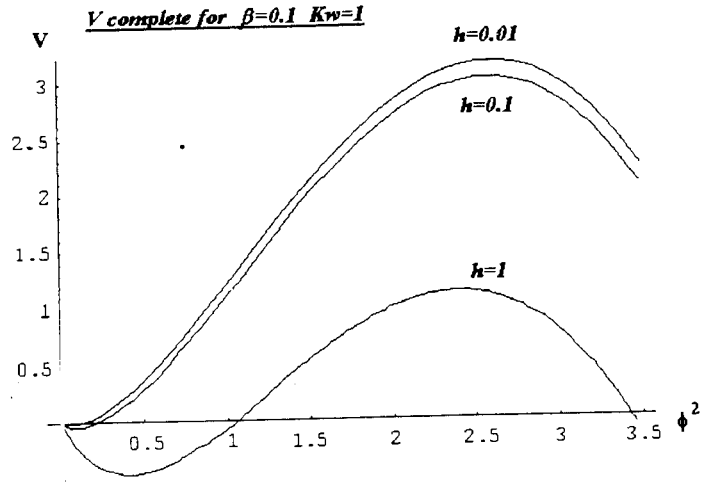
V complete for β=0.1 Kw=1
V
3
2.5
2
1.5
1
0.5
h=0.01
h=0.1
h=1
0.5
1
1.5
2
2.5
3
3.5
ϕ2

Fig.5

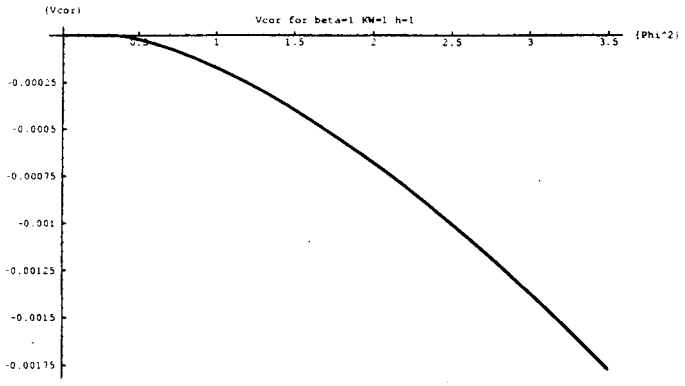
(Vcor)
Vcor for beta=1 KW=1 h=1
(Phi^2)
1
1.5
2
2.5
3
3.5
-0.00025
-0.0005
-0.00075
-0.001
-0.00125
-0.0015
-0.00175

Fig.6

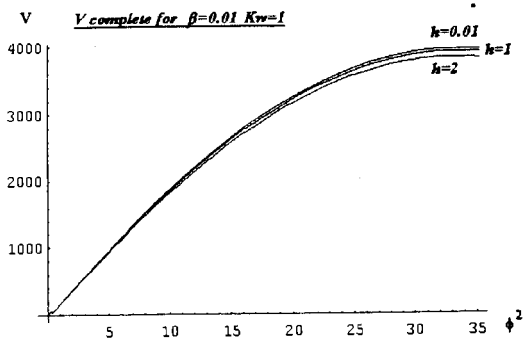
V
V complete for β=0.01 Kw=1
h=0.01
h=1
h=2
4000
3000
2000
1000
5
10
15
20
25
30
35
Φ²

Fig.7

Energy spectrum of the 5-dim hydrogen-like atom on the $SU(2)$ instanton background

M. V. Pletyukhov, E. A. Tolkachev

Institute of Physics, National Academy of Sciences of Belarus
Minsk 220072 Scorina av., 70
E-mail: plet@dragon.bas-net.by, tea@dragon.bas-net.by

Using the oscillator representation for the Schrödinger equation of the 5-dim hydrogen-like atom on the background of the $SU(2)$ instanton we construct the energy spectrum of the problem.

1. Introduction

It is well-known that non-relativistic quantum-mechanical problem about the hydrogen atom (on the Dirac's monopole background or without it) can be interpreted in terms of the 4-dim isotropic (singular) oscillator with constraints [1]. The convenience of such representation is apparent. It enables to construct the set of the coherent states and to pass consistently to the classical limit [2, 3], to develop the geometric quantization technique [4] and to calculate the energy spectrum [5]. The latter can be readily done due to the approach based on the dynamic symmetries of singular oscillator which have been investigated in [6, 7].

In the present work we are interested in the hydrogen-like systems in the dimensions higher than 3 allowing the oscillator representation on the analogue with the hydrogen case. In particular, we consider [8] the 5-dim hydrogen-like atom on the background of the BPST (Belavin-Polyakov-Schwartz-Tyupkin) instantonic potential [9]

$$\left(\frac{\pi_\mu^2}{2} - \frac{\alpha}{R}\right)\varphi = \varepsilon\varphi, \tag{1}$$

where $\pi_\mu = -i\partial_\mu - A_\mu^a \Lambda_a$, $\mu = 0, \ldots, 4$, $a = 1, 2, 3$; $R^2 = r_\mu r_\mu$; Λ_a are the generators of the $SU(2)$ representation with 'isospin' equal l ; $\varphi \in L^{(2l+1)}$– linear space of the representation; A_μ^a are the components of 1-form of the BPST-instantonic connection:

$$A_\mu^i dr^\mu = \frac{1}{R(R + r_0)}(-r_4 dr_a + r_a dr_4 - \varepsilon_{abc} r_b dr_c.) \tag{2}$$

Our goal is to calculate the energy spectrum of (1).

2. 5-dim hydrogen-like atom as 8-dim singular oscillator

Consider 8-dim singular oscillator with the Hamiltonian

$$H = -\frac{1}{2}\sum_{i=1}^{8}\frac{\partial^2}{\partial x_i^2} + \frac{\omega x^2}{2} - \frac{2l(l+1)}{x^2} \qquad (x^2 = \sum_{i=1}^{8} x_i x_i). \tag{3}$$

Following [10] we bind the coordinates in $\dot{R}^5$ and $\dot{R}^8$ by means of the Hurwitz transformation

$$r_\mu = C_\mu^{ij} x_i x_j. \tag{4}$$

This transformation possesses the property

$$r_\mu r_\mu = (x_i x_i)^2 \quad \text{or} \quad R = x^2. \tag{5}$$

There is the set of the operators X_a [11] obeying the $SU(2)$ commutation relations $[X_a, X_b] = i\varepsilon_{abc}X_c$, such that every of them removes the function depending on r_μ only: $X_a f(r_\mu) = 0$.

It is shown [11] that the Schrödinger equation for the Hamiltonian (3)

$$H\Psi^{(8)} = E\Psi^{(8)} \tag{6}$$

with the constraint

$$\mathbf{X}^2\Psi^{(8)} = l(l+1)\Psi^{(8)} \tag{7}$$

is equivalent to (1). The connection between these two problems is set up by means of (4) and with due regard for the relations binding the wavefunctions, energies and parameters:

$$\Psi^{(8)} = \sum_m D^l_{mm'}(\mathbf{z})\varphi(r_\mu), \tag{8}$$

$$\alpha = E/4, \qquad \varepsilon = -\omega^2/8 \tag{9}$$

where $D^l_{mm'}(\mathbf{z})$ are the Wigner functions depending on the auxiliary coordinates $\mathbf{z}$ [11], index l is fixed (for instance, $m' = 0$ for integer l and $m' = l$ for half-integer l).

3. Energy spectrum

The eigenvalues of the Hamiltonian (3) are given by [6, 7]

$$E_{nj} = 2\omega\left(n + 1/2 + \sqrt{-l(l+1) + j(j+3) + 9/4}\right), \tag{10}$$

where j takes integer and half-integer values.

Taking into account the relations (9) one can readily find

$$\varepsilon_{nj} = -\frac{\alpha^2}{2\left(n+1/2+\sqrt{-l(l+1)+j(j+3)+9/4}\right)^2}. \tag{11}$$

But such consideration doesn't make clear what values j *exactly* takes.

To obtain the expression (11) in the closed form we shall use the approach based on the ideas of the dynamic symmetries. Consider the operators

$$\begin{aligned} B_2^+ &= -i\omega a_j^+ a_j^+ - i\frac{2l(l+1)}{x^2}, \\ B_2 &= i\omega a_j a_j + i\frac{2l(l+1)}{x^2}, \\ H &= \omega(a_j^+ a_j + 4) - \frac{2l(l+1)}{x^2}. \end{aligned} \tag{12}$$

The creation $a_j^+ = \frac{1}{\sqrt{2\omega}}(\omega x_j - \partial_j)$ and annihilation $a_j = \frac{1}{\sqrt{2\omega}}(\omega x_j + \partial_j)$ operators obey the usual relations

$$[a_j, a_j^+] = \delta_{ij}.$$

Let us introduce the operators

$$K_0 = \frac{H}{2\omega}, \quad K_+ = \frac{B_2^+}{2\omega}, \quad K_- = \frac{B_2}{2\omega} \tag{13}$$

which satisfy the standard $SU(1,1)$ commutation relations

$$[K_0, K_\pm] = \pm K_\pm, \quad [K_-, K_+] = 2K_0. \tag{14}$$

The representation of the $SU(1,1)$ is constructed as follows [7]

$$\begin{aligned} K_0|n,k\rangle &= (n+k)|n,k\rangle, \\ K_+|n,k\rangle &= \sqrt{(n+1)(n+2k)}|n+1,k\rangle, \\ K_-|n,k\rangle &= \sqrt{n(n+2k-1)}|n-1,k\rangle, \end{aligned} \tag{15}$$

where $n = 0, 1, \ldots$ and $k(k-1)$ are the eigenvalues of the Casimir operator

$$C_2 = K_0^2 - K_0 - K_+ K_-. \tag{16}$$

From the formal relation

$$\frac{E}{2\omega} = n + k \tag{17}$$

and by force of (9) the next formula derives

$$\varepsilon_{nk} = -\frac{\omega_{nk}^2}{8} = -\frac{\alpha^2}{2(n+k)^2}. \tag{18}$$

Here n takes the arbitrary integer non-negative values. One should figure out what values k takes.

Let us express C_2 through the operator of the squared $SO(8)$ angular momentum F^2

$$C_2 = \frac{1}{4}F^2 + 2 - l(l+1), \tag{19}$$

where $F^2 = \sum_{j \le m} F_{jm}F_{jm}$, $F_{jm} = i(x_j\partial_m - x_m\partial_j)$, $1 \le j < m \le 8$.

In [12] the complete set of the wavefunctions of the 8-dim oscillator has been constructed by means of the consideration of the subgroup chain $SO(8) \supset SO(4) \times SO(4) \supset U(1) \times U(1) \times U(1) \times U(1)$. The obtained wavefunctions $Y^j_{j_1 m_{11} m_{12} j_2 m_{21} m_{22}}$ are the simultaneous eigenfunctions of the mutually commuting operators F^2, $\mathbf{I}^2 = \mathbf{I}_1^2 = \mathbf{I}_2^2$, $\mathbf{N}^2 = \mathbf{N}_1^2 = \mathbf{N}_2^2$, I_{1_3}, I_{2_3}, N_{1_3}, N_{2_3} with eigenvalues

$$\begin{aligned}
F^2 Y^f &= f(f+6)Y^f, \\
\mathbf{I}^2 Y^f &= j_1(j_1+1)Y^f, \\
\mathbf{N}^2 Y^f &= j_2(j_2+1)Y^f, \\
I_{1_3} Y^f &= m_{11}Y^f, \\
I_{2_3} Y^f &= m_{12}Y^f, \\
N_{1_3} Y^f &= m_{21}Y^f, \\
N_{2_3} Y^f &= m_{22}Y^f,
\end{aligned} \tag{20}$$

where

$$0 \le f \le 2n-2, \quad n \text{ integer}, \quad f \text{ even},$$

$$1 \le f \le 2n-1, \quad n \text{ half-integer}, \quad f \text{ odd};$$

$$0 \le j_1 + j_2 \le f/2, \quad f \text{ even}, \quad j_1 + j_2 \text{ integer},$$

$$1/2 \le j_1 + j_2 \le f/2, \quad f \text{ odd}, \quad j_1 + j_2 \text{ half-integer};$$

$$-j_1 \le m_{11}, m_{12} \le j_1,$$

$$-j_2 \leq m_{21}, m_{22} \leq j_2.$$

Comparing the explicit form of the operators $\mathbf{I}_1$, $\mathbf{N}_1$ and $\mathbf{X}$ [12] one can immediately deduce that $\mathbf{I}_1 + \mathbf{N}_1 = \mathbf{X}$.

We recall that there exist the constraint (7). According to the angular momentum addition rules $l = j_1 - j_2, \ldots, j_1 + j_2$ (we put $j_1 \geq j_2$ for certainity), i.e. that l takes values dependent on j_1 and j_2. We shall rearrange the scheme (20) in order to make l the free index, i.e. taking the arbitrary integer and half-integer values: $l = 0, 1/2, 1, \ldots$.

Let us define $j = f/2$ and put $l = p - q$, where $q = j_1 + j_2$, $p = 0, 1, \ldots, 2j_2$. From the comment to (20) it follows that $j = q, q+1, \ldots = q + p'$, where $p' = 0, 1, 2, \ldots$. Fixing l we find $j = l + (p + p')$, where $p'' = 0, 1, 2, \ldots$

Mutual respect of the formulas (19) and (20) leads to the relation

$$k(k-1) = j(j+3) + 2 - l(l+1), \tag{21}$$

which allows to express k through j

$$k = 1/2 + \sqrt{-l(l+1) + j(j+3) + 9/4}. \tag{22}$$

Substituting it into (18) we obtain the energy spectrum for the 5-dim hydrogen-like atom on the background of the $SU(2)$ BPST-instanton

$$\varepsilon_{nk} \to \varepsilon_{nj} = -\frac{\alpha^2}{2\left(n + 1/2 + \sqrt{-l(l+1) + j(j+3) + 9/4}\right)^2}. \tag{23}$$

It exactly coincides with (11), but now we are convinced that

$$j = l, l+1, \ldots$$

In particular case $l = 0$ the result

$$\varepsilon_{nj} = -\frac{\alpha^2}{2(n+j+2)^2}. \tag{24}$$

is in the full correspondence with that derived in [13].

References

[1] Iwai T., Uwano Y. *J.Phys.* **A 21** (1988) 4083

[2] Gerry C. *Phys.Rev.* **A 33** (1986) 6

[3] Pris' I., Tolkachev E. *Sov.J.Nucl.Phys.* **58** (1991) 258

[4] Mladenov I., Tsanov V. *J.Phys.* **A 20** (1987) 5865

[5] Pris' I., Tolkachev E. *Yad.Fiz.* **54** (1991) 962

[6] Malkin I., Man'ko V. *Dynamic symmetries and coherent states of the quantum systems.* Moscow, 1979 [in Russian]

[7] Perelomov A. *Generalized coherent states and their applications.* Moscow, 1987 [in Russian]

[8] Pletyukhov M., Tolkachev E. In: *Proceedngs of the Second International Workshop "Quantum Systems : New Trends and Methods",* Minsk,1996 (eds. Kim Y.S. et al, World Scientific)

[9] Belavin A. et al *Phys.Lett.* **59B** (1975) 85

[10] Polubarinov I. *Higher Hypercomplex numbers and quantum mechanics.* Dubna, 1984 (Preprint JINR)

[11] Pletyukhov M., Tolkachev E. In: *Proceedngs of the Sixth Annual Seminar "Nonlinear Phenomena in Complex Systems",* Minsk,1997 (eds. Kuvshinov V.I. and Krylov G.G.) [in print]

[12] Trunk M. *Int.J.Mod.Phys.* **11** N 13 (1996) 2329

[13] Davtyan L. et al *J.Phys.* **A 20** (1987) 6121

Nonperturbative QCD effects

L. Babichev, V. Klenitsky, V. Kuvshinov, V. Shaporov, R. Shulyakovsky

Institute of Physics, Skorina 70, 220072 Minsk, Belarus
e'mal: kuvshino@dragon.bas-net.by

Here we consider analytically the possibility of existence and correlation properties of three nonperturbative QCD phenomena: squeezed gluon states in jets, strong instanton in DIS and temperature hysteresis phenomenon in the first order QGP phase transitions.

I Introduction

In this short review we try to demonstrate that not speaking on confinement their exist some new essentially nonperturbative QCD phenomena with interesting physical properties and which can be search at corresponding experiments.

First of them is gluon analogy quantum photon states and in particular quantum squeezed states which are actively studied now in quantum optics. We demonstrate that nonperturbative QCD evolution can lead to quantum gluon squeezed states in QCD jets.

Second phenomenon is strong instanton induced processes in DIS which can appear and are search now in H1 experiment at HERA. We study correlations between gluon in final state as a possible signal of such processes.

And third - is temperature hysteresis which as we show appear in QGP first order phase transitions and can be connected with the properties of chiral symmetry violation and confinement.

II Two gluon correlations at the nonperturbative stage of jet evolution.

There were a number of phenomenological attempts to describe hadron multiplicity distribution (MD) and KNO scaling functions for different high-energy processes by general squeezed state (SS) by analogy with quantum optics (QO). For example, MD of produced particles in e^+e^-collisions [1],[2] shows steady oscillatory behaviour that differentiates from the poissonian and negative binomial distributions (NBD).

These states can have reduced uncertainty of physical variable compared with coherent one, sub-poissonian (for coincide phases) and super-poissonian (for antiphases) statistics corresponding to antibunching and bunching of photons, can decrease quantum noise [3].

Earlier we have proved that gluon SS can appear at the nonperturbative stage of evolution due to gluon selfinteraction in jet both for collinear gluons [4] and noncollinear gluons at the small jet cone [5].

We have studied colour evolution of gluon state at the nonperturbative stage of QCD for the jet ring and for the total jet cone and also checked the fulfilment of the condition of squeezing for evolved vector [6] supposing that at the end of perturbative stage there is a set of gluon coherent states with MD close to NBD [7]. Not any initial gluon state can lead to SS. Only the product of coherent states $\prod_{b=1}^{8}\prod_{l=1}^{3} \mid \alpha_l^b(t) >$ corresponds to SS, i.e. it satisfyes the condition of squeezing.

In this paper we study the angular dependence of squeezed gluon second correlation function by well-known methods from QO.

By analogy with QO we can write the second normalized correlation function of gluons with colour charge in Schrödinger representation in the form

$$g_l^{b(2)} = \frac{\left\langle \hat{a}_l^{b+}\, \hat{a}_l^{b+}\, \hat{a}_l^{b}\, \hat{a}_l^{b} \right\rangle}{\left\langle \hat{a}_l^{b+}\, \hat{a}_l^{b} \right\rangle^2}. \qquad (1)$$

In particular, for a coherent field with a poissonian distribution of gluons $g_l^{b(2)}$ is equal 1. The averaging of $g_l^{(2)}$ here is carried out over the final state vector at the moment t after the beginning of nonperturbative stage.

If $g_l^{b(2)} > 1$ for $\forall l$ then bunching of gluons takes place and the gluon antibunching can occur in the case $g_l^{b(2)} < 1$.

In particular, for the squeezed coherent state of photons the second normalized correlation function at $0 < r_l < \frac{1}{4}$ is

$$g_l^{(2)} = 1 - \frac{r_l[\alpha_l^2 e^{-2i\delta} + (\alpha_l^*)^2 e^{2i\delta}]}{\mid \alpha_l \mid^4 - 2r_l \mid \alpha_l \mid^2 [\alpha_l^2 e^{-2i\delta} + (\alpha_l^*)^2 e^{2i\delta}]} \qquad (2)$$

It can be for real α both less than 1 in the case $\delta = 0$ (coincide phases), and more than 1 for antiphases ($\delta = \frac{\pi}{4}$) corresponding to antibunching (sub-poissonian MD) and bunching (super-poissonian MD) of photons for $\forall l$ [8].

At the beginning of the nonperturbative gluon cascade

$$g_l^{b(2)} = 1 \tag{3}$$

because the gluon state vector at this moment (t=0) is the product of the gluon coherent states of the type $\prod_{b=1}^{8}\prod_{l=1}^{3} \mid a_l^b(\theta_1,0), a_l^b(\theta_2,0) >$. Averaging $g_l^{b(2)}$ over the evolved vector $\prod_{b=1}^{8}\prod_{l=1}^{3} \mid a_l^b(\theta_1+d\theta,t), a_l^b(\theta_2+\theta,t) >$ which describes gluon squeezed state, we obtain

$$g_l^{b(2)}(\theta_1,\theta_2) = 1 - \frac{M_1(\theta_1,\theta_2)}{\mid \alpha_l^b \mid^4 -2 \mid \alpha_l^b \mid^2 M_1(\theta_1,\theta_2) + M_2(\theta_1,\theta_2)}. \tag{4}$$

Here the explicit form of the functions $M_1(\theta_1,\theta_2), M_2(\theta_1,\theta_2)$ are given for the colour index b=1 and an arbitrary vector component l and we supposed for symplicity that $\alpha_l^1 = \mid \alpha \mid e^{i\delta}$ for $\forall l$ and $\alpha_l^b = \mid \beta \mid e^{-i\gamma}$, when $b \neq 1$, for $\forall l$, $\delta - \gamma = \frac{\pi}{4}$:

$$M_1(\theta_1,\theta_2) = 24\, t\, u_4\, \pi \mid \alpha \mid^2 \mid \beta \mid^2 \sin(4\delta - \pi/2)\Big\{(1+\delta_{l1})(2+u_1-\delta_{l1}) \times$$
$$(\sin\theta_1 + \sin\theta_2) - \frac{1}{2}\, u_1(\sin^3\theta_1 + \sin^3\theta_2)\,(2\delta_{l1} - \delta_{l2} - \delta_{l3})\Big\}, \tag{5}$$

$$M_2(\theta_1,\theta_2) = 80\, t\, u_4\, \pi \mid \alpha \mid^3 \mid \beta \mid^3 \sin(2\delta - \pi/4)\Big\{(1+\delta_{l1})(2+u_1-\delta_{l1}) \times$$
$$(\sin\theta_1 + \sin\theta_2) - \frac{1}{2}\, u_1(\sin^3\theta_1 + \sin^3\theta_2)\,(2\delta_{l1} - \delta_{l2} - \delta_{l3})\Big\}, \tag{6}$$

where $u_1 = \left(1 - \frac{m_g^2}{k_0^2}\right)$, $u_4 = \frac{k_0^4}{4(2\pi)^3}\frac{g^2}{2}(u_1)^{\frac{3}{2}}$.

Unlike corresponding expression (2) in QO $g_l^{b(2)}(\theta_1,\theta_2)$ (4) has also function $M_2(\theta_1,\theta_2)$ which appears due to the Hamiltonian containing the various composition of the annihilation and production operators of gluons with the different colours and vector components.

An angle dependence of squeezed gluon correlation function is plotted on Fig. for b=1 at the time t=0.001 and $\theta_2 = 0$ under reasonable parameters γ, m_g, k_0.

From this figure we notice that as the angle θ_1 increases to some angle $\theta_{1\max} \approx 8.6^0$ for $\forall l$, $g_l^{b(2)}(\theta_1)$ decreases steeply down and after that it saturates and falls very smoothly down.

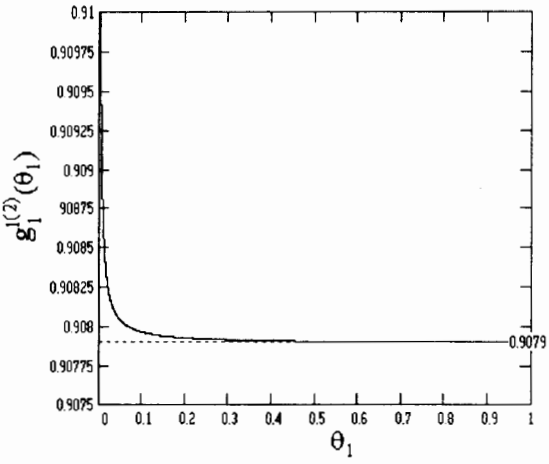

Figure 1: The angular dependence of the squeezed gluon correlation function $g_l^{1\,(2)}(\theta_1)$ at $\theta_2 = 0, g_l^{1\,(2)}(\theta_1 = 0) = 1$.

III Instanton induced correlations

As it is well-known, Yang-Mills gauge theories have highly degenerated vacuum structure even on the classical level [9, 10]. Quantum tunnelling transitions between different vacuum states are associated with the instantons [11], which are classical Euclidean field configurations with a finite action. These tunnelling transitions or instantons lead to the violation of certain fermionic quantum numbers, such as chirality (Q_5) in QCD and baryon (B) and lepton (L) charges in Standard Model of electro-weak interactions [12].

Possibility of the B and L numbers nonconservation is connected with the problem of the baryon and antibaryon asymmetry in the observable part of the Universe [13]. At low energies cross section of the $B + L$ is exponentially suppressed [14, 15]: $\sigma_{tunnelling} \sim exp(-\frac{4\pi}{\alpha_w}) = 10^{-169}$, where α_w is a coupling constant of the electro-weak interactions. In high energy particle collisions (in multi TeV regime) the cross section can increase exponentially if it is associated with multi $W^{\pm}$, Z^0 and H-bosons production in the weak instanton field [16, 17]: $\sigma_{tunnelling} \sim exp(\frac{4\pi}{\alpha_w}[-1 + \frac{1}{2}(\frac{3}{2}\frac{\sqrt{s}}{E_0})^{4/3} + ...])$, where $\sqrt{s}$ is a total energy of the processes; $E_0 \approx 14TeV$ is sphaleron

energy [18]. The needed energies are so high that it is very difficult to see such processes at the nowadays experiments.

From the other hand for strong $SU(3)$ instantons in QCD such phenomenon can exist at hundreds MeV [19] and be important in deep inelastic ep-scattering for decreasing Bjorken variable X_{Bj} and high photon virtuality Q^2 [20]. Search of QCD-instantons has started already in ep-collisions at HERA(H1). The processes have some features: instanton contribution to structure function $F_2(X_{Bj}, Q^2)$ rises strongly with decreasing X_{Bj}; σ^I_{tot} strongly peaks with decreasing of X_{Bj}; hadronic band emission of semi-hard partons is isotropic in the instanton rest system; current quark jet and characteristic flavour, strangeness-K^0, charm and muon flow take place [21, 22, 23]. Moreover instanton-induced processes manifest new mechanism of multiparticle production and can contribute to intermittency exponent [24].

We study properties of the second correlation function $C_2(y_1, y_2) = \rho_2(y_1, y_2) - \rho_1(y_1)\rho_2(y_2)$ as signature of $SU(3)$ instanton-induced multigluon state for classical instanton with the first quantum correction in QCD; $\rho_2(y_1, y_2)$ and $\rho_1(y)$ are inclusive distributions on rapidities of produced gluons.

We use the following natural assumption (in laboratory subsystem in ep-collision) [25]:

$$(k_i^L)^2 \gg (\vec{k_i^T})^2 \gg m_g^2, \qquad k_i^T \equiv \mid \vec{k_i^T} \mid = k^T,$$
$$E_i \approx k^T ch y_i, \qquad k_i^L \approx k^T sh y_i. \tag{7}$$

where E_i, m_g, k_i^T and k_i^L are energy, virtual gluon mass, transverse and longitudinal momenta of ith produced gluon correspondingly.

After all calculations the following formula for the second correlation function is obtained [26]:

$$C_2(y_1, y_2) = [-2A^2 + \frac{3}{2}\alpha A^2 \Pi(Y)] ch2y_1 ch2y_2 - 4\alpha A \pi ch(y_1 + y_2) th(y_1 - y_2) -$$
$$-2\alpha sh(y_1 - y_2) th(y_1 - y_2) + 2\alpha A shY [chy_1 ch2y_2 + chy_2 ch2y_1] +$$
$$+2\alpha A [arctg(\frac{chy_1}{shY}) ch2y_2 + arctg(\frac{chy_2}{shY}) ch2y_1], \tag{8}$$

where $A = 3(\frac{4}{g_s}\pi\sqrt{s}\rho^2 k^T)^2$, $\alpha = 8(k^T \frac{8}{g_s}\pi^2\rho^3(\sqrt{s})^2)^2$, g_s is a constant of strong interaction, ρ - instanton size.

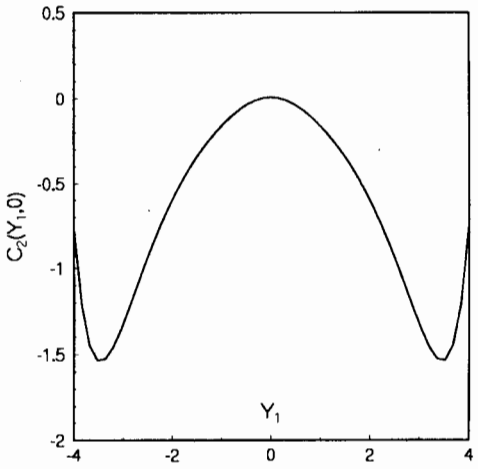

Figure 2: Correlation function vs. rapidity y_1 of one of the particle, when $y_2 = 0$.

Corresponding curve lies in negative region of the plot $C_2(y_1, 0)$, has maximum at $y_1 = 0$ and minima at $y_1 = \pm 3,5$ (see Fig.1). Central maximum corresponds to the quasiclassical approximation; two minima are contribution of the first quantum correction.

It should be noted, that for this effect the problem of taking into account the hadronization exists. Here it can be solved by the use of the local parton-hadron duality [27].

IV Temperature hysteresis in the first order QCD phase transition

The purpose of the section is to investigate the possibility of the existence of new and interesting features that characterize the QCD phase transition from quark-gluon plasma to hadrons.

Statistical QCD predicts that strongly interacting matter exists in two different states. Lattice gauge theory has shown that at low energy density it behaves as a gas of individual hadrons, whereas in the asymptotic limit of high density it is composed of quarks and gluons (quark-gluon plasma state). The lattice approach is very successful in the description of thermodynamical properties of strongly interacting matter in the hadron-free

environment. The critical behaviour of hadronic matter, however, can at present only be studied in the framework of phenomenological models.

There are three stages which usually are considered in high energy nuclear collisions where the production of quark-gluon plasma is expected. At the time immediately after the collision, multiple scattering between the primary and secondary constituents is supposed to lead to a rapid generation of entropy and thus eventually to thermalized state of quarks and gluons (quark-gluon plasma). What happens at this stage is of crucial relevance for the subsequent properties of the system, and much important work on this topic has appeared during the past years, based in particular on event generators using parton dynamics. Then, the evolution of quark-gluon plasma lead to hadrons by the phase transition. If nuclear collisions do indeed lead to a thermalized system of quarks and gluons, this hadronization stage, the final state in the evolution, will be independent of the initial thermal state of the primordial plasma. In other words, local hadronization properties of a plasma initially at a temperature of one GeV should be no different from those of a plasma of two hundred MeV. In contrast, global features such as multiplicities or flow effects on transverse momentum spectra will of course depend on the initial temperature. The lattice gauge calculation predicts that the phase transition may be both second order and first order, depending upon the number of quarks in the problem [28]. One of the differences between order of phase transition should be hysteresis phenomenon. Let us demonstrate this on the example of the Ginzburg-Landau model for phase transition from quark-gluon plasma to hadrons [29, 30].

The Ginzburg-Landau density of free energy is given by

$$F(\psi) = b|\psi|^2 + a|\psi|^4 + f|\psi|^6 \quad , \tag{9}$$

where ψ is uniform parameter order which characterize a hadron phase; the controlling parameters b, a, f are functions of the temperature in ways which are not known. In (9) $|\psi|^6$ term take into consideration for the description of first order phase trasition [29]. The phase transition take place due to the change of the controlling parameters with temperature. In fig.1 and fig.2 we show the plane of the controlling parameters $a, b, f = const$ of potential (9) and the dependence of ground state $|\psi_0|$ from parameters a, b respectively. The plane of the controlling parameters has four regions with the different form of potential which is shown in coresponding places

on the figure. As the controlling parameters change along lines 1 and 2, we have first and second order phase transition respectively. Hysteresis take place when the physical process is not completely reverse, i.e. direct and reverse phase transition occur at different values of the controlling parameters. So, the second order phase transition, both direct and reverse, occurs at $b \to 0, b, f = const$ near point of phase transition. The first order phase transition take place along line $b = \frac{1}{4f}a^2, a < 0$. In this case direct and reverse phase transition could occur at different values parameters b, a and hysteresis phenomenon is possible.In fig.2 a loop of hysteresis is shown. The existence of hysteresis phenomenon must lead to difference between the critical temperatures of the direct T_{c1} and reverse T_{c2} phase transitions. In fig.3 and 4 we show dependences $|\psi_0|$ vs. T for first and second order phase transitions. In case the first order phase transition $T_{c1} > T_{c2}$ and we have delay of the system in the quark-gluon plasma state. In case the second order phase transition such the difference does not. The theoretical and experimental search of differenses between consequences of the first and second order phase transitions can lead us to important results for registration of quark-gluon plasma in the nuclear collisions.

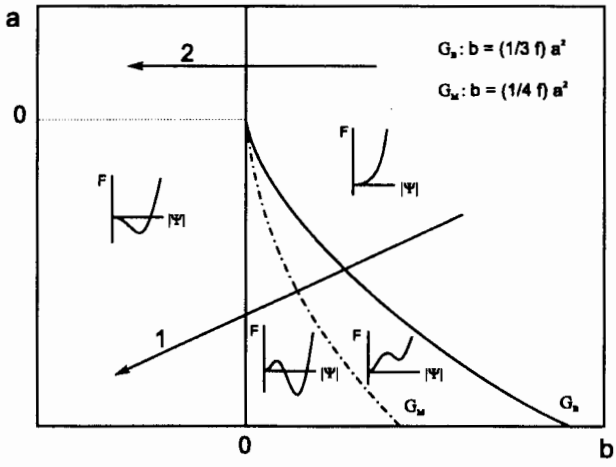

Figure 3: The plane of controlling parameters potential [29]

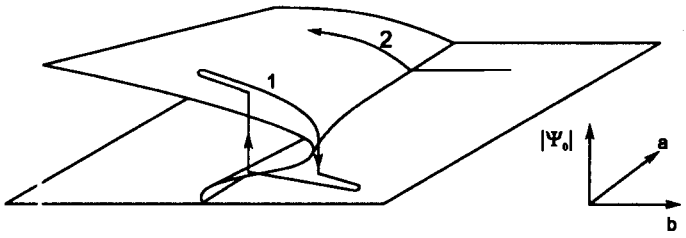

Figure 4: The dependence of ground state $|\psi_0|$ from controlling parameters a, b

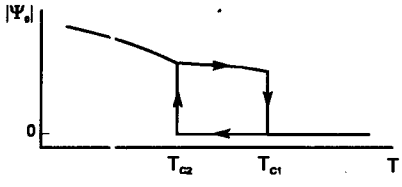

Figure 5 The dependence $|\psi_0|$ vs. T for first order phase transition

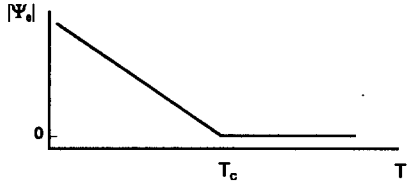

Figure. 6 The dependence $|\psi_0|$ vs. T for second order phase transition

V Conclusion

We show that three new QCD nonperturbative effects can be seen in the HEP experiments. Specific form of second correlation function of final gluons can be a signal of quantum gluon squeezed states in QCD jets and instanton induced events in DIS(HERA). Of course, here we need to overcome the hadronization properties. But it is known (LPHD) in doesn't spoil very much the quarks and gluons spectra. Also we see that temperature hysteresis, i.e. two different values of critical temperatures for transition to QGP phase transition and back exists in the first order QGP phase transition and can be search at experiments.

References

[1] DELPHI coll., Abreu P. et al., *Z.Phys.* **C50** (1991) 185.

[2] OPAL coll., Acton P.D. et al., *Z.Phys.* **C53** (1992) 539.

[3] D.F.Walls, G.J.Milburn, *Quantum Optics, Springer-Verlag*, NY.USA (1995) 351.

[4] V.Kuvshinov et al, *Proceed. 2nd Int. Workshop on Squeezed States and Uncertainty Relations* (Moscow,Russia,1992), NASA (1993) 301.

[5] V.Kuvshinov, V.Shaporov,*Proceed. of 4th Int. Sem. "Nonlinear Phenomena in Complex Systems"* (Minsk,Belarus,1995) (1996) 105.

[6] V.Kuvshinov, V.Shaporov,*Proceed. of 5th Int. Sem. "Nonlinear Phenomena in Complex Systems"* (Minsk,Belarus,1996) (to be published).

[7] E.Malasa, B.Webber, *Nuclear Physics* **B267** (1986) 702.

[8] S.Ya.Kilin, *Quantum Optics, Minsk*, (1990) 175 (in Russian).

[9] R.Jackiw and C.Rebbi, *Phys.Rev.Lett.* **37** (1976) 172.

[10] C.Callan, R.Dashen and D.Gross, *Phys.Lett.* **B63** (1976) 334.

[11] A.Belavin, A.Polyakov, A.Schwarz and Yu.Tyupkin, *Phys.Lett.* **B59** (1975) 85.

[12] S.Adler, *Phys.Rev.* **177** (1969) 2426.

[13] A.Sakharov, *JETP Lett.* **5** (1967) 1.

[14] G.'t Hooft, *Phys.Rev.Lett.* **37** (1976) 8.

[15] G.'t Hooft, *Phys.Rev.* **D14** (1976) 3432.

[16] A.Ringwald, *CERN-TH.* **6479/92** (1992) 1.

[17] A.Ringwald, *Nucl.Phys.* **B330** (1990) 1.

[18] N.Manton, *Phys.Rev.* **D28** (1983) 2019.

[19] D.Dyakonov and V.Petrov, *Proceed. of XXVI Winter School LINP* (1991) 8.

[20] I.Balitsky and V.Braun, *Phys.Lett.* **B314** (1993) 237.

[21] A.Ringwald and F.Schrempp, *DESY preprint* **94-197** (November,1994).

[22] M.Gibbs, A.Ringwald and F.Schrempp, *DESY preprint* **95-119** (June,1995).

[23] J.Feltesse (H1 Collaboration) *XXVII Int. Conf. on High Energy Physics* (Brussels, July 27-August 2, 1995), contributed paper **0489**.

[24] V.Kuvshinov and R.Shulyakovsky, *Proceed. of 2nd Int. Sem. "Nonlinear Phenomena in Complex Systems"* (Polatsk, Belarus,1993) 171.

[25] A.Ringwald and F.Schrempp, *DESY preprint* **96-125** (July,1996).

[26] V.Kuvshinov and R.Shulyakovsky, *Acta Phys.Pol* **B28** (1997) 1629.

[27] Ya.Azimov at. al., *Z.Phys.* **C27** (1985) 65.

[28] Karsch F. in *Quark-Gluon Plasma*, edited by R.C. Hwa (World Scientitific Singapore, 1990).

[29] Babichev L.F., Klenitsky D.V., Kuvshinov V.I Phys.Lett. **B345** (1995) 269.

[30] Hwa R. Nazirov M. Phys.Rev.Lett. **69** (1992) 741.

MAGNETIC POLARIZABILITIES OF PIONS AND KAONS IN RELATIVISTIC QUARK MODEL

S.I.Kruglov

National Scientific Centre of Particle and High Energy Physics
M.Bogdanovich Str.153, Minsk 220040, Belarus

The effective action for π, K-mesons in the external uniform static electromagnetic fields was obtained on the base of the relativistic quark model. The wave function of the meson ground state is the Airy function. Using the virial theorem we estimated the mean charge radii of π, K-mesons in terms of the string tension and the Airy function zero. On the base of the perturbative theory in the small external magnetic field we found the magnetic polarizabilities of π, K-mesons ($\beta_\pi = -0.8 \times 10^{-4}\ fm^3$, $\beta_{K^\pm} = -0.57 \times 10^{-4}\ fm^3$, $\beta_{K^0} = -0.23 \times 10^{-4}\ fm^3$).

1. Introduction

The recent development of the QCD string approach [1-7] showed good results at describing heavy quarkonia, barions and glueballs. The QCD string theory takes into account the main non-perturbative effects of strong interactions: the chiral symmetry breaking and the confinement of quarks. The chiral symmetry breaking gives nonzero quark condensate. As a result the light quarks (u, d - quarks) with the current masses $m_u \simeq m_d \simeq 7\ MeV$ acquire the dynamical masses $\mu_u \simeq \mu_d \simeq 320\ MeV$. The confinement of quarks does not allow them to be observed, i.e. quarks can not move inside of hadrons on large distances relatively each other. This was confirmed by the Monte-Carlo simulations and experiments. Both non-perturbative effects of strong interactions can be explained by introducing stochastic gluon vacuum fields with the definite fundamental correlators [3,4]. Then the linear potential between quarks appears and it provides the confinement of quarks. Besides the Regge trajectories are asymptotically linear with a universal slope [4].

It is important to calculate different intrinsic characteristics of hadrons on the base of the QCD string theory and to compare them with the experimental values. It will be the testing of this scheme. The charge radius (and electromagnetic form-factors) and electromagnetic polarizabilities of scalar mesons are fundamental constants which characterize the complex structure of particles. These values are known from the experimental data and therefore the estimation of them is reasonable. So we can check our notion about the vacuum structure by coinciding experimental data and theoretical predictions. In [8] we made the crude

estimation of the charge radius and the electric polarizability of pions and nucleons. Here we evaluate more precisely the mean squared radius using the virial theorem and the magnetic polarizability of pions.

The electromagnetic polarizabilities of hadrons α, β enter the induced electric $\mathbf{D} = \alpha\mathbf{E}$ and magnetic $\mathbf{M} = \beta\mathbf{H}$ dipole moments, where $\mathbf{E}$, $\mathbf{H}$ are the strengths of electromagnetic fields. As a result there is a contribution to the polarization potential [9,10] as follows

$$U(\alpha,\beta) = -\frac{1}{2}\alpha\mathbf{E}^2 - \frac{1}{2}\beta\mathbf{H}^2. \tag{1.1}$$

Electromagnetic polarizabilities are fundamental low-energy characteristics of strong hadron interactions and therefore they can be calculated in the framework of non-perturbative quantum chromodynamics – the QCD string theory.

The paper is organized as follows. In Sect. 2 after describing the general background we derive the effective action for pions and kaons in external electromagnetic fields. The ground state and charge radius of light mesons are found on the base of exact solutions and the virial theorem in Sect. 3. Sect. 4 contains the evaluation of the pion and kaon magnetic polarizabilities using the perturbative expansion in the small magnetic field. In the conclusion we made the comparison of our results with other approaches and experiments.

Units are chosen such that $\hbar = c = 1$.

2. Effective Action for Light Mesons

To get the effective action for pions in the external electromagnetic fields we proceed from the Fock-Schwinger representation of the Green function. For the sake of simplicity spins of quarks are neglected here. Starting with the approach [11] and introducing the external electromagnetic field with the vector-potential A_μ^{el} we write the Green function of the spinless quark in the Minkowski space

$$S(x,y) = \int_0^\infty \frac{ds}{i}\int_{z(0)=y}^{z(s)=x} Dz\; exp\Big\{i\Big(\int_0^s [\frac{1}{4}\dot{z}_\mu^2(t) - m^2 - e\dot{z}_\mu(t)A_\mu^{el}(z)]dt\Big)\Big\}\Phi(x,y), \tag{2.1}$$

where $z_\mu(t)$ is the path of the quark with the boundary conditions $z_\mu(0) = y_\mu$, $z_\mu(s) = x_\mu$ and

$$\Phi = P\; exp\{ig\int_y^x A_\mu dz_\mu\} \tag{2.2}$$

is the path ordered product (the parallel transporter), A_μ means the gluonic field and g is the coupling constant. Neglecting quark-antiquark vacuum loops and omitting the annihilation graph the Green function of mesons (the quark-antiquark system) takes the form [4]

$$G(x,\bar{x};y,\bar{y}) = < trS(x,y)\Phi(y,\bar{y})S(\bar{y},\bar{x})\Phi(\bar{x},x) > . \qquad (2.3)$$

Inserting (2.1) into (2.3) we find the expression

$$G(x,\bar{x};y,\bar{y}) = \int_0^\infty ds \int_0^\infty d\bar{s} \int_{z(0)=y}^{z(s)=x} Dz \int_{\bar{z}(\bar{0})=\bar{y}}^{\bar{z}(\bar{s})=\bar{x}} D\bar{z}\ exp\{i\int_0^s [\frac{1}{4}\dot{z}_i^2(t) - m_1^2 - \qquad (2.4)$$

$$e_1\dot{z}_\mu(t)A_\mu^{el}(z)]dt + i\int_0^{\bar{s}} [\frac{1}{4}\dot{\bar{z}}_\mu^2(\bar{t}) - m_2^2 - e_2\dot{\bar{z}}_\mu(\bar{t})A_\mu^{el}(\bar{z})]d\bar{t}\} < W(C) >,$$

where e_1, e_2 are charges and m_1, m_2 are current masses of the quark and antiquark; $z_\mu(t)$, $\bar{z}_\mu(\bar{t})$ are the paths of the quark and antiquark with the boundary conditions $z_\mu(0) = y_\mu$, $z_\mu(s) = x_\mu$, $\bar{z}_\mu(0) = \bar{y}_\mu$, $\bar{z}_\mu(\bar{s}) = \bar{x}_\mu$ and $\dot{z}_\mu(t) = \partial z_\mu/\partial t$. As compared with [12,13,4] we added the interaction of charged quarks with the external electromagnetic fields. The gage - and Lorentz invariant Wilson loop operator averaged over the external vacuum gluonic fields is given by

$$< W(C) >= \frac{tr}{N_C} < P\ exp\{ig\int_C A_\mu dz_\mu\} >, \qquad (2.5)$$

where N_C is the color number, C is the closed contour of lines $x\bar{x}$ and $y\bar{y}$ connected by paths $z(t)$, $\bar{z}(\bar{t})$ of the quark and antiquark. The Wilson operator (2.5) contains both the perturbative and non-perturbative interactions between quarks via gluonic fields A_μ. We suppose that pions consist of quarks which move slowly with respect to the time fluctuations of the gluonic fields ($T_q \gg T_g$). It is the potential regime of the string. Voloshin and Leutwyler remarked [14,15] that in another case ($T_q \ll T_g$) the dynamics is non-potential and the QCD sum rules can be used. We consider the case when the distance between quarks $r \gg T_g$. The Monte-Carlo calculations [16,17] gave $T_g \simeq 0.2 \div 0.3fm$. So we imply that the characteristic quark relative distance is $r \simeq 1fm$. This assumption will be confirmed below by the calculation of the quark-antiquark relative coordinate.

The avarage Wilson integral (2.5) at large distances in accordance with the area law can be represented in the Minkowski space as

$$< W(C) >= exp(i\sigma_0 S), \qquad (2.6)$$

where σ_0 is the string tension and S is the area of the minimal surface inside the contour C. The surface S can be parametrized by the Nambu-Goto form [18,19]

$$S = \int_0^T d\tau \int_0^1 d\beta \sqrt{(\dot{w}_\mu w'_\mu)^2 - \dot{w}_\mu^2 w'^2_\nu}, \tag{2.7}$$

where $\dot{w}_\mu = \partial w_\mu / \partial \tau$, $w'_\mu = \partial w_\mu / \partial \beta$. Using the approximation [4] that the coordinates of the string world surface $w_\mu(\tau, \beta)$ can be taken by straight lines for the minimal surface we write

$$w_\mu(\tau, \beta) = z_\mu(\tau)\beta + \bar{z}_\mu(\tau)(1 - \beta), \tag{2.8}$$

where τ is implied to be the proper time parameter for both trajectories $\tau = (tT)/s = (\bar{t}T)/\bar{s}$. For the uniform static external electromagnetic fields we have the representation of the vector potential through the strength tensor $F_{\mu\nu}$

$$A_\nu^{cl}(z) = \frac{1}{2} F_{\mu\nu} z_\mu, \qquad A_\nu^{cl}(\bar{z}) = \frac{1}{2} F_{\mu\nu} \bar{z}_\mu. \tag{2.9}$$

The paths z_μ, $\bar{z}_\mu$ are expressed via the center mass coordinate R_μ and the relative coordinate r_μ [4]

$$z_\mu(\tau) = R_\mu - \frac{\bar{s}}{s + \bar{s}} r_\mu, \qquad \bar{z}_\mu(\tau) = R_\mu + \frac{s}{s + \bar{s}} r_\mu \tag{2.10}$$

with the boundary conditions for $R_\mu(\tau)$, $r_\mu(\tau)$:

$$R_\mu(0) = \frac{\mu_1 y_\mu + \mu_2 \bar{y}_\mu}{\mu_1 + \mu_2}, \quad R_\mu(T) = \frac{\mu_1 x_\mu + \mu_2 \bar{x}_\mu}{\mu_1 + \mu_2},$$
$$r_\mu(0) = y_\mu - \bar{y}_\mu, \quad r_\mu(T) = x_\mu - \bar{x}_\mu.$$

The integrating with respect to z_μ, $\bar{z}_\mu$ in (2.4) is replaced by the integration over new variables R_μ, r_μ. As τ is a common time for the quark and antiquark (the time of the meson) the parametrization $z_\mu = (\tau, \mathbf{z})$, $\bar{z}_\mu = (\tau, \bar{\mathbf{z}})$ is possible [4]. This leads to the constraints: $R_0(\tau) = \tau$, $r_0(\tau) = 0$. In accordance with the approach [4] we introduce the dynamical masses μ_1, μ_2 by relationships

$$\mu_1 = \frac{T}{2s}, \qquad \mu_2 = \frac{T}{2\bar{s}}. \tag{2.11}$$

Replacing the integration with respect to s, $\bar{s}$ in (2.4) by the integration over $d\mu_1$ and $d\mu_2$ with the help of (2.6) - (2.10) we find [8] the two-point function

$$G(x, \bar{x}; y, \bar{y}) = T^2 \int_0^\infty \frac{d\mu_1}{2\mu_1^2} \int_0^\infty \frac{d\mu_2}{2\mu_2^2} \int DRDr \; exp\{iS_{eff}\} \tag{2.12}$$

with the effective action

$$S_{eff} = \int_0^T d\tau \Big[-\frac{m_1^2}{2\mu_1} - \frac{m_2^2}{2\mu_2} + \frac{1}{2}(\mu_1+\mu_2)\dot{R}_\mu^2 + \frac{1}{2}\tilde{\mu}\dot{r}_\mu^2 - \tag{2.13}$$

$$\frac{1}{2}F_{\nu\mu}e(\dot{R}_\mu R_\nu + \frac{1}{4}\dot{r}_\mu r_\nu) - \frac{q}{4}F_{\nu\mu}(\dot{R}_\mu r_\nu + \dot{r}_\mu R_\nu) - \int_0^1 d\beta\sigma_0\sqrt{(\dot{w}_\mu w'_\mu)^2 - \dot{w}_\mu^2 w'^2_\nu}\Big],$$

where $w_\mu = R_\mu + [\beta - \mu_1/(\mu_1+\mu_2)]r_\mu$; $\tilde{\mu} = \mu_1\mu_2/(\mu_1+\mu_2)$ is the reduced mass of the quark-antiquark system, $e = e_1+e_2$, $q = e_1-e_2$. The expression (2.13) defines the effective Lagrangian for light mesons (for example pions or kaons) in the external uniform static electromagnetic fields in accordance with the formulae $S_{eff} = \int_0^T \mathcal{L}_{eff}d\tau$. The expression (2.13) looks like nonrelativistic one at $F_{\mu\nu} = 0$, but it is not the truth. The author [4] showed that the relativism is contained here due to the $\tilde{\mu}$ - dependence and the spectrum is similar to that of the relativistic quark model.

The mass of the lowest states can be found on the base of the relationship [20]

$$\int DRDr\ exp\{iS_{eff}\} = \tag{2.14}$$

$$< R = \frac{\mu_1 x + \mu_2 \bar{x}}{\mu_1+\mu_2}, r = x - \bar{x} \mid exp\{-iT\mathcal{M}(\mu_1,\mu_2)\} \mid R = \frac{\mu_1 y + \mu_2 \bar{y}}{\mu_1+\mu_2}, r = y - \bar{y} >,$$

where the mass $\mathcal{M}(\mu_1,\mu_2)$ is the eigenfunction of the Hamiltonian. After that the Green function (2.12) is derived by integrating (2.14) over the dynamical masses μ_1, μ_2. In accordance with [4] we estimate the last integration on $d\mu_1$, $d\mu_2$ using the steepest descent method which gives a good accuracy when the Minkowski time $T \to \infty$. To have the correct formulas, it is necessary to go into Euclidian space and return into Minkovski space on completing the functional integration. We imply this procedure.

3. Ground State and Charge Radii

The last term in (2.13) can be approximated with the accuracy of $\sim 5\%$ [4] by the relation

$$\int_0^1 d\beta\sqrt{(\dot{w}_\mu w'_\mu)^2 - \dot{w}_\mu^2 w'^2_\nu} = \int_0^1 d\beta\sqrt{\mathbf{r}^2 - (\beta - \frac{\mu_1}{\mu_1+\mu_2})^2(\dot{\mathbf{r}} \times \mathbf{r})^2} \simeq \sqrt{\mathbf{r}^2}. \tag{3.1}$$

It is the potential regime at low orbital excitations of the string when the orbital quantum number l is small. As the equalities $R_0(\tau) = \tau$ $r_0(\tau) = 0$

are valid only 3-dimensional quantities are dynamical one. From (2.13) at the assumption (3.1) using the standard procedure we find the canonical 3-momentums corresponding to the center mass coordinate R_μ and the relative coordinate r_μ

$$\begin{aligned}\Pi_k &= \frac{\partial \mathcal{L}_{eff}}{\partial \dot{R}_k} = (\mu_1+\mu_2)\dot{R}_k - \frac{e}{2}F_{\nu k}R_\nu - \frac{q}{4}F_{\nu k}r_\nu, \\ \pi_k &= \frac{\partial \mathcal{L}_{eff}}{\partial \dot{r}_k} = \tilde{\mu}\dot{r}_k - \frac{e}{8}F_{\nu k}r_\nu - \frac{q}{4}F_{\nu k}R_\nu.\end{aligned} \tag{3.2}$$

The Hamiltonian $\mathcal{H} = \pi_k\dot{r}_k + \Pi_k\dot{R}_k - \mathcal{L}_{eff}$ found from (2.13) with the help of (3.1), (3.2) takes the form

$$\mathcal{H} = \frac{m_1^2}{2\mu_1} + \frac{m_2^2}{2\mu_2} + \frac{\mu_1+\mu_2}{2} + \frac{\mu_1+\mu_2}{2}\dot{R}_k^2 + \frac{\tilde{\mu}}{2}\dot{r}_k^2 - \frac{e}{2}(\mathbf{ER}) - \frac{q}{4}(\mathbf{Er}) + \sigma_0\sqrt{\mathbf{r}^2}. \tag{3.3}$$

where $E_k = iF_{k4}$ so that the equation for the eigenvalues takes the form

$$\mathcal{H}\Phi = \mathcal{M}(\mu_1,\mu_2)\Phi. \tag{3.4}$$

The terms contained the strength of the electric field in (3.3) describe the interaction of the dipole electric moment d with the external electric field. Using the definitions we have

$$\frac{e}{2}(\mathbf{ER}) + \frac{q}{4}(\mathbf{Er}) = \frac{1}{2}(e_1\mathbf{r_1} + e_2\mathbf{r_2})\mathbf{E} = \mathbf{dE} \tag{3.5}$$

and the interaction energy of the electric dipole moment with the uniform static electric field is $U = -\mathbf{dE}$. Bellow we investigate the case of the pure magnetic field when $\mathbf{E} = 0$. Using (3.2) the equation for the eigenfunction Φ of the auxiliary "Hamiltonian" $\tilde{\mathcal{H}} = \mathcal{H} - m_1^2/2\mu_1 - m_2^2/2\mu_2 - (\mu_1+\mu_2)/2$ is given by

$$\begin{aligned}&\left[\frac{1}{2\tilde{\mu}}\left(\pi - \frac{e}{8}(\mathbf{r}\times\mathbf{H}) - \frac{q}{4}(\mathbf{R}\times\mathbf{H})\right)^2 + \right. \\ &\left.\frac{1}{2(\mu_1+\mu_2)}\left(\mathbf{\Pi} - \frac{e}{2}(\mathbf{R}\times\mathbf{H}) - \frac{q}{4}(\mathbf{r}\times\mathbf{H})\right)^2 + \sigma_0\sqrt{\mathbf{r}^2}\right]\Phi = \epsilon(\mu,\mathbf{H})\Phi,\end{aligned} \tag{3.6}$$

where $\epsilon(\mu,\mathbf{H})$ is the eigenvalue. In accordance with the Noether theorem we come to the conclusion that the canonical momentum $\mathbf{\Pi}$ corresponding to the center mass coordinate is the constant, i.e. $\mathbf{\Pi} = const$. Therefore it is possible to choose the condition $\mathbf{\Pi} = 0$. Putting $\mathbf{\Pi} = 0$ and $\mathbf{R} = 0$ in (3.6) we arrive to the equation

$$\left[\frac{1}{2\tilde{\mu}}\left(\pi - \frac{e}{8}(\mathbf{r}\times\mathbf{H})\right)^2 + \frac{q^2}{32(\mu_1+\mu_2)}(\mathbf{r}\times\mathbf{H})^2 + \sigma_0\sqrt{\mathbf{r}^2}\right]\Phi = \epsilon(\mu,\mathbf{H})\Phi. \tag{3.7}$$

The second term in (3.7) describes the effect of the recoil of the string. Such term appears also in the non-relativistic models [21,9,10]. If we put $\mathbf{R} = 0$ in (2.13) this term would not appear [8].

In the quantum theory instead of the path integration in $\mathbf{r}$ we can use the replacement $\pi_k \to -i\partial/\partial r_k$. We can apply equation (3.7) for pions with light quarks with masses $m_1 = m_2 \equiv m$, $\mu_1 = \mu_2 \equiv \mu$ so that $\tilde{\mu} = \mu/2$ and for kaons when $m_1 \neq m_2$, $\mu_1 \neq \mu_2$.

The external magnetic field splits the energy levels like the Zeeman effect for atms. The difference of our case is we describe here the light quark-antiquark system in c.m.s. with the linear potential between quarks. Therefore the spectrum of the energy has another levels.

We can consider the small external magnetic field so that here the perturbative theory can be applied. We receive the first approximation when the external field $\mathbf{H}$ is switched off ($\mathbf{H} = 0$) and the equation for the eigenvalue is given by

$$\left(-\frac{1}{2\tilde{\mu}}\frac{\partial^2}{\partial r_i^2} + \sigma_0\sqrt{\mathbf{r}^2}\right)\Phi = \epsilon(\mu)\Phi. \tag{3.8}$$

Equation (3.8) gives the discrete values of the energy $\epsilon(\mu)$ due to the shape of the potential energy. The numerical solution of equation (3.8) was obtained in [22]. It is useful to find the solution to equation (3.8) for the ground state in the analytical form. After introducing the variables $\rho_k = (2\tilde{\mu}\sigma_0)^{1/3} r_k$, $\epsilon(\tilde{\mu}) = (2\tilde{\mu})^{-1/3}\sigma_0^{2/3} a(n)$ [4], equation (3.8) becomes

$$\left(-\frac{\partial^2}{\partial \rho_i^2} + \rho\right)\Phi(\rho) = a(n)\Phi(\rho). \tag{3.9}$$

The solution to equation (3.9) may be chosen in the form $\Phi(\rho) = R(\rho)Y_{lm}(\theta,\phi)$, where $Y_{lm}(\theta,\phi)$ are spherical functions. After setting the variable $R(\rho) = \chi/\rho$ we come to the equation for the radial function

$$\chi''(\rho) + \left(a(n) - \rho - \frac{l(l+1)}{\rho^2}\right)\chi(\rho) = 0, \tag{3.10}$$

where $\chi''(\rho) = \partial^2\chi(\rho)/\partial\rho^2$, l is an orbital quantum number. The solutions to equation (3.10) for the ground state $l = 0$ are the Airy functions $Ai(\rho - a(n))$, $Bi(\rho - a(n))$ [23]. The finite solution to (3.10) at $\rho \to \infty$ ($l = 0$) is

$$\chi(\rho) = NAi(\rho - a(n)). \tag{3.11}$$

The constant N can be found from the normalization condition

$$\int_0^\infty \chi^2(\rho)d\rho = 1. \tag{3.12}$$

The requirement that this solution satisfies the condition $\chi(0) = NAi(-a(n)) = 0$ gives the Airy function zeroes [23] $a(1) \equiv a_1 = 2.3381$, $a(2) \equiv a_2 = 4.0879$ and so on. The main quantum number $n = n_r + l + 1$, where n_r is the radial quantum number which defines the number of zeroes of the function $\chi(\rho)$ at $\rho > 0$. For the ground state we should take the solution (3.11) at $a(n) = a_1$ (here $n_r = 0$, $l = 0$):

$$\chi_0(\rho) = N_0 Ai(\rho - a_1). \tag{3.13}$$

Now let us estimate the mean squared radius for the state which is described by the function Φ (the solution of equation (3.8)). Multiplying (3.8) on the conjugated function Φ^* and integrating over the volume we find the relations

$$\begin{aligned} &< T > + < U >= \epsilon(\tilde{\mu}), \\ &< T >= -\frac{1}{\mu}\int \Phi^* \partial_k^2 \Phi dV, \quad < U >= \sigma_0 \int \sqrt{\mathbf{r}^2}\Phi^*\Phi dV. \end{aligned} \tag{3.14}$$

It is seen from (3.14) that the mean potential energy $< U >= \sigma_0 < \sqrt{\mathbf{r}^2} >$ is connected with the mean diameter $< \sqrt{\mathbf{r}^2} >$ (because $\mathbf{r}$ is the relative coordinate and quarks move around their center mass), which defines the size of mesons. In accordance with the virial theorem [24] we have the connection of the mean kinetic energy with the mean potential energy

$$2 < T >= k < U >, \tag{3.15}$$

where k is defined from the equality $U(\lambda r) = \lambda^k U(r)$. In our case of the linear potential $k = 1$ and from (3.14), (3.15) we get

$$< U >= \frac{2}{3}\epsilon(\tilde{\mu}) = \frac{2}{3}(2\tilde{\mu})^{-1/3}\sigma_0^{2/3}a(n). \tag{3.16}$$

The usage of the steepest descent method for the estimation of the integration in μ (at $\mathbf{H} = 0$) leads to the conditions [4]:

$$\frac{\partial \mathcal{M}(\mu_1, \mu_2)}{\partial \mu_1} = 0, \quad \frac{\partial \mathcal{M}(\mu_1, \mu_2)}{\partial \mu_2} = 0, \tag{3.17}$$

where the mass of the ground state $\mathcal{M}(\mu_1, \mu_2)$ is given by (see (3.3),(3.4))

$$\mathcal{M}(\mu_1, \mu_2) = \frac{m_1^2}{2\mu_1} + \frac{m_2^2}{2\mu_2} + \frac{\mu_1 + \mu_2}{2} + (2\tilde{\mu})^{-1/3}\sigma_0^{2/3}a(n). \tag{3.18}$$

Here we consider the more general case as compared with [4] when $\mu_1 \neq \mu_2$ ($m_1 \neq m_2$). This case is realized for K-mesons. It is assumed that the

current mass of u,d-quarks ($m_u = 5.6 \pm 1.1\ MeV$, $m_d = 9.9 \pm 1.1\ MeV$ [25]) m_1 is much less than the dynamical mass μ_1 ($\mu_1 \simeq 330\ MeV$), i.e. $m_1 \ll \mu_1$ and the mass of s-quark m_2 ($m_s = 199 \pm 33\ MeV$ [25]) is comparable with μ_1 but $m_2 < \mu_1$. Using these assumptions we neglect the term $m_1^2/2\mu_1$ in (3.18) and from (3.17) have the equations

$$(2\tilde{\mu}\sigma_0)^{2/3}a(n) = 3\mu_1^2, \quad 3m_2^2 + (2\tilde{\mu}\sigma_0)^{2/3}a(n) = 3\mu_2^2. \tag{3.19}$$

From (3.19) we arrive to the expression for the dynamical mass μ_2 (for s-quark)

$$\mu_2 = \sqrt{\mu_1^2 + m_2^2}. \tag{3.20}$$

To find μ_1 the perturbation in the parameter m_2^2/μ_1^2 will be assumed. Using the relation $\mu_2 \simeq \mu_1(1 + m_2^2/2\mu_1^2)$ which is obtained from (3.20) and the definition of the reduced mass $\tilde{\mu} = \mu_1\mu_2/(\mu_1 + \mu_2)$ from (3.19) we arrive to the equation

$$\mu_1 \simeq \sqrt{\sigma_0}\left(\frac{a(n)}{3}\right)^{3/4}\left(1 + \frac{m_2^2}{8\mu_1^2}\right). \tag{3.21}$$

In the zeroth order we come to the value $\mu_0 \equiv \mu_1^{(0)} = \sqrt{\sigma_0}(a(n)/3)^{3/4}$ [4]. The next order gives the relationship

$$\mu_1 \simeq \sqrt{\sigma_0}\left(\frac{a(n)}{3}\right)^{3/4} + \frac{m_2^2}{8\sqrt{\sigma_0}}\left(\frac{3}{a(n)}\right)^{3/4}. \tag{3.22}$$

In a particular case $m_2 = 0$ we arrive to $\mu_1 = \mu_2 = \mu_0 = \sqrt{\sigma_0}(a(n)/3)^{3/4}$ [4]. The value of the string tension $\sigma_0 = 0.15\ GeV^2$ was found from the comparison of the experimental slope of the linear Regge trajectories $\alpha' = 0.85\ GeV^{-2}$ and the variable $\alpha' = 1/8\sigma_0$ [4]. It leads for the lowest state $n_r = 0, l = 0, a(1) = 2.3381$ to the value $\mu_0 = 321\ MeV$ [4]. This means that for π-mesons when $m_1 = m_u$, $m_2 = m_d$ we have the dynamical masses of u, d-quarks $\mu_1 = \mu_2 = \mu_0$. For K-mesons using (3.20) and $m_2 = m_s \simeq 200\ MeV$ [25] from (3.22) we get the reasonable values

$$\mu_1 \simeq 337\ MeV, \quad \mu_2 \simeq 392\ MeV, \quad \tilde{\mu} \simeq 181\ MeV. \tag{3.23}$$

Inserting equation $< U >= \sigma_0 < \sqrt{\mathbf{r}^2} >$ into the l.h.s. of (3.16) one gives the expression

$$< \sqrt{\mathbf{r}^2} >= \frac{2}{3}(2\tilde{\mu}\sigma_0)^{-1/3}a(n). \tag{3.24}$$

From (3.20), (3.22) using the first order in the parameter m_2^2/μ_1^2 we find

$$2\tilde{\mu} \simeq \mu_0\left(1 + \frac{3m_2^2}{8\mu_0^2}\right) \qquad \left(\mu_0 = \sqrt{\sigma_0}\left(\frac{a(n)}{3}\right)^{3/4}\right). \tag{3.25}$$

Eq.(3.24) with the help of (3.25) gives the approximate relation for the mean relative coordinate

$$< \sqrt{r^2} >= \frac{2}{\sqrt{\sigma_0}} \left(\frac{a(n)}{3}\right)^{3/4} \left[1 + \frac{3m_2^2}{8\sigma_0} \left(\frac{3}{a(n)}\right)^{3/2}\right]^{-1/3}. \qquad (3.26)$$

For pions putting $m_2 = 0$ in (3.26) we arrive to

$$< \sqrt{\mathbf{r}^2} >_\pi = \frac{2}{\sqrt{\sigma_0}} \left(\frac{a(n)}{3}\right)^{3/4}. \qquad (3.27)$$

The same expression (3.27) was found in [8] using another method. With the help of the definition of the center mass coordinate and the values of the current masses $m_u \simeq 5\ MeV$, $m_d \simeq 10\ MeV$ [25] we can write the approximate relation for the mean charge radius of $\pi^\pm$-mesons [1]

$$\sqrt{< r^2_{\pi^\pm} >} \simeq \frac{m_d}{m_u + m_d} < \sqrt{\mathbf{r}^2} >_\pi = 0.67 < \sqrt{\mathbf{r}^2} >_\pi . \qquad (3.28)$$

At $\sigma_0 = 0.15\ GeV^2$ [4,8] and $a(1) = 2.3381$ Eq.(3.27), (3.28) give

$$\sqrt{< r^2_{\pi^\pm} >} \simeq 0.56\ fm \quad (< \sqrt{\mathbf{r}^2} >_\pi = 0.84\ fm). \qquad (3.29)$$

The calculated value (3.29) is close to the experimental data $< r^2_{\pi^\pm} >_{exp} = (0.44 \pm 0.02)\ fm^2$ $(\sqrt{< r^2_{\pi^\pm} >}_{exp} \simeq 0.66\ fm)$ [26]. For neural pions the mean radius is

$$\sqrt{< r^2_{\pi^0} >} \simeq \frac{1}{2} < \sqrt{\mathbf{r}^2} >_\pi = 0.42\ fm. \qquad (3.30)$$

Value (3.30) characterizes the radius of the sphere where the wave function of the π^0-meson is concentrated (remember that r is the distance between quarks).

For calculating the relative coordinate of K-mesons we should use Eq.(3.24) or (3.26) with conditions $\mu_1 = \mu_u$ for $K^\pm$ and $\mu_1 = \mu_d$ for K^0-mesons and $\mu_2 = \mu_s$ (3.23). As a result formulae (3.24) gives the value of the mean relative coordinate of kaons

$$< \sqrt{\mathbf{r}^2} >_K = 0.79\ fm. \qquad (3.31)$$

With the help of this relation we can estimate the mean charge radius of K-mesons

[1] The relationship $\sqrt{< r^2 >} \simeq < \sqrt{\mathbf{r}^2} >$ is confirmed by the numerical calculations

$$\sqrt{< r_K^2 >} \simeq \frac{\mu_2}{\mu_1 + \mu_2} < \sqrt{\mathbf{r}^2} >_K = 0.54 < \sqrt{\mathbf{r}^2} >_K = 0.43\ fm \qquad (3.32)$$

The experimental data of the mean charge radius of $K^{\pm}$-mesons are different $\sqrt{< r_{K^\pm}^2 >} = (0.53 \pm 0.05)\ fm$ [27], $< r_{K^\pm}^2 > = (0.34 \pm 0.05)\ fm^2$ [26] and for neutral K^0-mesons $\sqrt{< r_{K^0}^2 >} = (0.28 \pm 0.09)\ fm$ [27]. So the calculated value (3.32) is in agreement with the experiment with the accuracy of two standard deviations.

4. Perturbative Expansion and Magnetic Polarizabilities

To calculate the magnetic polarizability of pions and kaons in accordance with (1.1) we should know the Hamiltonian depending on the magnetic field $\mathbf{H}$. From (3.7) we arrive to the expression of the auxiliary "Hamiltonian"

$$\tilde{\mathcal{H}} = -\frac{1}{2\tilde{\mu}}\frac{\partial^2}{\partial r_k^2} + \frac{e}{8\tilde{\mu}}\mathbf{HL} + \left(\frac{e^2}{128\tilde{\mu}} + \frac{q^2}{32(\mu_1+\mu_2)}\right)[\mathbf{r}^2\mathbf{H}^2 - (\mathbf{rH})^2] + \sigma_0\sqrt{\mathbf{r}^2}, \qquad (4.1)$$

where $\mathbf{L} = -i(\mathbf{r}\times\partial)$ $(\partial_k = \partial/\partial r_k)$ is the angular momentum. Considering the external magnetic field $\mathbf{H} = (0,0,H)$ expression (4.1) is rewritten as

$$\tilde{\mathcal{H}} = -\frac{1}{2\tilde{\mu}}\frac{\partial^2}{\partial r_i^2} + \frac{eH}{8\tilde{\mu}}L_3 + \left(\frac{e^2}{4\tilde{\mu}} + \frac{q^2}{\mu_1+\mu_2}\right)\frac{H^2}{32}(r_1^2 + r_2^2) + \sigma_0\sqrt{\mathbf{r}^2}, \qquad (4.2)$$

where $L_3 = i(r_2\partial_1 - r_1\partial_2)$ is the third projection of the angular momentum.

Now let us consider the magnetic polarizability of pions on the base of the perturbative theory. We can rewrite (4.2) in the form

$$\tilde{\mathcal{H}} = \mathcal{H}_0 + \frac{eH}{8\tilde{\mu}}L_3 + \left(\frac{e^2}{4\tilde{\mu}} + \frac{q^2}{\mu_1+\mu_2}\right)\frac{H^2r^2sin^2\theta}{32}, \qquad (4.3)$$

where θ is the angle between $\mathbf{H}$ and the relative coordinate $\mathbf{r}$ and the free Hamiltonian is given by

$$\mathcal{H}_0 = -\frac{1}{2\tilde{\mu}}\frac{\partial^2}{\partial r_k^2} + \sigma_0\sqrt{\mathbf{r}^2}.$$

For the small magnetic fields $\mathbf{H}$ the second and third terms of (4.3) can be considered as a perturbation. Then using the standard perturbative

method [28], we find the shift of the energy in the state $\mid n >$ with the accuracy of the second order in **H**

$$\Delta E_n =< n \mid \frac{eH}{8\tilde{\mu}} L_3 + \left(\frac{e^2}{4\tilde{\mu}} + \frac{q^2}{\mu_1 + \mu_2} \right) \frac{H^2 r^2 sin^2\theta}{32} \mid n > + \sum_{n'} \frac{|< n \mid eHL_3/8\tilde{\mu} \mid n >|^2}{E_n - E_{n'}}. \tag{4.4}$$

For the ground state $l = 0$ (s-state) the first and third terms of (4.4) do not give the contribution to the energy because $L_3 \mid 0 >= 0$. Taking the mean value and using the condition $(1/4\pi) \int sin^2\theta d\Omega = 2/3$, from (4.4) we come to

$$\Delta E_0 = \left(\frac{e^2}{4\tilde{\mu}} + \frac{q^2}{\mu_1 + \mu_2} \right) \frac{H^2}{48} < r^2 > . \tag{4.5}$$

Comparing (4.5) with (1.1) we find the magnetic polarizability of light mesons

$$\beta = -\frac{1}{24} \left(\frac{e^2}{4\tilde{\mu}} + \frac{q^2}{\mu_1 + \mu_2} \right) < r^2 > . \tag{4.6}$$

It should be noticed that here $< r^2 >$ means the mean squared relative coordinate of the quark-antiquark system. Expression (4.6) is similar to the Langevin formula for the magnetic susceptibility of atoms. It is seen that we have here only the diamagnetic part of the polarizability ($\beta < 0$) because π, K-mesons are spinless particles and the paramagnetic part is absent. For estimation of (4.6) we can use the experimental values of $< r^2_{\pi,K} >_{exp}$ instead of $< r^2 >$ in accordance with formulas (3.28), (3.30)-(3.32) or expressions (3.26), (3.27). Inserting parameters $e = e_1 + e_2$, $q = e_1 - e_2$ and values for pions $\mu_1 = \mu_2 = \mu_0 = \sqrt{\sigma_0}(a(n)/3)^{3/4}$(3.25), (3.27) into Eq.(4.6) one yields

$$\beta_\pi \simeq -\frac{(e_1^2 + e_2^2)}{6} \left(\frac{a(n)}{3} \right)^{3/4} \sigma_0^{-3/2}, \tag{4.7}$$

which is similar to the expression for the electric polarizability of pions $\alpha_{\pi^\pm}$ [8]. Calculating equation (4.7) for charged pions at $\sigma_0 = 0.15\ GeV$, $e_1 = 2e/3$, $e_2 = e/3$, $e^2 = 1/137$, $n = 1$ in Gaussian units one takes the value

$$\beta_{\pi^\pm} \simeq -0.8 \times 10^{-4}\ fm^3. \tag{4.8}$$

In rationalized units, the polarizability is 4π times greater. For the neutral pions (π^0) the equalities

$$< \pi^0 \mid (e_1 - e_2)^2 \mid \pi^0 >= \frac{10e^2}{9}, \quad < \pi^0 \mid (e_1 + e_2)^2 \mid \pi^0 >= 0$$

occur [9] and Eq.(4.7) gives the same value $\beta_{\pi^0} = -0.8 \times 10^{-4}\ fm^3$ as for charged pions. In accordance with the dispersive integral [9] the sum of the electromagnetic polarizabilities is $(\alpha+\beta)_{\pi^\pm} = (0.39 \pm 0.04) \times 10^{-4}\ fm^3$ for charged pions and $(\alpha+\beta)_{\pi^0} = (1.04 \pm 0.07) \times 10^{-4}\ fm^3$ for neutral pions. Using the calculated value (4.8), the equality $\beta_{\pi^0} = \beta_{\pi^\pm}$ and the dispersion sum rules we arrive to the values of the electric polarizabilities

$$\alpha_{\pi^\pm} = 1.2 \times 10^{-4}\ fm^3, \quad \alpha_{\pi^0} = 1.8 \times 10^{-4}\ fm^3. \tag{4.9}$$

The pion polarizabilities obtained from the model of the instanton vacuum gave the greater values [29]. The values (4.9) are in reasonable agreement with the experimental data $\alpha_{\pi^\pm} = (2.2 \pm 1.6) \times 10^{-4}\ fm^3$ [30], $(\alpha-\beta)_{\pi^0} = (0.8 \pm 2.0) \times 10^{-4}\ fm^3$ [31]. In [8] we made the crude estimation of the pion electric polarizability which proved to be less as compared with the presented evaluation. Obviously that it is more easier to calculate the magnetic polarizability using the perturbative expansion than to calculate the exact eigenvalues of Hamiltonian (3.3).

For charged kaons $K^+ = u\bar{s}$, $K^- = s\bar{u}$, Eq.(4.6) at the values (3.23), (3.31) ($< r^2 > \simeq < \sqrt{\mathbf{r}^2} >$) leads to the magnitude

$$\beta_{K^\pm} = -0.57 \times 10^{-4}\ fm^3. \tag{4.10}$$

There is an experimental restriction only on the electric polarizability of kaons: $-15 \times 10^{-3} \leq \alpha_{K^-} \leq 7 \times 10^{-3}\ fm^3$ [32]. So our predictions concerning kaon polarizabilities can be checked in new experiments. Using the mean radius (3.31), the equalities [9]

$$< K^0 \mid e^2 \mid K^0 >= 0, \quad < K^0 \mid q^2 \mid K^0 >= \frac{4e^2}{9}$$

and the approximate relation $< \mathbf{r}^2 > \simeq < \sqrt{\mathbf{r}^2} >^2$ we arrive to the value

$$\beta_{K^0} = -0.23 \times 10^{-4}\ fm^3. \tag{4.11}$$

Unfortunately there are not experimental data of kaon polarizabilities yet.

5. Conclusion

The QCD string theory allows to estimate the mean squared radii and electromagnetic polarizabilities of π, K-mesons which are in reasonable agreement with experimental data. These quantities were derived as functions of the string tension which is a fundamental variable in this approach. Here we considered spinless quarks so that the accuracy of

calculations can be improved due to taking into account spins of quarks. Then more precise calculation of the electromagnetic polarizabilities can be done on the base of Hamiltonian (3.3) by finding the exact eigenvalues of it. It is not difficult to calculate the magnetic polarizabilities of excited states of pions and kaons using this approach. For that we should take the quantum numbers $n_r = 1$, $l = 0$ $(n = 2)$ and evaluate the mean relative coordinate in accordance with (3.26). Then Eq. (4.6) gives the necessary polarizabilities.

Our results of evaluations of the pion electromagnetic polarizabilities are close to the chiral perturbation theory (ChPT) predictions $\alpha_{\pi^\pm} = -\beta_{\pi^\pm} = 2.8 \times 10^{-4}\ fm^3$ [33-36]. Unfortunately the effective Lagrangian of the ChPT contains 12 constants L_i and it is the phenomenological one which is not obtained from the first principles of QCD yet. Nevertheless the ChPT prediction is quite reliable because the evaluation of the necessary constant combination $(L_9^r + L_{10}^r)$ is based on the pion decay $\pi^+ \to e^+\nu_e\gamma$.

The Nambu-Jona-Lasinio (NJL) model [37] having a good basing in the framework of QCD [38] describes the chiral symmetry breaking but not the confinement of quarks [4,39]. In our opinion it is why the NJL model leads to the greater value $\alpha_{\pi^\pm} \simeq \alpha^{cl} = e^2 < r_\pi^2 > /3m_\pi \simeq 15 \times 10^{-4}\ fm^3$ [40] as compared with the experimental data. Besides this model has free parameters and the calculated polarizabilities of pions and kaons are parameter dependent.

The instanton vacuum theory (IVT) developed in [41-43] does not give the confinement of quarks phenomenon [4]. This theory is like the NJL model [39] and takes into account only the chiral symmetry breaking. Therefore the calculation of the pion electromagnetic polarizabilities on the base of the IVT gave the similar result $\alpha_{\pi^\pm} \simeq \alpha^{cl}$ [29] as in the NJL model.

The evaluation of π, K meson polarizabilities in the framework of the current algebra leads to the values [44,9] $\alpha_{\pi^\pm} = -\beta_{\pi^\pm} = (2.4 \pm 0.7) \times 10^{-4}\ fm^3$, $\alpha_{K^\pm} = -\beta_{K^\pm} = (1 \pm 0.3) \times 10^{-4}\ fm^3$, which are close to our calculations. The necessary parameters h_A, h_V were taken from decays $\pi \to e\nu\gamma$, $\pi^0 \to 2\gamma$, and therefore the calculated polarizabilities are quite reliable.

All this shows that the obtained good agreement of the theoretical evaluation of the pion electromagnetic polarizabilities and the experimental data is the consequence of a good description the chiral symmetry breaking and confinement of quarks in the framework of the QCD string theory. Naturally that theory was derived on the base of the non-perturbative QCD, i.e. first principals of QCD. The accuracy of the experimental data

of pion electromagnetic polarizabilities can be improved in the new electron accelerators by reducing the statistical errors. There is an analysis [47] of the most favorable kinematical regions of the reaction $\gamma\pi \to \gamma\pi$ to get the information on the pion polarizabilities. It allows to plan new experiments to obtain more precise values of pion electromagnetic polarizab lities. The more difficult task is measuring electromagnetic polarizabilities of kaons.

There are also the other models of the estimation of π, K-meson polarizabilities [45,46].

References

[1] H. G. Dosch, Phys. Lett. **B190** (1987) 177.

[2] U. Marquard and H. G. Dosch, Phys. Rev. **D35** (1987) 2238.

[3] H. G. Dosch and Yu. A. Simonov, Phys. Lett. **B205** (1988) 339; Yad. Fiz. **57** (1994) 152; Z. Phys. **C45** (1989) 147.

[4] Yu. A. Simonov, Nucl. Phys. **B308** (1988) 512, ibid. **B324** (1989) 67; Phys. Lett. **B226** (1989) 151, ibid. **228** (1989) 413; Yad. Fis. **54** (1991) 192, ibid. **57** (1994) 1491, ibid. **58** (1995) 113; Usp. Fiz. Nauk **166** (1996) 337.

[5] M. Schiestl and H. G. Dosch, Phys. Lett. **B209** (1988) 85.

[6] A. Yu. Dubin, A. B. Kaidalov, Yu. A. Simonov, Yad. Fiz **56** (1993) 213, ibid. **58** (1995) 348.

[7] A. M. Badalyan and V. P. Yurov, Yad. Fiz. **56** (1993) 239.

[8] S. I. Kruglov, Phys. Lett **B390** (1997) 283, ibid. **B397** (1997) 283.

[9] V. A. Petrun'kin, Sov. Part. Nucl., **12** (1981) 278.

[10] A. I. L'vov, Int. J. Mod. Phys. **A8** (1993) 5267.

[11] M. B. Halpern and Senjanović, Phys. Rev. **D15** (1977) 1655.

[12] S. Samuel, Nucl. Phys. **B149** (1979) 517.

[13] J. Ishida and A. Hosoya, Progr. Theor. Phys. **62** (1979) 544.

[14] M. B. Voloshin, Nucl. Phys. **B154** (1979) 365.

[15] H. Leutwyler, Phys. Lett. **B98** (1981) 447.

[16] M. Campostrini, A. Di Giacomo, G. Mussardo, Z. Phys. **C25** (1984) 173.

[17] A. Di Giacomo and H. Panagopoulos, Phys. Lett. **B285** (1992) 133.

[18] Y. Nambu, Lectures at the Copenhagen Summer Symposium, 1970.

[19] T. Goto, Progr. Theor. Phys. **46** (1971) 1560.

[20] R. P. Feynman and A.R. Hibbs. Quantum Mechanics and Path Integrals (N. Y. : Mc Graw - Hill, 1965).
[21] J. L. Friar, Ann. of Phys. (N. Y.) **95** (1975) 170.
[22] E. Eichten et al., Phys. Rev. **D17** (1978) 3090.
[23] Handbook of Mathemetical Functions with Formulas, Graphs and Mathematical Tables, Ed. by M. Abramowitz and I. A. Stegun, 1964.
[24] V. A. Fok, Nachala Kvantovoy Mehaniki (M., Nauka, 1976 (in Russian)).
[25] Review of Part. Properties, Phys. Rev. **D50** (1994) 1173.
[26] Z. R. Amendolia et al., Nucl. Phys. **B277** (1986) 168; Phys. Lett. **B146** (1984) 116; **B178** (1986) 435.
[27] O.Dumbrajs at al., Nucl. Phys. **B216** (1983) 277.
[28] S. Flügge, Practical Quantum Mechanics 1 (Springer - Verlag, Berlin - Heidelberg - New York, 1971).
[29] S. I. Kruglov, J. Phys. **G22** (1996) 461.
[30] MARKII Coll. (J. Boger et al.), Phys. Rev. **D42** (1990) 1350.
[31] A. Kaloshin, V.Serebryakov, Yad. Fiz. **54** (1991) 1732; Phys. Lett. **B278** (1992) 198.
[32] G. Backenstoss et al., Phys. Lett. **B43** (1973) 431.
[33] J. F. Donoghue, B. R. Holstein and J.-C. Lin, Phys. Rev. **D37** (1988) 2423.
[34] J. Bijnens and F. Cornet, Nucl. Phys. **B296** (1988) 557.
[35] B. R. Holstein, Comments Nucl. Part. Phys. 19 (1990) 221.
[36] D. Babusci et al., Phys. Lett. **227** (1992) 158.
[37] S. P. Klevansky, Rev. Mod. Phys. **64** (1992) 649.
[38] S. I. Kruglov, Teor. Mat. Fiz. **84** (1990) 388.
[39] S. I. Kruglov, Acta Phys. Pol. **B20** (1989) 723, ibid. **B21** (1990) 985.
[40] V. Bernard and D. Vautherin, Phys. Rev. **D40** (1989) 1615.
[41] C. G. Callan, R. Dashen and D. J. Gross, Phys. Rev. **D17** (1978) 2717, ibid. **D19** (1978) 1826.
[42] E. V. Shuryak, Nucl. Phys. **B203** (1982) 93, 116, 160, ibid. **B214** (1983) 237.
[43] D.I. Dyakonov and V. Yu. Petrov, Nucl. Phys. **B245** (1984) 259, ibid. **B272** (1986) 457.
[44] M. V. Terent'ev, Yad. Fiz. **16** (1972) 1044 (Sov. J. Nucl. Phys. **16** (1973) 576); Yad. Fiz. **19** (1974) 1298 (Sov. J. Nucl. Phys. **19** (1974) 664.
[45] M. A. Ivanov and T. Mizutani, Phys. Rev. **D45** (1992) 1580.
[46] D. Ebert and M. K. Volkov, Yad. Fiz. **60** (1997) 891.
[47] D.Drechsel and L. V. Fil'kov, Z. Phys. **C349** (1994) 177.

Local properties of local multiplicity distributions

S.V.Chekanov*

High Energy Physics Institute Nijmegen (HEFIN),
University of Nijmegen/NIKHEF, NL-6525 ED
Nijmegen, The Netherlands

Abstract

Some aspects of applications of bunching parameters are discussed. It is investigated to what extent Monte-Carlo models, which have been tuned to reproduce global event-shape variables and single-particle inclusive distributions, agree with each other.

1 Introduction

One of the simplest observable, which contains information about the dynamics of multiparticle production beyond single-particle densities, is the multiplicity distribution. While the study of the multiplicity distribution P_N in full phase space deals with limited dynamical information influenced by charge- and energy-momentum conservation, the investigation of the evolution of the probabilities $P_n(\delta)$ of detecting n particles in ever smaller sizes δ of phase-space windows (bins) can provide detailed information on QCD multihadron production without these trivial constraints. A deviation of this distribution from that expected for purely independent particle production can be attributed to dynamical local multiplicity fluctuations.

The important quest behind such a study is the understanding of the origin of short-range correlations between final-state particles, leading

*On leave from Institute of Physics, AS of Belarus, Skaryna av.70, Minsk 220072, Belarus.

to the appearance of dynamical multiparticle spikes in individual events. As a consequence of these correlations, the normalized factorial moments (NFMs)

$$F_q(\delta) \equiv \frac{\langle n^{[q]} \rangle}{\langle n \rangle^q}, \tag{1}$$

$$\langle n^{[q]} \rangle = \sum_{n=q}^{\infty} n^{[q]} P_n(\delta), \qquad n^{[q]} = n(n-1)\dots(n-q+1), \tag{2}$$

of the local multiplicity distribution $P_n(\delta)$ exhibit a power-like increase with decreasing δ, namely $F_q(\delta) \propto \delta^{-\phi_q}$ [1]. The constants ϕ_q are called intermittency indices. This phenomenon reflects the peculiarity of $P_n(\delta)$ to become broader with decreasing δ. Since NFMs satisfy the scaling property $F_q(\lambda\delta) = \lambda^{-\phi_q} F_q(\delta)$, this is widely regarded as evidence that the correlations exhibit a self-similar underlying dynamics.

Experimentally, local fluctuations in e^+e^--processes have already been studied by the TASSO, HRS, CELLO, OPAL, ALEPH, DELPHI and L3 Collaborations [2]. The data do exhibit approximate power-like rise of the NFMs with a saturation at small δ. The conclusion has been reached that such a phenomenon is a consequence of the multi-jet structure of events, i.e., groups of particles with similar angles resulting in spikes of particles as seen in selected phase-space projections. The hard gluon radiation significantly affects the NFMs, so that they have stronger increase in 3-jet events than in 2-jet events. It has been found that for the statistics used at that time current Monte-Carlo models can, in general, describe the data, even without additional tuning.

Recently, it has been realized that the factorial-moment method poorly reflects the information content of local fluctuations, since the NFM of order q contains a trivial contamination from lower-order correlation functions (see reviews [3]). As a result, rather different event samples can exhibit a very similar behavior of the NFMs. The fact that subtle details in the behavior of $P_n(\delta)$ are missing, together with the small statistics used, may be the reason why different Monte-Carlo models can reasonably describe the local fluctuations measured in e^+e^- annihilation so far.

Another shortcoming of the factorial-moment measurement is that in moving to ever smaller phase-space bins, the statistical bias due to a finite event sample ($N_{ev} \neq \infty$) becomes significant, especially for high-order moments q. This is because in actual measurements the NFMs at small bin size are determined by the first few terms in (2). In most cases this

leads to a significant underestimate of the measured NFMs with respect to their true values.

Cumulants are a more sensitive statistical tool (see [3] and references therein). However, their measurement is rather difficult and was rarely attempted. Besides, the cumulants are expected to be influenced by the statistical bias to even larger degree, since they are constructed from the factorial moments of different orders q.

2 Local Properties

An important step towards an improvement of experimental measurements of the local multiplicity distribution was made in [4,5], where it was shown that any complex distribution can be represented as

$$P_n(\delta) = P_0(\delta)\frac{\lambda^n}{n!}L_n, \qquad L_n = \prod_{i=2}^{n}\eta_i^{n-i+1}(\delta),$$

where $\lambda = P_1(\delta)/P_0(\delta)$. The factor L_n measures a deviation of the distribution from a Poisson with $L_n = 1$. Non-poissonian fluctuations exhibit themself as a deviation of L_n from unity. The L_n is constructed from the bunching parameters (BPs)

$$\eta_q(\delta) = \frac{q}{q-1}\frac{P_q(\delta)P_{q-2}(\delta)}{P_{q-1}^2(\delta)}, \qquad q > 1. \tag{3}$$

The values of the BPs and NFMs for most popular distributions are shown in Table 1. The most interesting observation is that while the NFM is an "integral" characteristic of the $P_n(\delta)$ and the BP is a "differential", both tools have values larger than unity if the distribution is broader than a Poisson. Generally, however, one should not expect that all BPs are larger than unity for a broad distribution; BPs probe the distribution locally, i.e. they are simply determined by the second-order derivative from the logarithm of $P_n(\delta)$ with respect to the n. Note, that in the case of local distributions, the width of distributions is mainly determined by $\eta_2(\delta)$. This observation is based on the simple fact that $P_n(\delta)$ ceases to be bell-shaped at sufficiently small δ.

Distribution	P_n	NFMs	BPs
Pos. Binomial	$C_n^N p^n (1-p)^{N-n}$	$\prod_{i=1}^{q}(1-\frac{i}{N}) < 1$	$\frac{q-1-N}{q-2-N} < 1$
Poisson	$p^n \exp(-p)/n!$	1	1
Neg. Binomial	$\frac{\Gamma(n+k)}{\Gamma(n+1)\Gamma(k)} p^n (1+p)^{-(k+n)}$	$\prod_{i=1}^{q}(1+\frac{i}{k}) > 1$	$\frac{q-1+k}{q-2+k} > 1$
Geometric	$p^n (p+1)^{-n-1}$	$\prod_{i=1}^{q}(1+i) > 1$	$\frac{q}{q-1} > 1$

Table 1. *NFMs and BPs for positive-binomial, Poisson, negative-binomial and geometric distributions.*

BPs are more sensitive to the variation in the shape of $P_n(\delta)$ with decreasing δ than are the NFMs [6]. In the case of intermittent fluctuations, one should expect $\eta_2(\delta) \propto \delta^{-d_2}$. For multifractal local fluctuations, the $\eta_q(\delta)$ are δ-dependent functions for all $q \geq 3$, while for monofractal behavior $\eta_q(\delta) = const$ for $q \geq 3$ [4].

¿From an experimental point of view, the BPs have the following important advantages [5]:

1) They are less severely affected by the bias from finite statistics than the NFMs, since the qth-order BP resolves only the behavior of the multiplicity distribution near multiplicity $n = q - 1$;

2) For the calculation of the BP of order q, one needs to know only the q-particle resolution of the detector, not any higher-order resolution.

The problem we are dealing with in this paper is to investigate whether different Monte-Carlo (MC) models, which were tuned to reproduce the global-shape variables and single-particle inclusive densities, can lead to the same structure of the local multiplicity fluctuations which are determined by *many*-particle inclusive densities. We study JETSET 7.4 PS [7], ARIADNE 4.08 [8] and HERWIG 5.9 [9] models. The models have been tuned as described above by the L3 Collaboration [10].

3 Monte-Carlo Analysis

1) *Horizontal BPs:*

In order to reduce the statistical error on the observed local quantities when analyzing experimental data, we use the bin-averaged BPs [4,5]:

$$\eta_q(M) = \frac{q}{q-1}\frac{\bar{N}_q(M)\bar{N}_{q-2}(M)}{\bar{N}^2_{q-1}(M)}. \tag{4}$$

$$\bar{N}_q(M) = \frac{1}{M}\sum_{m=1}^{M} N_q(m,\delta), \tag{5}$$

where $N_q(m,\delta)$ is the number of events having q particles in bin m and $M = \Delta/\delta$ is the total number of bins (Δ represents the size of full phase-space volume). To be able to study non-flat distributions, like for rapidity, we have to carry out a transformation from the original phase-space variable to one in which the underlying density is approximately uniform, as suggested by Bialas, Gadzinski and Ochs [11].

2) *Generalized integral BPs:*

To study the distribution for spikes, we will consider the generalized integral BPs [5] using the squared pairwise four-momentum difference $Q^2_{12} = -(p_1 - p_2)^2$. In this variable, the definition of the BPs is given by

$$\chi_q(Q^2) = \frac{q}{q-1}\frac{\Pi_q(Q^2)\Pi_{q-2}(Q^2)}{\Pi^2_{q-1}(Q^2)}, \tag{6}$$

where $\Pi_q(Q^2)$ represents the number of events having q spikes of size Q^2 in the phase-space of variable Q^2_{12}, irrespective of how many particles are inside each spike. To define the spike size, we shall use the so-called Grassberger-Hentschel-Procaccia counting topology for which a many-particle hyper-tube is assigned a size Q^2 corresponding to the maximum of all pairwise distances (see [5] for details). For purely independent particle production, with the multiplicity distribution characterized by a Poissonian law, the BPs (6) are equal to unity for all q.

3.1 In rapidity variable

In order to study fluctuations inside jets, in most investigations the fluctuations have been measured in the rapidity y defined with respect to the

thrust or sphericity axis [2]. The Monte Carlo analysis for this variable is performed in the full rapidity range $|Y| \leq 5$. Fig. 1 shows the results for the BPs (4) for rapidity after the Białas-Gazdzicki-Ochs transformation. The second-order BP for JETSET model decreases with increasing M up to $M \simeq 20$, which is found to correspond to the value of M at which the maximum of the multiplicity distribution $P_n(\delta)$ first occurs at $n = 0$. At large M, all BPs show a power-law increase with increasing M, $\eta_q \sim M^{\alpha_q}$. This indicates that the fluctuations in y defined with respect to the thrust axis are multifractal scale invariant.

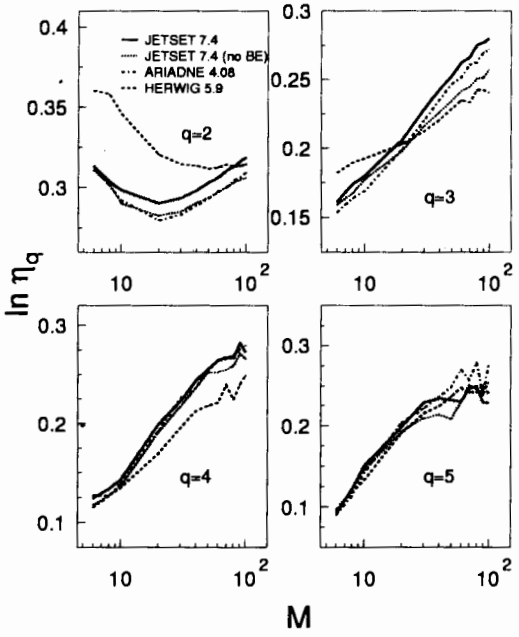

Figure 1. *BPs as a function of the number M of bins in rapidity defined with respect to the thrust axis. The shaded areas represent the statistical and systematical errors on the JETSET predictions.*

Note that the conclusion that fluctuations have a multifractal structure is possible without the necessity of calculating the intermittency indices ϕ_q. In contrast, to reveal multifractality with the help of the NFMs, one first needs to carry out fits of the NFMs by a power law.

HERWIG predictions (dashed lines) significantly overestimate the second-order BP obtained from LUND MCs. Since, for small phase-space cells, the second-order BP is determined by the dispersion of the distribution [4,5], this means that the HERWIG produces too broad local multiplicity distributions. Such a result confirms that obtained by the ALEPH Collaboration [12].

To study the disagreement between Monte-Carlo models in more detail, one can split η_2 into two BPs:

$$\eta_2 = \eta_2^{(\pm\pm)} + \eta_2^{(+-)}. \tag{7}$$

Here $\eta_2^{(\pm\pm)}$ is defined by (4) with $N_2(m,\delta) = N_2^{(\pm\pm)}(m,\delta y)$, $N_2^{(\pm\pm)}(m,\delta y)$ being the number of events having like-charged two-particle combinations inside bin m of size δy. Analogously, $\eta_2^{(+-)}$ is constructed from the number of events $N_2^{(+-)}(m,\delta y)$ having unlike-charged two-particle combinations. Note that due to a combinatorial reason, $\eta_2^{(\pm\pm)} < \eta_2^{(+-)}$.

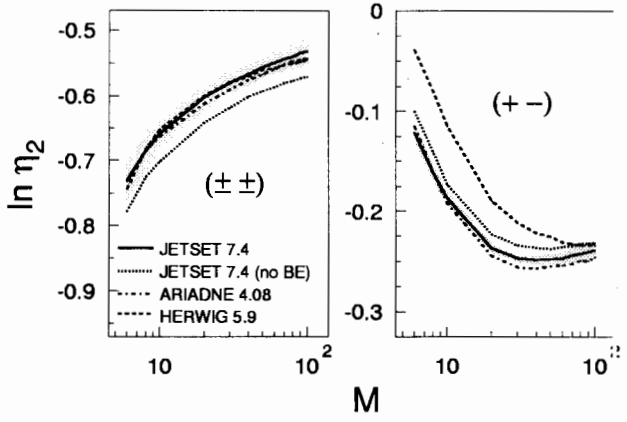

Figure 2. *The second-order BP as a function of the number M of bins in rapidity defined with respect to the thrust axis for like-charged and unlike-charged particle combinations.*

Fig. 2 shows that $\eta_2^{(\pm\pm)}$ and $\eta_2^{(+-)}$ indeed behave completely differently. While $\eta_2^{(\pm\pm)}$ shows the expected rise, $\eta_2^{(+-)}$ shows a strong decrease at low

M and the onset of an increase at large M. The structure of η_2 observed in Fig. 2 is a combination of these two effects.

Note that η_2 is strongly effected by the Bose-Einstein (BE) interference incorporated into the JETSET generator[1]. This is not unexpected since $\eta_2 \sim P_2/P_1^2$, which is very similar to the correlation functions used for Bose-Einstein studies.

Let us remind that in order to model the BE interference in JETSET, the momenta of identical final-state particles are shifted to reproduce the expected two-particle correlation function. The main disadvantage of such *ad hoc* method is that it spoils overall energy-momentum conservation and it is necessary to modify also momenta of non-identical particles to compensate for this. This effect in JETSET model can be seen in Fig. 2.

The strong anti-bunching tendency seen for unlike-charged particles at $M < 30$ can be attributed to resonance decays and to chain-like particle production along the thrust axis, as expected from the QCD-string model [13]. The latter effect leads to local charge conservation with an alternating charge structure. Evidence for this effect was recently observed by DELPHI [14]. As a result, there is a smaller rapidity separation between unlike-charged particles than between like-charged and $\eta_2^{(+-)}$ is much larger than $\eta_2^{(\pm\pm)}$ at small M. Having correlation lengths $\delta y \sim 0.5 - 1.0$ in rapidity, the resonance and the charge-ordering effects, however, become smaller with increasing M.

Note that to distinguish the NFMs calculated for different charge combinations in a bin-splitting technique is difficult due to insufficient sensitivity of this tool and a purely combinatorial reason.

3.2 In the four-momentum difference

The study of BPs described above can help us to understand a tendency of the particles to be grouped into spikes inside small phase-space intervals. Another question is how the multiplicity of these spikes fluctuates from event to event when the spike size goes to zero. To study this, we will use the BPs defined in (6).

Fig. 3 shows the behavior of χ_q as a function of $-\ln Q^2$. The full lines represent the behavior of the BPs in the Poissonian case. In contrast, all BPs obtained from the Monte Carlo models rise with increasing $-\ln Q^2$

[1]Here and below, we show JETSET predictions with the BE interference disabled after the retuning of this model to describe global-shape variables.

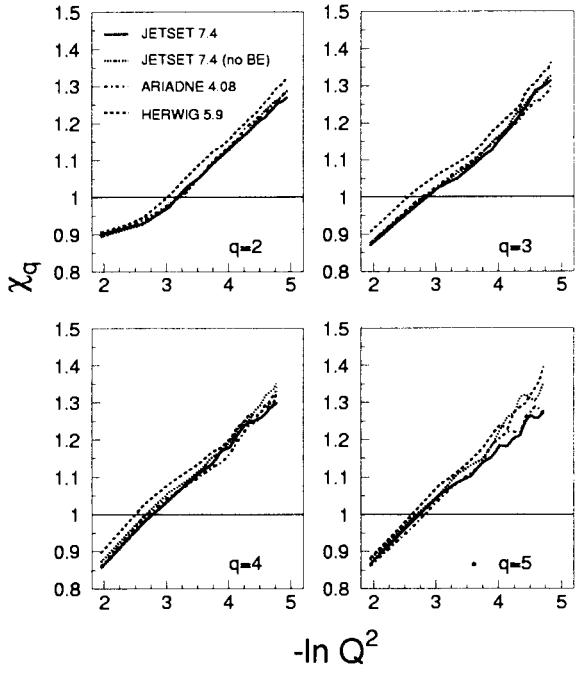

Figure 3. *Generalized integral BPs as a function of the squared four-momentum difference Q^2 between two charged particles.*

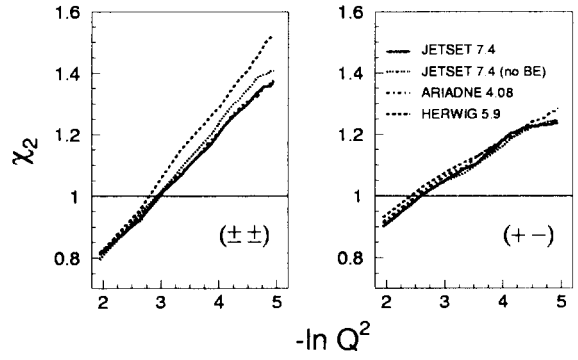

Figure 4. *Generalized second-order BP as a function of the squared four-momentum difference Q^2 between two charged particles.*

(decreasing Q^2). This corresponds to a strong bunching effect of all orders, as expected for multifractal fluctuations. The anti-bunching effect ($\chi_q < 1$) for small $-\ln Q^2$ is caused by the energy-momentum conservation constraint [5].

To learn more about the mechanism of multiparticle fluctuations in Q^2_{12} variable, we present in Fig. 4 the behavior of the second-order BP as a function of $-\ln Q^2$ for multiparticle hyper-tubes (spikes) made of like-charged and those of unlike-charged particles, separately. A significant difference is observed for like-charged combinations between HERWIG and LUND MCs.

4 Discussion

Local multiplicity fluctuations in Monte Carlo models have been studied by means of bunching parameters. Since all high-order BPs show a power-like rise with decreasing the size of phase-space interval, none of the conventional multiplicity distributions given in Table 1 can describe the local fluctuations observed in the MC models.

For e^+e^- interactions, one can be confident that, at least on the parton level of this reaction, perturbative QCD can give a hint for the understanding of the problem. Analytical calculations based on the DLLA of perturbative QCD show that the multiplicity distribution of partons in ever smaller opening angles is inherently multifractal [15]. Qualitatively, this is consistent with our results on the BPs for rapidity. Quantitatively, however, the QCD predictions disagree with the e^+e^- data and MC models [16].

In this paper we show that the power-law behavior of BPs is mainly due to like-charged particles. JETSET gives the same power-law trend even without the BE effect. This means that the intermittency observed for like-charged particles appears to be largely a consequence of QCD parton showers and hadronization.

The predictions of the ARIADNE 4.08 model are comparable with those of the JETSET 7.4 PS model. This is essentially due to the same implementation of hadronization, which is based for both models on string fragmentation.

A noticeable disagreement, however, is found between LUND and HERWIG models. The conversion of the partons into hadrons in the first models is based on the Lund String Model [13]. However, the hadronization

in HERWIG is modelled with a cluster mechanism [9]. This can be a rather natural candidate to explain the observed difference between local fluctuations in these models. A particular concern is the large difference between MC's for η_2. The behavior of η_2 for not very small intervals is sensitive to low-multiplicity events, for which hadronization details could play a significant role.

Acknowledgments

I wish to express my gratitude to W.Kittel and W.J.Metzger for many useful discussions.

References

[1] A.Białas and R.Peschanski, Nucl. Phys. B273 (1986) 703 Nucl. Phys. B308 (1988) 857.

[2] TASSO Collab., W.Braunschweig *et al.*, Phys. Lett. B231 (1989) 548 ; K.Sugano (HRS Collab.), Proc. Santa Fe Workshop "Intermittency in High-Energy Collisions", Eds. F.Cooper *et al.* (World Scientific, Singapore, 1991) p.1 ; CELLO Collab., H.J.Behrend *et al.*, Phys. Lett. B256 (1991) 97 ; OPAL Collab., M.Z.Akrawy *et al.* Phys. Lett. B262 (1991) 351 ; ALEPH Collab., D.Decamp *et al.*, Z. Phys. C53 (1992) 21 ; DELPHI Collab., P.Abreu *et al.*, Phys. Lett. B247 (1990) 137 ; A.De Angelis, Mod. Phys. Lett. A5 (1990) 2395 ; DELPHI Collab., P.Abreu *et al.*, Nucl. Phys. B386 (1992) 471 L3 Collab., B. Adeva *et al.*, Z. Phys. C55 (1992) 39.

[3] P.Bożek, M.Płoszajczak and R.Botet, Phys. Rep. 252 (1995) 101 ; E.A.De Wolf, I.M.Dremin and W.Kittel, Phys. Rep. 270 (1996) 1.

[4] S.V.Chekanov and V.I.Kuvshinov, Acta Phys. Pol. B25 (1994) 1189 ; S.V.Chekanov, W.Kittel and V.I.Kuvshinov, Acta Phys. Pol. B27 (1996) 1739 ; S.V.Chekanov and V.I.Kuvshinov, J. Phys. G22 (1996) 601.

[5] S.V.Chekanov, W.Kittel and V.I.Kuvshinov, Z. Phys. C73 (1997) 517.

[6] S.V.Chekanov, V.I.Kuvshinov, J.Phys. G23 (1997) 951.

[7] T.Sjöstrand, Comp. Phys. Comm. 82 (1994) 74.

[8] L.Lönnblad, Comp. Phys. Comm. 71 (1992) 15.

[9] G.Marchesini and B.R.Webber, Nucl. Phys. B310 (1988) 461 ; G.Marchesini *et al.*, Comp. Phys. Comm. 67 (1992) 465.

[10] J.Casaus, L3 Note 1946 (1996);
Sunanda Banerjee and Swagato Banerjee, L3 Note 1978 (1996) ; I.G.Knowles and T.Sjöstrand (conveners), "QCD Event Generators", Physics at LEP2, CERN-96-01, Vol. 2 (1996) p.103.

[11] A.Białas and M.Gazdzicki, Phys. Lett. B252 (1990) 483 ; W.Ochs, Z. Phys. C50 (1991) 339.

[12] ALEPH Collab., D.Buskulic *et al.*, Z. Phys. C69 (1995) 15.

[13] B.Andersson, G.Gustafson, G.Ingelman, T.Sjöstrand, Phys. Rep. 97 (1983) 31.

[14] DELPHI Collab., P.Abreu *et al.*, Phys. Lett. B407 (1997) 174.

[15] W.Ochs and J.Wosiek, Phys. Lett. B289 (1992) 159 ; B304 (1993) 144 ; Z. Phys. C68 (1995) 269 ; Ph.Brax, J.-L.Meunier and R.Peschanski, Z. Phys. C62 (1994) 649 ; Yu.Dokshitzer and I.M.Dremin, Nucl. Phys. B402 (1993) 139.

[16] S.V.Chekanov (for the L3 Collaboration), Presented at the 32th Rencontres de Moriond, "QCD and High Energy Hadronic Interactions" Les Arcs, France (1997) hep-ex/9707012; S.V.Chekanov, "Local Multiplicity Fluctuations and Intermittent Structure Inside Jets', Thesis, (1997), Nijmegen, The Netherlands.

Variational Perturbation Theory in QCD and its Applications

A.N. Sissakian[a] and I.L. Solovtsov[ab]

[a] *Bogoliubov Laboratory of Theoretical Physics, JINR, Dubna, Moscow region, 141980, Russia*

[b] *Gomel Polytechnical Institute, Gomel 246746, Belarus*

1 Introduction

In these lectures the nonperturbative approach to quantum field theory, variational perturbation theory (VPT), is briefly reviewed.

Solution of many physical problems is based on approximation of a quantity under consideration by a finite number of terms of a certain series. In quantum field theory this is conventionally an expansion into a perturbative series. This approach combined with the renormalization procedure is now a basic method for computations. As is well-known, perturbative series for many interesting models including realistic models are not convergent. Nevertheless, at small values of the coupling constant these series may be considered as asymptotic series and could provide a useful information. However, even in the theories with a small coupling constant, for instance, in quantum electrodynamics there exist problems which cannot be solved by perturbative methods. Also, a lot of problems of quantum chromodynamics require nonperturbative approaches.

Many approaches have been devoted to the development of nonperturbative methods. Among them is the summation of a perturbative series (see reviews [1] and monograph [2]). The difficulty is that the procedure of summation of asymptotic series is not unique as it contains a functional arbitrariness. A correct formulation of the problem of summation is ensured by further information on the sum of a series [3]. At present information of that kind is known only for the simplest field-theoretical models [4]. Moreover, in many cases of physical interest, the series of perturbative theory is not Borel summable.

There have been approaches that are not directly based on the perturbative series. Many of nonperturbative approaches make use of a variational procedure for finding the leading contribution. However, in this case there is no always an algorithm of calculating corrections to the value

found by a variational procedure, and this makes difficult to answer the question how adequate is the so-called main contribution to the object under investigation and what is the range of applicability of the obtained estimations.

Therefore, useful approaches to the study of the nonperturbative structure of quantum field theory are the methods that combine an expansion of a given quantity in a series that defines the algorithm of calculating the correction with an optimizing procedure. The nonperturbation Gaussian effective potential for a quantum system has been constructed by an approach of that sort in refs. [5, 6, 7, 8]. There exist the various optimizing procedures. In [9, 10], for example, the principle of minimal sensitivity has been applied to the third–order calculation of $R_{e^+e^-}$. Different ways of constructing the variational procedures for scalar models of quantum field theories are discussed in refs. [11, 12, 13]. However, even if the algorithm of calculating corrections, i.e. terms of a certain approximating series, exists, it is not still sufficient. Here of fundamental importance are the properties of convergence of a series. Indeed, unlike the case when even a divergent perturbative series in the weak coupling constant approximates a given object as an asymptotic series, the approximating series in the absence of a small parameter should obey more strict requirements. Reliable information in this case may be obtained only on the basis of convergent series.

We shall consider the method of a series construction with the aid of a variational procedure of the harmonic type. It has been observed empirically in [14] that the results seem to converge if the variational parameter is chosen, in each order, according to the principle of minimal sensitivity. This induced–convergence phenomenon is discussed in detail in ref. [15]. In ref. [16]] the proof of convergence of an optimized δ–expansion is given in the cases of zero and one dimensions. The proof of convergence of variational series in the case of anharmonic procedure is given in ref. [12] . Here, we discuss a method which allows one to systematically determine the low energy structure in quantum chromodynamics. We shall construct the expansion which is based on a new small parameter and apply this method to the nonperturbative renormalization group analysis in quantum chromodynamics. Applications to the definition of the QCD running coupling in the timelike domain and to the semileptonic decay of the τ lepton will be considered. The main results concerning the method of variational theory and some its applications can be found in the papers [5, 10, 11, 12, 13]

and [17, 18, 19, 20, 21, 22] (see also references therein).

2 Toy model

To represent a simple explanation of the basic idea of the method, let us first make a start with very transparent example, simple integral of the form

$$W(g) = \int_{-\infty}^{\infty} dx \, \exp(-S[x]) . \tag{2.1}$$

The expression (2.1) can be considered as the zero-dimensional analog of the ϕ^4-model. The function $S[x]$ plays the role of "the action functional"

$$S[x] = S_0[x] + S_I[x] = x^2 + g\,x^4 . \tag{2.2}$$

In the quantum field theory we can calculate the Gaussian functional integrals. Let us imagine that in this simple case we have to operate with Gaussian integrals as well. Thus, we can try to evaluate the quantity (2.1) by using the Gaussian integrals of the sort

$$\int dx \, P(x) \, exp(-a\,x^2) \tag{2.3}$$

with some polynomial $P(x)$ of x.

The standard method of calculations is the expansion of the expression $\exp(-S[x])$ in the power series of the "coupling constant" g. Indeed, in this case, one uses the Gaussian integrals (2.3) and obtains the standard asymptotic perturbative series

$$W(g) = \sum_{k=0}^{\infty} \omega_k \tag{2.4}$$

with the coefficients

$$\omega_k = \frac{1}{k!} \int_{-\infty}^{\infty} dx \, (-g\,x^4)^k \, \exp(-S_0[x]) . \tag{2.5}$$

Whereas the expansion of the function (2.1) in the series (2.4) with coefficient (2.5) is unique, the inverse procedure of finding the sum of the series (2.4) without using additional information about the function (2.1) is nonunique. For example, the same series (2.4) has also the function $W(g) + \exp(-1/g)$ that has different from $W(g)$ asymptotic behavior at

large values of the coupling constant g. The reason for the incorrectness of the summation procedure is the asymptotic nature of the perturbative expansion (2.4). Therefore, the perturbation series by itself without any additional information about its sum cannot be used to evaluate the function (2.1) for sufficiently large values of the coupling constant. Of course, in this simple case, we know the needed additional information about $W(g)$ and can apply to the series (2.4) some method of summation, for example, the Borel method. But, in the real field theory models, we do not know this information about function that is represented by functional integral and the problem requires special attention.

The VPT approach makes it possible to construct different expansion for the function (2.1) and for quantum field models using the Gaussian quadratures. In this section we will demonstrate how the VPT idea allows one to construct a nonperturbative expansion which is based on a new small expansion parameter.[1]

By using a new split of the action let us rewrite Eq. (2.2) in the form

$$S[x] = S_0'[x] + S_I'[x], \tag{2.6}$$

where we have introduced a new free action $S_0'[x] = \zeta^{-1}x^2$ and an action of interaction $S_I'[x] = gx^4 - (\zeta^{-1} - 1)x^2$. Here ζ is an auxiliary parameter of a variational type. Actually, the original quantity $W(g)$ does not depend on this parameter, therefore, when studying a finite number of the terms of the series it is possible to choose the variational parameter on the basis of some principle of optimization [12, 23].

The VPT series for (2.1) can written down as follows

$$W(g) = \sum_{n=0}^{\infty} W_n, \tag{2.7}$$

where the terms of the VPT expansion have the form

$$\begin{aligned} W_n &= \frac{1}{n!}\int dx\,(-S_I'[x])^N \exp(-S_0'[x]) \qquad (2.8)\\ &= \sum_{k=0}^{n}\frac{1}{(n-k)!\,k!}\int dx\,(-g\,x^4)^k\left[(\zeta^{-1}-1)\,x^2\right]^{n-k}\exp(-S_0'[x]). \end{aligned}$$

[1]Here, we use the so-called harmonic variational procedure. Other choices of the trial VPT functionals have been considered in [11, 12, 13, 22].

It is convenient to rewrite the free action as follows

$$S_0'[x] = \zeta^{-1} x^2 \Rightarrow \left[1 + \kappa (\zeta^{-1} - 1) \right] x^2 \qquad (2.9)$$

and set $\kappa = 1$ after all calculations. In this case, any power of $(\zeta^{-1} - 1)x^2]$ in Eq. (2.8) we can obtain by differentiations with respect to κ. The remaining polynomial $(-g x^4)^k$ has the standard perturbative form, therefore, we have a possibility to apply to calculations the standard diagram technique with modified propagator

$$\Delta = \frac{1}{1 + \kappa (\zeta^{-1} - 1)} . \qquad (2.10)$$

For $\kappa = 1$, one finds $\Delta = \zeta$.

The terms of the VPT expansion can be written down in the form

$$W_n = \sum_{k=0}^{n} \frac{1}{(n-k)!} \left(- \frac{\partial}{\partial \kappa} \right)^{n-k} \omega_k , \qquad (2.11)$$

where the coefficients

$$\omega_k = \frac{1}{k!} \int dx \, (-g x^4)^k \exp \left(- x \Delta^{-1} x \right) \qquad (2.12)$$

are given by the standard diagrams of perturbation theory with the propagator (2.10).

Consider a structure of the VPT term (2.11). First of all, note that the differentiation with respect to parameter κ gives the additional factor $(1 - \zeta)$

$$\frac{1}{m!} \left(- \frac{\partial}{\partial \kappa} \right)^m \Delta (\kappa = 1) = (1 - \zeta)^m \Delta (\kappa = 1) . \qquad (2.13)$$

Secondly, it is easy to see that in this model the number of internal lines (L) in any diagram (here, all diagrams are vacuum diagrams) equal to the double number of vertices (V): $L = 2V$. The internal line corresponds to propagator and leads to the factor ζ, and the vertex gives the factor g. Thus, schematically, one can write down

$$W_n \sim (g \zeta^2)^n + (1 - \zeta)(g \zeta^2)^{n-1} + \cdots + (1 - \zeta)^{n-1} (g \zeta^2) + (1 - \zeta)^n . \qquad (2.14)$$

N	0	1	2	3	4	6	8
C	1.14	2.64	3.56	5.46	6.12	871	11.33
D(g=10) %	2.76	4.83	0.26	0.73	0.038	0.006	0.0012
D(g=1000) %	5.01	6.52	0.56	1.13	0.089	0.017	0.0033

Table 1: *The relative error* $D(g) = |W_{\text{theor.}}(g)/W_{\text{exper.}}(g) - 1|$.

From (2.14). we can see that if the value of $(1-\zeta)$ will be proportional to $(g\zeta^2)$, the expression W_n will contain the common factor $(1-\zeta)^n$. So, let the parameter ζ obeys to equation

$$1 - \zeta = C g \zeta^2 \tag{2.15}$$

with some positive constant C. We see from (2.15) that for all values of the initial coupling constant g the new expansion parameter $a = 1 - \zeta$ obeys the inequality: $0 \leq a < 1$. The remained parameter C is independent on the value of the coupling constant g and can be found by different ways. For example, if we consider the first non-trivial order $W^{(1)}(g) = W_0(g) + W_1(g)$ and use so-called "fastest apparent convergence", from point of view of which an absolute value of the last calculated term in the expansion should be minimal or vanishes, and require that $W_1 = 0$ we find $C = 3/2$. In this case, we have the approximation $W(g)$ by the expression $W^{(1)}(g)$ (with $W_1 = 0$) with an accuracy better then six percent for all interval of g. In particular, at $g \to \infty$, the relative error of approximation is about 5.1%. Similar results can be obtained if one uses the principle of minimum sensitivity, or a normalization at some "experimental" value $W(g_0) = W_{\text{experim.}}$. If one includes to our consideration the next orders of the VPT expansion we will obtain a best approximation of $W(g)$.

In Table 1 we can see a dependence of the parameter C of the order expansion and the relative error $D(g) = |W_{\text{theor.}}(g)/W_{\text{exper.}}(g) - 1|$. Here, to find the parameter C one makes use the normalization condition $\min|W(g_0) - W_{\text{exper.}}| = \min|W(g_0) - W_{\text{exact}}(g_0)|$ at $g_0 = 1$.

3 Variational perturbation theory in QCD

To explain the basic idea of the method in the QCD case, let us first consider the pure Yang–Mills theory (quarks can be included without prob-

lems). The Lagrangian density has the form

$$\begin{aligned} L_{YM} &= -\frac{1}{4}(F_{\mu\nu})^2 - \frac{1}{2}\,g\,F_{\mu\nu}\,[A_\mu \times A_\nu] + \frac{1}{4}\,g^2\,[A_\mu \times A_\nu]^2 + L_{g.f.} + L_{F.P.} \\ &= L_0(A) + g\,L_3(A) + g^2\,L_4(A) \quad , \end{aligned} \tag{3.1}$$

where $F_{\mu\nu} = \partial_\mu A_\nu - \partial_\nu A_\mu$, $L_{g.f.}$ and $L_{F.P.}$ are gauge fixing and Faddeev–Popov terms.

The $L_3(A)$ generates the three–gluon and ghost–gluon–ghost vertices. This interaction is the Yukawa type interaction. The term $L_4(A)$ generates the four–gluon vertices. Let us introduce the $\chi_{\mu\nu}$ field and transform the term $L_4(A)$ to the Yukawa type diagrams

$$\begin{aligned} \exp\left\{ i\,\frac{g^2}{4}\int dx\ [A_\mu \times A_\nu]^2 \right\} &= \int D\chi \exp\left\{ -\frac{i}{2}\int dx\,\chi^2_{\mu\nu} \right. \\ &+ \left. i\frac{g}{\sqrt{2}}\int dx\,\chi_{\mu\nu}[A_\mu \times A_\nu] \right\} . \end{aligned} \tag{3.2}$$

The action functional can be written in the form

$$S = S_0(\chi) + S(A,\chi) + S^{Yuk.}_{YM}(A)\,, \tag{3.3}$$

where

$$S(A,\chi) = \frac{1}{2}\int dx\,dy\ A^a_\mu(x)\,\left[D^{-1}(x,y|\chi)\right]^{ab}_{\mu\nu}\,A^b_\nu(y) \tag{3.4}$$

and the gluon propagator $D(x,y|\chi)$ in the χ–field is defined as

$$\left[D^{-1}(x,y|\chi)\right]^{ab}_{\mu\nu} = \left[-\partial^2 g_{\mu\nu}\delta_{ab} + g\sqrt{2}f_{abc}\chi^c_{\mu\nu} + \text{gauge terms}\right]\delta(x-y). \tag{3.5}$$

The Green's functions can be written as

$$G(\cdots) = \langle\, G_{Yuk.}(\cdots|\chi)\,\rangle\ , \tag{3.6}$$

where

$$G_{Yuk.}(\cdots|\chi) = \int DA\,[\cdots]\,\exp\left\{ i\,\left[S(A,\chi) + S^{Yuk.}_{YM}(A) \right] \right\}\ , \tag{3.7}$$

and

$$\langle\cdots\rangle = \int D\chi\,[\cdots]\,\exp\left[\,i\,S_0(\chi)\right]\,. \tag{3.8}$$

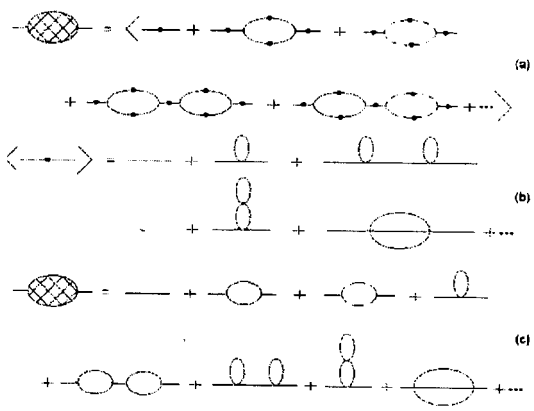

Figure 1: *The perturbation expansion of the full gluon propagator by using the χ–transformation. The gluon line with point corresponds to the function $D(\chi)$.*

The Green's functions $G_{Yuk.}(\cdots|\chi)$ contain only the Yukawa type diagrams appearing inside the brackets $\langle\cdots\rangle$ with the gluon propagator $D(x,y|\chi)$. In Fig. 1 (a), the full gauge propagator is shown. The expansion $D(x,y|\chi)$ in perturbation theory generates the four–gluon graphs [Fig. 1 (b)] that are added to the Yukawa diagrams, and in this case we obtain the standard perturbation expansion [Fig. 1 (c)].

Let us rewrite the Lagrangian in the form

$$\begin{aligned} L(A,\chi) &= L_0(A,\chi) + L_I(A,\chi), \\ L_0(A,\chi) &= \zeta^{-1}\, L(A,\chi) + \xi^{-1}\, L(\chi), \\ L_I(A,\chi) &= \eta\left[g\, L_{YM}^{Yuk.}(A) - (\zeta^{-1}-1)\, L(A,\chi) - (\xi^{-1}-1)\, L(\chi)\right], \end{aligned} \tag{3.9}$$

where ζ and ξ are the parameters of variational type. The original quantity $L(A,\chi)$ does not depend on ζ and ξ. Therefore, the freedom in choosing ζ and ξ can be used to improve the series properties . In the variational perturbation series a new action of interaction is used for constructing the expansion. It is clear that if the parameters $0 < \zeta < 1$ and $0 < \xi < 1$, we "strengthen" the new free Lagrangian and, at the same time, "weaken" the Lagrangian of interaction. After all calculations we put $\eta = 1$. This parameter will be also written in the propagator $D(x,y|\chi)$

in the combination with the coupling constant. The VPT series for the Green's function is given by

$$
\begin{aligned}
G(\cdots) &= \sum_n G_n(\cdots), \\
G_n(\cdots) &= \frac{1}{n!}\eta^n \int D\chi DA\,[\cdots]\,[i\,S_I(A,\chi)]^n \exp\,[\,i\,S_0(A,\chi)\,], \qquad (3.10) \\
&= (i\,\eta)^n \sum_{k=0}^{n} \frac{1}{(n-k)!\,k!} \int D\chi DA\,[\cdots]\,\Big[\,g\,S_{YM}^{Yuk}(A)\Big]^k \\
&\quad \Big[(\zeta^{-1}-1)\,S(A,\chi) + (\xi^{-1}-1)\,S(\chi)\Big]^{n-k} \exp\;\; i\,S_0(A,\chi)\,].
\end{aligned}
$$

We redefine the $L_0(A,\chi)$ for convenience of calculations as follows:

$$
L_0(A,\chi) \Rightarrow L_0'(A,\chi) = [1+\kappa(\zeta^{-1}-1)]L(A,\chi)+[1+\kappa(\xi^{-1}-1)]L(\chi). \quad (3.11)
$$

In this case, any power of $[(\zeta^{-1}-1)\,S(A,\chi) + (\xi^{-1}-1)\,S(\chi)]$ in (3.10) can be obtained by the corresponding number of differentiation of the expression $\exp[iS_0'(A,\chi,\kappa)]$ with respect to κ. After all calculations we set $\kappa = 1$.

From Eqs. (3.10) and (3.11) we have

$$
G_n = \eta^n \sum_{k=0}^{n} \frac{1}{(n-k)!}\left(-\frac{\partial}{\partial\kappa}\right)^{n-k} \langle\, g_k(\kappa)\,\rangle \quad , \qquad (3.12)
$$

where the functions

$$
\begin{aligned}
g_k(\kappa) &= \frac{i^k}{k!}\int DA\;\,[\cdots]\,\Big[\,g\;S_{YM}^{Yuk}(A)\Big]^k \\
&\quad \exp\left\{\,i\,[\,1+\kappa(\zeta^{-1}-1)\,]\int dx\;L(A,\chi)\right\} \qquad (3.13)
\end{aligned}
$$

correspond to the Yukawa diagrams of the Yang–Mills theory with gluon propagator $[1+\kappa(\zeta^{-1}-1)]^{-1}D(x,y|\chi) \to \zeta D(x,y|\chi)$ for $\kappa = 1$. The propagator of χ–field includes the factor $[1+\kappa(\xi^{-1}-1)]^{-1}$ transformed into ξ for $\kappa = 1$.

The operator of differentiation $(-\partial/\partial\kappa)^l/l!$ gives the factor $(1-\zeta)^l$ for the gluon propagator and $(1-\xi)^l$ for the propagator of the χ–field.

It is easy to verify that the Nth order of the VPT series contains the Nth order of a perturbation series with the correction $O(\,g^{N+1}\,)$, therefore, the VPT expansion does not contradict the perturbative results obtained for the small coupling constant.

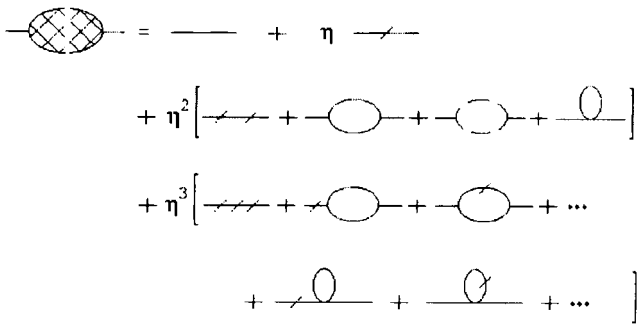

Figure 2: *The diagrams for the VPT expansion of the full gluon propagator.*

The diagrams corresponding to the new expansion of the full gluon propagator are shown in Fig. 2. The gluon line with slash signifies the differentiation over κ and contains the factor $(1-\zeta)$. If this line arises due to the χ-field propagator, the corresponding factor is $(1-\xi)$.

The outline of the VPT expansion structure can be written as

$$1 + \eta(1-\zeta) + \eta^2\left[(1-\zeta)^2 + g^2\zeta^3 + g^2\xi\right] \qquad (3.14)$$
$$+ \eta^3\left[(1-\zeta)^3 + g^2\zeta^3(1-\zeta) + g^2\xi(1-\zeta) + g^2\xi(1-\xi)\right] + \cdots$$

The construction of expansions for the Green's functions corresponding to three-, four-gluon, ghost-gluon-ghost vertices are introduced in similar manner.

If we choose $\xi = \zeta^3$ and $(1-\zeta)^2 = C\lambda\zeta^3$, where C is a positive constant, we obtain that the nth order term of our series contains the factor $(1-\zeta)^n$ and the expansion parameter $a = (1-\zeta) < 1$ for all values of the initial coupling constant. Now, one can perform the renormalization procedure and define the renormalization constants a power series of a [18, 19].

Consider the connection between the perturbative and non-perturbative regimes of the running coupling constant $\alpha_s(Q^2)$. To fix the parameter C we will use non-perturbative information from meson spectroscopy and derive $\alpha_s(Q^2)$ in the perturbative region at large Q^2. In other words, we will find the connection between the universal tension σ in the linear part of

the quark-antiquark static potential $V_{\rm lin}(r) = \sigma r$, which can be determined from meson spectroscopy, and the description of high energy physics. If, as usual, we assume that the quark potential in momentum space can be written as $V(q^2) = -16\pi\alpha_s(q^2)/3q^2$, where $\alpha_s(q^2)$ describes both large and small momentum, and that $\alpha_s(q^2)$ has the singular infrared asymptotics $\alpha_s(q^2) \sim q^{-2}$, we obtain, by taking the three-dimensional Fourier transform, the large-distance linear potential in coordinate space. The corresponding singular infrared behaviour of $\lambda = \alpha_s/(4\pi)$ conforms to the asymptotics of the β-function: $\beta(\lambda) \to -\lambda$ for a large coupling constant.

In the framework of this approach consider the functions $\beta^{(2)}$, $\beta^{(3)}$, $\beta^{(4)}$ and $\beta^{(5)}$ that are obtained if we take into consideration the terms $O(a^2)$, $O(a^3)$, $O(a^4)$ and $O(a^5)$ in the corresponding renormalization constant Z_λ. As has been shown [19], the values of $-\beta^{(k)}(\lambda)/\lambda$ as functions of the coupling constant for parameters $C_2 = 0.977$, $C_3 = 4.1$, $C_4 = 10.4$ and $C_5 = 21.5$ go to 1 at sufficiently large λ. The increase of C_k with the order of the expansion is explained by the necessity to compensate the high order contribution. A similar situation takes place also in zero- and one-dimensional models. The behaviour of the functions $-\beta^{(k)}(\lambda)/\lambda$ gives evidence for the convergence of the results, in accordance with the phenomenon of induced convergence. At large coupling, $-\beta^{(k)}(\lambda)/\lambda \simeq 1$, which corresponds to $\alpha_s(Q^2) \sim Q^{-2}$ at small Q^2.

The value of the coefficient σ in the linear part of the quark-antiquark static potential $V_{\rm lin}(r) = \sigma r$ is $\sigma \simeq 0.15 \div 0.20$ GeV^2. At a small value of Q^2 the corresponding behaviour of $\alpha_s(Q^2)$ is $\alpha_s(Q^2) \simeq 3\sigma/2Q^2$. Here we will use this equation at a certain normalization point Q_0 and the value $\sigma = 0.1768$ GeV^2 which has been obtained in [24]. The renormalization group method gives the following equation for the Q^2-evolution of the expansion parameter a:

$$Q^2 = Q_0^2 \exp[\,\phi(a, N_f) - \phi(a_0, N_f^0)\,] \tag{3.15}$$

with

$$\phi(a, N_f) = \int^{\lambda} \frac{d\lambda}{\beta(\lambda)}\,. \tag{3.16}$$

In an appropriate region of the momentum, the value of $\sigma(Q^2) = 2/3\,Q^2\,\alpha_s(Q^2)$ is almost independent of the choice of Q_0 and lies in the interval $0.15 \div 0.20$ GeV^2. This result agrees with the phenomenology of meson spectroscopy. Thus, we have found all the parameters and can now

consider the behaviour of the effective coupling constant at large Q^2. For example, we find $\alpha_{\rm eff}(m_Z) = 0.126$. It should be stressed that we have obtained this result by evolution of the effective coupling starting from a very low energy scale. Taking into account this fact the value of $\alpha_{\rm eff}(m_Z)$ obtained in such a way seems to be quite reasonable.

4 Renormalon representation and τ decay

In this section we will concentrate on a description of the inclusive decay of the τ lepton taking into account renormalon contributions (for detais, see [25]). Consider the Adler D-function $D(Q^2) = -Q^2 d\Pi/dQ^2$ corresponding to the vector hadronic correlator in the massless case. The two-loop perturbative approximation is given by $D(t,\lambda) = 1 + 4\lambda(\mu^2)$, where $t = Q^2/\mu^2$. Standard renormalization group improvement leads to the substitution $\lambda(\mu^2) \to \overline{\lambda}(t,\lambda)$, which implies a summation of the leading logarithmic contributions. However, due to the ghost pole of the running coupling at $Q^2 = \Lambda^2_{QCD}$ this substitution breaks the analytic properties of the D-function in the complex $q^2 = -Q^2$ plane, namely that the D-function should only have a cut on the positive real q^2 axis. We may correct this feature by noting that the above solution of the renormalization group equation is not unique. The general solution is a function of the running coupling with the asymptotic behaviour $1 + 4\lambda$, for small λ. To maintain the analytic properties[2] of the D-function we can write it as the dispersion integral of $R(s) = (1/\pi){\rm Im}\Pi(s+i\epsilon)$, and use RG improvement on the integrand rather than D itself. This method leads to $D(t,\lambda) = 1 + 4\lambda_{\rm eff}(t,\lambda)$ with $\tau = s/Q^2$. The Borel representation of $\lambda_{\rm eff}(t,\lambda)$ has the form

$$\lambda_{\rm eff}(t,\lambda) = \int_0^\infty db\, {\rm e}^{-b/\overline{\lambda}(t,\lambda)}\, B(b)\,, \qquad (4.1)$$

with $B(b) = \Gamma(1+b\beta_0)\,\Gamma(1-b\beta_0)$. Here $\beta_0 = 11 - 2/3N_f$ is the first coefficient of the β-function, and N_f is the number of active flavours. Thus, in the Borel plane there are singularities at $b\beta_0 = -1, -2, \ldots$ and $b\beta_0 = 1, 2, \ldots$ corresponding to ultraviolet and infrared (IR) renormalons respectively.

The first IR singularity at $b\beta_0 = 1$ is probably absent since there is no corresponding operator in the operator product expansion. Although

[2] Recently, in [26, 27], it has been shown that requiring the correct analytic properties for the running coupling leads to the non-perturbative power corrections of the form $\exp(-1/(\overline{\lambda}(Q^2)\beta_0))$.

this issue is not currently settled, it seems reasonable to assume that the first IR renormalon occurs at $b = 2/\beta_0$, and we would like to use this property of the operator product expansion as an additional constraint on the choice of solution to the renormalization group equation. This can be simply achieved (by judicious integration by parts), and as result we obtain the following expression for $\lambda_{\rm eff}$:

$$\lambda_{\rm eff}(t,\lambda) = \int_0^\infty d\tau\, \omega(\tau) \frac{\overline{\lambda}(kt,\lambda)}{1 + \overline{\lambda}(kt,\lambda)\beta_0 \ln\tau}\,, \tag{4.2}$$

in which the factor k reflects the renormalization scheme an biguity and the function $\omega(\tau) = 2\tau/(1+\tau)^3$ describes the distribution of virtuality usually associated with renormalon chains. The function $B(b)$ in the Borel transform of (4.2) has the form

$$B(b) = \Gamma(1 + b\beta_0)\,\Gamma(2 - b\beta_0)\,. \tag{4.3}$$

Thus in this representation for $\lambda_{\rm eff}$ the positions of all ultraviolet singularities remain unchanged, but the first IR renormalon singularity at $b = 1/\beta_0$ is absent.

In order to render Eq. (4.2) integrable we must combine this method with the nonperturbative a-expansion in which from the beginning the running coupling has no ghost pole. Separating the QCD contribution to R_τ-ratio as Δ_τ and writing $R_\tau = R_\tau^0(1 + \Delta_\tau)$, where R_τ^0 is the well-known electroweak factor, we obtain the expression [25]

$$\Delta_\tau = 48 \int_0^{M_\tau^2} \frac{ds}{M_\tau^2} \left(\frac{s}{M_\tau^2}\right)^2 \left(1 - \frac{s}{M_\tau^2}\right) \tilde{\lambda}(ks)\,, \tag{4.4}$$

in which the factor k again parametrizes the renormalization scheme and $\tilde{\lambda} = a^2(1+3a)/C$. In what follows we shall use the $\overline{MS}$ scheme, in which $k = \exp(-5/3)$. Note that the renormalon representation obtained for the coupling modifies the polynomial in the integral so that the maximum now occurs near $s = (2/3)M_\tau^2$.

Taking as input the experimental value of $R_\tau^{\rm exp} = 3.56 \pm 0.03$ [28], three active quark flavours and the variational parameter $C = 4.1$, we find $\alpha_s(M_\tau^2) = 0.339 \pm 0.015$ which differs significantly from that obtained ($\alpha_s(M_\tau^2) = 0.40$ in leading order [22]) without the renormalon-inspired representation for the coupling. The method, applying the matching procedure in the physical s-channel and using standard heavy quark masses, leads to $R_Z = 20.90 \pm 0.03$, which agrees well with experimental data.

5 Conclusion

In these lectures we have considered an approach to quantum field theory – the method of variational perturbation theory. The original action functional is rewritten using some variational addition and an expansion in the effective interaction is made. Therefore, in contrast to many nonperturbative approaches, in the VPT the quantity under consideration from the very beginning is written in the form of a series which makes it possible to calculate the needed corrections. The VPT method thereby allows for the possibility of determining the degree to which the principal contribution found variationally using some variational principle adequately reflects the problem in question and determining the region of applicability of the results obtained.

The possibility of performing calculations using this approach is based on the fact that the VPT, like standard perturbation theory, uses only Gaussian functional quadratures. Here, of course, the VPT series possesses a different structure and, in addition, some of the Feynman rules are modified at the level of the propagators and vertices. The form of diagrams themselves does not change, which is very important technically. The diagrams contributing to the Nth order of the VPT expansion are of the same form as those contributing to the Nth order of ordinary perturbation theory.

The variational parameters arising in the VPT method allow the convergence properties of the VPT series to be controlled. In [8, 12] has been shown that in the case of the anharmonic variational procedure for the scalar φ^4 model there is a finite region of parameter values in which the VPT series converges for all positive values of the coupling constant. For the harmonic variational procedure there are indications that VPT series can be also converge on the sense of so-called induced convergence, by fine-tuning the variational parameters from order to order. Note also, that a possibility of constructing Leibnitz series in field models is interesting, because, in this case, the first few terms of the series can be used to obtain two-sided estimates of the sum of the series, and existence of variational parameters makes it possible to narrow these estimates the maximum amount in a given order of VPT (see [23]).

Here, we have mainly concentrated upon the application of the method to quantum chromodynamics (see also [29]), where the VPT idea leads to an expansion with a new small expansion parameter. This parameter

obeys an equation whose solution is always smaller than unity for any value of the coupling constant. Therefore, while remaining within the limits of applicability of this expansion it is possible to deal with considerably lower energies than in the case of perturbation theory. An important feature of this approach is the fact that for sufficiently small value of the running coupling constant $\bar{\alpha}_s$ it reproduces perturbative predictions. Therefore, all the high-energy physics is preserved in the VPT method. In going to lower energies, where standard perturbation theory ceases to be valid, $\bar{\alpha}_s \simeq 1$, the VPT running expansion parameter $\bar{a}$ remains small and we do not find ourselves outside the region of applicability of the method.

References

[1] D.I. Kazakov and D.V. Shirkov, Fortschr.Phys. **28** (1980) 465 ; J. Zinn-Justin, Phys.Rep. **70** (1981) 109.

[2] J. Zinn-Justin, Quantum Field Theory and Critical (Phenomena. Clarendon Press. Oxford, 1989).

[3] M. Reed and B. Simon, Methods of modern mathematical physics. Vol. 4 Analysis of operators (New York, San Francisco, London: Academic Press, 1978).

[4] J. Glimm and A. Jaffe, Quantum Physics. A Functional Integral Point of View. (New York, Heidelberg, Berlin: Springer 1981).

[5] P.M. Stevenson, Phys.Rev. **D 30** (1985) 1712 ; Phys.Rev **D 32** (1985) 1389 .

[6] A. Okopinska, Phys.Rev. **D 35** (1987) 1835; Phys.Rev. **D 36** (1987) 2415 .

[7] I. Stancu andP.M. Stevenson, Phys.Rev. **D 42** (1990) 2710 .

[8] A.N. Sissakian, I.L. Solovtsov and O.Yu. Shevchenko, Phys.Lett. **B 313** (1993) 367.

[9] J. Chyla, A.L. Kataev and S.A. Larin, Phys. Lett. B **267** (1991) 269.

[10] A. Mattingly and P.M. Stevenson, Phys. Rev. Lett. **69** (1992) 1320; Phys. Rev. D **49** (1994) 437.

[11] A.N. Sissakian and I.L. Solovtsov, Phys.Lett. **A157** (1991) 261; Z.Phys. C **54** (1992) 263.

[12] A.N. Sissakian, I.L. Solovtsov and O.Yu. Shevchenko, Phys. Lett. B **297** (1992) 305; Phys. Lett. B **313** (1993) 367; Int. J. Mod. Phys. A **9** (1994) 1797; Int. J. Mod. Phys. A **9** (1994) 1929.

[13] L.D. Korsun, A.N. Sissakian and I.L. Solovtsov, Theor. and Math. Phys. **90** (1992) 37, Int. J. Mod. Phys. A **8** (1993) 5129.

[14] W.E. Caswell, Ann. Phys. **123** (1979) 153; J. Killingbeck, J. Phys. **A14** (1981) 1005.

[15] P.M. Stevenson, Nucl. Phys. **B231** (1984) 65.

[16] I.R.C. Buckley, A. Duncan and H.J. Jones, Phys. Rev. D **47** (1993) 2554; A. Duncan and H.J. Jones, Phys. Rev. D **47** (1993) 2560.

[17] A.N. Sissakian, I.L. Solovtsov, and O.P. Solovtsova, Phys. Lett. B **321** (1994) 381.

[18] I.L. Solovtsov, Phys. Lett. B **327** (1994) 335.

[19] I.L. Solovtsov, Phys. Lett. B **340** (1994) 245.

[20] I.L. Solovtsov and O.P. Solovtsova, Phys. Lett. B **344** (1995) 377.

[21] H.F. Jones and I.L. Solovtsov, Phys. Lett. B **349** (1995) 519.

[22] H.F. Jones, I.L. Solovtsov and O.P. Solovtsova, Phys. Lett. B **357** (1995) 441.

[23] A.N. Sissakian and I.L. Solovtsov, Phys. Part. Nucl **25** (1994) 478.

[24] R. Levine and Y. Tomozawa, Phys. Rev. D **19** (1979) 1572.

[25] H.F. Jones, A. Ritz and I.L. Solovtsov, Mod. Phys. Lett. A **12** (1997) 1361.

[26] D.V. Shirkov and I.L. Solovtsov, JINR Rapid Comm. No. 2[76]-96, 5, hep-ph/9604363.

[27] D.V. Shirkov and I.L. Solovtsov, Phys. Rev. Lett. **79** (1997) 1209.

[28] Particle Data Group, Phys. Rev. D **50** (1994); CLEO Collaboration, Phys. Lett. B **356** (1995) 580.

[29] H.F. Jones and I.L. Solovtsov, In Proc. Int. Europhysics Conference on High Energy Physics, Brussels, 27 July–2 August, 1995, Editors J. Lemonne, C. Vander Velde and F. Verbeure, World Scientific (Singapore) 1996, p. 242; H.F. Jones, A.N. Sissakian and I.L. Solovtsov, In Proc. 28th Int. Conference on High Energy Physics, Warsaw, 25–31 July, 1996, Editors Z. Ajduk and A.K. Wroblewski, World Scientific (Singapore) 1997, Vol. II, p. 1650.

Normalized factorial moments for the instanton-induced multigluon production processes in deep inelastic scattering

V.Kuvshinov, R.Shulyakovsky

Institute of Physics, Academy of Sciences of Belarus
Minsk 220072 Scorina av., 70
E-mail: kuvshino@dragon.bas-net.by

The instanton-induced multiparticle events in deep inelastic scattering (DIS) are considered in nonperturbative quantum chromodynamics (QCD). Normalized factorial moments are calculated for these processes. The first quantum correction to the classical instanton configuration is taken into account.

We believe, that specific behaviour of moments can be a new criterion for the identification of the instantons in H1 experiment at HERA (DESY, Hamburg).

I. Introduction

As it is well-known, Yang-Mills gauge theories have highly degenerated vacuum structure even on classical level [1]. As a rule, quantum-tunnelling transitions between different vacuum states are called "instantons".

The existence of the instantons [2] leads to the significant consequences of the quantum field theory: nonconservation of the baryon and lepton charges in the Standard Model electro-weak interactions, chiral symmetry broken in QCD [3].

In according to theoretical calculations, instantons in electro-weak theory can be observed in high energy particle collisions at multi-TeV regime [4,5]. In QCD such phenomena require much smaller energies (about some hundreds MeV [6]). Experimental search of the QCD-instantons has already goes at HERA (DESY, Hamburg) in lepton-hadron deep inelastic scattering [7,8].

The distinct event topology of instanton induced event allows to discriminate them from normal DIS events. There are following theoretically predicted features of instanton-induced multiple states.

1. *High parton multiplicity:* number of produced quarks in each instanton induced event $n_q = 2n_f - 1$ [3], where n_f is number of flavours; average gluon multiplicity $< n_g > \sim 3 - 10$ [6,7].

2. *Isotropically parton distribution* in the instanton rest system [3].

3. *Homogeneous quarks flavours distribution* (large fraction of strangeness and charm in final states as compared with normal DIS) [3].

4. Instanton induced total cross section σ_{tot}^{I} strongly peaks with decreasing of x [6].

5. Second structure function $F_2(x,Q^2)$ rises strongly with decreasing Bjorken variable x [7].

6. Two-particle correlation function in dependence on rapidities of produced gluons has specific form [9].

We study properties of the normalized factorial moments as a new criterion for the experimental identification of the instantons. Our calculations contain contribution of the first quantum correction to the quasiclassical approximation.

II. Distribution on multiplicity for the instanton induced multigluon events in DIS

On the basis of the instanton solution [2]: $A_{\mu}^{aI}(x) = (2/g)\eta_{\mu\nu}^{a}x_{\nu}(x^2+\rho^2)^{-1}$, one obtained the following formula for the multiplicity distribution for the instanton induced multigluon events in DIS (in quasiclassical approximation) [6,7]:

$$P_n^{(cl)} = e^{-A}\frac{A^n}{n!}, \tag{2.1}$$

where $A = \frac{4\pi}{\alpha_s(Q^2)}(\frac{1-x}{x})^2$, ρ is instanton size, α_s denotes coupling constant of strong interaction ($\alpha_s(Q^2) = 0.2$ for $Q^2 = 2500GeV^2$), $\eta_{\mu\nu}^{a}$ is a 't Hooft symbol [3].

The first quantum correction to the expression (2.1) is calculated on the basis on the gluon propagator on the instanton background [10] and leads to the following distribution [4,7]:

$$P_n^{(cl+qu)} = P_n = N\left(\frac{A^n}{n!} - B\frac{A^{n-2}}{(n-2)!}\right), \tag{2.2}$$

where $B = \frac{1}{2}(\frac{1-x}{x})^3$; normalization factor $N = e^{-A}(1-B)^{-1}$. Expression (2.2) is obtained for the $x > 0.5$; there are not exact formula for the small values of Bjorken variable.

III. Calculation of the normalized factorial moments for the instanton induced DIS processes

Let us remind the well-known definition [11]:

$$F_q = \frac{1}{< n >^q}\frac{d^qQ(z)}{dz^q}\bigg|_{z=1}, \quad Q(z) = \sum_{n=0}^{\infty}P_nz^n, \quad < n >= \frac{dQ(z)}{dz}\bigg|_{z=1}, \tag{3.1}$$

where F_q is qth normalized factorial moment, $< n >$ is average multiplicity, $Q(z)$ is so-called generating function.

In the case of quasiclassical approximation (2.1) of instanton induced multiparticle production processes (Poisson multiplicity distribution) we have trivial result $F_q = 1$.

If we take into account first quantum correction (distribution (2.2)) the following formula takes place:

$$F_q = (1-B)^{q-1} \frac{A^q(1-B) - 2qA^{q-1}B - q(q-1)A^{q-2}E}{(A(1-B)-2B)^q}. \qquad (2.3)$$

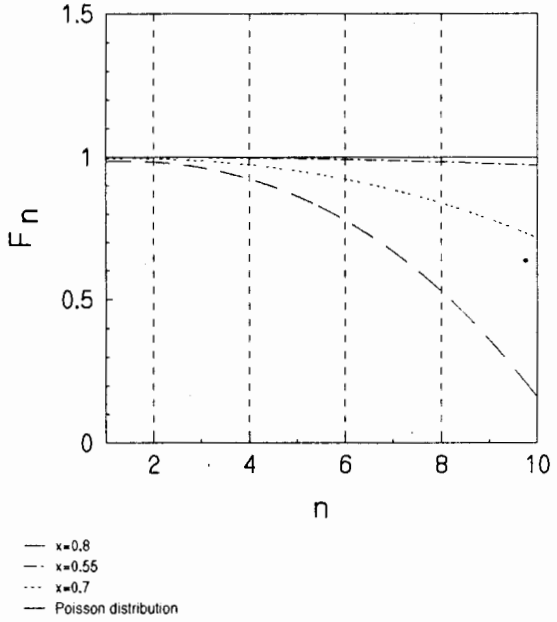

Fig.1. Normalized factorial moments for the different values of Bjorken variables x and fixed 4-momentum transfer $Q^2 = 2500GeV^2$.

Thus, F_q for the distribution of the instanton-induced DIS processes are decreased with moment number growth. Deflection of the normalized factorial moments from Poisson distribution is increased with increasing Bjorken variable x (see Fig.1).

IV. Conclusion

In this note we have calculated normalized factorial moments for the instanton-induced processes of multiparticle production in deep inelastic

scattering. Quasiclassical approximation gives trivial results. If we take into account the first quantum correction, that F_q have specific form. Thus, we have obtained new feature of instanton induced events in addition to the known footprints.

It should be noted, that our results are obtained for the parton distribution. Local parton-hadron duality [12] allows to apply them to hadrons and to compare with experimental data.

The authors are grateful for the support in part to Basic Science Foundation of Belarus (Projects F95-013, M96-023).

References

[1] R.Jackiw and C.Rebbi, *Phys. Rev. Lett.* **37** (1976) 172.

[2] A.Belavin, A.Polyakov, A.Schwarz and Yu.Tyupkin, *Phys.Lett.* **B59** (1975) 85.

[3] G.'t Hooft, *Phys.Rev.Lett.* **37** (1976) 8;
G.'t Hooft, *Phys. Rev.* **D14** (1976) 3432.

[4] D.Dyakonov and V.Petrov, *Proceed. of XXVI Winter School LINP* (1991) 8.

[5] A.Ringwald, *Nucl.Phys.* **B330** (1990) 1;
A.Ringwald, *CERN-TH.* **6479/92** (1992).

[6] I.Balitsky and V.Braun, *Phys.Lett.* **B314** (1993) 237.

[7] A.Ringwald and F.Schrempp, *DESY preprint* **94-197** (November, 1994);
M.Gibbs, A.Ringwald and F.Schrempp, *DESY preprint* **95-119** (June,1995);
A.Ringwald and F.Schrempp, *DESY preprint* **96-203** (October, 1996).

[8] T.Carli and M.Kuhlen, *Talk on XVIII Int. Sumposium on Lepton-Photon Interaction, Hamburg* (1997).

[9] V.Kuvshinov and R.Shulyakovsky, *Acta Phys. Pol.* **B28** (1997) 1629.

[10] L.Brown, R.Carlitz, D.Creamer and C.Lee, *Phys. Rev.* **D17** (1978) 1583.

[11] I.M.Dremin, E. De Wolf and W.Kittel, *Usp. Fiz. Nauk* **163** (1993) 3.

[12] Ya.Azimov at. al. *Z.Phys.* **C27** (1985) 65.

Труды Международной школы-семинара «Актуальные проблемы физики частиц»

Proceedings of International School-Seminar «Actual Problems of Particle Physics»

Ответственный за подготовку сборника к печати
В.С.Румянцев

E1,2-98-307

Том II

Макет Н.А.Киселевой

Рукопись сборника поступила 27.10.98. Подписано в печать 18.11.98
Формат 60 × 90/16. Офсетная печать. Уч.-изд. листов 17,0
Тираж 170. Заказ 50996. Цена 35 р.

Издательский отдел Объединенного института ядерных исследований
Дубна Московской области